République Algérienne Démocratique et Populaire
Ministère de L'Enseignement Supérieur et de la Recherche Scientifique
Université de KASDI MERBAH Ouargla
Faculté des Sciences Appliquées
Département de Génie Electrique

Thèse de Doctorat

Présentée pour l'obtention du grade de **DOCTEUR**

En : Electrotechnique

Spécialité : Electrotechnique

Par : El Mouatez Billah MESSINI

Thème

Sizing, optimization and energy management of a hybrid system based on three generators

Soutenue publiquement, le **26/02/2025**, devant le jury composé de :

M.	DJAFOUR Ahmed	Prof.	Université Kasdi Merbah Ouargla	Président
M.	BOUREK Yacine	MCA	Université Kasdi Merbah Ouargla	Directeur de thèse
M.	MAKHLOUFI Salim	Prof.	Université Ahmed DRAIA. ADRAR	Examinateur
M.	AISSAOUI Faris	MCA	Université de Ghardaia	Examinateur
M.	SADAOUI Fares	MCA	Université Kasdi Merbah Ouargla	Examinateur
M.	BOUHAFS Ali	MCA	à Université Kasdi Merbah Ouargla	Examinateur
M.	AMMARI Chouaib	MCB	Université Kasdi Merbah Ouargla	Invité (Co-directeur de thèse)

Année universitaire 2024/2025

People's Democratic Republic of Algeria
Ministry of Higher Education and Scientific Research
Kasdi Merbah University of Ouargla
Faculty of Applied Sciences
Department of Electrical Engineering

Ph.D. Thesis

Presented for the attainment of the degree of **Ph.D.**

In : Electrotechnics

Specialty : Electrotechnics

By : El Mouatez Billah MESSINI

Topic

Sizing, optimization and energy management of a hybrid system based on three generators

Publicly defended on **26/02/2025**, before the jury composed of:

M.	DJAFOUR Ahmed	Professor	Kasdi Merbah University of Ouargla	President
M.	BOUREK Yacine	Senior Lecturer (MCA)	Kasdi Merbah University of Ouargla	Thesis Supervisor
M.	MAKHLOUFI Salim	Professor	Ahmed Draia University, Adrar	Examiner
M.	AISSAOUI Faris	Senior Lecturer (MCA)	University of Ghardaia	Examiner
M.	SADAOUI Fares	Senior Lecturer (MCA)	Kasdi Merbah University of Ouargla	Examiner
M.	BOUHAFS Ali	Senior Lecturer (MCA)	Kasdi Merbah University of Ouargla	Examiner
M.	AMMARI Chouaib	Lecturer (MCB)	Kasdi Merbah University of Ouargla	Guest (Co-supervisor)

Academic Year 2024/2025

Abstract

This thesis covers modeling, optimal sizing, and energy management of a Hybrid Renewable Energy System intended for supplying electrical energy to oil and gas facilities located in southern Algeria. The globally increasing demand for energy, which is accompanied by environmental concerns calling for cleaner sources of energy, presents an urgent need for the integration of renewable sources in industries, especially within the oil and gas industry. This work investigates one such transition from conventional natural gas systems to renewable sources of energy, addressing the resultant techno-economic and environmental challenges associated with integrating renewables. A complete simulation-driven methodology has been applied by using MATLAB for the representation of the various system components including photovoltaic (PV) modules, wind turbines (WT), gas turbines (GT), Battery Energy Storage Systems (BES), and Hydrogen Energy Storage (HES). In the given work, the optimization methodology was implemented through sophisticated optimization algorithms such as Non-dominated Sorting Genetic Algorithm II (NSGA-II), multi-objective particle swarm optimization (MOPSO), and Fick's Law Algorithm (FLA) combined with energy management techniques, based on the load flow between generated power and priority between storage means, toward better system efficiency with low cost and low emissions. All these settings were taken into consideration: completely renewable integrated systems and partial transitions of 20%, 50%, and 80%, while the used strategies included the storage integration of BES and HES. The results indicate that while full integration of renewables can bring Carbon Dioxide Emission (CDE) factor as low as nearly zero, the cost of energy is higher. In contrast, partial integration of Renewable Energy Sources(RES) shows a more balanced approach in which lower Cost of Energy (COE) values can be achieved while it reduces CDE significantly. For instance, a PV-WT-BES-HES based system, emerged as the most efficient configuration to meet 0% Loss of Powe Supply Probability (LPSP) with optimal COE and environmental performance. Results have pointed out the feasibility and efficiency of the integration of renewable energy sources into the oil and gas industry, hence providing an opportunity to cut carbon emission while transitioning towards sustainable energy systems.

Keywords: Hybrid Renewable Energy System (HRES); Optimal Sizing; Energy Management Strategy (EMS); Oil and Gas Facilities; Photovoltaic (PV); Wind Turbine (WT); Battery Energy Storage (BES); Hydrogen Energy Storage (HES); Techno-Economic Analysis; Carbon Emissions Reduction.

Résumé

Cette thèse porte sur la modélisation, le dimensionnement optimal et la gestion de l'énergie d'un système hybride d'énergie renouvelable destiné à l'approvisionnement en électricité des installations pétrolières et gazières situées dans le sud de l'Algérie. L'augmentation mondiale de la demande en énergie, accompagnée de préoccupations environnementales appelant à des sources d'énergie plus propres, souligne l'urgence d'intégrer les sources renouvelables dans les industries, en particulier dans le secteur pétrolier et gazier. Ce travail explore cette transition d'un système conventionnel à base de gaz naturel vers des sources d'énergie renouvelables, en abordant les défis technico-économiques et environnementaux qui en résultent.

Une méthodologie complète basée sur la simulation a été appliquée en utilisant MATLAB pour la représentation des différents composants du système, notamment les modules photovoltaïques (PV), les éoliennes (WT), les turbines à gaz (GT), les systèmes de stockage d'énergie par batteries (BES) et le stockage d'énergie par hydrogène (HES). Dans ce travail, la méthodologie d'optimisation a été mise en œuvre à l'aide d'algorithmes d'optimisation avancés tels que l'algorithme génétique à tri non-dominé II (NSGA-II), l'optimisation par essaim particulaire multi-objectifs (MOPSO) et l'algorithme basé sur la loi de Fick (FLA), combinés avec des techniques de gestion de l'énergie basées sur le flux de charge entre la puissance générée et la priorité entre les moyens de stockage, dans le but d'améliorer l'efficacité du système à faible coût et faibles émissions.

Les scénarios étudiés incluent des systèmes intégrés entièrement renouvelables ainsi que des transitions partielles à hauteur de 20 %, 50 % et 80 %, avec des stratégies incorporant l'intégration du stockage via BES et HES. Les résultats indiquent que, bien que l'intégration complète des énergies renouvelables puisse réduire presque à zéro les émissions de dioxyde de carbone (CDE), le coût de l'énergie reste plus élevé. En revanche, une intégration partielle des sources d'énergie renouvelables (RES) offre une approche plus équilibrée permettant d'obtenir un coût de l'énergie (COE) plus bas tout en réduisant considérablement les CDE. Par exemple, un système combinant PV-WT-BES-HES s'est révélé être la configuration la plus efficace pour atteindre une probabilité de perte

d'alimentation (LPSP) de 0 %, avec un COE optimisé et de bonnes performances environnementales. Les résultats mettent en évidence la faisabilité et l'efficacité de l'intégration des énergies renouvelables dans l'industrie pétrolière et gazière, offrant ainsi une opportunité de réduction des émissions de carbone tout en assurant une transition vers des systèmes énergétiques durables.

Mots-clés : Système Hybride d'Énergie Renouvelable (SHER); Dimensionnement Optimal; Stratégie de Gestion de l'Énergie (SGE); Installations Pétrolières et Gazières; Photovoltaïque (PV); Éolienne (Éolienne); Stockage d'Énergie par Batterie (SEB); Stockage d'Énergie à l'Hydrogène (SEH); Analyse Technico-Économique; Réduction des Émissions de Carbone.

ملخص

تتناول هذه الدراسة نمذجة وتحديد الحجم الأمثل وإدارة الطاقة لنظام الطاقة المتجددة الهجين (HRES) الذي يهدف إلى تزويد منشآت النفط والغاز في جنوب الجزائر بالطاقة الكهربائية. مع تزايد الطلب العالمي على الطاقة وظهور مخاوف بيئية تدعو إلى استخدام مصادر طاقة أنظف، أصبح دمج مصادر الطاقة المتجددة في الصناعات، وخاصة صناعة النفط والغاز، أمرًا بالغ الأهمية. تبحث هذه الدراسة في التحول الجزئي من الأنظمة التقليدية التي تعتمد على الغاز الطبيعي إلى مصادر الطاقة المتجددة، مع معالجة التحديات التقنية والاقتصادية والبيئية الناتجة عن دمج الطاقة المتجددة.

تم استخدام منهجية تعتمد على المحاكاة باستخدام برنامج MATLAB لتمثيل مكونات النظام المختلفة، بما في ذلك الألواح الضوئية (PV) والتوربينات الهوائية (WT) والتوربينات الغازية (GT) وأنظمة تخزين الطاقة بالبطاريات (BES)وأنظمة تخزين الطاقة بالهيدروجين(HES).

في هذا العمل، تم تنفيذ منهجية المثلى باستخدام خوارزميات تحسين متقدمة مثل خوارزمية الفرز الجيني غير المسيطرة (NSGA-II) IIوخوارزمية تحسين حركة السرب متعددة الأهداف (MOPSO) وخوارزمية المعتمدة على قانوني فيك للانتشار (FLA)، مع تقنيات إدارة الطاقة بهدف تحقيق كفاءة أفضل للنظام بتكلفة منخفضة وانبعاثات قليلة. شملت هذه الإعدادات تقييم أنظمة الطاقة المتجددة الكاملة والانتقالات الجزئية بنسبة 20٪ و50٪ و80٪، باستخدام استراتيجيات تضمنت دمج أنظمة التخزين BES وHES.

تشير النتائج إلى أنه رغم أن الدمج الكامل للطاقة المتجددة يمكن أن يقلل من انبعاثات ثاني أكسيد الكربون (CDE) إلى ما يقرب من الصفر، فإن تكلفة الطاقة تكون أعلى. على النقيض من ذلك، يظهر الدمج الجزئي لمصادر الطاقة المتجددة نهجًا أكثر توازنًا، حيث يمكن تحقيق قيم منخفضة لتكلفة الطاقة (COE) مع تقليل كبير للانبعاثات. على سبيل المثال، أثبت النظام القائم على PV-WT-BES-HESأنه التكوين الأكثر كفاءة لتحقيق احتمالية انقطاع إمداد الطاقة (LPSP)بنسبة 0%، مع تكلفة طاقة (COE) مثلى وأداء بيئي جيد. وتبرز النتائج جدوى وكفاءة دمج مصادر الطاقة المتجددة في قطاع النفط والغاز، مما يوفر فرصة لتقليل انبعاثات الكربون مع ضمان الانتقال نحو أنظمة طاقة مستدامة.

الكلمات المفتاحية

نظام الطاقة المتجددة الهجين(HRES) ؛ تحديد الحجم الأمثل؛ استراتيجية إدارة الطاقة(EMS) ؛ منشآت النفط والغاز ؛ الألواح الضوئية(PV) ؛ التوربينات الهوائية(WT) ؛ تخزين الطاقة بالبطاريات(BES) ؛ تخزين الطاقة بالهيدروجين (HES)؛ التحليل التقني والاقتصادي؛ تقليل انبعاثات الكربون.

Acknowledgements

First and foremost, I thank **ALLAH**, the Almighty, for granting me the strength and determination to complete this research work.

I would like to express my deepest gratitude to my thesis supervisors, Pr. **Yacine Bourek**, Senior Lecturer, and Dr. **Chouaib Ammari**, Lecturer at the University of Ouargla, for their constant guidance, continuous support, and invaluable advice. This work was carried out at the Electrical Engineering Laboratory (LAGE) of the Scientific Research Center of the University of Ouargla, under the supervision of Pr. **Yacine Bourek**. I offer my sincere thanks for initiating and supporting my work, for his patience, and for the trust he placed in me throughout this thesis. A few lines will never suffice to express the extent of my gratitude toward him.

Furthermore, I would like to extend my immense thanks to Dr. **Chouaib Ammari**, who was always available and provided me with unconditional support throughout this research journey. His assistance, both scientific and personal, was instrumental in the successful completion of this work.

Additionally, I would like to give special thanks to Pr. **Dimitrios Ipsakis**, Professor at the Technical University of Crete, for welcoming me and guiding me during my internship at the aforementioned university. His scientific and professional guidance significantly contributed to the effective and high-quality realization of this work.

I also express my heartfelt thanks to Pr. **DJAFOUR Ahmed**, Senior Lecturer at the Kasdi Merbah University of Ouargla, for accepting to evaluate this work and for the honor of presiding over the jury.

Lastly, I extend my sincere gratitude to Pr. **MAKHLOUFI Salim**, Pr. **AISSAOUI Faris**, Dr. **SADAOUI Fares**, and Mr. **BOUHAFS Ali** for their interest and for accepting to evaluate this work as examiners.

I would also like to thank all the individuals whom I could not mention here but who contributed, directly or indirectly, to the realization of this work.

Finally, I cannot conclude without expressing my heartfelt gratitude to my parents, my wife, and all my family members for their unwavering support and encouragement throughout this journey,

enabling me to complete this work.

Dedication

It is with immense joy that I dedicate this modest work to the dearest people in the world—my beloved parents—for all their moral support throughout these years of study and for the unconditional love they have always shown me.

I also dedicate this work to my beloved wife, for her unwavering support and tireless efforts in helping me complete my thesis.

I dedicate this work to all my family members—each of my brothers, sisters, and their families, both small and large, and especially my cousin El Haj Zaki.

I also dedicate this work to my work colleagues at the Algerian Petroleum Institute, especially my office collaborators (Xabi, Aissa, Taki, and Mohammed).

Contents

List of Figures

List of Tables

Abbreviations

AC Alternating current.

ACS Annualized cost of system.

AI Artificial intelligence.

ALO Ant Lion Optimizer.

ARO Artificial rabbit optimization.

BESS Battery Energy Storage System.

BSO OS Brainstorm Optimization in Objective Space.

BSS Battery storage systems.

CAPEX Initial/capital expenditure.

CE Carbon emission.

CES Chemical energy storage.

CFOE Carbon footprint of energy.

CO Carbon monoxide.

CO_2 Carbone dioxide.

COE Unit electricity cost.

CRF Capital Recovery Factor.

CS Cuckoo Search.

CSP Concentrated solar power.

DC Direct current.

DMGWO Discrete multiobjective grey wolf optimization.

DNI Annual direct normal irradiance.

DP Dynamic programming.

DPB Discounted Payback Period.

DPSP Deficiency of Power Supply Probability.

EE Embodied energy.

EENS Expected Energy Not Supplied.

EL Electrolyzers.

EMS Energy Management Strategies.

EO Equilibrium Optimizer.

FA Firefly Optimization Algorithm.

FC Fuel Cells.

FE Fuel emission.

FLA Fick's Law Optimization Algorithm.

FOWT Floating offshore wind turbines.

GA Genetic Algorithms.

GHG Greenhouse gas.

GHI Global horizontal irradiance.

GOA Grasshopper Optimization Algorithm.

GT Gas Turbine.

GTG Gas turbogenerators.

GWO Grey Wolf Optimizer.

H2 Hydrogen.

HESS Hydrogen Energy Storage System.

HHV Higher Heating Value.

HIL Hardware-in-the-loop.

HPS Hybrid power systems.

HRES Hybrid renewable energy systems.

HS Harmony Search.

IRR Internal Rate of Return.

JC Job creation.

JFF Job formation factor.

KPI Key performance indicators.

LCA Life cycle assessment.

LCC Lifecycle costing.

LCOE Levelized cost of energy.

LCOWP Levelised Cost of Water Pumped.

LF Load Following.

LOEE Loss of Energy Expected.

LOLE Loss of Load Expected.

LOLP Loss of Load Probability.

LPSP Loss of Power Supply Probability.

LTE Local transport-based employment.

LWSP LossofWaterSupplyProbability.

MCDA Multi-criteria decision analysis.

MCDM Multi-Criteria Decision-Making.

MFO Moth Flame Optimization.

MFOA Moth-Flame Optimization Algorithm.

MILP Mixed-Integer Linear Programming.

MOCSA Multi-objective crow search algorithm.

MPC Model predictive control.

MPSO Multi-Objective Particle Swarm Optimization.

MToe Million tonnes of oil equivalent.

NGPP Natural Gas Power Plant.

NPC Net Present Cost.

NPV Net Present Value.

NSGA-II Non-dominated Sorting Genetic Algorithm II.

O-EMS Optimized Energy Management Strategies.

OFs Objective functions.

OPEX Operation and maintenance costs.

PAT Small hydro turbine generator.

PEM Proton Exchange Membrane.

PEMEL Proton Exchange Membrane Electrolyzer.

PEMFC Proton Exchange Membrane Fuel Cell.

PPS Power production scheduling.

PSO Particle Swarm Optimization.

PV Photovoltaic.

R-EMS Rule-based Energy Management Strategies.

RE Renewable energy.

RF Renewable Fraction.

RHO Receding horizon optimization.

RHS Rolling horizon strategy.

ROI Return on investment.

RTOP Renewable energy production simulation.

S-SSA Simplified Squirrel Search Algorithm.

SA Simulated Annealing.

Sa Social acceptance.

SCC Social cost of carbon.

SCS Supercapacitors.

SDM Single Diode Model.

SFS Stochastic Fractal Search.

SKTM Shariket Kahraba wa Taket Moutadjadida.

SMA Slime Mould Algorithm.

SO2 Sulfuric Dioxide.

SOC State of Charge.

SOS Symbiotic Organisms Search.

ST Stirling engine.

TAC Total Annual Cost.

TACS Total Annual Cost of System.

TAEP Total annual energy production.

TDM Triple Diode Model.

TEG Thermoelectric generation.

TES Thermal Energy Storage.

TNPC Total Net Present Cost.

TOPSIS Technique for Order Preference by Similarity to an Ideal Solution.

UES Unit electricity cost.

WAsP Wind Atlas Analysis and Application Program.

WECs Wave energy converters.

WOA Whale Optimization Algorithm.

WT Wind Turbine.

ZBF Zinc bromine flow battery.

Note: Author abbreviations are shown in alphabetical order in their corresponding reference entry.

Nomenclature

Term	Description	Units
C_B	BES capacity	(Wh)
$C_{BES-\text{init}}$	Initial capacity in BES (kWh)	(kWh)
C_{tk}	H_2 tank capacity	(kg)
HHV_{H_2}	Higher heating value for H_2	(kWh/kg)
I	Current of photovoltaic module	(A)
I_{ph}	Photon current	(A)
I_{sd}	Diode current	(A)
I_{sh}	Shunt resistor current	(A)
I_{ssd}	Diode saturation current	(A)
N_{BES}	Number of BES	—
N_{pv}	Number of photovoltaic modules	—
P_{BT}	Power of the inverter	(kW)
P_{EL}	Electrolyzer power (kW)	—
P_{FC}	Fuel cell power	(kW)
P_{GT}	Power of gas turbine generators	(kW)
P_{tot}	Total power supplied to the load	(kW)
Q_{H_2}	Quantity (mass) of H_2 in storage tank	(kg)
$Q_{H_{2-\text{end}}}$	Final H_2 quantity in tank	(kg)
$Q_{H_{2-\text{init}}}$	Initial H_2 quantity in tank	(kg)
R_s	Series resistance of PV module	(Ω)
R_{sh}	Branch resistance of PV module	(Ω)

Term	Description	Units
V	Voltage of photovoltaic module	(V)
Δt	Time span for the simulation	(hour)
η_{EL}	Efficiency of electrolyzer	(%)
η_{FC}	Efficiency of fuel cell	(%)
η_{GT}	Efficiency of gas turbine generators	(%)
γ	Actual interest rate	—
σ	Battery hourly self-discharge	(%/day)
f	Inflation rate	—
i	Interest rate	—
k	Boltzmann constant	(J/K)
n	Diode ideal factor	—
q	Electron charge	(C)
t	Time	(hour)

General Introduction

The increasing demand for energy is intrinsically linked to improvements in the quality of life worldwide. As societies advance, their energy needs grow, creating a pressing demand for reliable and abundant energy sources. Historically, fossil fuels such as coal, oil, and natural gas have been the cornerstone of global energy supply. However, the continued reliance on these finite resources raises concerns over their eventual depletion and the significant environmental repercussions associated with their use. Chief among these concerns is global warming, driven by the accumulation of greenhouse gases in the atmosphere, resulting in rising global temperatures. This issue has garnered international attention, leading to global accords such as the Paris Agreement, which aims to mitigate climate change by reducing carbon emissions.

In response to these challenges, there is a global shift towards renewable and clean energy sources. Renewable energy technologies, including solar, wind, and hydropower, offer the promise of a sustainable energy future with minimal environmental impact. However, these technologies face significant hurdles, primarily their intermittent nature and the high initial capital investment required. The variability of renewable energy sources necessitates the integration of storage systems or the supplementation with conventional energy sources to ensure a stable and continuous energy supply.

To address the limitations of standalone renewable energy systems, hybrid renewable energy systems (HRES) have been developed. These systems combine various renewable sources, such as solar and wind, with conventional energy generators like natural gas power plants and diesel generators, alongside diverse storage technologies including batteries, hydrogen storage, thermal batteries, and hydraulic and pneumatic systems. The hybrid approach aims to balance the intermittency of renewable sources with the reliability of conventional power, thereby enhancing the overall system efficiency and reliability.

A critical aspect of HRES is the management of diverse load demands. These demands encompass

not only electrical loads but also thermal (heating/cooling) and hydrogen supply loads, with varying profiles depending on the application—whether residential, industrial, or communal. Effective load management requires precise matching of supply with demand to ensure optimal system performance.

The optimal sizing and installation of HRES components are essential to achieve a balance between energy supply and demand. This necessitates sophisticated energy management systems (EMS) that can dynamically allocate power flows, minimize power losses, reduce system costs, and lower environmental impacts. The EMS must be capable of integrating and managing multiple energy sources and loads to ensure a continuous power supply throughout the system's lifespan.

To enhance the efficiency of HRES, artificial intelligence (AI) techniques are increasingly being employed. These techniques include Genetic Algorithms (GA), Particle Swarm Optimization (PSO), Grey Wolf Optimization (GWO), and other advanced methods. AI-based optimization enables the precise sizing of system components, ensuring an optimal trade-off between various performance indicators such as cost, efficiency, and environmental impact. AI techniques can be categorized into four main groups: swarm-based techniques (e.g., PSO), evolutionary-based techniques (e.g., GA), physics law-based techniques (e.g., Simulated Annealing), and human behavior-based techniques (e.g., Harmony Search). Each category offers unique advantages in solving complex optimization problems in the design and operation of HRES.

Consequently, the transition to a sustainable energy future necessitates the development of innovative solutions like hybrid renewable energy systems. These systems, through the integration of diverse energy sources and advanced management strategies, promise to meet the rising energy demands while mitigating environmental impacts. The application of AI in optimizing these systems represents a significant step forward in achieving efficient, cost-effective, and environmentally friendly energy solutions for various sectors, including the oil and gas industry.

The primary objective of this study is to develop a hybrid renewable energy system that seamlessly integrates renewable energy sources with existing fossil fuel-based energy production facilities. The focus is on an oil and gas processing facility located in the southeastern region of Algeria, which currently preprocesses natural gas. The existing energy production system at this facility relies on a Natural Gas Turbine coupled with a synchronous generator, commonly referred to as a Natural Gas

Power Plant (NGPP). The proposed system aims to partially incorporate renewable energy sources into the current setup, thereby reducing its environmental footprint.

In particular, this study will explore the integration of renewable energy technologies such as solar and wind power with the existing NGPP infrastructure. Additionally, the system will incorporate advanced storage solutions, including batteries and hydrogen storage systems, to manage the intermittency of renewable sources and ensure a stable energy supply. The optimal sizing of these components will be guided by an energy management strategy that prioritizes the maximum feasible integration of renewable energy sources (RES).

The performance of the proposed hybrid system will be evaluated using three key performance indicators (KPIs). The technical indicator will focus on the probability of power supply loss and excess energy production. The economic indicators will include the total annualized cost of the system and the cost of energy production. Lastly, the environmental indicator will assess the reduction in carbon dioxide emissions, reflecting the system's impact on mitigating climate change.

This study's final aim is to achieve an optimal trade-off between these KPIs through the physical modeling of system components and the application of advanced artificial intelligence (AI) techniques. By employing AI methods such as Genetic Algorithms (GA), Particle Swarm Optimization (PSO), and other relevant optimization algorithms, the study will determine the optimal sizing for each system component. These AI-based optimization techniques will ensure that the system meets the desired technical, economic, and environmental performance targets.

Furthermore, this research will culminate in providing comprehensive recommendations to stakeholders and policymakers. These recommendations will be instrumental in making informed decisions regarding the adoption and implementation of clean energy systems. By demonstrating the feasibility and benefits of integrating renewable energy with existing fossil fuel-based infrastructure, the study aims to contribute significantly to the advancement of sustainable energy solutions in the oil and gas sector.

In summary, the study's objective is to design and optimize a hybrid renewable energy system that enhances the sustainability of an oil and gas processing facility in Algeria. By integrating renewable energy sources and advanced storage technologies with the existing NGPP, and optimizing the system

using AI techniques, the study seeks to achieve a balance between technical performance, economic viability, and environmental impact. The insights and recommendations derived from this research will support the transition towards cleaner energy systems and inform strategic decision-making processes in the energy sector.

This thesis is organized as follows: following this general introduction, the first chapter (Chapter I) is dedicated to an extensive literature review and the problem statement concerning the hybrid renewable energy systems under study. This literature review provides a historical overview of renewable energy sources (RES) and their impact across technical, economic, and environmental dimensions. Additionally, it includes an analysis of previous works on the modeling, optimal sizing, and energy management of multi-source hybrid renewable systems. The chapter concludes by highlighting our unique contribution to this field, emphasizing the novelty of the techniques employed to address the energy problem. The second chapter (Chapter II) forms the core of our study, focusing on the modeling and optimal sizing of the system based on AI techniques, along with energy management for the oil and gas processing facility. This section begins with the data collection and description of the study region, including weather and load data profiles. It then delves into the extensive and detailed physical modeling of each system component, including generators, storage systems, and converters. Various energy management strategies and optimization techniques are developed and utilized to solve the optimization problem, guided by the previously mentioned key performance indicators (KPIs).
The final part of this thesis (Chapter III) is devoted to the presentation and discussion of the study's outcomes. Here, the key performance indicators are evaluated and discussed, comparing the behavior of the employed optimization algorithms. Additionally, a sensitivity analysis of the studied system is conducted to assess the limitations of the adopted methods.
The thesis concludes with a general conclusion and suggestions for future work, providing a comprehensive overview of the research findings and outlining potential directions for further investigation in the realm of hybrid renewable energy systems for oil and gas facilities.
In summary, this thesis not only addresses the technical and economic challenges of integrating renewable energy with existing fossil fuel systems but also contributes to the broader goal of sustainable energy solutions. Through a systematic approach combining literature review, detailed modeling, AI-based optimization, and rigorous analysis, this research aims to advance the understanding and implementation of hybrid renewable energy systems, ultimately aiding stakeholders and policymakers in making informed, strategic decisions for a cleaner energy future.

Chapter I

State of the Art and Problem Statement

I.1 Algeria Energy Sector

The rise in global lifestyle quality has led to a significant increase in energy demand. Currently, hydrocarbon fuels are the primary source of energy, accounting for approximately 70% of the global energy demand. Due to the urgent economic growth worldwide, these fuels are expected to remain a leading energy source for the foreseeable future [1–3]. Algeria stands out as a major player in the global energy landscape. It is the largest producer of natural gas in Africa, the second-largest supplier of natural gas to Europe, and among the top three oil producers on the continent. The country's conventional hydrocarbon reserves are substantial, spread across just over 200 oil and gas deposits (Fig. I.1, source : [4]) [2, 4]. The hydrocarbon sector is a cornerstone of Algeria's economy, with oil and natural gas production reaching around 155 million tonnes of oil equivalent (MToe). The energy demand in Algeria is growing rapidly, exceeding a 6% annual increase. The nation's extensive reserves of oil and natural gas are projected to meet consumption needs for the next 50 years for oil and 70 years for natural gas, assuming current consumption rates persist. To capitalize on these resources, Algeria has implemented fiscal incentives aimed at attracting foreign investment, particularly for exploring unconventional resources such as shale gas [5]. Moreover, Algeria is not solely focused on fossil fuels; it is also keen on expanding its renewable energy (RE) sector. The country has set an ambitious strategic plan to achieve a 40% share of renewable energy in electricity production by 2030, with a particular emphasis on solar energy. This plan positions Algeria as a potential leader in

the global renewable energy sector [1, 5–13].

Algeria possesses significant potential for renewable energy generation, including solar, wind, biomass, geothermal, and hydropower sources. Despite being rich in non-renewable energy sources, with 98% of energy production coming from such sources, the country aims to diversify its energy mix by investing in renewable energy technologies. The Algerian government has set ambitious targets to install around 22 GW of renewable energy capacity by 2030, encompassing various sources like bio-power, solar PV, Concentrated Solar Panel(CSP), geothermal, cogeneration, and wind power. The country's Renewable Energy and Energy Efficiency Development Plan focuses on large-scale solar and wind generation, as well as geothermal and biomass technologies, to reduce dependency on fossil fuels and promote sustainable energy practices. This shift towards renewable energy aligns with the country's goal of transitioning to a cleaner and more sustainable energy system, showcasing its commitment to environmental preservation and energy security [14–18].

Algeria benefits from exceptionally high solar insolation intensities, making it one of the world's most promising regions for solar energy development. The country's solar potential is estimated at 13.9 TWh/year. The average annual sunshine duration is approximately 2650 hours in the coastal region, 3000 hours in the high plateau, and 3500 hours in the Sahara [2, 15, 19]. Correspondingly, the average annual direct normal irradiance (DNI) in these regions is estimated at 1700, 1900, and 2650 kWh/m^2/year, respectively, which is highly favorable for the development of concentrated solar power (CSP). Additionally, Algeria's global horizontal irradiance (GHI) ranges from 2100 kWh/m^2/year in the north to 2400 kWh/m^2/year in the south, further supporting the potential for photovoltaic (PV) installations. Fig. I.2 (source: [20]) illustrates the geographic locations best suited for CSP and PV based on DNI and GHI values. This high level of solar insolation makes Algeria ideally suited for both CSP and PV technologies. The extensive solar resources could significantly contribute to the country's energy mix, reducing dependency on fossil fuels and aligning with Algeria's strategic goals for renewable energy development. The deployment of solar technologies could harness this abundant energy, potentially transforming Algeria into a leader in renewable energy within the region [2, 14, 15, 19].

Algeria's heavy reliance on fossil fuels has led to the rapid depletion of natural resources and a significant increase in greenhouse gas (GHG) emissions. Hydrocarbon fuels are the primary contributors to these emissions, highlighting the urgent need for climate action. The COP28 summit has

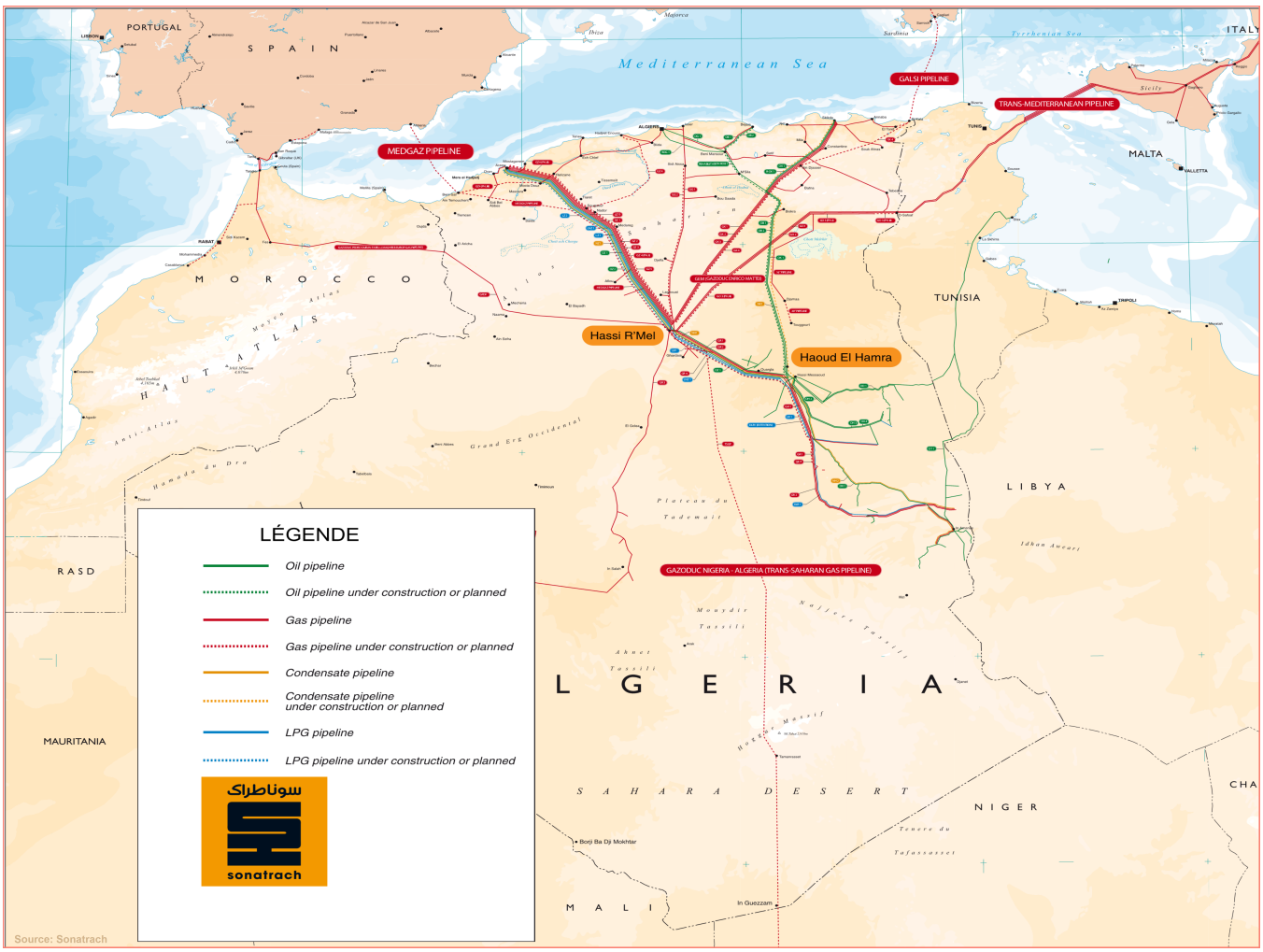

Figure I.1: Algeria Oil and Gas map.

emphasized the necessity for serious climate measures, advocating for a clear phase-out of fossil fuels to achieve net-zero emissions by 2050. This transition aims to mitigate the environmental impact of hydrocarbon fuels and promote sustainable practices while maintaining economic stability. Given this context, Algeria's dependence on oil and gas demands urgent attention at all levels to bolster the nation's energy security. Addressing energy sustainability, environmental protection, and economic factors is crucial. Exploring alternative energy sources is essential to diversify and strengthen the energy mix, enhancing Algeria's overall energy sustainability [3, 21].

Wind energy in Algeria varies significantly across different regions due to diverse topographical and climatic conditions. The first wind speed measurement campaign in Algeria dates to the 1910s. Historically, wind speed measurements were averaged from three daily readings taken at 7 a.m., 1 p.m., and 6 p.m. to determine daily average wind speeds [15]. More recent assessments have utilized

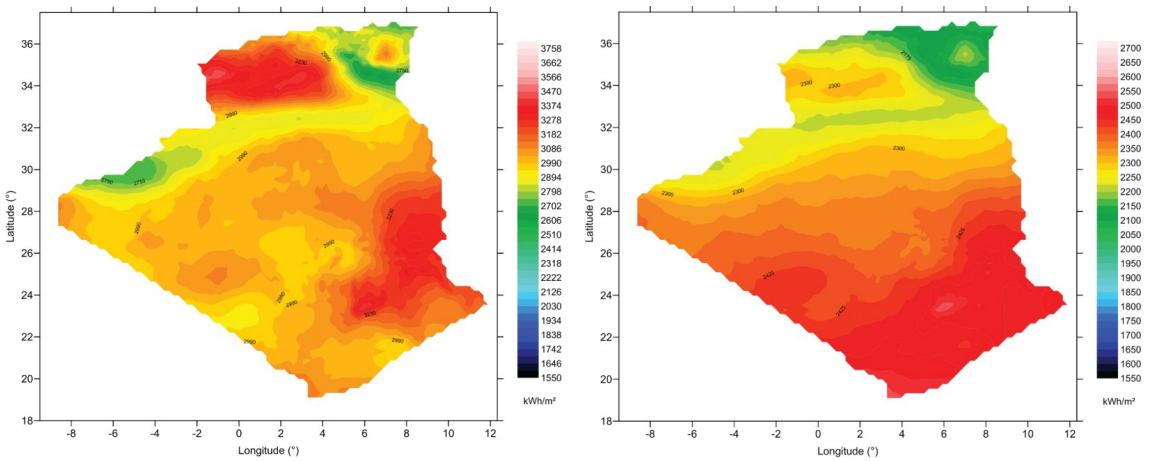

Direct Normal Irradiation. Global Horizontal Irradiance.

Figure I.2: Global resource potential for CSP and PV.

advanced methodologies and tools like the Wind Atlas Analysis and Application Program (WAsP) to map wind speeds at 37 locations across the country. Fig. I.3 (source: [15, 22]) shows that the most promising wind resources are in the southwestern part of Algeria, particularly in the Sahara. Here, the annual mean wind speeds exceed 5 m/s, making it suitable for wind power generation. Regions such as Tindouf, Ain Salah, and Adrar exhibit particularly high wind potential, with average wind speeds reaching 6 m/s. These conditions are ideal for the installation of wind farms, which could significantly contribute to the country's renewable energy capacity. Wind power can be particularly useful in areas with an annual mean wind speed around 5–6 m/s, which is sufficient to support wind energy projects aimed at both small and large-scale applications. The southwestern region's significant wind potential makes it a strategic location for future wind energy developments, contributing to Algeria's overall renewable energy strategy and enhancing energy security [2, 14, 15, 22–24].

Algeria's commitment to renewable energy is reflected in its ambitious targets and international cooperation agreements. As part of its efforts to reduce greenhouse gas emissions, Algeria has signed the Kyoto Protocol and the Copenhagen Accord. The country has also established bilateral cooperation agreements with various nations, including the USA, France, Germany, Spain, Brazil, and China. These partnerships are aimed at fostering investment growth, promoting technology transfer, reinforcing interconnections, and creating the Maghreb electricity market.

As of 2015, Algeria's installed renewable power generation capacity reached 533 MW, including 295 MW from solar, 228 MW from hydro, and 10 MW from wind. The country plans to significantly increase this capacity to 22 GW by 2030, with specific targets for different renewable sources: 1 GW

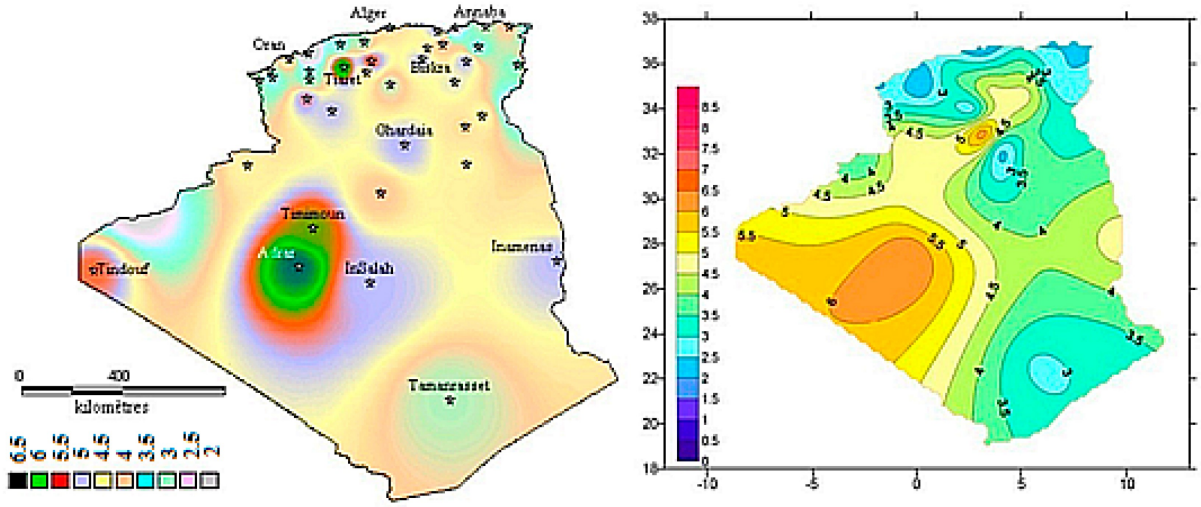

Figure I.3: Map showing wind speed measurement 10 m AGL in Algeria.

from bio-power, 13.5 GW from solar PV, 2 GW from CSP, 15 MW from geothermal, 400 MW from cogeneration, and 5 GW from wind. These projects will be implemented in two stages, with the first stage (2015–2020) focusing on developing 4525 MW of renewable energy capacity and the second stage (2021–2030) enhancing electrical interconnections to facilitate the deployment of renewable power plants in strategic regions such as In Salah, Adrar, Timimoun, and Béchar. Most renewable energy projects are expected to be installed in the Sahara regions, positioning these areas as pioneers in Algeria's renewable energy exploitation. Table I.1 provides details on 14 installed PV parks and one wind farm managed by Sonelgaz-Énergies Renouvelables (ex. SKTM), a subsidiary of SONELGAZ [15].. These projects are essential for Algeria's transition to a sustainable energy future and its potential role as a major exporter of renewable energy [2, 14, 15, 22–24].

In the context of Algeria's substantial conventional (especially oil and gas) and renewable energy potentials, it is imperative to consider a transition towards cleaner energy sources while ensuring the growing load demand is met. This transition necessitates the integration of Hybrid Renewable Energy Systems (HRES), which combine conventional and renewable energy sources to provide a stable and reliable energy supply.

Table I.1: Installed capacity and energy output of renewable energy projects in Algeria

Site	Region	Area Project (km^2)	Installed Capacity (MW)	Energy Output at June 2017 (GWh)	Commissioning Date
El Hadjira	Ouargla	0.6	30	9.738	2017
Oued Nechou PV	Ghardaia	0.05	1.1	4.593	2014
Tindouf	Tindouf	0.18	9	6.376	2015
Djanet	Illizi	0.06	3	10.729	2015
Tamanrasset	Tamanrasset	0.26	13	36.41	2015
Aoulef	Adrar	0.1	5	12.557	2016
Zaouiate Kounta	-	0.12	6	15.213	2016
Reggane	-	0.1	5	12.221	2016
Timimoune	-	0.18	9	23.8222	2016
In Salah	-	0.1	5	12.328	2016
Kaberten (PV)	-	0.06	3	9.584	2015
Adrar	-	0.4	20	59.585	2015
Kaberten (wind farm)	-	0.33	10.2	51.579	2014

I.2 Literature review on Hybrid Renewable Energy Systems

I.2.1 Electrification of rural/isolated/remote loads

To ensure a cost-effective electrification of rural areas and distant isolated loads, grid connection proves its techno-economic infeasibilities. In other words, the grid extension approach tends to be expensive and unviable. In this context, off grid (isolated from the national network) become the most suitable solution [25].

I.2.2 Electrification using fossil fuels

The most feasible solution to overcome the energy and especially electricity access to those remote areas is to consider fossil fuel-based energy grid systems. However, this solution suffers from its environmental infeasibility. For instance, diesel generator (DG) which is the most considered solution for remote off grid suffers from emission like Carbone dioxide (CO_2) and sulfuric Dioxide (SO_2). These emissions occur not only during their utilization but also during its transportation which are against sustainability recommendations [9, 26].

I.2.3 Consideration of RE and HRES

The non abondance, the global availability, and emission-free for renewable energy (RE) sources make them a very promising solution for energy supply to remote and isolated areas. However, full integration still suffers from several drawbacks such as intermittency, randomness, and reliability. Considering full shift to renewable energy sources such as solar photovoltaics (PV) and wind power source is still not the optimal solution to ensure continuous energy demands [27–30]

I.2.3.1 The need for Hybrid Renewable Energy System (HRES)

Limitations present in all the suggested solutions from the techno-economic and environmental aspect and the drawbacks present in the standalone renewable energy power plants, the concept of Hybrid Renewable Energy System (HRES) is suggested. The HRES consists of the coexistence of multiple renewable energy sources alongside with energy storage means and reserve sources [31, 32]. During the functioning of the HRES, the renewable sources are considered as the primary source for the load demand insurance. However, as stated earlier, the intermittent behavior of RE sources make them in most operational time in a surplus or deficit regarding the load demand, In this case, comes the importance of the energy storage system which will work as an energy balance in both situations by charging-discharging processes [33, 34]

I.2.3.2 The need for non-renewable sources

On the other hand, developments are still in progress to reduce the economic impact of RE sources, full renewable energy supply even with an appropriate storage medium is still economically infeasible due to the need of high size for the storage system. In this regard, partial integration of RE into existing fossil-fuel based systems or the new development of a system that co-consider both RE and non-RE sources is considered as a promising solution [1, 35]. The primary objective of considering Hybrid Renewable Energy Systems (HRES) is to ensure that energy load demands are met, particularly for isolated loads, while adhering to specific design goals. These objectives include:

- **Technical Objectives**: Ensuring that the energy load is met consistently at a defined level required by the consumer. This level is often quantified as the percentage of unmet load or the percentage of time during which the load, or a portion of it, remains unmet.
- **Economic Objectives**: A critical consideration in the design of HRES, typically measured by metrics such as the levelized cost of energy (LCOE), total system cost, or return on investment

(ROI). These economic indicators help in evaluating the financial viability of the system.

- **Environmental Objective**s: This objective emphasizes the importance of minimizing the environmental impact when sizing an HRES. Most research in this area focuses on the carbon emission (CE) factor, assessing how effectively the system reduces greenhouse gas emissions.
- **Social Objectives**: Although often given less attention in research, the social objective is crucial for ensuring the designed system's alignment with global sustainability goals. Social objectives can include metrics such as the Human Development Index (HDI), job creation (JC), portfolio risk (PR), social acceptance (Sa), and the social cost of carbon (SCC).

These factors contribute to the broader societal acceptance and benefits of the HRES. By integrating these objectives, the designed HRES can effectively balance technical performance, economic feasibility, environmental responsibility, and social impact, thereby promoting a sustainable and comprehensive approach to energy management.

I.2.3.3 The need for optimal sizing

Ensuring a trade-off between the four previously stated objectives—technical, economic, environmental, and social—is a challenging task due to their often-conflicting nature. Failing to achieve an acceptable balance among these objectives can lead to technical inefficiencies, such as undersizing, or economic inefficacies, such as oversizing. Additionally, improper allocation and load sharing between sources may result in environmental issues if the system is not optimally designed and sized. Therefore, optimal sizing of HRES is a crucial step in the design process. Determining the optimal capacity configuration of each component in an HRES at the planning stage is essential. An undersized configuration may lead to insufficient power supply, whereas an oversized configuration can result in high investment costs and considerable energy curtailment. Hence, the optimization of off-grid HRES has garnered extensive academic and industrial attention. Effective sizing optimization ensures that the system configurations consistently meet the defined objectives, utilizing renewable energy sources efficiently and economically. In the literature, numerous studies address the optimal sizing of HRES, highlighting the importance of this process in achieving a balanced and sustainable energy solution. By integrating advanced optimization techniques and comprehensive performance evaluations, these studies provide valuable insights into the development of HRES that align with technical, economic, environmental, and social goals. This optimization is not only crucial for enhancing system efficiency but also for promoting the broader adoption of renewable energy technologies in a cost-effective and environmentally responsible manner [31, 35, 36].The recent studies regarding optimal sizing of

a HRES consider PVs and Wind Turbines WTs in most cases, alongside with storage system based on batteries (BTs) and/or Hydrogen storage systems. The metaheuristic optimization algorithms are among the most used methods for sizing and allocating of HRES.

The paper by [37] presents a comprehensive technical and economic analysis for the optimal sizing of a hybrid photovoltaic-wind power system for an industrial site in Tlemcen, Algeria. Utilizing the Loss of Power Supply Probability (LPSP) algorithm, the study determines the most cost-effective configuration, balancing technical performance with economic viability. A significant finding is the critical role of the storage system, accounting for 52% of the total investment cost. The optimal configuration identified consists of 61 PV panels and nine wind turbines, achieving a competitive energy cost comparable to European standards. However, the study highlights the challenge posed by government-subsidized public grid costs, which are substantially lower. This research underscores the potential for hybrid systems to contribute to sustainable energy solutions in regions with substantial renewable resources. It also points to the need for supportive policy frameworks to enhance their economic attractiveness.

Authors in [38] conduct an in-depth financial and technical analysis for the optimal sizing of renewable energy microgrids in Biskra, Algeria. Utilizing the HOMER software, the study evaluates three configurations: photovoltaics, photovoltaics/wind, and photovoltaics/wind/diesel. The analysis reveals that the configuration combining photovoltaics, wind, and diesel achieves the lowest Levelized Cost of Energy (LCOE) at \$0.188/kWh and the highest Net Present Value (NPV) of \$10.2M, demonstrating superior financial viability. Sensitivity and risk analyses further solidify the robustness of these findings, highlighting the significance of financial indicators such as NPV, Internal Rate of Return (IRR), and Discounted Payback Period (DPB) in guiding investment decisions. This research underscores the potential of hybrid systems to meet local energy demands efficiently while mitigating financial risks.

Bacha et al. [39] present an optimization study for the sizing of a hybrid microgrid system in a rural area of Biskra, Algeria, aiming to alleviate energy poverty. The research employs novel optimization algorithms—Stochastic Fractal Search (SFS) and Symbiotic Organisms Search (SOS)—alongside the traditional Particle Swarm Optimization (PSO) to compare performance. Results demonstrate that the SFS algorithm yields the lowest Levelized Cost of Energy (LCOE) at \$0.09138/kWh for the optimal configuration. The study effectively highlights the importance of incorporating multiple renewable energy sources, such as solar and wind, along with diesel generators and battery storage, to ensure a reliable and cost-effective energy supply. This work underscores the potential of hybrid

systems to provide sustainable energy solutions for isolated regions while emphasizing the efficiency of advanced optimization techniques.

In [40], authors present a novel approach for the optimal sizing of a hybrid PV-wind water pumping system in Adrar, Algeria, employing recent metaheuristic algorithms such as Equilibrium Optimizer (EO), Slime Mould Algorithm (SMA), and others. The study integrates the Levelised Cost of Water Pumped (LCOWP) and Loss of Water Supply Probability (LWSP) as objective and constraint functions, respectively. Results demonstrate the superior accuracy and efficiency of the EO algorithm, achieving an optimal LCOWP of \$1.181/m^3 at a 45m head with 0% LWSP. The study emphasizes the economic and technical benefits of hybrid systems without batteries or diesel generators, highlighting the significant potential of EO in optimizing complex renewable energy systems for sustainable water pumping solutions.

Researchers in [41] conduct a detailed techno-economic analysis to determine the optimal hybrid energy system for the rural area of Bankhwar Utrar in Kalam, Pakistan. The study evaluates multiple configurations involving solar PV, wind turbines, hydro turbines, and diesel generators using HOMER Pro software, considering economic, technical, operational, and environmental criteria. The multi-criteria decision analysis (MCDA) identified a hybrid system of solar PV, wind turbines, hydro turbines, and battery banks as the most efficient, with an NPC of \$166,173.78 and an LCOE of \$0.14/kWh. This configuration also achieved zero GHG emissions, contrasting sharply with the high costs and emissions of diesel-based systems. The research underscores the potential for hybrid renewable systems to provide sustainable and economically viable energy solutions in remote regions.

In order to cover the most relevant research studies in this field regarding the 04 previously stated objectives (Technical, Economic, environmental and social) as well as used algorithms/methods of optimal sizing and modeling , in addition to system configuration, Table I.2 gives a summary on recent published research in this field.

Table I.2: Summary of recent hybrid renewable energy studies with optimization techniques.

Ref.	**Config.**	**OFs**	**Optim. Techs.**	**Highlight**
[42]	PV-WT, DG, BT	LPSP, NPC, LCOE, RF	Improved Archimedes Optimization Algorithm (IAOA)	The study introduces the Improved Archimedes Optimization Algorithm (IAOA) to optimize the design of a Hybrid Renewable Energy System (HRES) for a microgrid in the Farafra region of Egypt. Three scenarios are considered based on PV panels, wind turbine systems, diesel generators, and a battery energy storage system, aiming to minimize the net present cost (NPC) while meeting constraints related to renewable fraction index, loss of power supply probability, and availability. Simulation results show that the proposed IAOA outperforms other algorithms like AOA, AEFA, EO, GWO, and HHO, achieving an efficient HRES design with Levelized Cost of Energy(LCOE) of 0.213/kWh, while maintaining high reliability and renewable fraction index .
[1]	PV, GT, Hydrogen	LPSP, COE, CDE, RF	Fick's Law Optimization Algorithm (FLA)	Utilizing a multidisciplinary approach encompassing engineering, economics, and environmental analysis, the research identifies the electrolyser system as the primary cost contributor in the SHRES. The optimized system balances energy sources with 45% from PV modules, 35% from fuel cells, and 20% from gas turbines, showcasing a significant reliance on renewable energy while ensuring required power generation. The study emphasizes the importance of the electrolyser system and the distribution of power generation sources in optimizing the SHRES for sustainability in the oil and gas industry.

Ref.	**Config.**	**OFs**	**Optim. Techs.**	**Highlight**
[43]	PV-WT, BG, BT	NPC, LCOE, LCOH, PBP, PI, RF	HOMER Pro software	The proposed system generates 2,009,492 kWh/yr of electricity and 30,199 kg/yr of Hydrogen, with reported values for Net Present Cost (NPC), Levelized Cost of Energy (LCOE), Levelized Cost of Hydrogen (LCOH), and payback period. After considering the effective rate after digestate, the costs are reduced, and HOMER determines the breakeven grid extension distance. The optimized system showcases the economic viability and sustainability of utilizing hybrid renewable energy sources for electric vehicle charging and hydrogen refueling, providing valuable insights for future energy policies.
[44]	PV-WT, BT	EPSP, NPC, RF	HOMER Pro software	A techno-economic analysis was conducted for on-site hydrogen refuelling stations powered by hybrid renewable energy systems in Niğde, Türkiye, and Zaragoza, Spain. Different power system scenarios were evaluated to refuel 24 vehicles per day in each region, with optimal system architectures identified for each location based on cost metrics and CO2 emissions reductions. The study emphasizes the role of renewable energy systems in achieving net-zero emissions targets and reducing reliance on fossil fuels in the transportation sector, aligning with United Nations Sustainable Development Goals .
[41]	PV-WT-Hydro, DG, BT	NPC, LCOE, GHG	HOMER Pro software	A multi-criteria decision analysis (MCDA) approach was utilized to identify the most efficient and sustainable system, resulting in a hybrid configuration of solar PV, wind turbine, hydro turbine, and battery bank. This system demonstrated superior economic efficiency with an LCOE of 0.14$/kWh, and zero GHG emissions, outperforming traditional diesel generator-based systems in both economic and environmental aspects.

Ref.	**Config.**	**OFs**	**Optim. Techs.**	**Highlight**
[45]	PV-WT, DG, BT	LPSP, NPC, GHG	HOMER Pro software	Through quantitative simulations, the biomass-battery-based system emerges as the most economically optimal, with an NPC of approximately 1.07 M$ and a COE of 0.118$/kWh, while maintaining environmentally safe emission levels. Additionally, the grid-tied RE technology demonstrates cost-effectiveness, with an NPC of 348,318 and a COE of 0.0112$/kWh, providing valuable insights for policymakers to integrate hybrid RE systems in urban settings for sustainable energy generation .
[46]	PV-WT, BT	TAC(CT)	The firefly algorithm	Contributions of the study include incorporating a battery degradation model, stochastic modeling for islanded system planning, and accounting for uncertainties in load and renewable power. Numerical results show low planning costs for the hybrid system using renewable resources, with batteries providing flexibility to cover power oscillations. The firefly algorithm efficiently finds optimal solutions, and stochastic modeling, while increasing planning costs, offers more reliable solutions without additional costs for the battery degradation model .
[47]	Pump As Turbine (PAT)-PV-Hydro, DG, BT	LCC, LCA, Cumulative Environmental Burdens	NSGA-II	The paper introduces a model focusing on optimizing the economic and environmental impacts of a hybrid renewable energy and battery storage system for off-grid farms, utilizing micro-hydropower and photovoltaics as primary renewable energy sources, with batteries and a diesel generator as potential backup systems. A modified Non-dominated Sorting Genetic Algorithm II (NSGA-II) is employed to provide various energy supply technology solutions based on economic (life cycle costing or LCC) and environmental (life cycle assessment or LCA) constraints. The study conducted in Southern Spain revealed that systems heavily reliant on batteries could achieve cost efficiency and lower impacts on climate change and energy resources, while systems minimizing material resource consumption resulted in higher fuel costs. The optimal solutions utilized a significant portion of the total energy generated, with sensitivity to energy production-demand distributions .

Ref.	**Config.**	**OFs**	**Optim. Techs.**	**Highlight**
[48]	WT - Hydrogen	LPSP, TNPC, COE	ELECTRE	The study utilizes a hybrid optimization approach to determine the optimal location and size of wind turbines and hydrogen storage systems in rural areas with high wind energy potential across three Iranian provinces. The ELECTRE decision-making method is employed to identify Assadabad Nehbandan as the optimal site for wind farm implementation. The comparison between a hybrid system with wind turbines and batteries versus one with hydrogen storage focuses on cost minimization and reliability maximization. Results indicate that the battery-based hybrid system has a lower cost of energy at 0.373 ($/kWh) compared to the hydrogen storage-based system at 0.609($/kWh). Sensitivity analysis reveals that higher wind speeds lead to decreased total net present cost and cost of energy, while increased interest rates have the opposite effect. The economic justification favors the battery-based hybrid system over the hydrogen storage-based system due to lower initial costs .
[49]	PV-WT, BT-H2	Capacity Shortage, TNPC, COE	HOMER Pro software	The article proposes a hybrid energy model combining various stand-alone and grid-connected systems (e.g., photovoltaic, wind turbine, fuel cell) to meet the power needs of an educational institute in Pakistan. These systems were optimized for techno-economic feasibility, considering electricity demand, geographic, and climatic data. The results obtained show that grid-connected hybrid systems offer the lowest net present cost (M$ 1.536859) and cost of energy ($0.155/kWh). Solar and wind resources were also shown to be viable for hydrogen production and power generation, with hydrogen being a more affordable long-term energy storage option than batteries.

Ref.	**Config.**	**OFs**	**Optim. Techs.**	**Highlight**
[50]	PV-TEG	Energy Factor	Arithmetic Optimization (ARO)	This paper proposes a theoretical model for a hybrid power generation system combining photovoltaic (PV) and thermoelectric generation (TEG) to improve power efficiency. It addresses partial shielding conditions (PSC) that cause power loss and component mismatch by using an artificial rabbit optimization (ARO) algorithm to reconfigure the electrical connections among PV and TEG arrays, enhancing overall power output. The effectiveness of the ARO algorithm is verified through simulation tests on 4 × 4 and 20 × 15 arrays, showing power output improvements of 34.05% and 23.10%, respectively. Further validation through hardware-in-the-loop (HIL) experiments confirms the feasibility of the proposed reconfiguration strategy.
[51]	PV-H2	Model Chain, LCOE, LCOH	commercial solver Gurobi 9.5.1	The paper presents a capacity optimization model for PV–hydrogen hybrid systems, utilizing physical solar power curve modeling to enhance accuracy. It also incorporates government subsidies into the economic analysis, aiming to maximize annual profits. Applied in Heilongjiang Province, China, the study finds that a 1-MW PV plant needs a 226.9 kW transformer, 366.8 kW electrolyzers, and 3 compressors. Physical modeling improves annual profit by 38.9%, with key factors including subsidy policies, costs, and PV power utilization significantly influencing system optimization and economic viability.
[52]	Grid-PV-DG	COE, NPC	HOMER Pro software	This paper presents a techno-economic assessment of a hybrid electricity supply system comprising PV, diesel generator (DG), and grid components for 132 locations in India, using HOMER software. It estimates the Net Present Cost (NPC) and Cost of Electricity (CoE) for 25 selected locations and compares these with a conventional grid+DG system. The study finds that the proposed grid+PV+DG system has 9.5%–36.6% lower NPC and 16%–33.6% lower CoE compared to the conventional system at all 25 locations. The inclusion of the PV component reduces grid electricity purchases and significantly decreases DG operation hours.

Ref.	Config.	OFs	Optim. Techs.	Highlight
[53]	Floating Offshore Wind Turbines (FOWT), Wave Energy Converters (WECs)	Radius, Draft, PTO Damping, Layout	Eigenfunction, AQWA	This paper develops a practical model to analyze the performance of a hybrid system with semi-submersible floating offshore wind turbines (FOWT) coupled to point-absorbing wave energy converters (WECs). The model uses the matching-method of eigenfunctions to solve the boundary value problem, decomposing the velocity potential into radiation and diffraction problems. It accounts for wind forces, mooring lines, power take-off (PTO) systems, and viscous effects, and is applied to the OC4-DeepCwind platform combined with an array of WECs. The study performs a multiparameter effect analysis, examining the impact of WEC radius, draft, PTO damping, layout, base column submergence, wave heading, and frequency on the system's motion response and WECs' mean capture width ratio. The model's accuracy is validated through convergence analysis and case studies, providing detailed insights into optimizing the hydrodynamic performance of the hybrid FOWT-WEC system.
[54]	Hydro-PV	–	Real-time Dispatch, Parallel Dynamic Programming	This paper proposes a real-time dispatch method for hybrid hydro-photovoltaic (PV) systems to address the uncertainty of large-scale PV output. The method includes a multi-scale nested joint operation model for short-term and real-time strategies, formulating different reserve capacity operation strategies based on PV output deviations. A case study on the Beipan River, China, demonstrates that considering PV uncertainty can reduce total monthly water consumption by 4.29% and decrease the number of monthly passes through the vibration zone by 53, improving economic performance and minimizing the negative impact of PV fluctuations on hydropower units, though it may cause spatial loss during extreme weather conditions.

Ref.	**Config.**	**OFs**	**Optim. Techs.**	**Highlight**
[55]	Offshore Wind Turbine and WECs	–	OpenFAST-AQWA	This study introduces a complete toolkit based on the OpenFAST-AQWA framework for optimizing the layout and evaluating the performance of a hybrid system combining floating offshore wind turbines and wave energy converters (WECs). The DeepCWind-Wave Stars hybrid system is proposed to validate this new tool, with key WEC parameters optimized based on local wave contours influenced by the platform. The evaluation under various wind and wave conditions shows that integrating WECs does not compromise system stability, reduces mooring force fluctuations, and slightly increases average mooring force. Additionally, the generated wave power effectively supplements wind power, particularly at low wind speeds.
[56]	WT-PV-Battery	–	EMTP	The research focuses on analyzing lightning transient overvoltages in a hybrid wind turbine-photovoltaic-battery energy storage system by developing a hybrid system model in the EMTP environment. High-frequency models of various components like PV string, inverter, cable, power transformer, wind tower, DC/DC converter are established to study overvoltages caused by lightning strikes at different points. The study delves into the installation of surge protection devices within the PV system and examines how different wind farm and PV system topologies affect lightning surge. Results indicate that lightning surges from the PV system do not impact the wind farm or battery energy storage system. Furthermore, significant voltage reductions of 72.8% in the PV system's string structure and 63.4% in the wind farm's star structure compared to radial connection are observed when facing lightning surges from the substation side.

Ref.	**Config.**	**OFs**	**Optim. Techs.**	**Highlight**
[57]	Nuclear Power, CSP, Thermal Storage	–	EBSILON Software	A hybrid system combining nuclear power, concentrated solar power, and thermal storage is proposed to enhance peak shaving ability, with a focus on operation flexibility and energy efficiency. Under design conditions, the hybrid system demonstrates an energy efficiency of 35.74% and an equivalent solar-to-power efficiency of 24.05%. The hybrid system's performance under off-design conditions was studied, showing that increasing direct normal irradiance (DNI) from 500 W/m2 to 900 W/m2 led to a 6.25% increase in the equivalent solar-to-power efficiency. Additionally, maintaining constant core power allows the hybrid system to achieve a peak shaving depth of up to 25%, offering potential guidance for enhancing flexibility and energy efficiency in pressurized water reactor nuclear power plants.
[58]	PV-Wind and Hydropower	LPSP, NPC, COE	MOGA	The study focused on determining the optimal system size for a hybrid renewable energy system (combining solar PV, wind, and hydro energy) to achieve sustainable electrification of remote areas. By using the multi-objective genetic algorithm optimization technique, the study found that a configuration of PV 88 kW, wind 18 kW, Hydro1 215 kW, and Hydro2 197 kW provided the best performance in terms of cost-effectiveness and energy production. The results showed that this hybrid renewable energy system had the lowest levelized cost of electricity (COE) and net present cost (NPC), making it a viable solution for providing reliable load servicing over a 25-year period without the need for an energy storage device. This demonstrates the potential for implementing sustainable energy systems to meet the long-term energy needs of remote communities while achieving sustainable development goals.

I.2.4 HRES Components and optimal sizing

The literature considers various topologies when designing an optimal Hybrid Renewable Energy System (HRES) for isolated loads. A fundamental HRES configuration typically includes energy sources (both renewable and non-renewable), energy storage systems, and power converters. Additionally, loads play a crucial role as they represent the power sink within the system [31, 32, 35, 36, 59]. This section will provide an in-depth analysis of each component of the HRES and their roles in the system. We will examine how these elements are integrated and managed to ensure an efficient and reliable energy supply. The focus will be on understanding the considerations and methodologies applied in the design and optimization of each part of the HRES. This includes evaluating different energy sources, assessing the capacity and efficiency of energy storage systems, and exploring the functionality of power converters. Additionally, we will discuss the significance of load management in achieving an optimal balance between supply and demand.

I.2.4.1 Energy Sources

The literature delves into the complexities of designing optimal Hybrid Renewable Energy Systems (HRES), considering various topologies to address these challenges. The complementary behavior between solar irradiation and wind speed, while advantageous, also presents significant challenges. Solar irradiation, for instance, exhibits a random pattern, increasing from sunrise to a peak at midday before decreasing to zero after sunset. The duration and intensity of solar presence are higher in the summer compared to other seasons [60]. In contrast, wind is present throughout the day, although its intensity fluctuates randomly, typically peaking during spring and winter [29]. These characteristics make wind and solar energy rarely sufficient as sole energy sources in HRES. Despite the synergistic potential of wind and solar energy, the inherent uncertainties associated with these renewable sources cannot be eliminated. Off-grid HRES that rely entirely on renewable energy face significant techno-economic challenges in meeting load demand [61]. This underscores the necessity of incorporating storage systems and/or non-renewable backup sources in the design of such systems.

Furthermore, the literature suggests that the future of HRES could be even more promising with the inclusion of other energy sources. These additional sources, as documented, encompass a wide range of possibilities. Hydropower [62, 63], thermal solar energy, commonly referred to as Concentrated Solar Power (CSP) [64–66], hydrokinetic (often known as tidal) energy [67, 68], biomass [69], biogas, and diesel generators [69] have all been identified as viable components of HRES. These insights highlight that while wind and solar energy form the cornerstone of most HRES due to their comple-

mentary nature, their variability necessitates the inclusion of additional energy sources and storage systems to ensure a reliable and efficient energy supply.

I.2.4.2 Energy Storage (ES) systems

The objective of energy storage (ES) systems within Hybrid Renewable Energy Systems (HRES) is to mitigate the imbalance between energy production, with its inherent intermittency, and load demand, which exhibits stochastic behavior. Integrating ES into HRES significantly enhances the overall techno-economic quality of the system across various sectors. One of the key advantages of this integration is the improvement in energy efficiency, achieved by effectively managing the production-consumption mix [36, 70–73]. In the literature, energy storage systems are categorized based on the type of storage medium, considering the medium's availability, cost, and roundtrip efficiency, which refers to the efficiency of the energy storage system in both storing and retrieving energy [36, 71–73]. In isolated or remote HRES, the types of energy storage systems include electrochemical (e.g., various types of batteries), electromagnetic (e.g., supercapacitors), chemical (e.g., hydrogen-based energy storage), mechanical (e.g., pumped hydro storage, compressed air energy storage, and gravity energy storage), and thermal (e.g., molten salt thermal energy storage) [36, 71–73]. Each type of ES presents specific advantages and challenges during installation, operation, and management. To address these challenges and optimize the benefits, hybridizing two or more energy storage systems within a single HRES may be considered. In such cases, the energy storage system will determine the size and the participation percentage of each storage medium in the total stored energy at each operational step [72, 74].The integration of ES technologies is not just a component, but a crucial element for the efficient operation of HRES. It ensures reliability and stability in energy supply, and its advancements and innovations continue to play a vital role in the development and optimization of HRES.

I.2.4.2.a Electrochemical storage systems

Typically known as the battery energy storage system. Batteries are the most common energy storage component in off-grid HRES applications. The types of batteries commonly used in these systems are Lithium-ion [75–81], Lead-acid [75–81] , Nickel-Cadmium [75] , Sodium Sulphur [77] , Vanadium redox flow [76, 80, 81], Absorbent Glass Mat [78] and Zinc–Bromine [79, 80] batteries. The storage medium in this type of storage is a chemical product that can release/store electrical energy through electrochemical reactions initiated due to the flow of electrons between the cathode

and anode. A battery's typical components are:

- The cathode, the positively charged electrode, which receives electrons from the anode and is reduced during the electrochemical reaction;
- The anode, another key player, is the negative electrode that is oxidized and actively supplies electrons to the load, making it an integral part of the energy transfer process;
- The electrolyte, which transfers electrons between the two electrodes;
- The separators, which prevent direct contact between the positive and negative electrodes, ensuring electrical insulation and preventing short circuits.

Electrochemical processes at both electrodes move electrons via an external circuit during discharge. An external voltage between the electrodes switches electrochemical processes during charging, with the anode releasing electrons and the cathode accepting them. The study [82], authors present a comprehensive framework for the optimal sizing of photovoltaic (PV) systems combined with battery storage systems (BSS) for residential microgrids. The research highlights the critical role of lithium-ion batteries in enhancing energy autonomy and reducing grid dependency by efficiently storing excess solar energy generated during peak sunlight hours. Through a multi-objective optimization approach, the paper addresses critical factors such as battery degradation, depth of discharge (DoD), and the influence of various azimuth and tilt angles on the PV array's performance. The results underscore the importance of an appropriately sized battery system to match the temporal variability of solar generation with the residential load profile, thus ensuring a reliable energy supply and maximizing economic benefits. By evaluating scenarios in different geographical locations, the study provides practical guidelines for microgrid designers to achieve optimal system performance and cost-effectiveness, emphasizing the necessity of balancing capital investment with operational savings. This work significantly contributes to the understanding of how BSS can mitigate the intermittency of renewable energy sources in microgrid applications, paving the way for more resilient and autonomous residential energy systems.

Authors in [81] evaluated four battery energy storage technologies: lead-acid, lithium-ion, vanadium redox, and zinc bromine flow batteries within a solar PV/diesel generator hybrid system for isolated Indian islands. Using HOMER software, the zinc bromine flow battery (ZBF) emerges as the most cost-effective for overcoming renewable intermittency. The ZBF system showcases the highest return on investment and renewable penetration, with the lowest payback period and pollutant emissions. This highlights its superior performance and economic viability, making it an optimal choice

for hybrid renewable energy systems in remote island settings. In [75], researchers employed meta-heuristic algorithms to optimize the sizing of a hybrid PV/wind system with electrochemical storage devices, comparing lead-acid, lithium-ion, and nickel-cadmium batteries. The research demonstrates the JAYA algorithm's effectiveness in minimizing the unit electricity cost (UEC) while ensuring reliability through various LPSP levels. Results indicate that lithium-ion batteries, despite higher initial costs, offer competitive UEC with extended lifetime and higher depth of discharge (DOD). Sensitivity analysis reveals significant cost reductions with improved battery lifespan and cost efficiency, highlighting lithium-ion's potential to outperform traditional lead-acid batteries in hybrid renewable energy systems. The study [77] presents a unified model optimizing the configuration of BES systems using multiple types of batteries, specifically lead-acid, lithium-ion, and sodium-sulfur (NaS) batteries. By accounting for capacity degradation dynamics, the model determines the optimal battery types and capacities to minimize the total cost of hybrid power systems (HPS) with wind, PV, and biomass generation. Results indicate that combining lead-acid and lithium-ion batteries achieves the lowest total cost, with significant economic advantages over single-type BES system configurations. The study underscores the importance of considering degradation characteristics in optimizing BES system for HPS.

I.2.4.2.b Chemical storage systems (Hydrogen Energy Storage systems)

Chemical energy storage (CES) systems, including hydrogen energy storage (HES), are essential for storing energy in the chemical bonds of molecules and releasing it through chemical reactions [71, 72, 83].

These systems, which are environmentally friendly, offer high storage capacities, providing a robust solution for managing the intermittency of renewable energy sources [72, 83, 84] . HES, a specific type of CES, plays a crucial role in this process through a reversible power-to-hydrogen conversion cycle. The main components of HES, such as electrolyzers, compressors, hydrogen tanks, and fuel cells, determine its technical performance. The types of electrolyzers and fuel cells commonly used are alkaline, proton exchange membrane, and solid oxide [36]. The technical performance of HES is determined by the conversion efficiency of both the electrolyzer and fuel cell, along with the higher heating value of hydrogen [36].

In the context of hybrid renewable energy systems (HRES), the integration of HES is particularly significant due to the variable output of photovoltaic (PV) systems. Achieving optimal energy management requires precise sizing of the storage system, involving the determination of the rated power

for the electrolyzer (P_{EL}), fuel cell (P_{FC}), and hydrogen tank capacity (m_{tank}) [1].

Hydrogen, produced via electrolysis, serves as a perfectly sustainable and clean energy carrier, further enhancing the stability and continuity of power supply in HRES [72, 85]. By complementing renewable energy sources and reducing dependency on fossil fuels, HES contributes significantly to sustainable energy solutions and the reduction of harmful emissions [71]. Compared to batteries-based BES systems, which suffer from drawbacks such as large size, limited lifespan, and high-cost hydrogen (H2) emerges as a renewable energy storage solution [84]. Integrating Fuel Cells (FCs) into hybrid renewable energy systems (RES) not only reduces the size of the BES but also extends the system lifespan and enhances overall performance. Notably, HES systems boast a longer lifespan of approximately 25 years compared to lithium-ion batteries, maintaining consistent performance without significant deterioration [84].

The study in [86] has explored a grid-linked integrated energy system incorporating HES for collective energy communities. By utilizing surplus electricity to electrolyze water, hydrogen is produced and stored, providing a robust solution to balance energy supply and demand. The hybrid operation strategy significantly enhances system performance, achieving an annual hydrogen supply of 81 673 kg. The study highlights the high energy density, scalability, and cost-effectiveness of hydrogen storage, demonstrating its superior role in mitigating the intermittency of renewable energy sources and improving the overall efficiency and reliability of integrated energy systems.

In [87], Izadi et al. optimize a hybrid renewable energy system (HRES) comprising solar PV, wind turbines, and hydrogen storage for zero-energy buildings across various climate conditions using a neural network-genetic algorithm. Hydrogen storage is central to the system, capturing excess energy via electrolyzers and storing it in hydrogen tanks. The stored hydrogen is then converted back to electricity through fuel cells when renewable generation is insufficient. The results demonstrate that integrating hydrogen storage significantly enhances system reliability, reducing grid dependency and improving energy supply stability. The optimization method effectively balances installation costs, CO2 emissions, and LPSP, showcasing hydrogen storage's vital role in overcoming renewable intermittency.

Authors in [88] utilized a whale optimization algorithm (WOA) to design a hybrid photovoltaic-biowaste energy system with hydrogen storage. The system integrates PV panels, biowaste units, and a hydrogen fuel cell storage system to ensure a reliable and cost-effective energy supply. Hydrogen is produced through water electrolysis using surplus energy and stored in high-pressure tanks. This hydrogen is later converted back to electricity via fuel cells during periods of low renewable

generation. Results demonstrate the hybrid system's ability to achieve minimum total net present cost (TNPC) and improved reliability. The incorporation of hydrogen storage significantly mitigates the intermittency of renewable sources, ensuring continuous and stable energy supply.

In their study, [89] Ammari et al. conducted a techno-economic analysis of a stand-alone photovoltaic (PV) system using three different storage systems—lead-acid batteries, lithium-ion batteries, and hydrogen storage—to supply energy to isolated houses in southern Algeria. The results demonstrate that hydrogen storage is the most cost-effective and reliable option, with the lowest investment cost and no unmet load or excess energy. Hydrogen storage, utilizing a 7 kW electrolyzer and a 6 kg storage tank, outperforms lead-acid and lithium-ion batteries by offering a longer lifespan and higher efficiency. This highlights the significant role of hydrogen storage in mitigating the intermittency of solar energy and ensuring a stable energy supply for remote locations. Another forms of chemical energy storage can be considered when HRES energy storage includues synthetic natural gas (SNG), and methane [36, 72, 90].

I.2.4.2.c Thermal energy storage (TES) systems

According to the US Department of Energy, Thermal Energy Storage (TES) held a significant share of 1.9%, equivalent to 3.3 GW, in energy storage as of 2017 [71]. TES technologies aim to address the intermittent nature of renewable energy sources by storing surplus energy during periods of abundant generation, thereby mitigating fluctuations in supply and demand. This approach not only supports a more competitive and scalable method for reducing carbon emissions in heat and power production but also ensures durability, cost-effectiveness, and scalability. The versatility of TES is evident in its various applications, including industrial process heat, electricity production, and district heating systems, making it a technology of great potential [91, 92].

TES can be categorized based on heat storage principles into latent heat storage, sensible heat storage, and thermochemical storage [36, 72, 93]. The simplest and most widely used method is sensible heat storage, which utilizes the temperature difference in materials like molten salt or solid thermal media to store electrical energy. This method is crucial in supporting heating, cooling, and steam generation—constituting over 45% of industrial and domestic energy demand—while offering lower investment costs compared to other energy storage types [71, 72].

A TES system consists of three essential components: a heat generator (typically an electric heater) that converts electricity to heat, a thermal storage tank or medium that stores heat in an insulated reservoir, and a heat transfer mechanism that delivers heat directly to the load demand or indirectly

through thermodynamic process cycles for electrical load demands [71, 92]. Although the round-trip efficiency from electricity to electricity, which measures the energy losses during the storage and retrieval process, is limited by the low efficiency of Rankine or Brayton cycles. TES offers acceptable energy density (80–250 Wh/kg) and shallow heat loss (self-discharge typically at 1% per day) [71, 92]. These attributes make TES a valuable component in hybrid renewable energy systems (HRES), particularly for isolated or remote applications where it helps ensure a stable and reliable energy supply.

The research done by [94] examines the techno-economic feasibility of solar power plants integrating photovoltaic (PV) and concentrated solar power (CSP) systems with thermal energy storage (TES) and electrical battery storage. The analysis shows that TES, with its lower investment cost and high storage capacity, provides superior economic and reliability performance compared to battery storage in current scenarios. However, as battery costs decrease to around 160 USD/kWh, they become competitive with TES, offering flexibility and rapid response times. The study concludes that hybrid systems combining PV, CSP, TES, and batteries can achieve optimal economic and reliability outcomes, demonstrating the vital role of TES and the increasing potential of batteries in future energy systems.

In [95] authors proposed a wind-photovoltaic-thermal energy storage (TES) hybrid power system utilizing an electric heater (EH) to stabilize power output. The TES system, comprised of molten salt storage, effectively captures excess energy from wind and PV generation, converting it into thermal energy for later use. This hybrid system, optimized through a multi-objective particle swarm optimization (MOPSO) algorithm, shows that incorporating TES significantly enhances reliability and economic performance by smoothing renewable energy fluctuations and maximizing the utilization rate of transmission channels. Comparisons reveal that TES offers superior reliability and cost-effectiveness compared to battery storage, especially for large-scale applications.

Authors in [96] suggest an optimization of a hybrid renewable energy system (HRES) incorporating PV, wind, and concentrated solar power (CSP) plants with thermal energy storage (TES) and battery storage. The CSP system employs molten salt TES, which stores excess energy as heat to be later converted to electricity, ensuring a steady power supply. The analysis reveals that the TES, integrated with an electric heater, is more economical than battery storage alone for large-scale applications. However, integrating batteries improves flexibility and reliability, especially for meeting variable loads. The proposed multi-objective optimization highlights that combining TES with batteries effectively mitigates renewable intermittency, achieving a balanced trade-off between cost and reliability.

In [97] a regional multi-energy system (RMES) incorporating medium-high temperature solar thermal (MHTST) technology with thermal energy storage (TES) is investigated. The system integrates photovoltaic (PV) and wind energy sources, utilizing MHTST for dispatchable power generation. TES, using heat transfer oil (HTO), captures excess solar heat and stores it for later electricity generation or direct heating. The optimization model highlights TES's role in enhancing the system's flexibility and reliability, particularly during periods of low solar irradiance and high energy demand. The results indicate that TES effectively balances operational costs and carbon emissions, demonstrating superior performance compared to conventional PV systems without TES. [98] presented the optimal configuration and operation of a hybrid CSP/PV/wind power cogeneration system incorporating thermal energy storage (TES) and BES system. The TES, using molten salt, stores excess thermal energy from CSP for electricity generation during low solar periods. The system's two modes—TES heat production without BES system and with BES system—demonstrate different economic and reliability outcomes. TES without BES system achieves a lower LCOE of \$0.0526/kWh but higher LPSP of 6.86%. Incorporating BES system lowers LPSP to 4.83% but increases LCOE to \$0.160/kWh. The study underscores the importance of combining TES and BES system to enhance system reliability and economic efficiency.

I.2.4.2.d Electromagnetic energy storage (ECMS) systems

Supercapacitors (SCs) represent a pivotal class of electromagnetic energy storage technologies, leveraging electrostatic and redox processes across positive and negative electrodes. SCs function by storing energy in the form of electrostatic fields created between electrodes separated by a dielectric medium. This design allows for quick energy storage and retrieval. These devices, categorized into electric double-layer capacitors and pseudo-capacitors, are often coupled with batteries in hybrid energy systems due to their high power density and rapid response capabilities, enhancing overall regulation performance [36]. Notably, SCs exhibit power densities between 1000–5000 W/kg and can endure approximately 500,000 cycles at full depth-of-discharge, offering charge/discharge efficiencies up to 95% within 0.3 to 30 seconds [36, 99]. These attributes make SCs robust and durable, as they avoid the chemical reactions that typically limit battery life, maintaining efficiency levels between 80% and 95% while requiring power electronics for voltage regulation [72]. Additionally, their characteristics make them suitable for high-power and medium-energy applications such as peak energy consumption management, output power smoothing, and energy recovery in mass transit systems [71, 100]. With power ratings ranging from 10 to 75 kW and energy ratings between 4 and 70 Wh,

SCs can be easily scaled through series or parallel connections [101]. Despite their high specific energy and power densities, SCs face challenges such as high self-discharge rates and significant capital costs [102]. However, their robustness, adaptability to diverse environments, and minimal maintenance requirements make them a viable option for a range of applications [71, 103–106]. SCs, particularly those with porous carbon electrodes and liquid electrolytes, offer considerable advantages in terms of specific energy and power densities. These systems, whether symmetrical or asymmetrical, provide enhanced energy density and reduced leakage currents, making them suitable for both small to medium and large-scale applications [71, 107]. Their ability to support pulsed power demands in high-tech applications underscores their potential in advanced energy storage solutions for hybrid renewable energy systems, including those intended for oil and gas facilities [71, 108].

In [109], authors explored the optimal design and energy management of a fully renewable energy system that integrates batteries and supercapacitors. The research focuses on enhancing the reliability and efficiency of isolated, off-grid hybrid renewable energy systems (HRES). The hybrid energy storage system (HESS) comprising lithium-ion batteries, lead-acid batteries, and supercapacitors aims to address the intermittency and variability of renewable energy sources. The integration of supercapacitors alongside batteries significantly improves the system's dynamic response and stability. Supercapacitors effectively reduce voltage overshoots and power fluctuations during abrupt changes in wind speed and solar radiation. This complementary use of batteries and supercapacitors ensures a more stable and reliable power supply, enhancing the overall performance of the HRES. The study highlights the techno-economic benefits and the potential for scalable application in remote and off-grid areas.

I.2.4.3 Energy Management Strategies (EMS)

The Energy Management Strategy (EMS) serves as the central control mechanism for the optimal sizing and operation of a Hybrid Renewable Energy System (HRES). The EMS coordinates power circulation within the system's components to achieve defined operational goals and performance within certain constraints [1, 36]. Specifically, the EMS aims to ensure a cost-effective energy supply to meet load demand. This involves promoting the use of efficient, low-cost energy sources and optimizing energy storage methods.

A well-designed EMS is crucial for maintaining high system efficiency and reliability throughout

the year. It extends the lifetime of system components, reduces operating costs, and maximizes overall system performance by managing the energy flow in a technically and economically feasible manner [31]. The EMS achieves these objectives by considering actual load demand, energy generation, and storage states, and then determining the optimal power flow coordination. This approach ensures high efficiency by maximizing resource harvesting, minimizing operational costs, favoring low-cost energy generators, ensures low carbon emissions, and prolonging the system's lifespan [1, 31, 36, 84, 110, 111].

In off-grid applications, the basic objective of an EMS is to reliably satisfy load demand. EMS can be classified into predefined rule-based EMS and real-time optimized EMS. Furthermore, integrating demand-side management (DSM) with supply-side energy management can achieve a higher degree of supply-demand matching, thereby enhancing system reliability and reducing the required storage capacity. The strategic control through an EMS ensures the consistent supply of electricity to the load, optimizes resource utilization, minimizes operational costs, and extends the system's lifetime [31, 36, 112]

.

The EMS regulates the power circulation within the proposed HRES configuration, striving to fulfill electricity demand while simultaneously reducing overall environmental and operational expenses. This dual focus on operational efficiency and environmental sustainability underscores the importance of a robust EMS in the effective deployment of HRES [31, 84, 110].

I.2.4.3.a Predefined rules-based EMS

A predefined rule-based Energy Management Strategy (R-EMS) operates using a predetermined flowchart that defines the interaction between energy production, load demand, and storage. This type of EMS involves various scenarios that may occur at each time step of the system's operation. When multiple storage systems or different energy sources are available, the EMS must prioritize among them to optimize performance. The literature identifies four major strategies for rule-based EMS to coordinate production and load demand while accounting for storage, thereby overcoming the intermittency of renewable energy (RE) sources and the stochastic nature of load demand:

- **Separating Low Power and High Power Demands**: This strategy allocates different power demands to the appropriate source or storage system based on the operating characteristics and capabilities [113].

- **Long-term and Short-term Storage Priorities**: This involves prioritizing between storage systems based on the energy density and self-discharging rate [114, 115].

- **Threshold-based Operation**: This defines thresholds for power blocks to determine their operation based on the maximization of the blocs efficiency and limiting shut-downs [34].

- **Allocation Factor Definition**: This involves setting allocation factors between different energy storge to ensure that these storage will work effectively within their operation range [116].

For a typical system composed of photovoltaic (PV) panels, wind turbines (WT), batteries (BT), and diesel generators (DG)—referred to as a PV-WT-BT-DG system—the EMS can follow either a Load Following (LF) or Cycle Charging (CC) strategy. In the LF EMS, the battery is prioritized for both charging (using surplus RE production) and discharging (to meet deficits in RE generation). If the battery is insufficient, the diesel generator covers the remaining deficit, operating at partial load. During periods of excess RE generation, if the battery cannot store all the surplus energy, the excess energy is curtailed. Conversely, in the CC EMS, the diesel generator operates at its full rated power to charge the battery and maintain a predefined level of charge. This strategy ensures that the battery is sufficiently charged, providing a reliable energy reserve. These strategies highlight the importance of a well-designed EMS in managing the balance between energy production, storage, and load demand. By implementing such strategies, HRES can achieve higher efficiency, reliability, and sustainability.

In order to examine the effect of these two different strategies, [117] applied both Load Following Operation Strategy (LF) and Cycle Charging Operation Strategy (CC) in optimizing the energy management of a hybrid renewable energy system (HRES) for Sachs Harbour, a remote community in Northern Canada. LF was found to be more suitable for integrated systems, as it operates the diesel generator only when renewable energy sources and battery storage cannot meet the demand, thus minimizing fuel consumption. Conversely, CC, which runs the diesel generator at full capacity until the battery reaches a preset state of charge, proved more effective for electricity-only systems. The study demonstrates that an appropriate energy management strategy can significantly impact the overall system efficiency, fuel consumption, and cost-effectiveness, offering valuable insights for sustainable energy planning in remote areas.

In [118], authors conducted a techno-economic analysis of a hybrid energy system (HES) for an educational institution in Tamil Nadu, India, utilizing both on-grid and off-grid configurations.

The energy management strategy focuses on two dispatch strategies: Load Following (LF) and Cycle Charging (CC), optimized using HOMER software. LF strategy was found to be more effective for on-grid systems, where the generator operates only to meet the load demand, thus reducing operational costs and emissions. Conversely, the CC strategy, which charges batteries with surplus power from the generator, was more suitable for off-grid systems. The study highlights that the on-grid system with LF strategy achieved a lower Net Present Cost (NPC) of $7.66 million and Cost of Energy (COE) of $0.127/kWh, demonstrating its economic feasibility and environmental benefits over the off-grid system. This comparative analysis underscores the importance of selecting appropriate EMS strategies to optimize performance and cost in HES deployments.

In the study conducted by [119], authors have investigated the optimal sizing of a hybrid PV-WT-battery storage system, examining the impacts of split-Stirling engine (ST) and combined ST with organic Rankine cycle (ORC) back-ups under circuit charging (CC) and load following (LF) dispatch strategies. The energy management strategy uses a rule-based approach with four if-then constructs to manage energy flow, prioritizing battery storage before deploying back-ups. For CC, the back-ups charge batteries with any excess power, whereas in LF, back-ups strictly follow the load. Results indicate that using ST + ORC back-ups in LF mode reduces the levelized cost of energy (LCOE) by 60.70% and CO2 emissions by 33.71%, compared to a traditional diesel generator (DG) base case, although with a slight increase in LPSP. In contrast, the split ST in CC mode achieved reductions of 61.4% in LCOE, 33% in CO2 emissions, and 24.47% in LPSP. These findings highlight the significant potential of biomass-powered ST and ST + ORC back-ups to enhance the reliability, cost-efficiency, and environmental performance of HRES configurations over conventional DG systems.

I.2.4.3.b Optimized EMS

Unlike predefined rule-based EMS (R-EMS), optimized EMS (O-EMS) involves greater computational time and complexity. This is because O-EMS focuses on ensuring optimal functioning in the short term and evaluating the future implications of current decisions, rather than relying on a fixed set of rules to achieve long-term objectives. While R-EMS ensures global techno-economic or techno-economic and environmental objectives for the entire operation period, O-EMS dynamically assesses and selects the best available short-term scenarios. This approach allows O-EMS to adapt and respond more effectively to the variability of renewable energy sources and load demands. O-EMS can be considered a double-layer optimization strategy. The inner layer focuses on short-term optimization, refining the operational behavior of the system, while the outer layer provides an optimal

sizing framework and sets boundaries for the inner layer. The inner layer then offers feedback to the outer layer, creating a continuous loop of improvement and adaptation. This method allows O-EMS to explore various short-term scenarios rather than merely following a predefined rule based on energy balance. By dynamically adjusting to current conditions and predicting future states, O-EMS aims to maximize system efficiency, minimize operational costs, and reduce environmental impact, thus ensuring a more reliable and sustainable energy supply.

In literature, different methods are applied to HRES to achieve an O-EMS including finite automata [120] , dynamic programming (DP) [121, 122], stochastic programming [123], mathematical programming [123], receding horizon optimization (RHO) [124, 125], model predictive control (MPC) [126, 127], fuzzy logic controller [128].

In [122], Chedid et al. presented an optimized energy management system (O-EMS) for a university campus micro-grid reliant on an unreliable grid. The O-EMS uses a combination of Genetic Algorithm (GA) and Dynamic Programming (DP) to achieve optimal sizing of PV and BES system. The GA performs the initial sizing, while the DP focuses on optimal dispatch strategies, dynamically managing the power flow within the system. The O-EMS operates in two distinct modes: during active hours, it employs DP to optimize power flow, prioritizing renewable energy and battery usage to minimize reliance on DG and reduce grid energy purchases during peak tariffs. During passive hours, a rules-based algorithm takes over, managing battery charging using the lowest tariff rates. This dual-layer approach ensures short-term optimization while providing feedback for continuous improvement and long-term system efficiency. Results show significant reductions in operational costs and emissions, with the O-EMS phasing out nearly all DG usage and optimizing energy purchase from the grid. The O-EMS's dynamic and adaptive strategy demonstrates superior performance in managing the variability of renewable energy sources and load demands, ensuring a reliable and sustainable energy supply for the campus. Authors in [120] have introduced an (O-EMS) for a standalone hybrid PV/BT/DG/hydrogen system using a finite automata-based framework. The O-EMS dynamically generates multiple energy management strategies and evaluates them to identify the most efficient scenario. The framework operates in three steps: initial sizing based on an analytical and economic approach, generating various EMS using finite automata, and evaluating these strategies to develop an optimized EMS. The O-EMS employs a dual-layer optimization strategy. The inner layer focuses on short-term optimization, dynamically adjusting the system's operations based on current conditions and predicted future states. The outer layer provides an optimal sizing framework, guiding the inner layer and incorporating its feedback for continuous improvement. This approach allows the system to

adapt to the variability of renewable energy sources and load demands, ensuring maximum efficiency and cost-effectiveness. The study demonstrates that the integrated framework significantly reduces the size of the PV system from 140 kW to 60 kW and cuts the diesel generator working hours by 35%. Additionally, the optimized EMS lowers the LCOE by 40% and increases the utilization of renewable energy sources, highlighting the potential of O-EMS to enhance the performance and sustainability of hybrid renewable energy systems. In another study conducted by Forough et al. [124], they have introduced a novel optimized energy management system (O-EMS) for a hybrid renewable energy system (HRES) using a receding horizon optimization (RHO) approach. The O-EMS employs a dual-layer strategy where the outer layer focuses on the optimal sizing of system components, while the inner layer dynamically adjusts the operational behavior based on real-time data. The receding horizon strategy optimizes the control variables at each time step, using a mixed integer convex programming method. This approach allows the O-EMS to dynamically manage the energy flows among PV, wind turbines, batteries, and a diesel generator. The framework captures the variability of renewable energy resources and demand profiles, optimizing short-term operations while providing feedback for continuous improvement. Results demonstrate that the O-EMS significantly enhances economic performance and renewable energy utilization, increasing the share of renewable energy from 68.5% to 81.4% and reducing diesel fuel consumption. By adjusting the prediction horizon length, the system achieves more effective battery scheduling and reduces the overall operation cost. This O-EMS approach highlights the potential for improved reliability, cost efficiency, and environmental sustainability in HRES applications.

Another study that uses the RHO as an O-EMS is considered in [125]. In this study, authors proposed an (O-EMS) for designing off-grid microgrids in rural areas using a multi-objective optimization approach. The O-EMS employs the Non-dominated Sorting Genetic Algorithm II (NSGA-II) and Direct MultiSearch (DMS) algorithms to optimize multiple economic indicators simultaneously, such as Net Present Value (NPV) and Modified Internal Rate of Return (MIRR). The dual-layer strategy includes an outer layer for optimal sizing and an inner layer for dynamic operational optimization. The inner layer utilizes a rolling horizon strategy (RHS), forecasting load profiles and renewable production to minimize operational costs over a 24-hour horizon. The RHS adjusts energy dispatch in real-time, improving system efficiency and reducing costs. Results indicate that the O-EMS achieves a significant reduction in Net Present Cost (NPC) and enhances profitability by increasing renewable energy utilization and minimizing load curtailment. This method ensures a balanced trade-off between investment costs and operational efficiency, providing reliable and sustainable energy supply for rural

microgrids in developing countries.

I.2.5 Optimal sizing of a HRES

The ultimate objective of optimal sizing for Hybrid Renewable Energy Systems (HRES) is to minimize initial costs while ensuring load demand is met. Oversizing a system results in higher initial costs, whereas undersizing leads to a loss of power supply. Consequently, optimal sizing is essential to ensure a techno-economically reliable operation [35].

To analyze each HRES, several critical steps must be undertaken: identifying the energy source types, developing mathematical models for the energy sources, calculating the energy balance, identifying the decision variables, defining the objective functions, and establishing the constraints. Due to variations in HRES configurations, selecting an appropriate and efficient sizing strategy is necessary. The mathematical interplay and the conflicting behavior of objectives, constraints, and decision variables highlight the complexity and difficulty of attaining an optimal solution for an optimization problem [35, 129]. In previous sections of this work, we have described the energy sources (section I.2.4.1), energy storage (section I.2.4.2), and energy management systems (section I.2.4.3). This part will focus on the objective functions, decision variables, and optimization algorithms employed in the optimal sizing of HRES. Optimal sizing requires defining objective functions that typically aim to minimize costs, maximize efficiency, and ensure reliability. Decision variables may include the capacities of various energy sources and storage systems, and the operational parameters of the system. Constraints are often related to technical limitations, resource availability, and environmental regulations.

I.2.5.1 Objective Functions

In optimization problems, an objective function is a mathematical expression that depends on system output variables and decision variables. This function must be optimized (minimized or maximized) by the optimization algorithm during the optimization process. Based on the studied HRES, both single and multiple objective problems may be considered. Objective functions, often referred to as key performance indicators (KPIs) for HRES, can be classified into four main categories: Technical, Economic, Environmental, and Social. These KPIs are evaluated to be minimized or maximized by the optimization process and significantly affect system capacity (usually decision variables) [35, 129].

I.2.5.1.a Technical Indicator

Due to the intermittency of sources and the stochastic behavior of load demand, ensuring reliable load demand becomes a challenging task. For this reason, technical KPIs are considered when optimally sizing an HRES. Technical KPIs mainly include the LPSP [1], Loss of Load Probability (LOLP) [130], Expected Energy Not Supplied (EENS) [131], Deficiency of Power Supply Probability (DPSP) [132], Loss of Load Expected (LOLE) [133], and Loss of Energy Expected (LOEE) [133]. The energy target is often represented by the LPSP of the system, a metric that measures the percentage of time when the available power is insufficient to meet the required load. The reliability of load demand is crucial, and a system that consistently provides enough electrical energy to meet demand over a specific period will have a lower LPSP value. This metric is widely employed by authors in the literature [1, 134].

The study conducted by [134] integrates LPSP as a crucial reliability indicator for optimizing hybrid renewable energy systems (HRES) for rural telecom towers. LPSP measures the likelihood of power supply shortfalls, highlighting the system's reliability. The authors developed a discrete multiobjective grey wolf optimization (DMGWO) algorithm to minimize LPSP alongside cost and excess energy generation. By incorporating LPSP, the algorithm ensures a reliable power supply, achieving a low LPSP value of 0.07, indicating high system reliability. This approach effectively balances economic feasibility with the necessity of uninterrupted power supply, crucial for remote telecom operations.

I.2.5.1.b Economic Indicator

Economic indicators, along with technical KPIs, are crucial in the development and integration of renewable energy systems worldwide. The significance of economic indicators lies in evaluating the feasibility of the designed systems. Typically, the economic assessment includes initial/capital expenditure (CAPEX), operation and maintenance costs (OPEX), replacement costs, and other relevant expenses [35, 36]. Commonly used economic KPIs in the literature include Net Present Cost (NPC) [135–137], COE [138], levelized cost of energy (LCOE) [139–141] , life cycle cost (LCC) [142, 143], Total Annual Cost (TAC) [132, 138, 144–147] , and annualized cost of system (ACS) [1, 148–150]. These KPIs provide a comprehensive evaluation of the economic performance and viability of HRES, ensuring that the systems are not only technically sound but also economically feasible and sustainable over the long term.

The study by [135] conducts a comprehensive economic analysis for optimal sizing of a hybrid renewable energy system (HRES) comprising photovoltaic (PV) panels, fuel cells (FC), and diesel generators (DG). The economic evaluation focuses on minimizing the Net Present Cost (NPC), incorporating capital costs, operation and maintenance costs, and replacement costs of each component. They utilize a multi-objective crow search algorithm (MOCSA) to balance TNPC against the reliability indicator, LPSP. The analysis includes sensitivity assessments of fuel prices and costs of FC equipment, demonstrating that integration of hydrogen energy technology can significantly reduce the NPC, particularly when FC costs are decreased by 30-50%.

I.2.5.1.c Environmental Indicator

One of the main objectives of considering HRES is mitigating environmental pollution by reducing greenhouse gas (GHG) emissions and promoting cleaner energy sources. Conventional fossil fuel-based energy sources emit significant quantities of CO_2 and SO_2 gases. Integrating renewable energy (RE) sources into the energy production sector helps mitigate carbon emissions and leads to more environmentally friendly power production. To account for environmental factors during the optimal sizing of HRES, several indicators are considered in the literature. These include carbon emission (CE) [1, 143, 150, 151], embodied energy (EE) [152], carbon footprint of energy (CFOE) [153, 154], life cycle assessment (LCA) [155–159], and fuel emission (FE) [149]. These environmental KPIs provide a comprehensive assessment of the environmental impact of HRES, ensuring that the systems contribute to reducing pollution and promoting sustainability.

Bortolini et al. in their study [154] integrated environmental indicators by evaluating the Carbon Footprint of Energy (CFOE) within their hybrid renewable energy system (HRES) model. CFOE measures the total greenhouse gas emissions in CO2 equivalents per kWh produced over the system's lifetime. The model accounts for emissions from manufacturing, transportation, installation, operation, maintenance, and end-of-life disposal of system components, including PV modules, BES, and diesel generators. By adopting a bi-objective design approach, the study identifies configurations that minimize both CFOE and Levelized Cost of Electricity (LCOE). Their results indicate that integrating higher capacity BES and PV reduces CFOE by up to 50%, demonstrating significant environmental benefits over traditional diesel-only systems.

Authors in [155] conducted a study that evaluates the environmental indicators through a comprehensive Life Cycle Assessment (LCA) of various hybrid renewable energy system (HRES) configurations for remote rural communities. The environmental sustainability assessment considers 18

potential impact categories, such as climate change, ozone depletion, acidification, and more. The study evaluates the impacts of using different configurations, including solar photovoltaics (PV), wind turbines, diesel generators, and battery storage. Results show that hybrid systems with combined PV and wind resources significantly reduce environmental impacts compared to stand-alone systems. For instance, integrating higher capacity battery storage with PV and wind reduces environmental impacts by up to 40%, making these hybrid configurations environmentally preferable. The study highlights that PV systems, when installed at the household level, have 15% higher impacts in a micro-grid than in individual home installations

I.2.5.1.d Social Indicator

In recent years, nearly all countries have promoted the development of clean energy sources through national policies. Consequently, the development of Hybrid Renewable Energy Systems (HRES) should align with these policy recommendations. However, due to the lack of evaluation methods for socio-political performance indicators, only a few studies have considered these parameters when designing and sizing HRES. Nevertheless, social indicators are crucial for assessing the acceptance of HRES by society, ensuring alignment with national policies for social development, and ensuring compliance with regulations [35, 160, 161].

In the literature, social indicators include the Human Development Index (HDI) [160, 162], job creation (JC) or job formation factor (JFF) [160, 162, 163], portfolio risk (PR) [164–167], social acceptance (Sa) [168], and social cost of carbon (SCC) [169]. These indicators play a significant role in determining the societal and regulatory feasibility of HRES, thus underscoring their importance in the optimal design and implementation of these systems.

In [162], Khan et al. addressed social indicators for hybrid renewable energy systems (HRES) by focusing on Human Development Index (HDI), job formation factor (JFF), and local transport-based employment (LTE). These social indicators are evaluated using the concept of excess energy utilization. The HDI improvement is linked to the availability of excess energy, which can support additional household and community activities, leading to better living standards. The JFF is assessed by calculating the jobs generated per megawatt of installed capacity for various components like solar PV, wind turbines, diesel generators, and battery storage. LTE estimates the employment generated through the use of excess energy for local transportation, such as battery-powered rickshaws. The study finds that HRES configurations with balanced excess energy and optimal technical design contribute significantly to social development, enhancing local employment opportunities and overall

human development in rural areas.

In another study conducted by [163], authors focused on social indicators in the context of hybrid renewable energy systems (HRES) through a multi-objective optimization approach that includes job creation and public lighting coverage. Job creation is quantified by considering the employment opportunities generated during the construction, installation, and operation phases of HRES components, such as photovoltaic panels, wind turbines, diesel generators, and battery storage systems. The study uses specific job creation factors for each technology to estimate the total number of jobs generated locally. Public lighting coverage is treated as a critical social indicator, aiming to improve living conditions and security in rural areas. The model prioritizes ensuring that public lighting needs are met, with a specific objective function to maximize the percentage of public lighting coverage. This comprehensive consideration of social impacts helps to align HRES projects with broader socio-economic development goals, ensuring that energy solutions contribute positively to the community's welfare.

The study, conducted by [160], delves into the social indicators for hybrid renewable energy systems (HRES) by focusing on the Human Development Index (HDI) and job creation. The study emphasizes HDI as a measure of social impact, correlating energy access with improved living standards, better education, and higher income levels. The authors propose that surplus energy generated by HRES can be used to power small workshops and businesses, thereby enhancing economic activities and elevating HDI. Additionally, job creation is quantified using job creation factors specific to each energy source, including PV, wind, biomass, and diesel generators. The study calculates the direct and indirect employment generated during the installation, operation, and maintenance phases of the HRES components. This dual focus on HDI and job creation highlights the potential of HRES to contribute significantly to social development, particularly in rural and remote areas.

I.2.5.2 Solution methods for HRES Optimal Sizing problems

I.2.5.2.a Traditional methods

The optimal sizing methodology for Hybrid Renewable Energy Systems (HRES) involves finding the best trade-off between the considered evaluation indicators. Several sizing methods exist in the literature, each aiming to solve the optimization problem by considering objective functions and system constraints. The goal is to determine the optimal set of decision variables that will minimize or maximize the objective function while ensuring that all constraints are met.

Among these methods are traditional methods such as Mixed-Integer Linear Programming (MILP)

[170], analytical methods [171], graphic construction methods [172], probabilistic methods [173], iterative methods [174], numerical methods [175], and software tools [31, 176] like (HOMER [177], iHOGA[178] , TRNSYS [179] and RETScreen [180]).

I.2.5.2.b Artificial intelligence (AI) based methods

According to studies by [31, 35], AI-based methods, especially metaheuristic algorithms, are widely employed in the optimal sizing of HRES due to their superior efficiency, accuracy, and rapid convergence. These algorithms can be categorized into four main classes as outlined by [181]: evolution-based methods, physics-based methods, swarm intelligence methods, and human behavior-based methods.

- **Evolution-Based Methods** (*eg. Genetic Algorithms (GA)*): These methods mimic the process of natural selection to find optimal solutions and are known for their robustness and flexibility [182–184];
- **Physics-Based Methods** (*eg. Simulated Annealing (SA)*): This probabilistic technique mimics the annealing process in metallurgy and is effective for finding global optimizations in a large search space [185, 186];
- **Swarm Intelligence Methods** (*eg. Particle Swarm Optimization (PSO) and Grey Wolf Optimizer (GWO)*): These methods simulate the social behavior of organisms like birds and wolves to explore the search space and find optimal solutions efficiently [187–191];
- **Human Behavior-Based Methods** (*eg. Harmony Search (HS)*): Inspired by the musical process of seeking harmony, this method is effective for a variety of optimization problems [186, 192].

These optimization techniques, with their diverse approaches and strengths, are crucial for the effective and efficient sizing of HRES. The selection of an appropriate method depends on the specific characteristics and requirements of the system being studied, ensuring that the optimal solution is tailored to the unique needs of each HRES.

In their comprehensive study, [193] evaluated ten metaheuristic optimization techniques for the optimal sizing of a hybrid photovoltaic (PV)/wind turbine/battery system. The algorithms assessed include Genetic Algorithm (GA), Cuckoo Search (CS), Simulated Annealing (SA), Harmony Search (HS), Jaya Algorithm, Firefly Optimization Algorithm (FA), Flower Pollination Algorithm (FPA), Moth Flame Optimization (MFO), Brainstorm Optimization in Objective Space (BSO-OS), and Simplified Squirrel Search Algorithm (S-SSA). The primary objective was to minimize the Total Net Present

Cost (TNPC) while maintaining reliability through Deficiency of Power Supply Probability (DPSP) constraints. The study finds FPA and SA to be particularly robust and accurate, with zero standard deviation in TNPC values across 50 runs, while FAO excels in execution speed. These results provide valuable insights for selecting suitable optimization techniques for HRES sizing, emphasizing SA's balance between robustness, accuracy, and execution time.

In another insightful study, [194] present a comprehensive evaluation of eight metaheuristic optimization algorithms for the optimal sizing of an isolated hydrogen-based micro-grid. The algorithms assessed include Moth-Flame Optimization Algorithm (MFOA), Genetic Algorithm (GA), Particle Swarm Optimization (PSO), Dragonfly Algorithm (DA), Salp Swarm Algorithm (SSA), Ant Lion Optimizer (ALO), Grey Wolf Optimizer (GWO), and Grasshopper Optimization Algorithm (GOA). The objective was to minimize the total net present cost (NPC) while ensuring the system's technical feasibility and cost-effectiveness. The study notably highlights the superior performance of MFOA in reducing the NPC compared to other algorithms, achieving a 2.1% and 3.2% cost reduction over GA and PSO, respectively. This research underscores the importance of advanced metaheuristic techniques in enhancing the economic and operational efficiency of micro-grid systems, providing a valuable reference for future studies in the domain of renewable energy systems.

I.3 Research gap and study novelties

After examining the literature regarding HRES for remote areas in our study region, several works have focused on configurations such as PV-BT, PV-WT-BT, and sometimes incorporating DG to ensure load availability during RE source/storage unavailability. However, these studies primarily consider small-sized or domestic-type loads, with no studies addressing heavy industrial load demands in Algeria. Globally, some studies have investigated incorporating renewable energy into various sectors, including enhancing chemical reactions [195], wastewater treatment [196], hydrogen production [197–200], and water desalination [201]. Other studies have explored the integration of solar energy into processes like crude oil upgrading and oil refining, showing promising results in terms of cost-effectiveness and environmental impact [197, 200].

In our study, we focus not on a fully renewable energy system but on a partial shift towards clean energy sources for electricity generation for heavy-duty industrial applications, particularly in the oil and gas sector in Algeria. The novelty of our approach lies in steering the backbone of Algeria's energy sector (oil and gas) towards cleaner energy solutions. This approach not only leverages sustainability opportunities but also employs high-level evaluation techniques based on artificial intelligence (AI)

methods and decision-making methodologies.

The suggested system will deeply focus on integrating renewable energy sources, particularly PV and WT, and evaluating single and dual storage technologies, including electrochemical (battery storage systems) and chemical (hydrogen storage systems). Hydrogen storage has emerged as a promising solution for green energy storage. Additionally, we consider energy management strategies alongside AI-based optimization techniques, including traditional ones like GA, PSO, NSGA-II, MOPSO, and newly developed ones post-2022, such as Fick's Law Algorithm (FLA), to solve sophisticated optimization problems. This approach aims to find the best trade-off regarding techno-economic, environmental, and social performance while ensuring effective synergy between generations, storage systems, and load demand. Our approach involves a comprehensive analysis of technical, economic, and environmental performance indicators to contribute to this field.

The utilization of the considered methods (FLA) as novel optimization tools, adopting this methodology, we guarantee a comprehensive evaluation of the prospective advantages and obstacles linked to the incorporation of HRES into oil and gas facilities for their electrification. Also, dual storage strategies and decision making technique like (TOPSIS and SAW) will be implemented and applied to the studied systems. The combination between traditional/novel optimization algorithms and decision-making techniques in order to address the challenges of designing renewable energy systems, establishing a standard for operational efficiency and sustainability in energy-intensive industries. These contributions have the potential to significantly impact the integration of renewable energy technologies and serve as a model that can be replicated in similar contexts worldwide. This represents a crucial step towards reducing carbon emissions in the oil and gas sectors through the integration of renewable energy solutions. The main contributions of this work are:

1. Designing and sizing a solar renewable energy system with different (dual/single) storage strategies based on a hybrid battery-hydrogen system;

2. Optimizing energy use and reducing reliance on fossil fuels by dynamically balancing energy production through renewable energy integration;

3. Using the novel optimization algorithm to optimize the size of system components, prioritizing meeting load demand and economic viability;

4. Utilizing the decision making methods to identify the most suitable system configuration among various feasible solutions.

By positioning our work within the context of previous studies, we address the gaps identified in

the literature and introduce novel approaches to the integration and optimization of HRES for heavy industrial applications like the oil and gas sector in Algeria. This research not only contributes to the academic field but also provides practical solutions for the sustainable development of the Algerian and worldwide energy sector.

I.4 Conclusion

This chapter represents an important contribution to the field because an extensive review of recent literature related to modeling, optimal sizing, and energy management in Hybrid Renewable Energy Systems is performed. System components-from different types of energy sources and storage systems to methods for their sizing-were discussed in broad detail.

Special importance was given to renewable energy sources, such as solar and wind, and the installation of storage facilities like BES system and hydrogen-based ESS to offset the intermittency of the latter.

This chapter also focused on the various EMS, which are essential to be considered in balancing load demand with renewable energy availability efficiently. These included the review of various rule-based systems and advanced optimization-based EMS approaches. The latter have become especially necessary to minimize the overall system costs while at the same time maintaining efficiency and reliability at high values.

The literature also calls for the optimum sizing methodologies applied on HRES. Herein, this work has reviewed several conventional and artificial intelligence-based optimization algorithms, including GA and PSO with their supporting software, such as HOMER and iHOGA.

These are appropriate for determining the best configuration of the renewable systems and storage units for the main objectives of minimum cost, maximum energy produced, and emissions reduction.

The literature review indeed gave insight, not only into current trends and methodologies but also revealed striking research gaps, particularly in addressing heavy industrial loads such as those in the oil and gas industry. This chapter therefore forms a basis for subsequent chapters where such gaps shall be addressed by incorporating renewable energy systems into fossil fuel-based industries, with a focus on advanced optimization techniques and dual storage strategies.

Chapter II

Modeling, sizing and Energy Management of a Hybrid Renewable Energy System

II.1 Introduction

Before embarking on the optimization process, it is essential to provide a comprehensive description and mathematical modeling of each system component. This section begins with an overview of the existing reference system, which involves the electrification of a natural gas (NG) power plant using NG power generation. The load profile and climate data are also discussed. Additionally, each subcomponent of the proposed Hybrid Renewable Energy System (HRES) is modeled. The reference system serves as a baseline for evaluating the potential improvements and benefits of the suggested HRES based on various objectives.

II.2 System description

II.2.1 Reference system

The main goal of this study is to evaluate the technical feasibility, economic viability, and environmental impact of integrating a Hybrid Renewable Energy System (HRES) into the oil and gas industry. The reference system considered is an upstream natural gas processing facility. The load demand is defined

as the electricity required to power the facility's operations, which include motor pumps, compressors, electric furnaces, and electric aero coolers. Currently, all electricity demand for this facility is met by a conventional natural gas power plant (Fig. II.1).

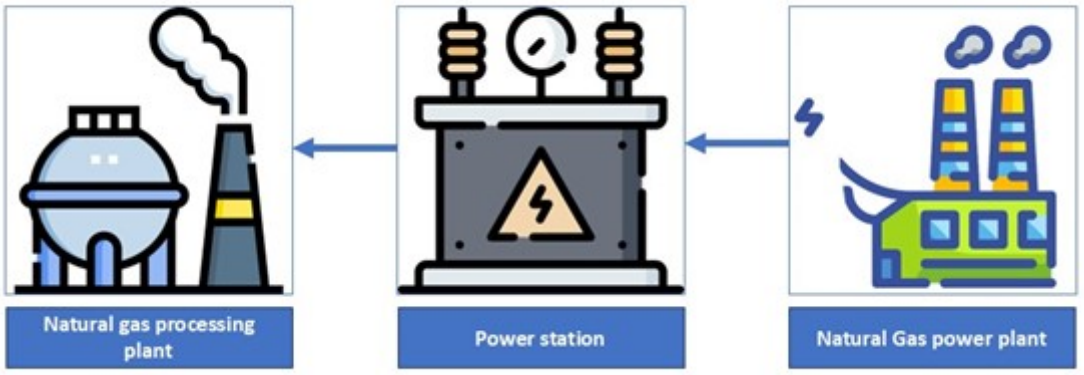

Figure II.1: Current power generation system.

II.2.2 Suggested system

The proposed Hybrid Renewable Energy System (HRES), illustrated in Fig. II.2 , represents a hybrid configuration that integrates the existing system (Fig. II.1) with renewable and conventional energy sources. The HRES consists of renewable energy sources, including Photovoltaic (PV) modules and Wind Turbines (WT), as well as conventional sources such as a Gas Turbine (GT). Additionally, the system incorporates energy storage solutions, including chemical storage (HES System, HESS) and electrochemical storage (Batteries). The HESS components include Fuel Cells (FC), Hydrogen Storage Tanks (ST), and Electrolyzers (EL). In this configuration, the GT supplies AC current to the AC bus, while the PV, WT, FC, and EL are connected to the DC bus. A DC/AC converter is utilized to ensure optimal and secure integration between the AC and DC buses.

The schematic depicted in Fig. II.2 represents the overall system configuration. However, various configurations may be explored to identify the most effective setup. These different configurations, which allow for comparative analysis, are detailed in Table II.1

II.2.3 Mdeling and optimization procedure

The evaluation of each configuration presented in Table II.1 must follow specific procedures to ensure a thorough techno-economic and environmental analysis. This analysis requires several data inputs,

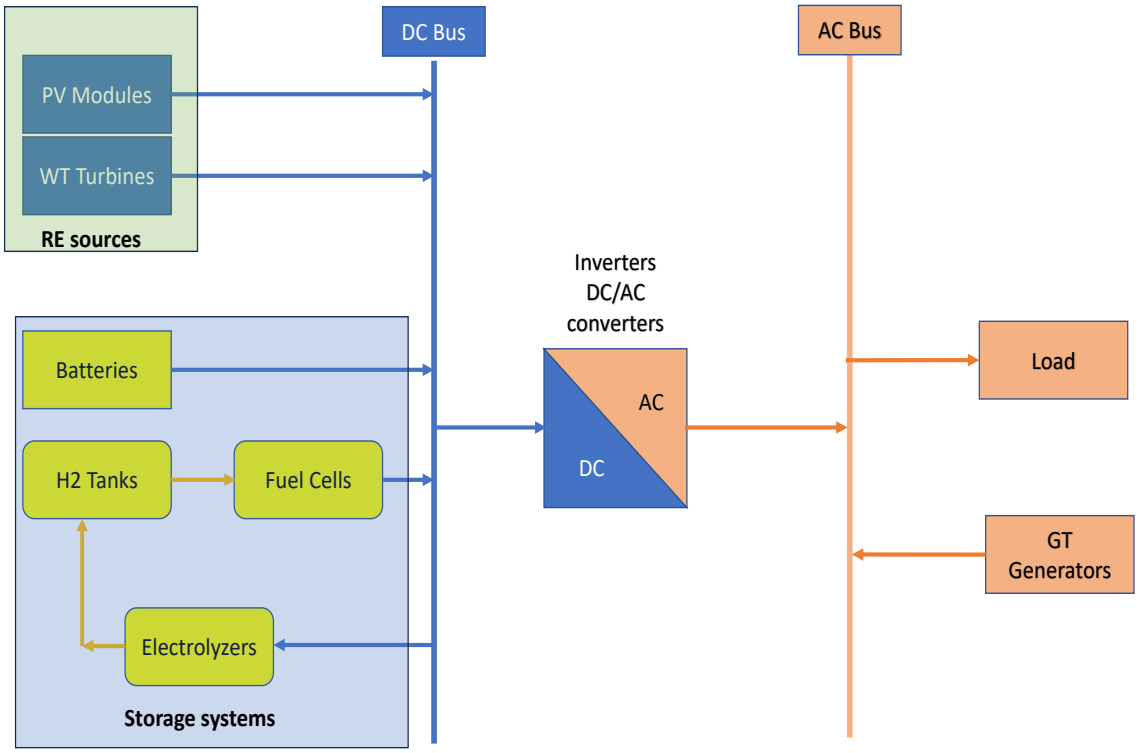

Figure II.2: Hybrid Renewable Energy System Scheme.

Table II.1: Case Studies Configuration

Configuration (Case study)	Description / Requirements	PV	WT	GT	HESS	BES system
Configuration 1	0% renewable			✓		
Configuration 2	100% Renewable	✓	✓		✓	
Configuration 3	100% Renewable	✓	✓			✓
Configuration 4	100% Renewable (dual storage)	✓	✓		✓	✓(p)
Configuration 5	100% Renewable (dual storage)	✓	✓		✓(p)	✓
Configuration 6	HRES ($RE \geq 20\%$)	✓		✓	✓	
Configuration 7	HRES ($RE \geq 50\%$)	✓		✓	✓	
Configuration 8	HRES ($RE \geq 80\%$)	✓	✓	✓	✓	
Configuration 9	HRES ($RE \geq 80\%$)	✓	✓	✓	✓	✓(p)
Configuration 10	HRES ($RE \geq 80\%$)	✓	✓	✓	✓(p)	✓

(p): Primary storage.

including component modeling, as well as economic and environmental modeling of each subsystem.

The process begins with an initialization step that includes the following:

- System Configuration: Selection of one configuration from Table II.1.
- Climate Data: Relevant data for the studied region.
- Load Profile: Load demand specific to the studied system (reference system).

- Technical and Economic Parameters: Parameters for each component considered within the system configuration.

Following initialization, the next phase involves the technical and economic modeling and optimization process. This process is guided by predefined rule-based Energy Management Strategy (EMS), objective functions, and system constraints. The goal is to determine the optimal system size and configuration that best meets the specified objectives. Finally, the optimal system configuration/size is evaluated against the objective functions and system operation. These evaluations are presented in the form of various plots, tables, and are followed by detailed discussions and analysis.

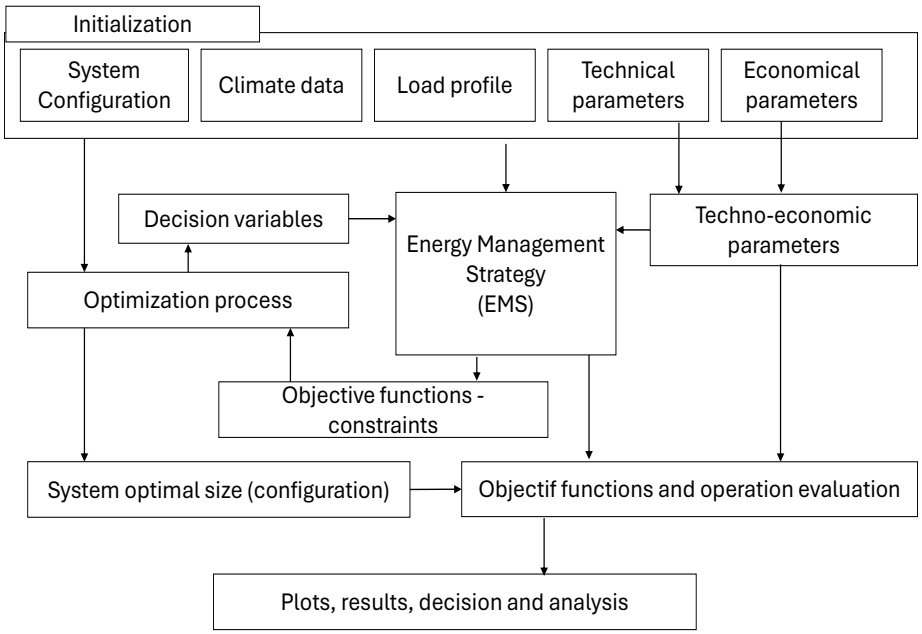

Figure II.3: HRES modeling and optimization procedures.

The evaluation of each configuration presented in Table II.1, must flow specific procedures to be done. The techno-economic and environmental analysis of each configuration necessitates several data inputs, components modeling as well as economic and environmental modeling of each subsystem. Firstly, an initialization stem that include: a system configuration (one from Table II.1), Climate data for the studied region, load profile for the studied system, technical and economic parameters for each considered component of the system configuration. This initialization step is followed by technical and economic modeling and optimization process based on predefined rule-based EMS, objective functions and system constraints in order to attain the final optimal system size and configuration.

Finally, the system optimal configuration/size is evaluated against the objective functions as well as system operation, these evaluations are presented in from of different adequate plots, tables followed by discussions and analysis. Fig. II.3 summarize this modeling and optimization procedure.

II.3 Climate data and solar/wind potential for the study region

The optimal sizing of the Renewable Energy System (RES) for covering the total electric load demand of the Natural Gas Processing Plant (NGPP) located in Hassi Messaoud, southeast Algeria, is heavily influenced by the regional climate conditions. Hassi Messaoud is situated at latitude 31°43'10.7" N and longitude 6°03'02.2" E (Fig. II.4 [1]), an area well known for its extensive oil and gas production infrastructure. To accurately model and optimize the RES, it is crucial to analyze the climate data for this specific location, focusing on solar irradiance, wind velocity and ambiant temperature, which are critical inputs for solar/wind-based energy systems.

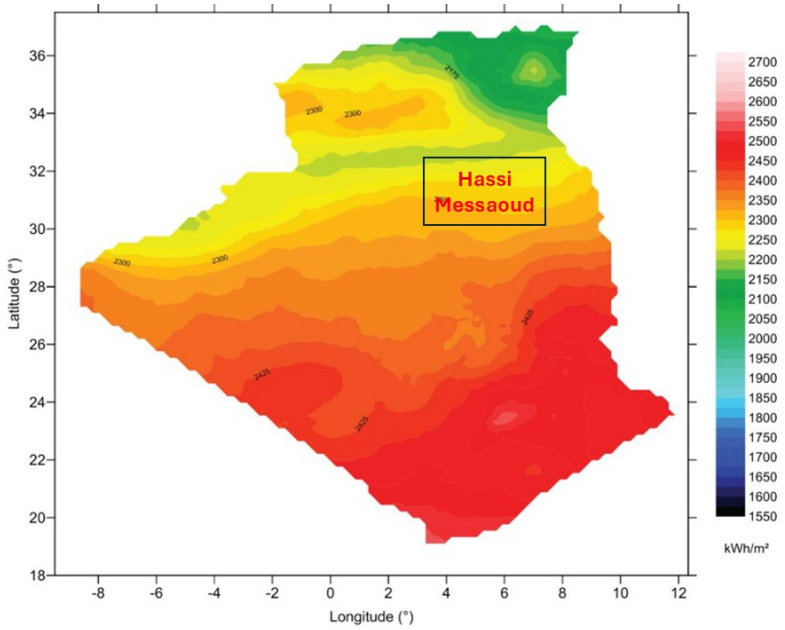

Figure II.4: GHI of the study location.

The climate data utilized in this study were obtained from comprehensive reanalysis datasets that offer a thorough spatio-temporal record of various meteorological variables [202, 203]. The hourly solar radiation and temperature data for the study area are presented in Figs. II.5 and II.6, respectively. These figures illustrate the significant variations in solar irradiance, temperature, and daylight hours experienced throughout the year, a pattern that can be attributed to the Earth's axial tilt and its impact on solar exposure.

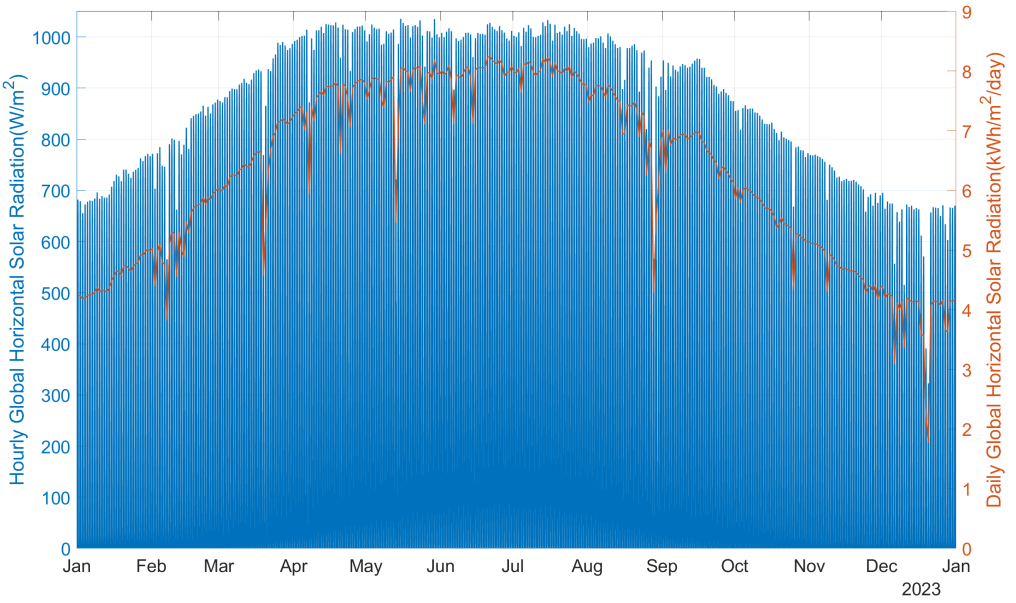

Figure II.5: Hourly Solar irradiation and temperature at the selected study area.

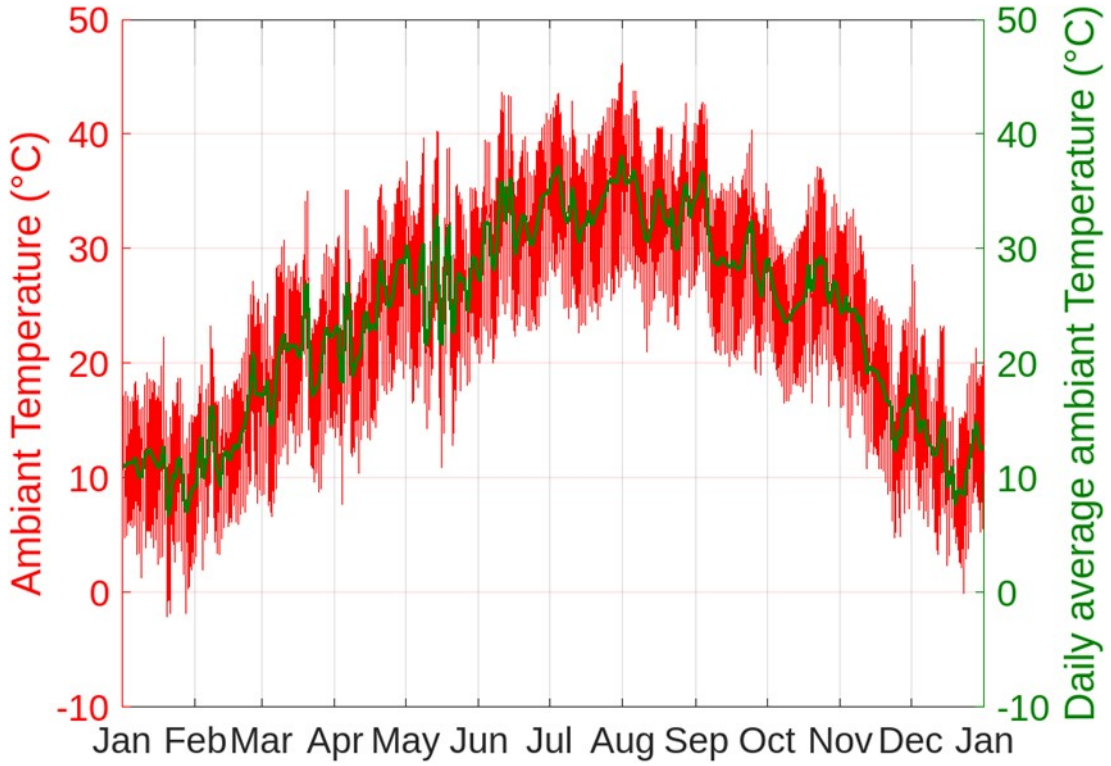

Figure II.6: Hourly and daily average of recorded temperature on the selected area for study.

In examining the solar irradiance data (Fig. II.5), it becomes evident that there is a pronounced increase in average daily solar irradiation during the spring season (Mar., Apr., May). The average

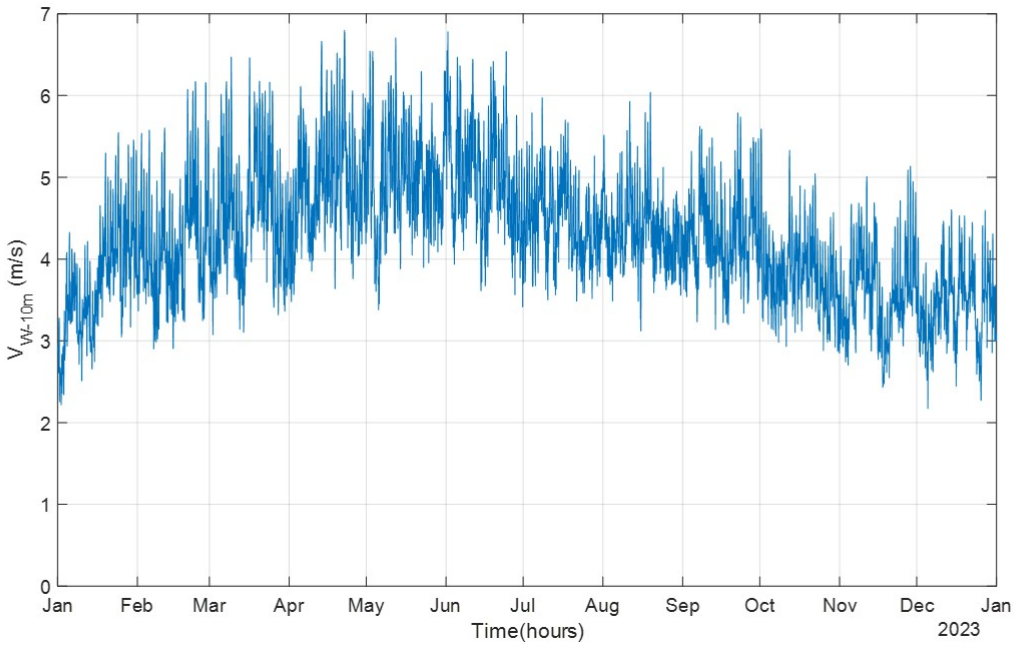

Figure II.7: Hourly wind velocity at 10m high of the selected study area.

daily solar irradiation during this period reaches a peak of 4882.86 kWh/m2, reflecting the abundant solar energy available in the region. Conversely, the winter season records the lowest average daily solar irradiation at 2508.52 kWh/m2, indicating a reduced level of solar energy during this time. The maximum daily solar irradiation, observed during the summer season, peaks at 5330.60 kWh/m2, a phenomenon driven by the extended daylight hours and intensified solar radiation typical of the summer months. In contrast, the fourth trimester exhibits the lowest peak daily solar irradiation at 3560.07 kWh/m2, highlighting the seasonal decline in solar energy availability.

There is also a clear correlation between solar irradiance and temperature patterns in the study region, as shown in Figs. II.5 and II.6. Both variables reach their highest levels during the summer season. The average daily temperature during this period rises to 33.18°C, with a peak daily temperature of 46.83°C. On the other hand, the winter season, records the lowest average daily temperature at 12.92°C, with a minimum daily temperature of -2.65°C. These variations underscore the influence of solar radiation on temperature, where increased sun exposure during summer months directly heats the Earth's surface and atmosphere, resulting in higher temperatures.

Based on the climate data analyzed, it is evident that solar energy holds significant potential for energy generation in the Hassi Messaoud region, with a daily average solar irradiance ranging from 3.3 to 8.7 kWh/m²/day , whereas wind speed seems to be unpredictable throughout the year (Fig. II.7). Consequently, solar photovoltaics have been selected as the principal source of renewable energy for

the proposed system. The selection is supported by the region's favorable solar potential, as indicated by the data and visualized through the accompanying figures and maps. These insights are crucial for the accurate sizing and optimization of the RES, ensuring it meets the energy demands of the NGPP efficiently and sustainably.

II.4 Load demand profile

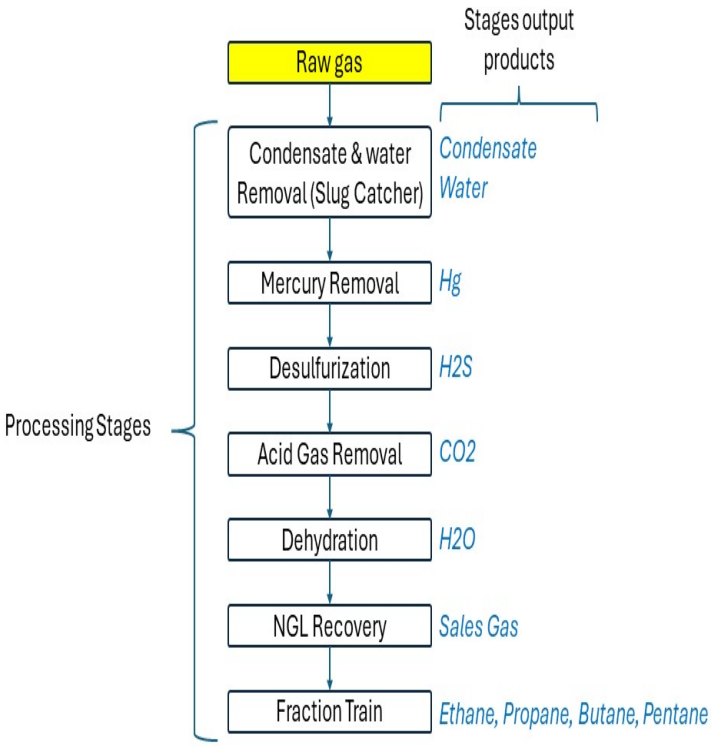

Figure II.8: Typical natural gas processing plant operations.

Natural gas processing plants (NGPPs) play a crucial role in converting raw gas extracted from wells into commercially valuable products. As depicted in Fig. II.8, a typical NGPP comprises multiple processing stages, including raw gas extraction and transportation, sweetening, and final product separation [3].

Initially, raw gas is extracted from wells and transported through pipelines to the processing plant. Upon arrival, the gas is first separated from any accompanying liquids through a process called gravity

separation. The gas then undergoes treatment to remove impurities such as hydrogen sulfide (H_2S), carbon dioxide (CO_2), and water vapor. This step, known as sweetening, is particularly energy-intensive, especially during the removal of CO_2 to comply with transportation standards [3, 204]. After sweetening, the gas is dehydrated to eliminate water vapor, enabling the separation of natural gas liquids (NGLs) like ethane, propane, and butane from methane, the primary component. Mercury removal is achieved by injecting nitrogen, and a cryogenic process using turbomachinery is employed to separate the NGLs from the remaining methane.

These stages demand substantial heat and electrical energy, which are required to power the turbomachinery and facilitate various thermal or chemical processes. Once processed, the methane, now purified, becomes "sale gas" and is ready for commercial use [3, 204].

The processing plant not only produces pure methane but also yields valuable byproducts, including NGLs and sulfur, which are recovered from the acid gases removed during processing. These byproducts are utilized across various industries. It is important to note the substantial energy requirements of this process. The plant's operations rely on internally generated power and steam, primarily produced by gas turbines. Additionally, natural gas with low levels of hydrogen sulfide, known as "fuel gas," is used to power turbines and boilers. For example, a plant processing 2.5 billion standard cubic feet of raw gas per day requires approximately 65 MW of electricity and 15,000 tons of steam daily, highlighting the significant energy demands of such facilities [3, 204].

In this study, accurately assessing the electrical energy requirements for the natural gas processing facility is of paramount importance. Our primary objective is to improve the environmental performance of these facilities by integrating renewable energy (RE) sources into the existing electricity production system described in section II.2.1. The facility selected for this study is located in southern Algeria and comprises two treatment trains, each with a capacity of 770 tons per hour.

The power station responsible for generating electricity for this facility consists of three 20 MVA gas turbogenerators (GTG). These thermal generators operate on natural gas produced on-site, with an estimated cost of $0.0366 per kWh of NG. Given the approximate efficiency of these thermal generators, which is around 30%, the specific cost of electricity production, including both variable and fixed costs, is approximately $0.075 per kWh of electricity.

The annual electrical power demand time-series, derived from the GTG production data, is illustrated in Fig. II.9. The load demand pattern closely follows typical industrial trends, exhibiting low fluctuations on both daily and seasonal scales. This stability is attributed to the consistent nature of

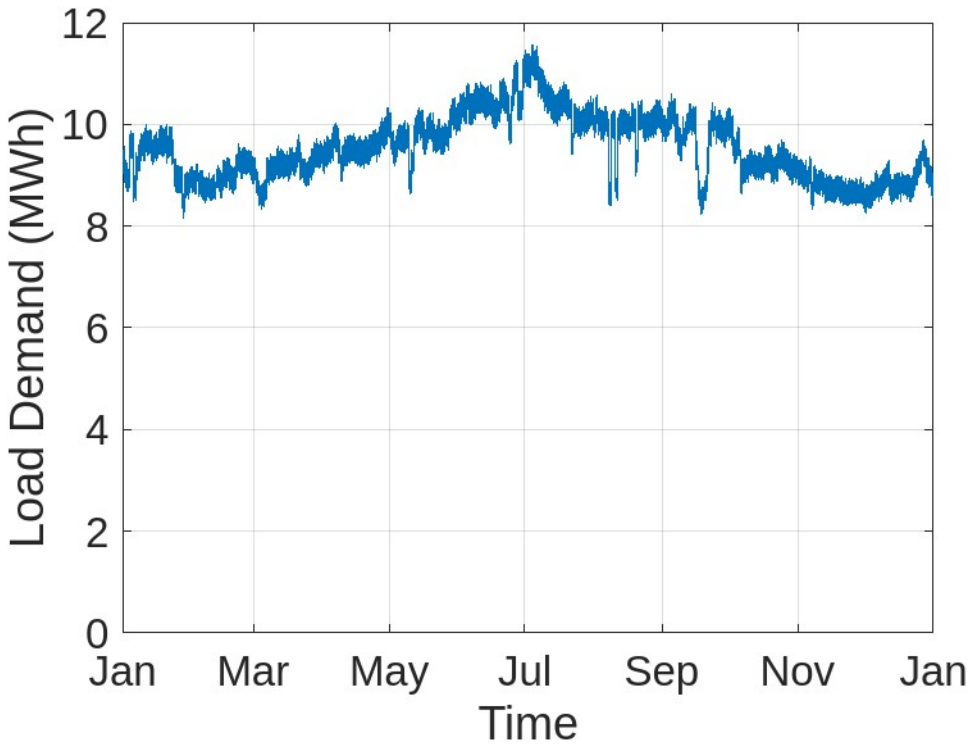

Figure II.9: Hourly electrical load demand profile during the year.

industrial operations, which remain relatively constant throughout the working period. Additionally, since the processing operations are only slightly influenced by ambient temperature and solar irradiance, there is a modest increase in load demand during the summer season.

Based on the presented (Fig. II.9) annual hourly time-series, the total annual electricity consumption is calculated to be 83,470.035 MWh. The annual peak and minimum power demands are 11.57 MW and 8.167 MW, respectively. The average daily electricity consumption is calculated to be 228.68 MWh.

II.5 Hybrid Renewable Energy System (HRES) modeling

As outlined in section II.2.2, the proposed system involves a comprehensive revamping of the existing system described in section II.2.1, evaluated from multiple perspectives, including performance indicators. To thoroughly assess the impact of integrating renewable energy, 10 distinct case studies were considered (Table II.1). These case studies range from a baseline scenario of 100% fossil fuel-based electrification (Configuration 1 in Table II.1) to scenarios that gradually increase the integration of renewable energy sources, culminating in a scenario with complete reliance on renewables (0% fossil

fuel).

The renewable energy sources and storage systems were selected based on an analysis of the available resources in the study region, with the goal of mitigating the intermittent nature of renewable sources and the stochastic behavior of load demand. In particular, specific configurations (Configurations 4, 5, 9, and 10) were designed to explore the effectiveness of hybrid storage systems, incorporating both BES system and HES systems (HESS).

This section presents the mathematical modeling of the proposed system, covering the technical, economic, and environmental aspects of all equipment used in the 10 suggested configurations. The models developed here will serve as the foundation for evaluating the performance and feasibility of each configuration, guiding the optimization process to achieve the best possible outcomes in terms of efficiency, cost-effectiveness, and sustainability.

II.5.1 Sources modeling

II.5.1.1 PV solar power modeling

The PV cell models considered in this study are based on diode models, as illustrated in Fig. II.10 [205]. Specifically, the Single Diode Model (SDM), Double Diode Model (DDM), and Triple Diode Model (TDM) are employed, all of which have been widely used by researchers in recent years. Generally, increasing the number of diodes in the circuit enhances the accuracy of the model but also adds to its complexity. In this section, these models have been developed and evaluated under various operating conditions to assess their performance and suitability for the study's objectives.

From equivalent circuits (a,b,c) in Fig. II.10, the relationship between the output voltage and current are V and I, respectively, is expressed in eq. (II.1)

$$\begin{aligned} I &= I_{ph} - I_{sh} - \sum_{i=1}^{n_D} I_{sd_i} \\ &= I_{ph} - \frac{V + IR_s}{R_{sh}} - \sum_{i=1}^{n_D} I_{ssd_i} \left[\exp\left(\frac{q\,(V + IR_s)}{A_i k T} \right) - 1 \right] \end{aligned} \tag{II.1}$$

Where I_{ph}, I_{sh}, I_{sd_i}, and I_{ssd_i} represent the photon current, shunt resistor current, diode (i) current, and diode (i) saturation current, respectively.

R_s, R_{sh}, and n_D represent the series resistance, branch resistance, and the number of diodes in

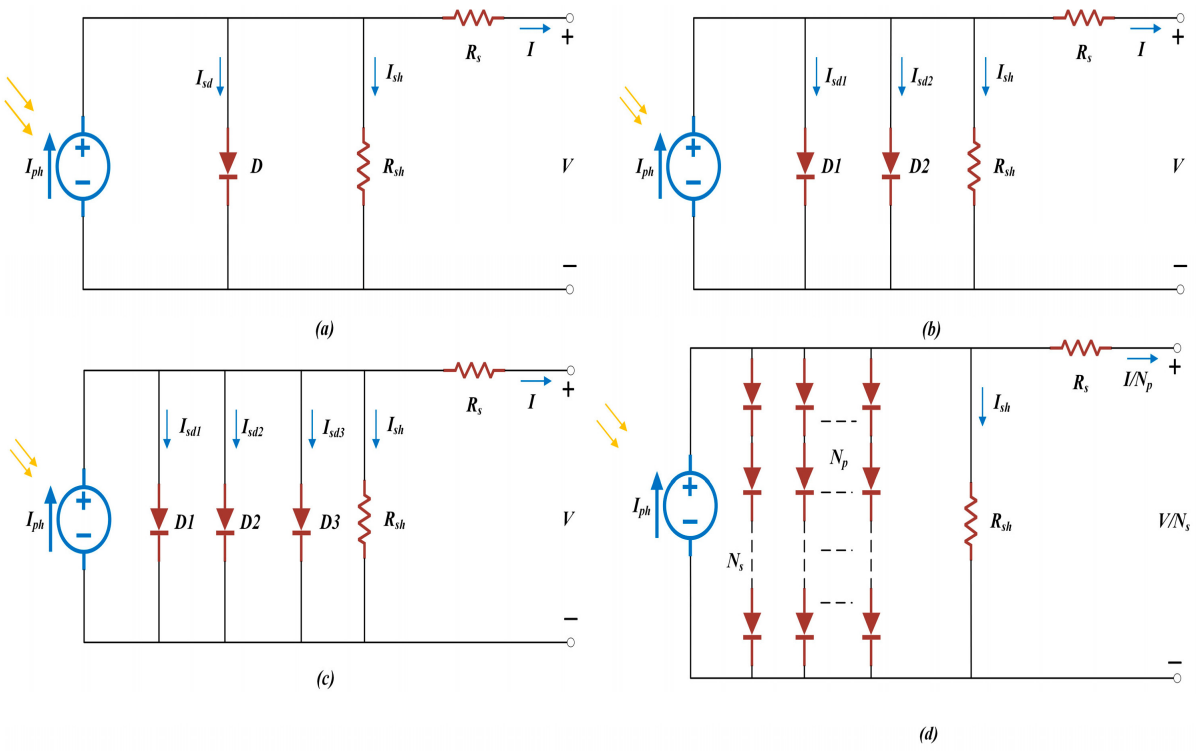

Figure II.10: PV models' circuits: (a) SDM; (b) DDM; (c) TDM; (d) PV module

the circuit, respectively.

A represents the ideality factor.

T, k, and q represent absolute temperature, the Boltzmann constant (1.3806×10^{-23} J/K), and unit charge (1.6022×10^{-19} C).

II.5.1.1.a I-V characteristics of PV module

From eq. (II.1) it is clearly apparent that the output voltage (V) of the PV module is highly dependent on its output current (I). For the objective of analyzing this characteristics under different conditions, a simulation model is developed under Matlab to evaluate the IV characteristics of JAP6-72-320/4BB solar panel (Fig. II.11). The parameters of this module are presented in Table II.2.

The relationship between the output voltage (V) and output current (I) of a PV module is a critical aspect of its performance, as indicated by eq. (II.1). To thoroughly analyze these characteristics under various conditions, a simulation model was developed using MATLAB to evaluate the I-V and P-V characteristics of the JAP6-72-320/4BB solar panel (Fig. II.11). The parameters of this PV module are detailed in Table II.2 . The equations governing the behavior of the photovoltaic (PV) module are outlined in the following set of equations eqs. (II.2) to (II.6), [1]:

$$P_{PV}(\text{hour}) = I_{PV} \cdot V_{PV} \tag{II.2}$$

$$I_{PV} = N_p \cdot I_{ph} - N_p \cdot I_s \left[\exp\left(\frac{q\left(V_{PV} + IR_s\right)}{N_s K A T_o}\right) - 1\right] \tag{II.3}$$

$$I_{ph} = \left[I_{sc} + K_i\left(T_o - T_{ref}\right)\right] \cdot \frac{G}{G_{ref}} \tag{II.4}$$

Reverse saturation current I_{rs} and Saturation current I_s is calculated by using eqs. (II.5) and (II.6):

$$I_{rs} = \frac{I_{sc}}{\exp\left(\frac{q \cdot V_{oc}}{N_s K A T_o}\right) - 1} \tag{II.5}$$

$$I_s = I_{rs}\left(\frac{T_o}{T_{ref}}\right)^3 \cdot \exp\left(\left(\frac{qE_g}{AK}\right) \cdot \left(\frac{1}{T_{ref}} - \frac{1}{T_o}\right)\right) \tag{II.6}$$

Table II.2: Photovoltaic Module Specifications

Parameter	Symbol	Value
Dimensions (LxWxH)	–	1960x991x40[mmxmmxmm]
Maximum power at STC (P_m)	P_m	320 W
Maximum power voltage (V_{mp})	V_m	36.95 V
Maximum power current ($_{mp}$)	I_m	8.66 A
Open circuit voltage (V_{oc})	V_{oc}	46.19 V
Short-circuit current (I_{sc})	I_{sc}	8.98 A
Total series cells	N_s	72
Total parallel cells	N_p	1
Ideality factor of diode	A	1.3
Cell short-circuit current temperature coefficient of I_{sc}	α	0.058%/°C
Cell open-circuit voltage temperature coefficient of V_{oc}	β	-0.330%/°C
Reference temperature	T_{ref}	25 °C
Solar Irradiance	G_{ref}	1000 W/m^2 at STC

The impact of varying solar irradiance on the I-V and P-V characteristics of the PV module is illustrated in Fig. II.12. The intensity of irradiance was varied from 200 W/m^2 to 1000 W/m^2 while

Figure II.11: Solar PV module of JAP6-72-320/4BB/RE

maintaining a constant temperature of 25°C. It was observed that the current remains steady as the voltage increases up to approximately 30 V, beyond which it begins to decrease. Additionally, an increase in irradiance intensity results in a higher current, indicating that irradiance significantly influences the short-circuit current. However, the open-circuit voltage remains relatively low, as shown in Fig. II.12. The maximum power output is clearly depicted in the power performance curves, where an increase in solar irradiance leads to a corresponding increase in power generation by the PV module.

Temperature exerts a notable influence on the output performance of the PV solar module when the irradiance intensity is held constant at $1000\,\mathrm{W/m^2}$. While the current exhibits only minor variations as the temperature fluctuates from 10°C to 70°C, the voltage demonstrates a decreasing trend in the I-V performance curve as the atmospheric temperature rises, as shown in Fig. II.13 (right). Consequently, the power output of the solar cell increases as the temperature decreases, as depicted in Fig. II.13 (left). This behavior highlights the inverse relationship between the temperature and the performance of the solar cell.

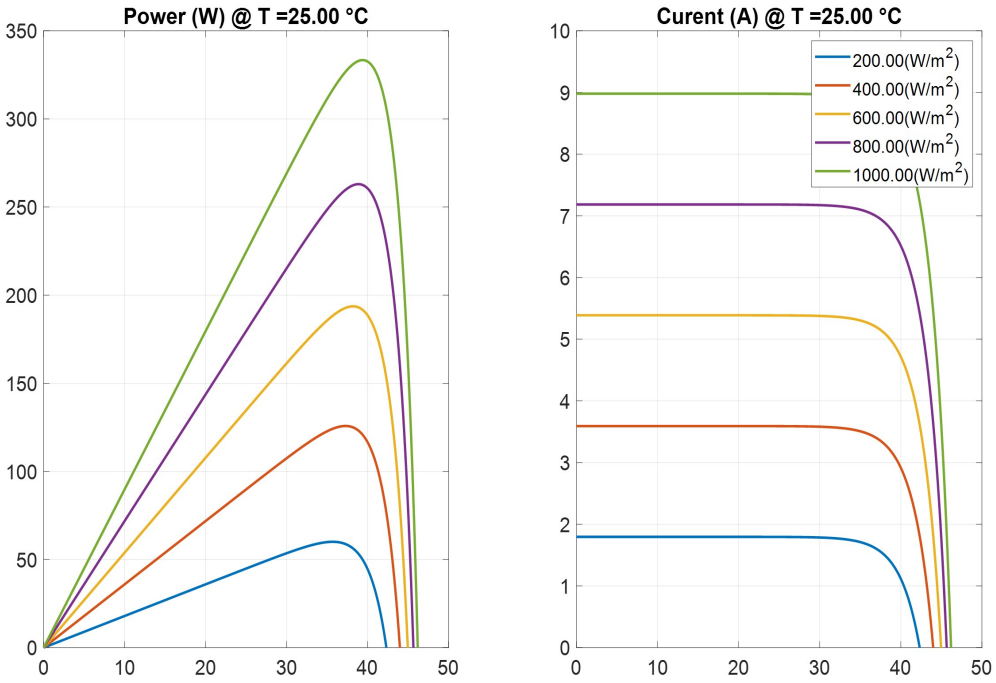

Figure II.12: P–V(left) and I-V(right) characteristics, varying solar radiation at constant temperature of 25°C.

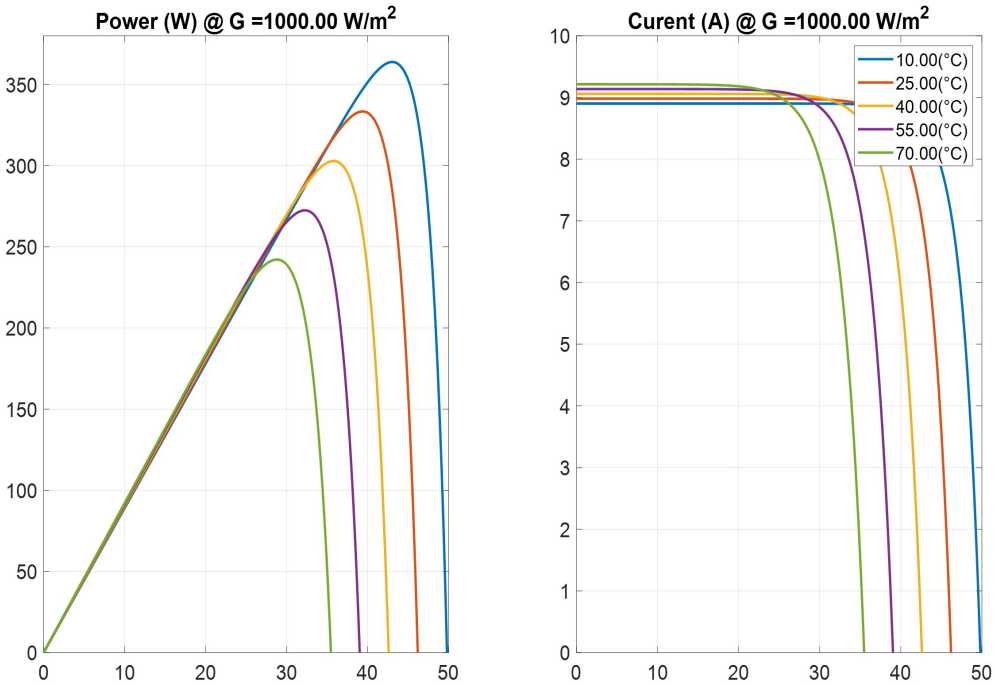

Figure II.13: P–V(left) and I-V(right) characteristics, varying temperature at constant solar radiation of 1000 W/m^2

II.5.1.1.b PV power generated in the study region

Based on climate data presented in section II.3, the power generated from one PV module of type JAP6-72-320/4BB/RE is presented in Fig. II.14

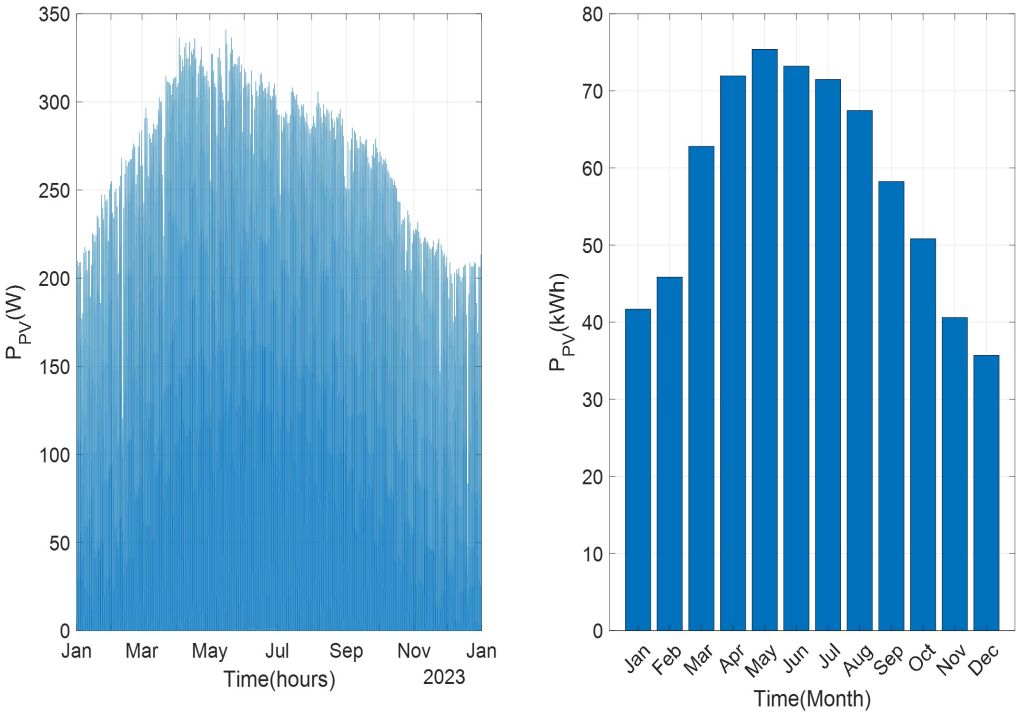

Figure II.14: hourly (left), total monthly (right) of PV power production in the study region

Fig. II.14 shows the hourly (left), total monthly (right) of PV power production in the study region based on the actual climate data. From the figure, it is clear that the region presents a high capacity of power generation from solar source especially in the summer season. However, the intermittent behaviour and the unavailability of this source are clear. In this regard, a complement source/storage become a necessity.

II.5.1.1.c PV module Parameters extraction using metaheuristic algorithm

The estimation of the PV module parameters is conducted using a metaheuristic algorithm based on measured I-V curves. This research provides a unique approach that employs a GA and PSO to find the characteristics of a solar panel. The major aim is to decrease the root mean square error (RMSE) between the measured currents and the currents that are estimated using different cell models presented in Fig. II.10. From eq. (II.1), I_{ph}, $I_{s_{ssd_i}}$, R_s, R_{sh}, and A_i are the parameters that require estimation. These characteristics offer an accurate representation of the electrical behavior

of the solar panel. The suggested approach is verified using experimental data that is gathered for a single situation of solar irradiance.

Objective function The objective function to be optimized is the Root Mean Square Error (RMSE) between the measured current I_{mes} from lab bench PV module (from the literature) and the estimated current from the 03 models developed above. The objective functions for the three models are recapitulated in eqs. (II.7) to (II.9).

Table II.3: Objective function

Objective function	Decision variables
$\text{RMSE}_1 = \sqrt{\sum_{i=1}^{N} (I_{mes}(i) - I_1(X_1)(i))^2}$ (II.7)	$X_1 = [I_{ph}, I_{ssd1}, A_1, R_s, R_{sh}]^T$
$\text{RMSE}_2 = \sqrt{\sum_{i=1}^{N} (I_{mes}(i) - I_2(X_2)(i))^2}$ (II.8)	$X_2 = [I_{ph}, I_{ssd1}, I_{ssd2}, A_1, A_2, R_s, R_{sh}]^T$
$\text{RMSE}_3 = \sqrt{\sum_{i=1}^{N} (I_{mes}(i) - I_3(X_3)(i))^2}$ (II.9)	$X_3 = [I_{ph}, I_{ssd1}, I_{ssd2}, I_{ssd3}, A_1, A_2, A_3, R_s, R_{sh}]^T$

The optimization problem is expressed as follow:

minimise $RMSE(X)$

subject to X

The upper and the lower bounds for the decision variable are presented in Table II.4

Table II.4: Lower and upper bounds for the decision variables

Parameter	Lower bound	Upper bound
R_s (Ω)	0.0	1.00
R_{sh} (kΩ)	0.10	10.00
I_{ph} (A)	3.6	6.00
I_{ss1} (μA)	10^{-3}	1000.00
I_{ss2} (μA)	10^{-3}	1000.00
I_{ss3} (μA)	10^{-3}	1000.00
A_1	1.00	3.00
A_2	1.00	3.00
A_3	1.00	3.00

Solution methods The minimization of the objective function is conducted using genetic algorithm (GA) and Particle swarm optimization (PSO) algorithms. The flow chart of the optimization process for GA is presented in Fig. II.16 [206], whereas the flowchart for the PSO algorithm is presented in Fig. II.15 [206].

Parameters extraction results and discussions The optimization process for each model and for each algorithm has been run 50 times in order to get a statistical behavior of both optimization

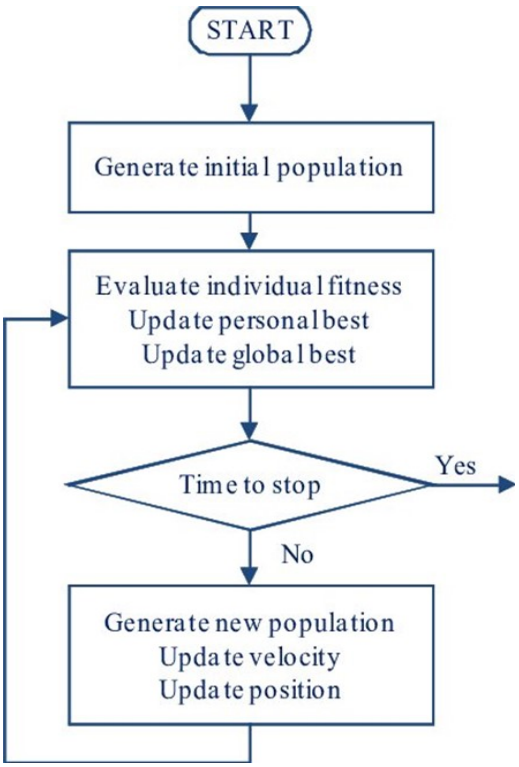

Figure II.15: PSO Flowchart

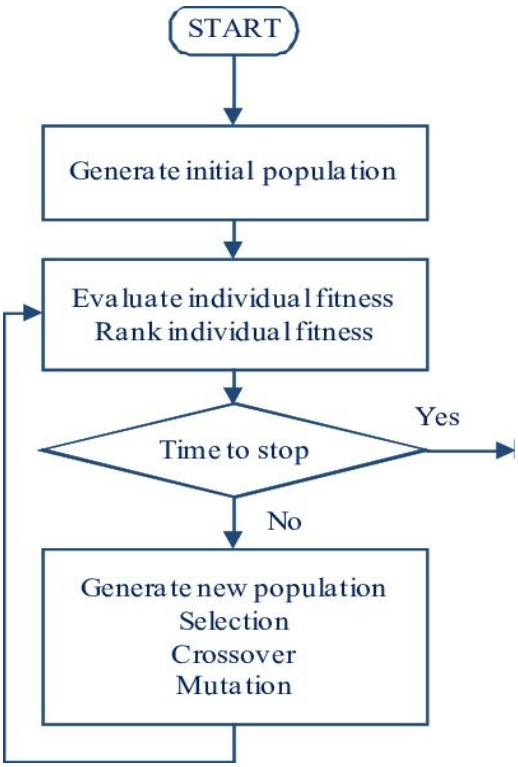

Figure II.16: GA Flowchart

techniques when applied to each model. Best, worst, mean and standard deviation for RMSE and elapsed time are recorded and presented in Table II.5.

Table II.5: Recapitulation of results after 50 optimization runs

		GA			PSO		
		SDM	DDM	TDM	SDM	DDM	TDM
$R_s(\Omega)$		0.0145	0.0394		0.3856	0.4421	
$R_{sh}(\mathrm{k}\Omega)$		9.3665	6.1465		10.00	1.49	
$I_{ph}(A)$		3.9066	3.8720	3.9073	3.8432	3.8478	3.8439
$I_{ss1}(\mu A)$		33.0680	10.8185	10.1159	0.2660	0.0030	0.2709
$I_{ss2}(\mu A)$		-	12.2589	0.2324	-	0.2631	0.4262
$I_{ss3}(\mu A)$		-	-	278.8820	-	-	0.1296
A_1		1.7099	1.5689	1.5592	1.2129	1.00	1.2143
A_2		-	2.0047	1.8124	-	1.2491	2.7581
A_3		-	-	2.9807	-	-	2.8257
RMSE(%)	best	5.4881	3.9114	4.9377	1.0164	0.7895	0.9356
	worst	20.8571	20.0861	17.9127	5.6924	6.7600	5.0558
	mean	14.1685	12.2437	10.8767	2.0549	1.7738	1.9830
	std	3.9678	3.6492	3.8247	0.9871	0.9357	0.9524
Time(s)	best	0.8650	83.6727	130.6713	0.4837	94.78	76.8896
	worst	9.3010	1151.2	1732.0	16.5894	2636.7	1987.5
	mean	1.9384	254.6078	431.317	6.0922	938.22	719.6401
	std	1.8298	232.8563	305.1968	3.6855	562.85	424.1028

Another insightful information after 50 runs of the optimization algorithms are presented in

Fig. II.17, this presentation shows that PSO surpass the GA in getting lower RMSE, when it comes to duration of the optimization process GA can give an acceptable results ($RMSE < 5\%$) with minimum time.

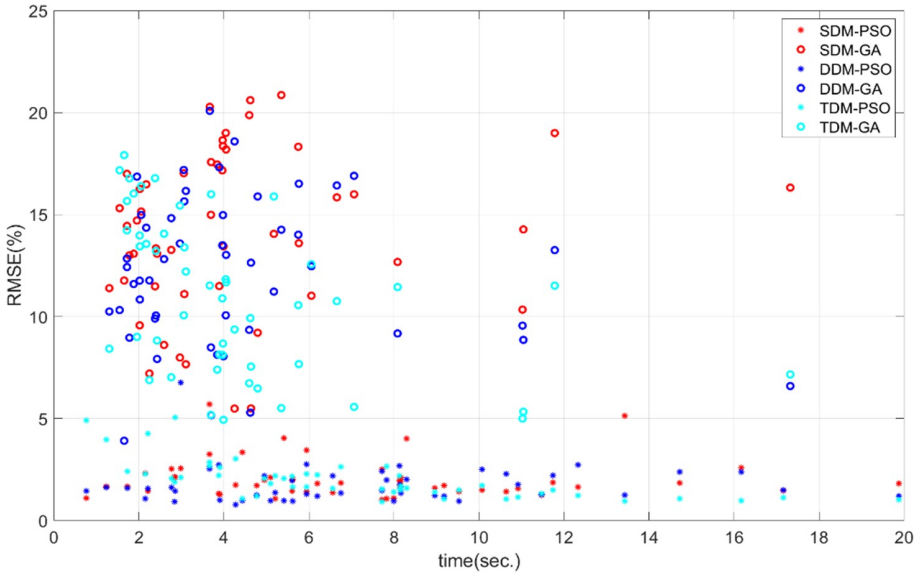

Figure II.17: 50 runs solutions

The comparison between the estimated and the measured current for each case is presented in Fig. II.18

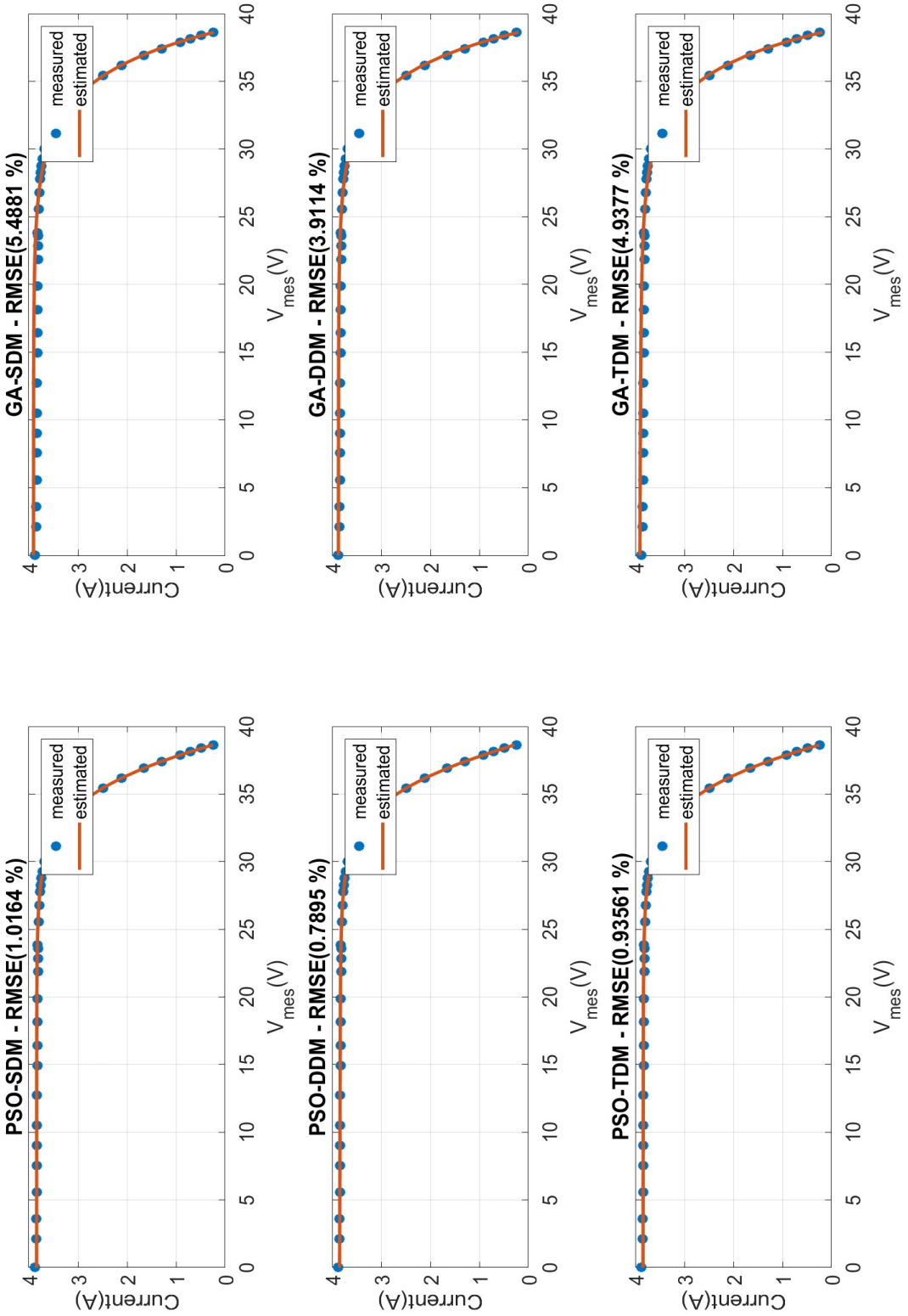

Figure II.18: measured and estimated currents

Figure II.17 shows that PSO surpass the GA in minimizing RMSE, the run time of the GA optimization process is acceptable when minimum (RMSE¡5%) is considered.

Additinally, figure II.18 presents a comparison between measured and estimated IV-curves, with an outcomes as follows: 5.49% (GA) and 1.02% (PSO) for the SDM, 3.91% (GA) and 0.79% (PSO) for the second model, and 4.94% (GA) and 0.94% (PSO) for the third model. The results show that the DDM using the PSO approach obtained greater accuracy in parameter extraction for PV module modelling. This is demonstrated by the average deviation of the estimated values from the actual measured values, confirming the efficiency of the method.

II.5.1.2 Wind Turbine (WT) power modeling

Given the wind potential in the study region, the power generated by the wind turbine is calculated using eq. (II.10) [69]

$$P_{WT}(\text{hour}) = \frac{1}{2} \times \rho \times C_{WT} \times A \times V_w^3(\text{hour}) \tag{II.10}$$

C_{WT} is the power coefficient of the wind turbine, ρ is the air density (kg.m^{-3}), and V_w is the instantaneous wind speed (m/s).

In the literature, the developed mathematical models for estimating wind energy power are highly dependent on wind velocity due to its significant variability compared to air density. In the optimization of HRES sizing, eq. (II.11) is widely used for estimating wind energy production, highlighting the critical role of wind velocity in the power output of wind turbines [137, 160, 207–209].

$$P_{WT}(t) = \begin{cases} 0, & \text{if } V_W(t) < V_{cut-in} \text{ or } V_W(t) > V_{cut-off} \\ P_r \left(\frac{V_W^3(t) - V_{cut-in}^3}{V_r^3 - V_{cut-in}^3} \right), & \text{if } V_{cut-in} < V_W(t) < V_r \\ P_r, & \text{if } V_r < V_W(t) < V_{cut-off} \end{cases} \tag{II.11}$$

Since the meteorological data for wind velocity is measured at a height of 10m, which is different from the wind turbine hub altitude, Equation II.12 [210] yields the wind velocity at turbine hub height, where H is the wind turbine hub altitude (m), $V_{w_{ref}}$ is the reference velocity (m/s) at a reference height H_{ref} (m), and α is the Hellman coefficient.

$$V_{w_H} = V_{w_{ref}} \left(\frac{H}{H_{ref}} \right)^{\alpha} \tag{II.12}$$

The Hellman exponent α, which is influenced by the coastline, the form of the ground's topography, and the air's stability, is 0.6 for this kind of terrain in stable air above populated regions [69, 211].

For the optimal selection of the wind turbine to be utilized in our study system, two different models were chosen and analyzed. These models were evaluated based on their operational ranges, specifically the cut-in speed (V_{cut-in}), cut-off speed (, $V_{cut-off}$) , and rated speed (V_r). The parameters of these wind turbine models are presented in Table II.4 [212]. Figs. II.19 and II.20 illustrate the wind velocity histogram and the Weibull distribution fit curve for the selected area, considering the hub height. The Weibull distribution factor provides a measure of the distribution of wind speeds over the course of a year. It is evident from this figure that the majority of wind velocities fall within the range of 5 to 13 m/s. Based on these parameters, Model 1, with a rated speed of 8.5 m/s, was selected as the most suitable option for this study.

Table II.6: WT chosen models for the system study

Parameter	**Model 1 [69]**	**Model 2: Bergey Wind Power's BWC Excel-R/48 [209]**
Rated capacity, P_r (kW)	20	7.5
Cut-in speed, V_{cut-in} ($m.s^{-1}$)	2.75	3.1
Rated speed, V_r ($m.s^{-1}$)	8.5	13.8
Cut-out speed, $V_{cut-off}$ ($m.s^{-1}$)	20	15.6
Hub height, H (m)	36	18
Capital Cost ($)	50 000	19 400

The power generated by WT (model 1) based on the wind speed of the selected study area is presented in Fig. II.21.

II.5.1.3 Gas turbine modeling

In the reference system (Case Study 1 in Table II.1) and HRES Case Studies 6 to 10 (Table II.1), Gas Turbines (GT) are integral components. To accurately model the fuel consumption of these turbines, a fuel consumption curve is utilized. In practice, the fuel consumption of a GT can be divided into two components: one component is associated with the rated power and accounts for the fuel consumed by cooling systems and auxiliary equipment, which remains constant regardless of the generator's output power. The second component of fuel consumption is directly related to the operational power output, varying in correlation with the actual operating power of the generator.

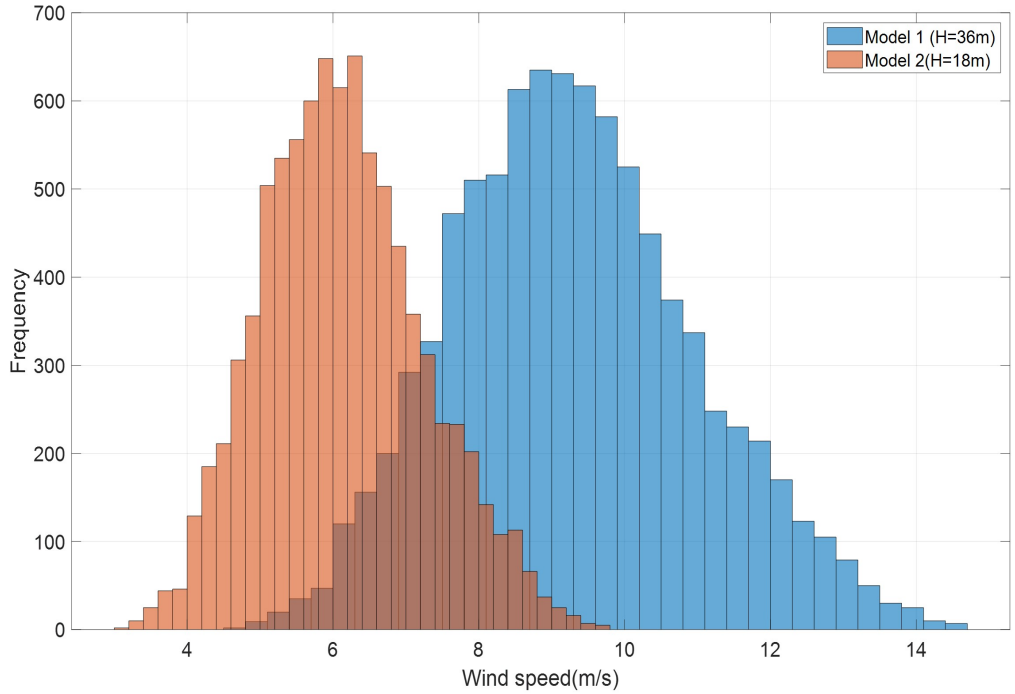

Figure II.19: Wind speed (at Hub height) frequency for selected WT models

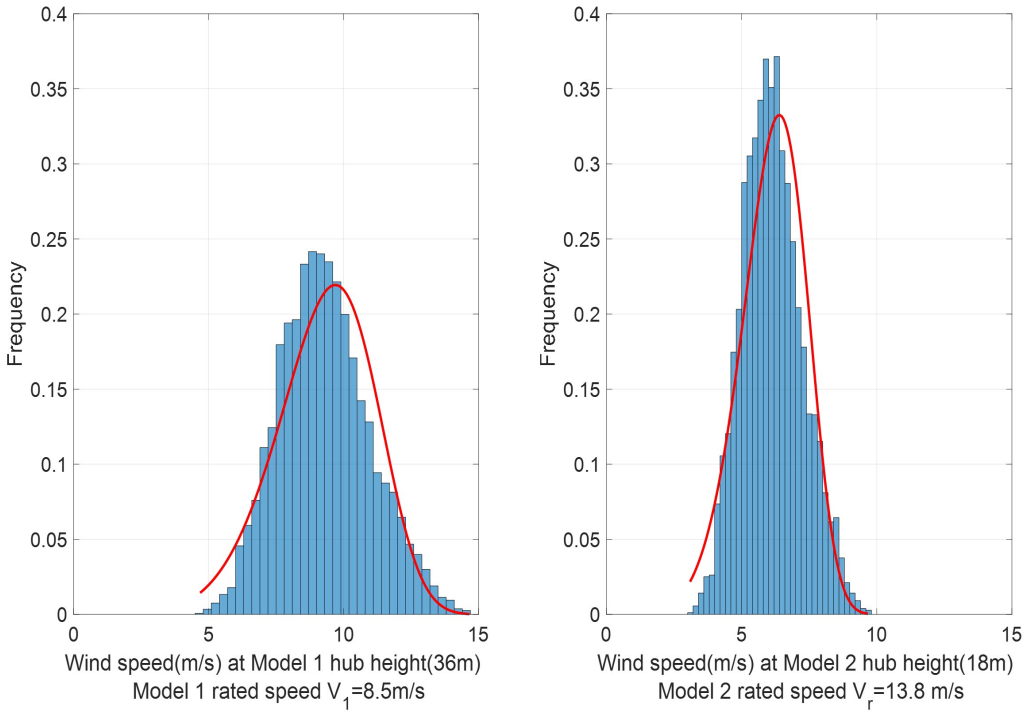

Figure II.20: Wind speed (at Hub height) frequency for selected WT models

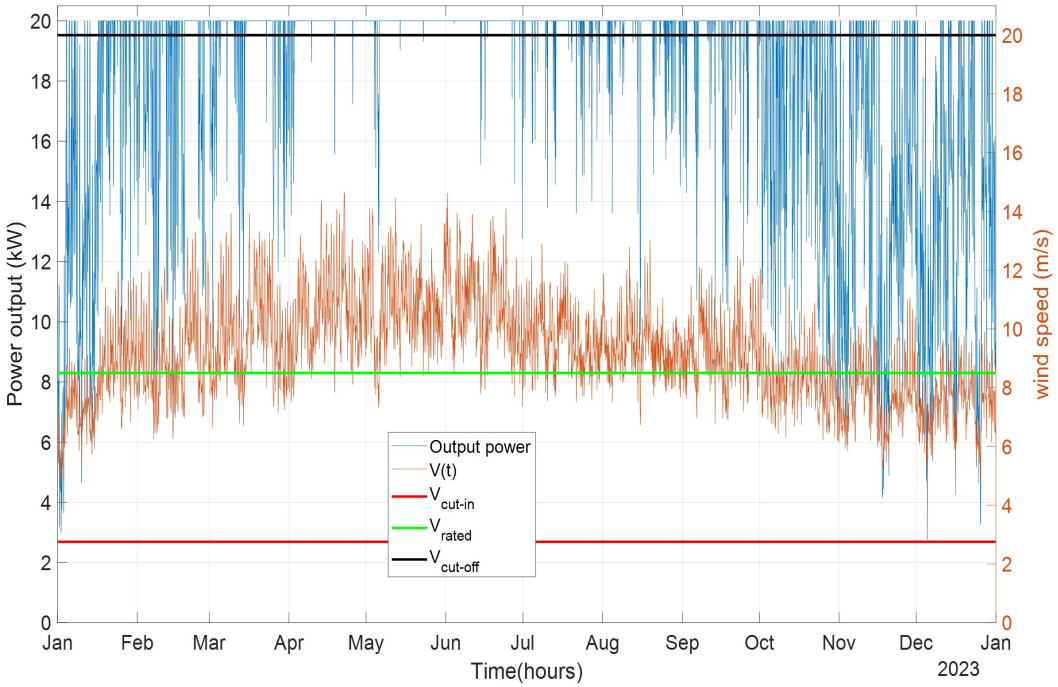

Figure II.21: Output power generated by WT (model 1) based on the wind speed at Hub height

eq. (II.13) is used to determine the fuel consumption of the GT:

$$fc_{GT}(t) = f_1 \times P_{rGT} + f_2 \times P_{GT}(t) \tag{II.13}$$

Where f_1 ($m^3h^{-1}.kW^{-1}$) and f_2 ($m^3h^{-1}.kW^{-1}$) are the fuel curve intercept coefficient and the slope, respectively. P_{rGT} and $P_{GT}(t)$ are the rated power and the hourly power generation of the MGT generator, respectively. All GT system parameters are presented in Table II.7.

The efficiency of the Gas Turbine (GT) can be calculated using the Higher Heating Value of Natural Gas (HHV_{NG}), as described in eq. (II.14). Fig. II.22 illustrates the relationship between efficiency and power output for the GT. From this curve, it is evident that the GT operates more efficiently when it is closer to its rated power. This emphasizes the importance of optimizing the GT's operational strategy to maintain performance near its rated capacity, thereby maximizing fuel efficiency and minimizing operational costs.

$$\eta_{GT}(t) = \frac{P_{GT}(t)}{fc_{GT}(t) \times HHV_{NG}} \tag{II.14}$$

Table II.7: GT system parameters

Parameter	Value
Rated Power P_{rGT} (kW)	20 000
Fuel curve intercept coefficient f_1 ($m^3h^{-1}.kW^{-1}$)	0.05
Fuel curve slope f_2 ($m^3h^{-1}.kW^{-1}$)	0.29
Higher Heating Value of Natural Gas HHV_{NG} (MJ/m^3)	32.5

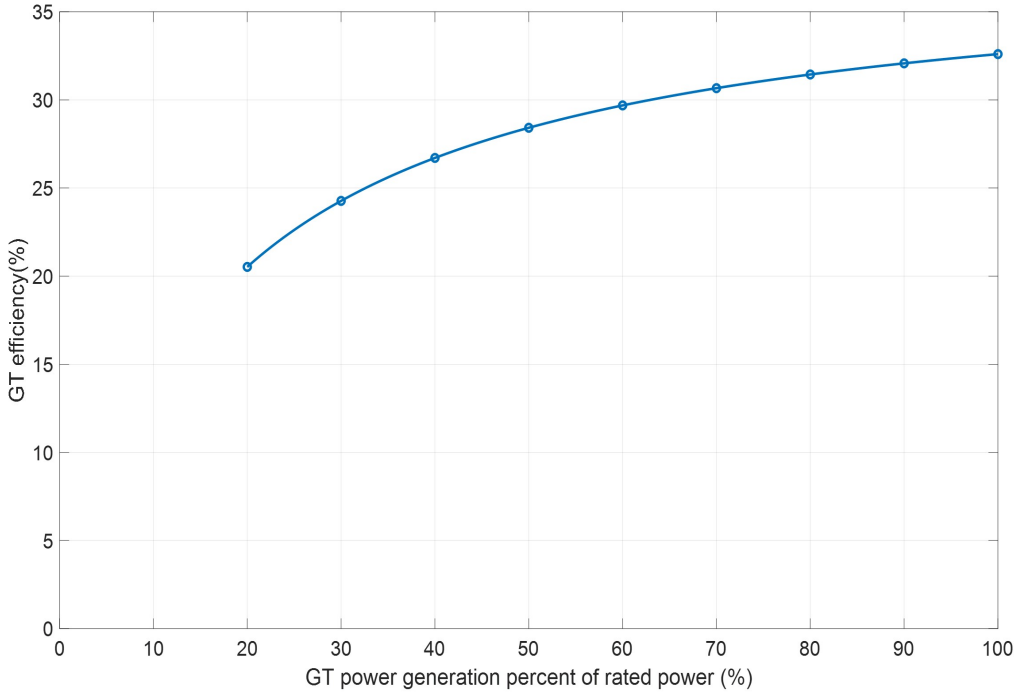

Figure II.22: Efficiency vs power curve for GT

II.5.2 Storage modeling

The storage system plays a critical role in balancing the energy generated from sources with the power demand from varying loads. At any given time, t during the evaluation of the HRES, the storage system may either be charged or discharged, depending on the power difference between generation and consumption. Based on the system configurations presented in Table 1, two types of storage systems are considered in this study: BES and Hydrogen-based Energy Storage (HES). These storage systems are integral to ensuring the stability and reliability of the HRES by managing the intermittency of renewable energy sources and the stochastic nature of load demands.

II.5.2.1 Battery Energy Storage (BES) modeling

BES systems utilize electrochemical conversion to store electrical energy during periods of surplus generation by converting it into chemical energy. During periods of energy deficit, when generation cannot meet consumption, the stored chemical energy is converted back into electrical energy to supply the load. Two critical parameters that must be considered during the modeling process are the actual BES capacity $C_{BES}(t)$ and the State of Charge SoC(t). These parameters can be determined using eq. (II.15), which calculate the BES capacity and state of charge based on the charging and discharging energy at each time step and the previous BES capacity $C_{BES}(t-1)$. These equations are fundamental for accurately modeling the performance and behavior of the BES system over time.

$$C_{BES}(t) = C_{BES}(t - \Delta t) \times (1 - \sigma_{BES}) + C_{BES}^{char}(t) - C_{BES}^{dischar}(t) \tag{II.15}$$

σ_{BES} is the parameter that quantifies the self-discharge of BES during time and is expressed as a percentage of capacity per time step (in this study $\sigma_{BES} = 5.7870 \cdot 10^{-5}\%/hour$ which means a 50% self discharge each year. $C_{BES}^{char}(t)$ and $C_{BES}^{dischar}(t)$ are the charging and discharging capacities at time t, and are expressed by eqs. (II.16) and (II.17):

$$C_{BES}^{char}(t) = \eta_{BES}^{char} \times P_{BES}^{char}(t) \times \Delta t \tag{II.16}$$

$$C_{BES}^{dischar}(t) = \frac{P_{BES}^{dischar}(t)}{\eta_{BES}^{dischar}} \times \Delta t \tag{II.17}$$

Where $P_{BES}^{char}(t)$ and $P_{BES}^{dischar}(t)$ are the BES charging and discharging power at time t. η_{BES}^{char} and $\eta_{BES}^{dischar}$ are the charging and discharging efficiencies of the BES system. Δt is the time step size; in our case, for hourly simulation, $\Delta t = 1$ hour.

To ensure the physical feasibility of the storage system, the state of the BES must always remain within a specific range. This range is defined by the maximum capacity ($C_{BES-max}$) and minimum capacity ($C_{BES-min}$) of the BES. Typically, $C_{BES-max}$ represents the nominal capacity of the entire BES system, which can be expressed using the following equation (eq. (II.18)):

$$C_{BES-max} = N_{Bat} \times C_{Bat-nom} \tag{II.18}$$

Where N_{Bat} is the total number of battery accumulators in the BES system, and $C_{Bat-nom}$ is the nominal capacity of a single battery accumulator.

$$C_{BES-min} \leq C_{BES}(t) \leq C_{BES-max} \tag{II.19}$$

The condition in eq. (II.19) is crucial for defining the upper limit of the storage system's capacity, ensuring that the BES operates within safe and efficient parameters throughout its use.

The State of Charge (SoC) of the BES system can be expressed as the percentage of the available capacity $C_{BES}(t)$ relative to the maximum allowed capacity $C_{BES-max}$. It is essential that the SoC remains within specified upper and lower limits to ensure the safe and efficient operation of the BES. The SoC and its limit conditions can be mathematically expressed as follows:

$$SoC(t) = \frac{C_{BES}(t)}{C_{BES-max}} \tag{II.20}$$

$$SoC_{min} \leq SoC(t) \leq SoC_{max} \tag{II.21}$$

This SoC must satisfy the following conditions:

Where SoC_{min} and SoC_{max} represent the minimum and maximum allowable state of charge, respectively. These conditions ensure that the battery operates within a safe range, preventing over-charging or deep discharging, which can affect the battery's lifespan and performance.

Another important parameter is the Depth of Discharge (DoD) of the BES system. The DoD is defined as the maximum allowable State of Charge (SoC) that can be utilized during the discharge process, as described in eq. (II.22). This parameter is significant because it directly impacts the number of charge-discharge cycles the battery can undergo, thereby influencing the overall health and lifespan of the battery. Proper management of the DoD is essential to ensure the longevity and efficiency of the BES system within the HRES.

$$DoD = SoC_{max} - SoC_{min} \tag{II.22}$$

Equation eq. (II.22) can be used to determine the values of SoC_{max}, SoC_{min}, and $C_{BES-min}$, and these parameters are calculated as follows eqs. (II.23) to (II.25):

$$SoC_{max} = \frac{C_{BES-max}}{C_{BES-max}} = 1 \tag{II.23}$$

$$SoC_{min} = 1 - DoD \tag{II.24}$$

$$C_{BES-min} = SoC_{min} \times C_{BES-max} = (1 - DoD) \times C_{BES-max} \tag{II.25}$$

The data used for the BES modelling are presented in Table C.1.

II.5.2.2 Hydrogen-based Energy Storage (HES)

The Hydrogen-based Energy Storage (HES) system is considered in several case studies (specifically, cases 2 and 4-10 in Table II.1). Like the BES system, the primary objective of the HES is to mitigate the intermittency of renewable energy generation and the variability of energy consumption. However, unlike BES, HES relies on the chemical conversion of energy between electricity and hydrogen. The HES process involves generating hydrogen (H_2) through water electrolysis during periods of surplus energy generation. The stored hydrogen can then be converted back into electrical energy as needed through the reverse process, utilizing a Fuel Cell (FC). One of the key advantages of HES is its lack of self-discharge over time, making it a promising option for renewable energy storage. However, it is important to note that the round-trip (charge-discharge) efficiency of HES is generally lower compared to BES. As outlined in section II.2.2, the HES system comprises Electrolyzers (EL), Fuel Cells (FC), and Hydrogen Storage Tanks (ST). The detailed modeling of these components will be presented in the subsequent sections.

II.5.2.2.a Electrolyzer modeling

In an off-grid, PV-dominant hybrid renewable energy system for Southern Algeria, PEM electrolyzers are preferable over alkaline and SOEC electrolyzers. With a more satisfactory dynamic response, they are better able to respond to unexpected shifts in the availability of renewable energy, allow optimal utilization, and minimize downtime—vital as the latter is based on renewable sources which have intermittent characteristics. Additionally, their small size makes them ideally adapted to rural

locations with limited space compared to larger alternatives. PEM electrolyzers also have the ability to generate high-purity hydrogen, which reduces the need for large-scale post-processing, hence being particularly useful in the oil and gas industry. Furthermore, the ability to operate effectively without a continuous grid supply means that they are ideally suited for the handling of renewable energy variability, further supporting their use for this project[213].

A PEM electrolyzer cell schematic diagram is shown in Fig. II.23 . The PEM electrolyzers uses typically a solid electrolyte to conduct H^+ ions. The overall chemical reaction mechanism the incolves PEM electrolyzer are presented in eq. (II.26). The performance of the electrolyzer is typically characterized by its current–voltage (I-V) characteristic curve, which is obtained from experimental measurements. The modeling of a PEM electrolyzer can be approached both non-linearly and linearly, with the resulting models being well-suited to curve-fitting based on experimental data. This modeling approach ensures accurate representation of the electrolyzers behavior under various operating conditions.

$$\begin{aligned} &\text{Anode:} \quad 2H_2O \rightleftharpoons O_2 + 4H^+ + 4e^- \\ &\text{Cathode:} \quad 4H^+ + 4e^- \rightleftharpoons 2H_2 \end{aligned} \tag{II.26}$$

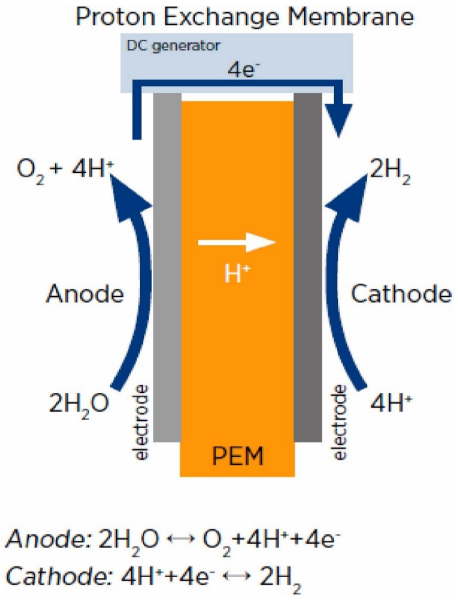

Figure II.23: PEM electrolyzer schematic diagram

The amount of hydrogen produced ($\dot{m}_{H2}(t)\,[kg/h]$), through water electrolysis depends on the current that passes through it based on the first Law of Faraday [214].

$$\dot{m}_{H_2}(t) = \eta_F \times n_c \times \frac{I_{EL}(t)}{Z \times F} \times M_{H_2} \times 3600 \tag{II.27}$$

Where $I_{EL}(t)$ is the current supplied to the electrolyzer (in A). The parameters presented in eq. (II.27) are described in Table II.8.

Table II.8: Parameters for electrolyzer model

Parameter (unit)	Description (value)
η_F (%)	The Faraday efficiency, typically equal to 97% [215]
n_c (-)	The number of PEM electrolyzer cell stacks
R ($J{\cdot}mol^{-1}{\cdot}K^{-1}$)	The gas constant, 8.314 $J{\cdot}mol^{-1}{\cdot}K^{-1}$
F ($C{\cdot}mol^{-1}$)	The Faraday constant, 96 485 C/mol
Z (-)	The excess number of electrons, which is 2 for hydrogen

I-V characteristic of PEM electrolyzer To accurately predict the amount of hydrogen produced by the electrolyzer, it is essential to determine the Current-Voltage (I-V) characteristics of the electrolyzer cell, as described in eq. (II.27). The I-V relationship is crucial for calculating the cell's current and voltage, which are key factors in hydrogen production. The I-V characteristics of the electrolyzer are represented by a highly non-linear model, expressed by eq. (II.28) [216, 217]. The coefficients in this model can be estimated through curve fitting techniques based on experimental data, allowing the model to closely match the actual performance of the electrolyzer under various operational conditions.

$$V_{ele}(t) = V_{nernst} + \frac{r_1 + r_2 T_{ele}}{A_{ele}} \times I_{EL}(t) + \left(s_1 + s_2 T_{ele} + s_3 T_{ele}^2\right) \times \log\left(\frac{t_1 + \frac{t_2}{T_{ele}} + \frac{t_3}{T_{ele}^2}}{A_{ele}} \times I_{EL}(t) + 1\right) \tag{II.28}$$

r_i, s_i, and t_i are the model parameters to be determined by curve fitting based on experimental I-V data (see Table B.1. $V_{ele}(t)$, V_{nernst}, T_{ele}, and A_{ele} denote the operation and Nernst voltages (V), the operating temperature (°C), and the electrode area (m^2), respectively.

The Nernst voltage depends on the temperature and pressure of the anode and cathode and can be calculated using eqs. (II.29) to (II.31) [216].

$$V_{nernst} = 1.229 - 0.85 \times 10^{-3} \times (T_{ele} - 25) + 4.3085 \times 10^{-5} \times (T_{ele} + 273.15) \times \log\left(P_{H_2} \times \sqrt{P_{O_2}}\right) \tag{II.29}$$

$$P_{H_2} = \frac{0.5 \times RH_a \times P_{H2O_{sat}}}{\left(RH_a \times \frac{P_{H2O_{sat}}}{P_{anode}}\right) \times \exp\left(\frac{1.635 \times \left(\frac{I_{EL}(t)}{A_{ele}}\right)}{(T_{ele}+273.15)^{1.334}}\right)} - 1 \tag{II.30}$$

$$P_{O_2} = \frac{0.5 \times RH_c \times P_{H2O_{sat}}}{\left(RH_c \times \frac{P_{H2O_{sat}}}{P_{cathode}}\right) \times \exp\left(\frac{4.192 \times \left(\frac{I_{EL}(t)}{A_{ele}}\right)}{(T_{ele}+273.15)^{1.334}}\right)} - 1 \tag{II.31}$$

The evolution of the cell I-V characteristic of PEM electrolyzer is presented in Fig. II.24.

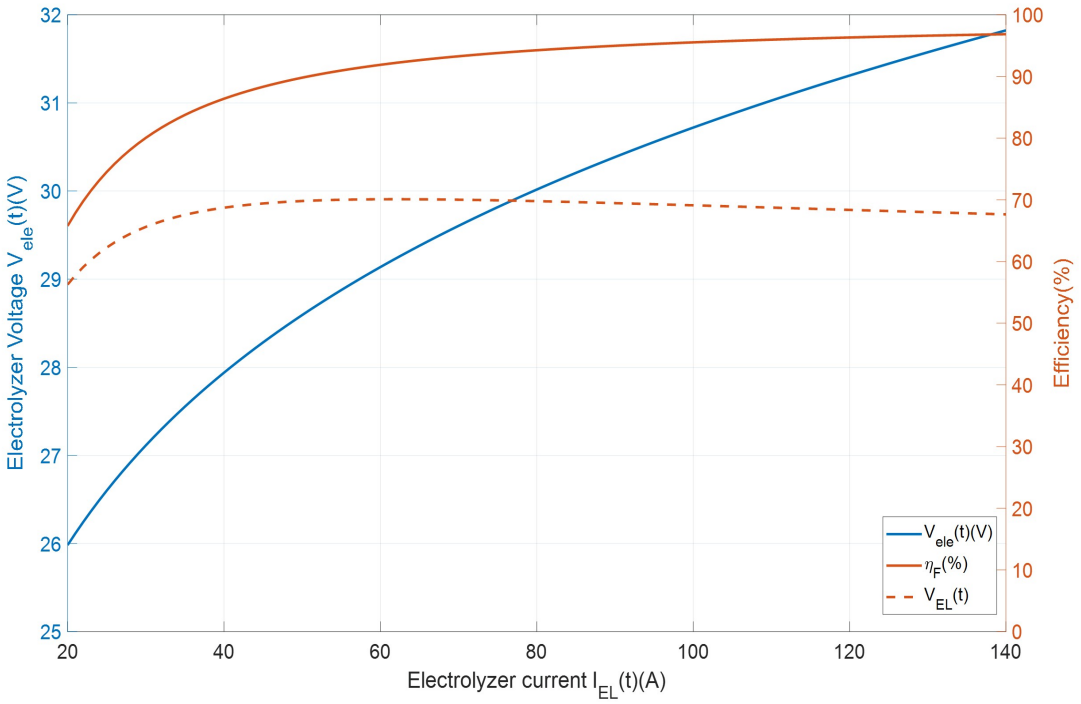

Figure II.24: PEM electrolyzer characteristics

Efficiency and Faraday Efficiency of PEM Electrolyzer The final step in electrolyzer modeling involves evaluating the efficiency of the device. Typically, the efficiency of an electrolyzer is defined as the ratio of the energy produced to the energy consumed. The produced energy is derived from the higher heating value (HHV) of the hydrogen generated, while the consumed energy is the electrical energy required for the electrolysis process. This efficiency metric is crucial for assessing the overall performance and viability of the electrolyzer within the energy storage system. The interpolated current–voltage (I-V) characteristic driven from the model represented by eq. (II.29) and visually depicted in Fig. II.24 as presented by [1, 216]. Before calculating the hydrogen production using eq. (II.27), it is necessary to estimate the Faraday efficiency η_F. As indicated in Table II.8, the

typical value of η_F is approximately 97% [215]. However, it is important to note that the Faraday efficiency is significantly influenced by the operating temperature of the electrolyzer. This temperature dependency can be expressed mathematically in eq. (II.32) [217].

$$\eta_F = B_1 \times \exp\left(\frac{B_2 + B_3 \times T_{ele} + B_4 \times T_{ele}^2}{\left(\frac{I_{EL}(t)}{A_{ele}}\right)} + \frac{B_5 + B_6 \times T_{ele} + B_7 \times T_{ele}^2}{\left(\frac{I_{EL}(t)}{A_{ele}}\right)^2}\right) \tag{II.32}$$

Where $B_i = [99.5, -9.5788, -.0555, 0, 1502.7083, -70.8005, 0]$; for $i = 1, 2, ..., 7$

The efficiency of the electrolyzer η_{EL} is than calculated using the $HHV_{H_2} = 39.39\ kWh/kg$, is expressed in eq. (II.33):

$$\eta_{EL} = \frac{\dot{m}_{H_2}(t) \times \Delta t}{P_{EL}(t)} \times HHV_{H_2} \tag{II.33}$$

II.5.2.2.b Fuel Cell modeling

As mentioned in the previous section, the Fuel Cell (FC) operates in a manner that is the reverse of the electrolyzer (EL). The Fuel Cell is activated when there is a deficit in generation relative to load demand, allowing it to convert stored hydrogen back into electricity. However, the operation of the FC is dependent on the availability of sufficient hydrogen in the Hydrogen Storage Tank (ST). In this study, a Proton Exchange Membrane Fuel Cell (PEMFC) is utilized. The schematic of the PEMFC, as described by [218] , is presented in Fig. II.25. The semi-empirical mathematical model for this equipment is described by the following paragraphs. The output voltage of a single PEMFC typically ranges from 0.9 to 1.23V, excluding entropy and irreversibility losses. To achieve a higher voltage, multiple cells are connected in series. On a standard current-voltage polarization curve for a PEMFC, the voltage initially drops sharply due to activation losses, then decreases more gradually and linearly because of Ohmic resistance. At high load conditions, the voltage declines more rapidly again, driven by diffusion over-potential. The total output voltage of a PEMFC stack is calculated using eq. (II.34) [218].

$$V_{FC}(t) = n_{c_{fc}} \times (V_{rev,fc} - V_{act,fc} - V_{ohm,fc} - V_{con,fc}) \tag{II.34}$$

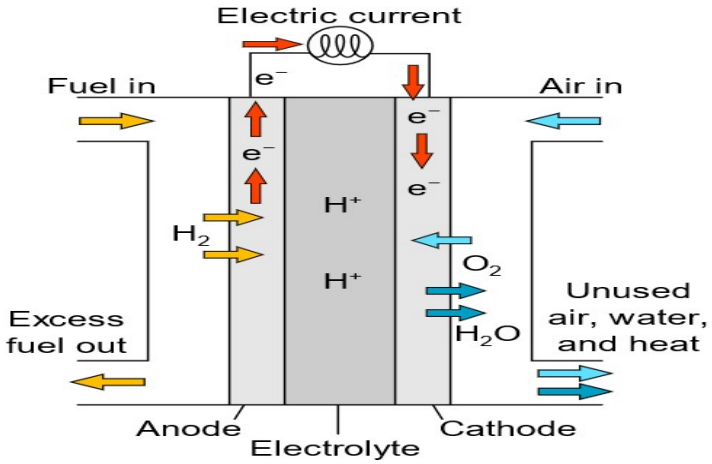

Figure II.25: PEM fuel cell Schematic

$n_{c_{fc}}$ is the number of cells connected in series for the FC stuck and V_{rev}, V_{act}, V_{ohm} and V_{con} are open circuit voltage, voltage drop due to activation over potential, voltage drop due to ohmic loss over cell and the connection over-potential drop per cell. These voltages are calculated using eqs. (II.35) to (II.42) [218].

$$V_{rev,fc} = 1.229 - 0.85 \times 10^{-3} \times (T_{fc} - 298.25) + 4.3085 \times 10^{-5} \times T_{fc} \times \ln\left(P_{H_2} \times \sqrt{P_{O_2}}\right) \tag{II.35}$$

$$P_{H_2} = \frac{RH_a \cdot P_{H_2O}}{2}\left[\frac{1}{\left(\frac{RH_a \cdot P_{H_2O}}{P_a} \cdot \exp\left(\frac{1.635 I_{fc}/A}{T_{fc}^{1.334}}\right)\right)} - 1\right]$$

$$P_{O_2} = RH_c \cdot P_{H_2O}\left[\frac{1}{\left(\frac{RHc \cdot P_{H_2O}}{Pc} \cdot \exp\left(\frac{4.192 I_c/A}{T_{fc}^{1.334}}\right)\right)} - 1\right]$$

$$P_{H_2O} = 2.95 \cdot 10^{-2}(T_{fc} - 273.15) - 9.18 \cdot 10^{-5}(T_{fc} - 273.15)^2 + 1.44 \cdot 10^{-7}(T_{fc} - 273.15)^3 - 2.18 \tag{II.36}$$

$$v_{act,fc} = -\left[\xi_1 + \xi_2 T_{fc} + \xi_3 T_{fc} \ln(C_{O_2}) + \xi_4 T_{fc} \ln(I_{fc})\right] \tag{II.37}$$

$$\xi_2 = 2.86 \cdot 10^{-3} + 2 \cdot 10^{-4} \ln(A_{fc}) + 4.3 \times 10^{-5} \ln(C_{H_2}) \tag{II.38}$$

$$\begin{aligned} C_{O_2} &= \frac{P_{O_2}}{5.08 \cdot 10^6} \cdot \exp\left(\frac{498}{T_{fc}}\right) \\ C_{H_2} &= \frac{P_{H_2}}{1.09 \cdot 10^6} \cdot \exp\left(\frac{-77}{T_{fc}}\right) \end{aligned} \tag{II.39}$$

$$V_{ohm,fc} = I_{fc}\,(R_m + R_c)\,; \quad R_m = \frac{\rho_m l}{A} \tag{II.40}$$

$$\rho_m = \frac{181.6\left[1 + 0.03\left(\frac{I_{fc}}{A}\right) + 0.062\left(\frac{T_{fc}}{303}\right)^2\left(\frac{I_{fc}}{A}\right)^{2.5}\right]}{\left[\lambda - 0.634 - 3\left(\frac{I_{fc}}{A_{fc}}\right)\right]\exp\left(4.18 \cdot \frac{T_{fc}-303}{T_{fc}}\right)} \tag{II.41}$$

$$v_{con} = -\beta \cdot \log\left(\frac{J_{max} - J}{J_{max}}\right) \tag{II.42}$$

Since the working principal of fuel cell is similar to the electrolyzer, and in order to evaluate the I-V curve and efficiency of fuel cell, eq. (II.43): can be used. The hydrogen consumption of the fuel cell can be calculated using the Faraday law as expressed in eq. (II.44) [218]:

$$\eta_{FC} = \frac{P_{FC}(t)}{\dot{m}_{H_2}(t) \cdot HHV_{H_2}} \tag{II.43}$$

$$\dot{m}_{H_2}(t) = n_{c_{fc}} \cdot \frac{I_{fc}(t)}{Z \cdot F \cdot \eta_F} \cdot M_{H_2} \cdot 3600 \text{ [kg/h]} \tag{II.44}$$

Figure II.26 presents the I-V characteristics as well as the efficiency of FC based on the parameters presented in Table II.9.

Table II.9: FC Parameters

Parameter (value)	Description
$n_{c_{fc}} = 14$	Number of cells connected in series
$A_{fc} = 300$ cm^2	Cell Area
$P_{n_{fc}} = 4.5$ kW	Rated power of FC
$RH_a = 1, RH_c = 1$	Relative humidity (anode/cathode)
$M_{\text{hydrogen}} = 2.01588 \times 10^{-3}$ kg/mol	Molar mass of hydrogen
$T_{fc} = 35°$C	Fuel cell operating temperature
$\beta = 108 \times 10^{-4}$	Empirical coefficient

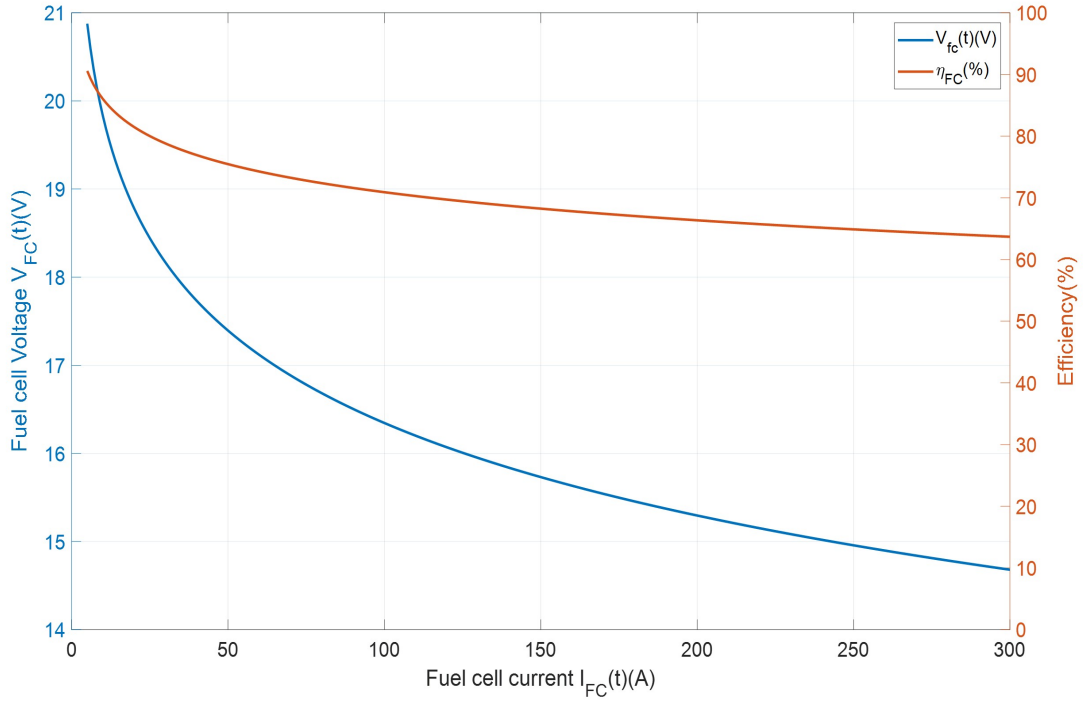

Figure II.26: PEM fuel cell Schematic

II.5.2.2.c Hydrogen storage tank (ST) modeling

The hydrogen tank is used to balance hydrogen production-consumption during the function of EL and FC. In our study we consider medium pressure hydrogen tank as a storage mean for hydrogen production/consumption. The Quantity of Hydrogen $Q_{H_2}(t)\,[kg]$, available in the tank at time t depends on the previous quantity $Q_{H2}(t-\Delta t)$ and the amount of hydrogen produced/consumed by EL/ FC respectively. This quantity is expressed by expressed using the mass conservation principal (eq. (II.45)):

$$Q_{H2}(t) = Q_{H2}(t-\Delta t) + \Delta t \cdot \begin{cases} \dot{m}_{H2_{produced}}, & \text{if Excess of production (Eq. eq. (II.27))} \\ -\dot{m}_{H2_{consumed}}, & \text{if Lack of production (Eq. eq. (II.44))} \end{cases} \tag{II.45}$$

II.5.3 Economic modeling of HRES

In this study, the economic performance is evaluated using the COE metric. This indicator is calculated by taking the ratio of the annualized cost of the system (ACS) to the total annual energy production (TAEP) generated by the proposed system (eq. (II.46)), ensuring that the electrical load demand is

consistently met [1, 35].

The annual cost of the system (ACS) as expressed in eq. (II.47) encompasses the capital expenditure (CAPEX), replacement costs, and operation and maintenance expenses (OPEX), all of which are converted into their respective annual values:

$$COE = \frac{ACS}{TAEP} \tag{II.46}$$

$$ACS = Ca_{cap} + Ca_{rep} + Ca_{o\&m} \tag{II.47}$$

Where $Ca_{cap}, Ca_{rep}, Ca_{om}$ represent the annual capital cost, replacement cost, and operation and maintenance cost, respectively. The capital cost is converted to its annual value using the Capital Recovery Factor (CRF). The CRF is a ratio used in determining the present value of a series of equivalent annual cash flows. The conversion between annual and total costs is expressed in eq. (II.48)) [1]:

$$\begin{cases} Ca_{cap} = CRF \cdot CAPEX \quad \text{and} \quad Ca_{o\&m} = CRF \cdot OPEX \\ CRF = \frac{\gamma(1+\gamma)^{N_{sys}}}{(1+\gamma)^{N_{sys}}-1} \end{cases} \tag{II.48}$$

Where N_{sys} is the lifespan of the system (in years), and γ is the actual interest rate and it can be determined using the formula in eq. (II.49):

$$\gamma = \frac{i-f}{1+f} \tag{II.49}$$

In eq. (II.49), i and f represent the nominal interest rate and the inflation rate, respectively. Similarly, to convert the replacement cost into its annual value, the Sinking Fund Factor (SFF) is used, which is calculated using the actual interest rate γ and equipment lifetime $LT(in\ years)$ (eq. (II.50)):

$$SFF = \frac{\gamma}{(1+\gamma)^{LT}-1} \tag{II.50}$$

The total replacement cost of each component (TC_{rep}) is then converted to its annual value (Ca_{rep})) using the eq. (II.51):

$$Ca_{rep} = SFF \cdot TC_{rep} \tag{II.51}$$

II.5.3.1 BES life estimation

A specific economic model for the annual replacement cost of the BES ($Ca_{rep-BES}$). In fact, as stated in section II.5.2.1 (eq. (II.22)), the lifetime of batteries expressed as the total cycle to failure and is highly dependent to the DoD (eq. (II.52)) as shown in Fig. II.27 [219]. The actual lifetime of the BES is expressed in eq. (II.52))

$$\text{BES}_{\text{cycle-to-failure}} = 1188.32 \times (\log(DoD))^2 - 11123.09 \times \log(DoD) + 27158.74 \tag{II.52}$$

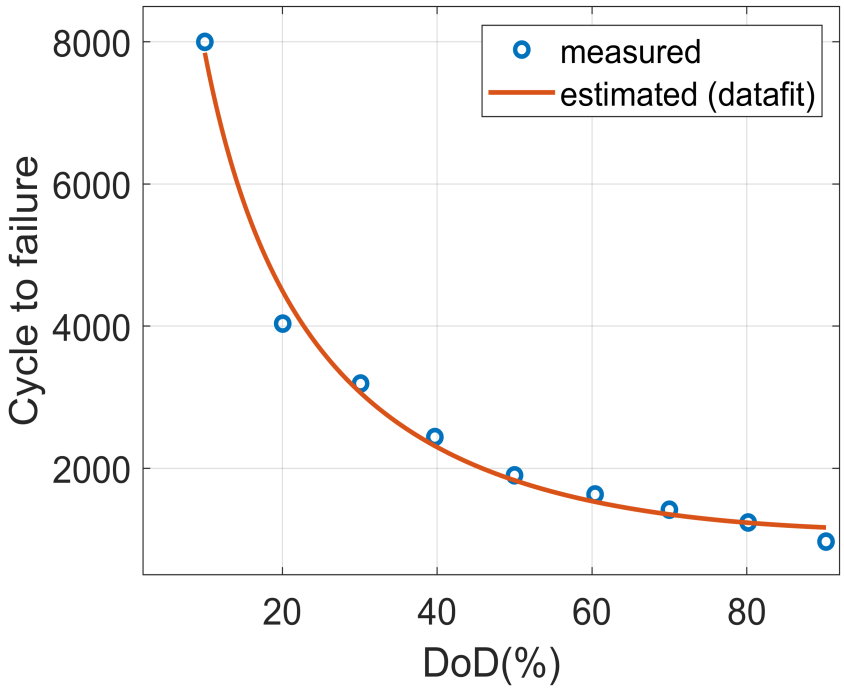

Figure II.27: Battery cycle life (cycles to failure) vs. depth of discharge (DOD).

The BES manufacturer provides in their datasheet, the total cycle that BES can reach during its life span $BES_{cycle,tot}$, to estimate the BES lifetime in years eq. (II.52)) is used and the total cycle provided by the manufacturer using eq. (II.53)):

$$BES_{\text{Lifetime}}(\text{years}) = \frac{BES_{\text{cycle-to-failure}}}{BES_{\text{cycle}}(1 \text{ year})} \tag{II.53}$$

II.5.3.2 Fuel cost of gas turbine

Another specific parameter that has to be taken into account is the (Ca_{om-GT}), this cost must include the fuel consumption during the year [1]. The fuel consumption as stated in [1] is calculated using

eq. (II.54) based on the NG fuel consumption fc_{GT} given by eq. (II.13) in section II.5.1.3:

$$GT_{\text{fuel-cost}}(\$/\text{year}) = \sum_{t=1h}^{t=8760h} (fc_{GT}(t) \times NG_p) \times \Delta t \tag{II.54}$$

Where NG_p is the local price for the natural gas (NG). The inclusion of fuel consumption will contribute to the overall operating and maintenance expenses associated with the use of gas turbines

II.5.4 Environmental modeling of HRES

The reference base system (Case Study 1 in in Table II.1), as well as other case studies presented in Table II.1, include Gas Turbines (GT) as a component of their energy sources. During the operation of the GT, emissions of greenhouse gases (GHGs) occur, including carbon monoxide (CO), carbon dioxide (CO2), and other GHGs. The assessment of GHG emissions from the gas turbine can be carried out using the Carbon Dioxide Emission (CDE) factor. This factor can be determined using the calculation provided in eq. (II.55) [1]:

$$CDE\ (\text{kg}CO_{2eq}/\text{year}) = \sum_{t=1h}^{t=8760h} (fc_{GT}(t) \times \lambda_{CO_2,NG}) \times \Delta t \tag{II.55}$$

where $\lambda_{CO_2,NG}$ ($\text{kg}CO_{2eq}/\text{m}^3$) represents the emission conversion factor of natural gas. This evaluation is crucial for understanding the environmental impact of the gas turbine within the overall energy system and for comparing the effectiveness of different case studies in reducing GHG emissions.

II.5.5 Social parameters modeling of HRES

One of the significant advantages of Hybrid Renewable Energy Systems (HRES) is their substantial contribution to the social development of society. The implementation of HRES aligns with both national and global policies and objectives for sustainable development. These objectives often include reducing the environmental impact on society and promoting the growth of industries with lower environmental footprints. In the literature, key parameters such as job creation (JC), the Human Development Index (HDI), and the Renewable Fraction (RF) are frequently used to assess the social impact of HRES. These metrics help quantify the broader societal benefits of transitioning to cleaner energy systems, demonstrating how HRES can contribute to both environmental sustainability and social progress [1, 35, 160].

The Renewable fraction is the fraction of the total yearly renewable energy supplied to the load to the total yearly load. The RF describes the limit of power supply as compared to non-renewable energy source to renewable energy source. The RF is given by eq. (II.56):

$$RF = \left(1 - \frac{\sum P_{GT}(t)}{\sum P_{Load}(t)}\right) \tag{II.56}$$

The $RF = 0$, means that a full NG-based system , contrary , a $RF = 1$ means a full renewable energy based system.

II.6 Hybrid Renewable Energy System (HRES) optimal sizing

After completing a comprehensive modeling process for all HRES components, an optimal sizing procedure is essential to determine the best capacities and configurations that minimize or maximize the considered objective functions while adhering to operational constraints. The optimization process involves defining the decision variables, objective functions, and constraints, as well as selecting the appropriate solution methods to address the problem. Additionally, the energy management strategy plays a critical role during optimization. As outlined in section II.2, this process is guided by a predefined rule-based Energy Management Strategy (EMS), which significantly influences the operational outcomes. The adopted EMS is utilized to calculate the outputs of the objective functions and constraints based on the given inputs (decision variables). Given that this study addresses multiple objective functions with various constraints, the optimization process is formulated as a multi-objective constrained optimization problem, which can be expressed by eq. (II.57):

$$\begin{aligned} \text{minimize/maximize} \quad & \{OF_i(\chi)\} \\ \chi \in \mathbb{R} \quad & Con_j(\chi) \leq C_j \end{aligned} \tag{II.57}$$

where χ represents the decision variable vector, $\mathbb{R}$ denotes the decision space of χ, $OF_i(\chi)$ is the i-th objective function, $Con_j(\chi)$ is the j-th constraint, and C_j is the limit for the j-th constraint.

Here, $i = 1, 2, \ldots, n_{OF}$ and $j = 1, 2, \ldots, m_{Con}$, where n_{OF} and m_{Con} represent the number of objective functions and the number of constraints, respectively. This formulation ensures that the optimization process systematically addresses all relevant factors, leading to a solution that balances multiple objectives within the defined constraints.

II.6.1 Decision variables

The reference system, which relies solely on the Gas Turbine (GT) for energy generation, is not included in the optimization process. Since the GT is the only energy source in this system, there is only one configuration that ensures power reliability and meets the load demand, leaving no room for optimization. However, to diversify power sources and capitalize on the lower costs and abundant availability of renewable energy (RE) resources in the study region, RE sources are integrated into the system. The capacities of these sources—specifically, the number of PV panels (N_{PV}) and the number of wind turbines (N_{WT}) will be optimized to attain a balance between initial costs and the required GT capacity.

Furthermore, to address the intermittency of RE sources and the stochastic and unpredictable nature of load demand, the capacities of the BES system (N_{BES}) and the HES system (the number of electrolyzers, fuel cells and hydrogen tanks, N_{EL}, N_{FC} *and* N_{ST}) will be adjusted accordingly. This adjustment is necessary to ensure that the system can effectively manage the variability of both generation and consumption.

Additionally, the initial energy quantities present in the storage systems significantly influence the system's performance. These initial amounts are crucial for balancing any shortfall or unavailability of renewable energy sources during the initial hours of the simulation. It is important to note that the simulation begins at 00:00 on January 1st of the studied year. During the first approximately eight hours, solar energy is unavailable. During this period, the initial energy levels in the storage systems—represented by ($C_{BES-init} = C_{BES}(t = 1h)$, *and* $Q_{H_2-init} = Q_{H_2}(t = 1h)$) play a critical role and are treated as decision variables in the optimization process. Therefore, the global decision variable is defined in eq. (II.58) :

$$\chi = [N_{PV},\ N_{WT},\ N_{Bat},\ N_{EL},\ N_{FC},\ N_{ST},\ N_{GT},\ C_{BES-init},\ Q_{H_2-init,\ DoD}]^T \tag{II.58}$$

II.6.2 Objective functions (OFs)

To compare the studied systems in terms of their techno-economic, environmental, and social performances, this study focuses on techno-economic and environmental objective functions. Although social performance indicators are crucial, they are not included in the optimization process to avoid overburdening the computational effort. However, these social indicators will be evaluated separately

for each system to assess the social impact of the different configurations.

II.6.2.1 Technical objective function

In this study, LPSP is considered the primary objective function. It serves as a critical metric for assessing the reliability of the energy system. The LPSP is defined as the proportion of time during which the system fails to meet the load demand due to insufficient power availability. The objective is to minimize the LPSP, thereby maximizing the system's reliability. The LPSP is mathematically expressed as follows in eq. (II.59):

$$OF_1 = LPSP = \frac{\sum_{t=1h}^{t=8760h} \text{Power failure time } (P_{LPS}(t) > 0)}{\text{Total time} = 8760} \ [\%] \tag{II.59}$$

Where $P_{LPS}(t)$ (eq. (II.60)) is the loss of power supply or the unmet load, $P_{supplied}(t)$ is the supplied power and $P_{Load}(t)$ is the load demand at time t.

$$P_{LPS}(t) = P_{Load}(t) - P_{supplied}(t) \tag{II.60}$$

In addition to LPSP, the Excess Energy (EE) factor is another technical metric evaluated for each configuration. EE measures the renewable energy that is generated but not consumed by the load due to an excess in generation capacity. The percentage of excess energy, which originates from renewable sources, is calculated using eq. (II.61):

$$EE = \frac{\sum_{t=1h}^{t=8760h} P_{EPS}(t) \times \Delta t}{\sum_{t=1h}^{t=8760h} P_{Load}(t) \times \Delta t} \tag{II.61}$$

Whereas $P_{EPS}(t)$ represents the Excess of power supply generated and not consumed by the load.

II.6.2.2 Economic objective function

The second objective function, eq. (II.62), to be considered in this study is the economic objective function. COE is chosen to the metric to be minimized by optimization process. The COE is expressed by eq. (II.46) presented in section II.5.3.

$$OF_2 = COE \ [\$/\text{kWh}] \tag{II.62}$$

II.6.2.3 Environmental objective function

The third objective function in this study, eq. (II.63), is to minimize the Carbon Dioxide Emission (CDE) factor, which is used to assess the environmental impact of the energy system. The CDE factor is mathematically expressed by eq. (II.55), as detailed in section II.5.4:

$$OF_3 = CDE \ [\text{kgCO}_{2eq}/\text{year}] \tag{II.63}$$

II.6.3 Constraints

Technical constraints are essential to include in the optimization process to ensure that the proposed system is logically and technically sound. The optimization must satisfy all these constraints to provide a feasible solution.

The first constraints are the linear inequality related to the initial energy quantities present in the storage systems, which must not exceed the total nominal capacities. This is represented by the following inequalities (eqs. (II.64) and (II.65)):

$$C_{BES-init} \leq N_{Bat} \times C_{Bat-nom} \implies \chi(8) - \chi(3) \times C_{Bat-nom} \leq 0 \tag{II.64}$$

$$Q_{H_2-init} \leq N_{ST} \times Q_{ST-nom} \implies \chi(9) - \chi(6) \times Q_{ST-nom} \leq 0 \tag{II.65}$$

Where $C_{Bat-nom}$ and Q_{ST-nom} are nominal capacity of a single battery accumulator in (kWh) , and the nominal capacity of one H_2 storage tank in (kg) respectvely.

Additionally, it is crucial to maintain the energy levels within the storage system throughout its operational lifespan. Specifically, the amount of energy remaining in the storage system at the end of the year must be equal to or greater than the energy level at the beginning of the year. This ensures that the leftover energy can serve as the starting point for the subsequent year. If this condition is not met, an external energy source, such as additional hydrogen or battery recharging, will be required annually to reset the system to its initial state. These constraints are mathematically expressed in eqs. (II.66) and (II.67).

$$Q_{H2}\,(\text{hour} = 8760) - Q_{H2}\,(\text{hour} = 1) \geq 0 \implies \chi(9) - Q_{H2}\,(\text{hour} = 8760) \leq 0 \tag{II.66}$$

$$C_{BES}\,(\text{hour} = 8760) - C_{BES}\,(\text{hour} = 1) \geq 0 \implies \chi(8) - C_{BES}\,(\text{hour} = 8760) \leq 0 \tag{II.67}$$

II.6.4 Energy management strategy (EMS)

In our study, to prioritize the use of renewable energy sources, these are designated as the primary means of meeting the load demand. However, given the inherent intermittency and unpredictability of renewable sources—compounded by the stochastic nature of the load—BES and/or HES systems are incorporated into the system configurations to balance these fluctuations.

Specifically, in case studies 4, 5, 9, and 10 (as outlined in Table II.1), both BES and HES coexist. In these scenarios, one storage system is prioritized during the charging and discharging processes. The prioritized storage system, designated as the "primary" storage, serves the short-term role (handling hourly charge/discharge cycles), while the secondary storage system operates in a long-term capacity (managing daily charge/discharge cycles). This approach allows for a detailed investigation of how each storage system performs when assigned to short-term versus long-term energy balancing tasks.

Finally, if the power generated by renewable energy sources and the storage systems cannot meet the load demand, the Gas Turbine (GT) will be activated (if included in the system configuration under study). If GT is not part of the configuration, the LPSP will appear. The EMS flowcharts illustrating these processes are presented in Figs. II.28 and II.29 [115].

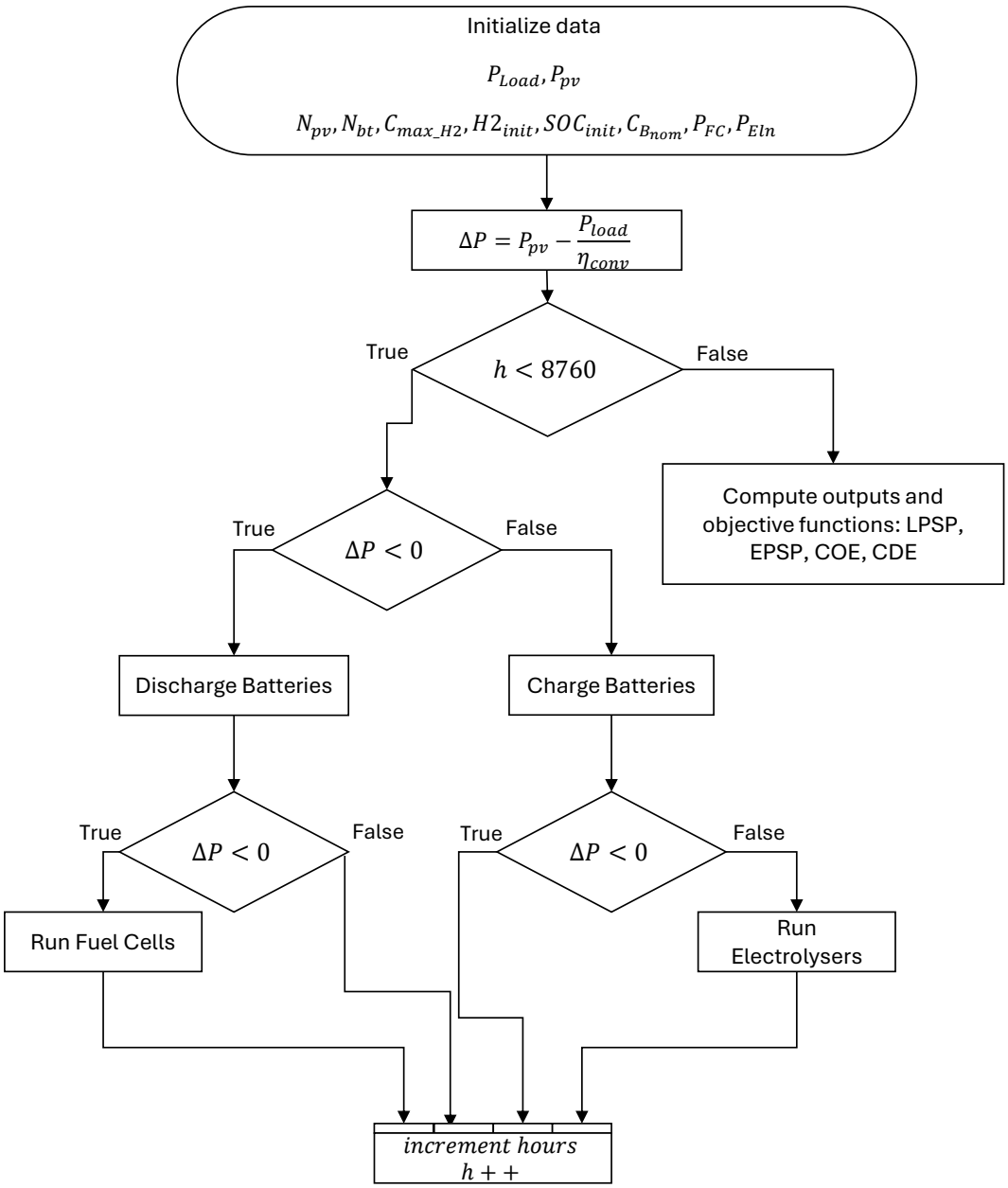

Figure II.28: EMS for case studies 4 and 9

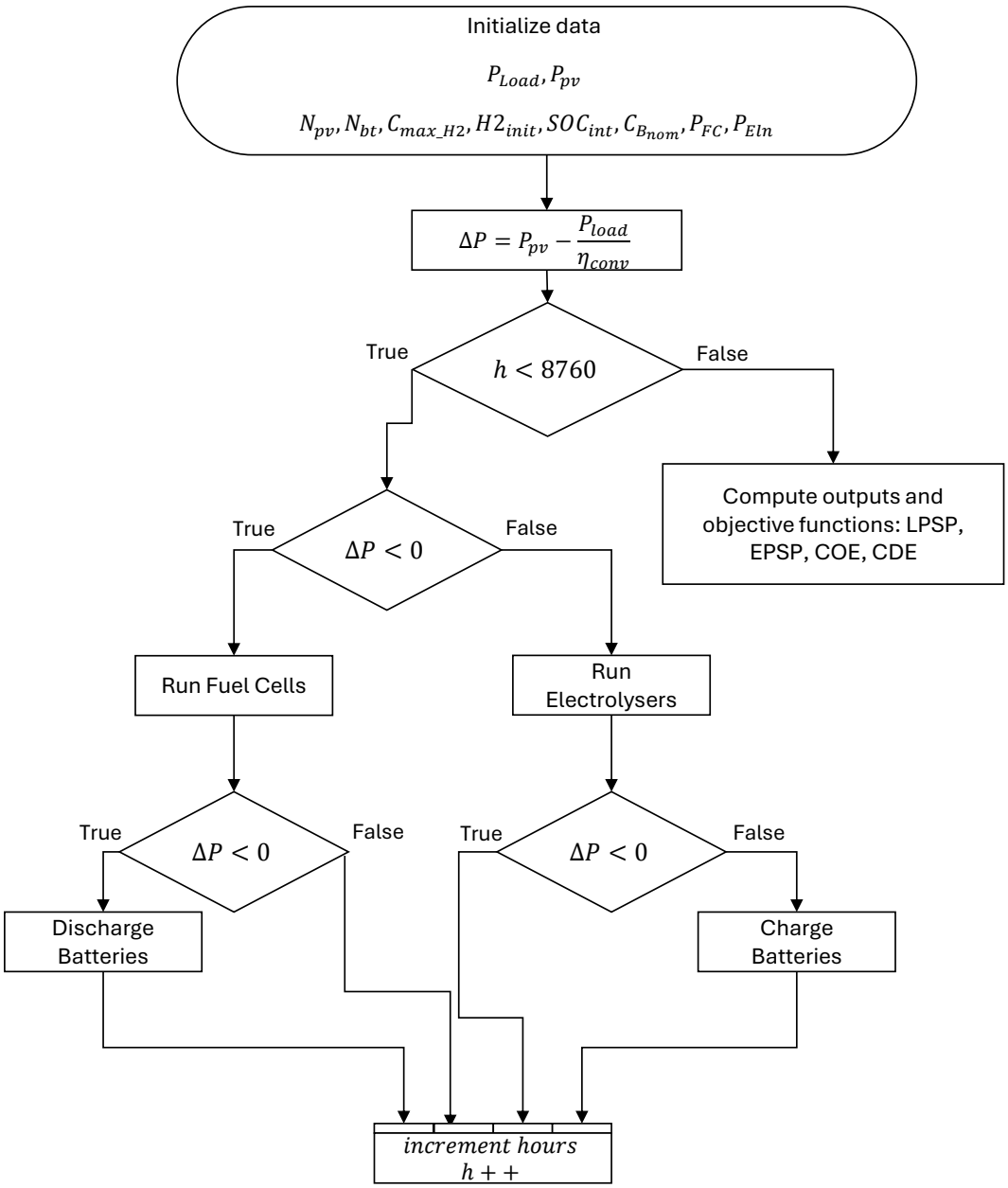

Figure II.29: EMS for case studies 5 and 10

II.6.5 Solution method

In the context of optimizing multi-objective problems, it is possible to optimize each objective function independently. However, finding a solution that satisfactorily meets all objectives simultaneously can be challenging, especially when these objectives conflict with one another. In multi-objective optimization (MOO) problems, the solution is often not unique; instead, a set of optimal solutions, known as Pareto-optimal solutions or non-inferior solutions, is identified. A solution is considered Pareto-optimal or non-dominated if there is no other feasible solution that can improve one objective without degrading at least one other objective.

In this study, to efficiently solve the MOO problem, three optimization algorithms are employed: the Non-Dominated Sorting Genetic Algorithm-II (NSGA-II) [220, 221], Multi-Objective Particle Swarm Optimization (MOPSO) [222, 223], and Fick's Law Optimization Algorithm (FLA) [1].

Additionally, the Pareto curve provides a comprehensive overview and exploration of the various trade-offs between objective functions, offering multiple options for implementing the optimal configuration. Given the conflicting nature of the selected objective functions (LPSP, COE, and CDE), selecting the best trade-off among Pareto non-dominated solutions is a crucial step in final system implementation. To assist in this decision-making process, Multi-Criteria Decision-Making (MCDM) methods are employed. Specifically, this study adopts the Technique for Order Preference by Similarity to an Ideal Solution (TOPSIS) [224, 225] and Simple Additive Weighting (SAW) [223, 224] as MCDM techniques to identify the most suitable solution from the Pareto set.

II.6.5.1 Non-Dominated Sorting Genetic Algorithm-II (NSGA-II)

The Non-dominated Sorting Genetic Algorithm II (NSGA-II), as proposed by [220] evaluates the quality of candidate solutions based on the Pareto dominance principle. This algorithm generates a set of Pareto-optimal solutions, representing a balance among the optimized objectives. Fig. II.30 illustrates the key steps involved in applying NSGA-II to our system for minimizing the objective functions described in eq. (II.57). The specific parameters of NSGA-II utilized in this study are outlined in Table II.10

II.6.5.2 Multi-Objective Particle Swarm Optimization (MOPSO)

The Multi-Objective Particle Swarm Optimization (MOPSO) algorithm is a metaheuristic, swarm-based algorithm designed for solving optimization problems. MOPSO is inspired by the simulation of social behavior in swarms. The algorithm begins by initializing a group of random particles, each

Table II.10: NSGA-II parameters used in the present study

Parameter	Values
Population size	200
Function Tolerance	$\mathbf{10}^{-6}$
Constraints Tolerance	–
Max number of generations	200 × Number of decision variables
No. of objectives	3
No. of variables	9 or 10
Mutation type	Gaussian
Crossover Fraction	0.8000

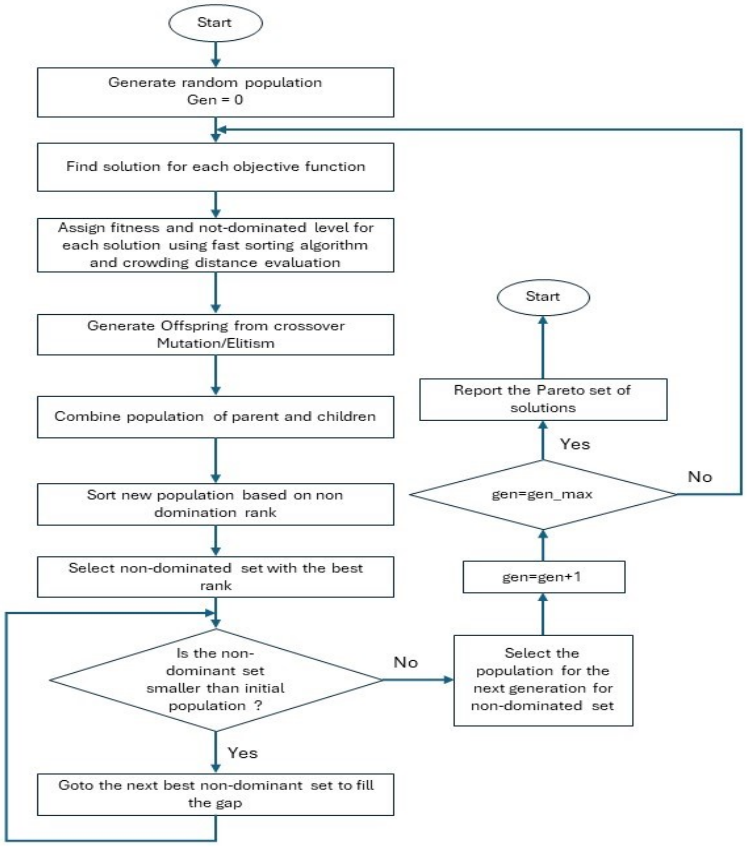

Figure II.30: Flow chart of NSGA-II

representing a potential solution within the decision variable space. During each iteration, non-dominant solutions (optima) are identified based on updates to the particles' positions, which are governed by their calculated velocities. The velocity $\Upsilon_i(t)$ and position $\chi_i(t)$ of each particle are

updated at each generation (iteration) using two key values. The first is the personal best P_{best}, which is the best solution achieved by that specific particle thus far. The second is the global best (G_{best}), which is the best solution found by any particle in the entire population. The implementation steps of the MOPSO algorithm can be summarized as follows:

1. **Initialization (eq. (II.68))**: Randomly generate an initial population of particles, each representing a potential solution within the decision variable space.

$$\chi_i^j(it=0) = LB_i + \text{rand} \times (UB_i - LB_i) \tag{II.68}$$

   Where χ_i^j is the $j-th$ particles of the $i-th$ decision variable, UB_i and LB_i are the upper and the lower bounds of the $i-th$ decision variable. Herein, $i = 1, 2, \ldots, n$ and $j = 1, 2, \ldots, p$, whereas n is the number of decision variables, in this study $n = 10$ (eq. (II.58)) and is p the number of particles. $rand$ is a random number between 0 and 1.

2. **Velocity update (eq. (II.69))**: each particle wanders around in the search space updating at each iteration it its own position $\chi_i^j(it)$ and velocity $\Upsilon_i^j(it)$ on the basis of its own past search experience (the historical own best position of χ_i^j : $P_{best}^j(it)$) and on that of the swarm (the historical best position encountered by any of the particles: G_{best}).

$$\Upsilon^j(it) = \omega \times \Upsilon^j(it-1) + c_1 \times r_1 \times \left(P_{best}^j(it) - \chi^j(it-1)\right) + c_2 \times r_2 \times \left(G_{best} - \chi^j(it-1)\right) \tag{II.69}$$

   Υ^j, χ^j and P_{best}^j are the array form of size $[1 \times n]$ of the $j-th$ particle velocity, position and its personal best. G_{best} is the global best for all particles. In this context, c_1 and c_2 are positive constants that denote the personal confidence factor and Swarm confidence factor, respectively. The variable ω represents the inertia weight, while r_1 and r_2 are two independent sequences of random numbers generated within the range [0, 1]. These random sequences serve to prevent entrapment in local minima and facilitate the divergence of a small subset of particles, thereby enabling a broader exploration of the search space. The MOPSO parameters used in this study are given in Table II.11.

3. **Position update (eq. (II.70))**: the particle position at the iteration (it) is updated as follows:

$$\chi^j(it) = \chi^j(it-1) + \Upsilon^j(it) \tag{II.70}$$

4. **Objective function Evaluation**: the OF are evaluated for each particle position.
5. **Non-Dominated Sorting**: non-dominant solutions are identified and archived to form a Pareto front.
6. **Iteration**: the process is repeated of updating velocities, positions, and identifying non-dominant solutions until the stopping criteria are met.
7. **Stopping criteria**: the stopping criteria is met when convergence occurs. the convergence is achieved when the positions of all particles converge to the same set of values.

Table II.11: MOPSO parameters used in the present study

Parameter	Values
Population Size	200
Max Iterations	1000
Inertia Weight (ω)	0.4
Cognitive Coefficient (c_1)	2
Social Coefficient (c_2)	2
Mutation Probability	0.5
Number of Variables	9 or 10
Number of Objectives	3

II.6.5.3 Fick's Law Optimization Algorithm (FLA)

The Fick's Law Optimization Algorithm (FLA), initially developed by [181], is a physics-based meta-heuristic approach inspired by the principles of diffusion. These principles describe the movement of particles undergoing random thermal motion, particularly their natural tendency to migrate from areas of higher concentration to those of lower concentration. The FLA algorithm has demonstrated robust optimization performance across various problem types, showcasing resilience and adaptability, which suggests its potential application in a wide range of fields. The primary strategies for searching to achieve optimal results include several key stages. The FLA method excels in both exploration and exploitation when seeking optimal solutions, making it a promising approach for addressing our problem. Furthermore, FLA has proven its applicability to a diverse array of optimization challenges, positioning it as a strong candidate for application to the current problem under study. However, the technique does have certain limitations, such as sensitivity to parameter settings and dependence on initialization. To mitigate these limitations, preliminary simulations were conducted to identify the optimal parameter settings tailored to our specific problem before implementing the method [1]. Additionally, the Fick's Law Algorithm (FLA), in its current form, is not capable of solving multi-objective problems directly. To address this limitation, the three objective functions presented in

section II.6.2 are combined into a single optimization problem using the Euclidean sum method. This approach aggregates the multiple objectives into a single objective function by summing the squared values of each individual objective function, thereby converting the multi-objective problem into a single-objective problem. The final objective function that will be introduced to FLA is expressed as follows (eq. (II.71)):

$$\mathrm{OF}_{FLA} = \sqrt{OF_{1n}^2 + OF_{2n}^2 + OF_{3n}^2} \tag{II.71}$$

Where OF_{in} is the normalization of the $i-th$ objective function over its maximum value(eqs. (II.71) to (II.73)).

$$OF_{1n} = 1 - \frac{LPSP}{\mathrm{LPSP}_{max}} \tag{II.72}$$

$$OF_{2n} = 1 - \frac{COE}{\mathrm{COE}_{max}} \tag{II.73}$$

$$OF_{3n} = 1 - \frac{CDE}{\mathrm{CDE}_{max}} \tag{II.74}$$

LPSP_{max} and COE_{max} are 1% and 1\$/kWh respectively and CDE_{max} is calculated based on full functioning of GT.

The implementation steps of the MOPSO algorithm can be summarized as follows (Table II.12):

II.6.5.4 Technique for Order Preference by Similarity to an Ideal Solution (TOPSIS)

The Technique for Order Preference by Similarity to an Ideal Solution (TOPSIS) method is a decision-making tool adopted in this study to select the best trade-off among Pareto non-dominant solutions. This method assists decision-makers in choosing the optimal design configuration by evaluating and ranking the alternatives based on predefined criteria. TOPSIS facilitates the identification of the solution that is closest to the ideal and farthest from the worst, ensuring that the selected configuration offers a balanced and effective compromise among the multiple objectives [224, 226].

The implementation steps of TOPSIS are as follows [115, 224, 226–228]:

1. **Define the problem and criteria**

Table II.12: The implementation steps of FLA

1: Initialization;
2: Insert parameters of D, C1, C2, C3, C4, C5;
3: Initiate the population X_i (i = 1, 2, ..., N) as random;
4: Clustering: Dividing the population into two clusters N_1 and N_2;
5: **for** $s = 1 : 2$ **do**
6: Calculate the fitness of each group molecule N_s;
7: Determine the best molecule with the best fitness value;
8: **end for**
9: **while** FES $\leq$ MAXFES **do**
10: **if** TF is greater than 0.9 **then**: (SSO)
11: **for** op = 1: nop **do**
12: Compute rate of diffusion;
13: Compute the step of motion factor;
14: Update position of the population;
15: **end for**
16: **else if** TF is fewer than rand **then** (EO)
17: **for** op = 1: nop **do**
18: Compute rate of diffusion;
19: Compute quantity of group relative;
20: Update position of the population;
21: **end for**
22: **else** (EO)
23: Compute flow direction;
24: Calculate molecules number tending to move to the region;
25: Update position of the population;
26: Update remaining molecules in region i;
27: Update region j molecules;
28: Update FES $\leftarrow$ FES + NP;
29: **end while**
30: Return best solution;

Establishing the problem and identifying the criteria that will be employed to assess the available options is essential. Our analysis focuses on three key performance indicators (KPIs): the technical LPSP, the economic COE and the environmental CDE indicators.

2. **Construct a decision matrix**

   Construct a decision matrix in which each row corresponds to an option or a combination of choice variables, and each column represents a criterion or an evaluation of the objective functions. Allocate scores to each option based on each criterion (LPSP, COE and CDE).

3. **Normalise the decision matrix** To achieve equal weighting for each criterion, it is necessary to normalise the decision matrix by dividing each score by the total sum of scores in the corresponding column. This function will transform the matrix into a matrix that is used for relative

performance evaluation. The equation for normalisation is eq. (II.75):

$$r_{ij} = \frac{x_{ij}}{\sqrt{\sum_{i=1}^{m} x_{ij}^2}}, i = 1, 2, ..., n \tag{II.75}$$

where r_{ij} is the normalized value, x_{ij} is the original value, m is the number of rows in the dataset, and n is the number of columns.

4. **Weighting the criteria** Determine the weights w_j for each criterion based on their respective significance in attaining the target. The total of all weights must equal 1. Subsequently, matrix multiplication between the normalized decision matrix and the weights matrix is performed to obtain the weighted normalized decision matrix v_{ij} (eq. (II.76).

$$v_{ij} = w_j r_{ij} \tag{II.76}$$

5. **Determine the ideal and negative-ideal solutions** Determine the best and worst values for each criterion. In the context of minimizing the LPSP and COE criteria, the ideal solution v_j^+ refers to the lowest value that can be obtained from a set of alternatives. Conversely, the negative-ideal solution v_j^- represents the highest value among the alternatives.

6. **Euclidean distance** Calculate the Euclidean distance of each alternative from the ideal best and the ideal worst values. The formula for Euclidean distance is:

$$D_i^+ = \sqrt{\sum_{j=1}^{n} \left(v_{ij} - v_j^+\right)^2} \tag{II.77}$$

$$D_i^- = \sqrt{\sum_{j=1}^{n} \left(v_{ij} - v_j^-\right)^2} \tag{II.78}$$

where D_i^+ and D_i^- are the distances of the alternative from the ideal and negative-ideal solutions respectively and n is the number of criteria.

7. **Relative closeness coefficient** the relative closeness coefficient is the ratio of the negative separation to the sum of the positive and negative separations. The formula for relative closeness

is (eq. (II.79)):

$$C_i = \frac{D_i^-}{D_i^- + D_i^+} \tag{II.79}$$

8. **Select an alternative which has maximum** C_i

The overall TOPSIS process is presented in the flowchart in Fig. II.31 [227].

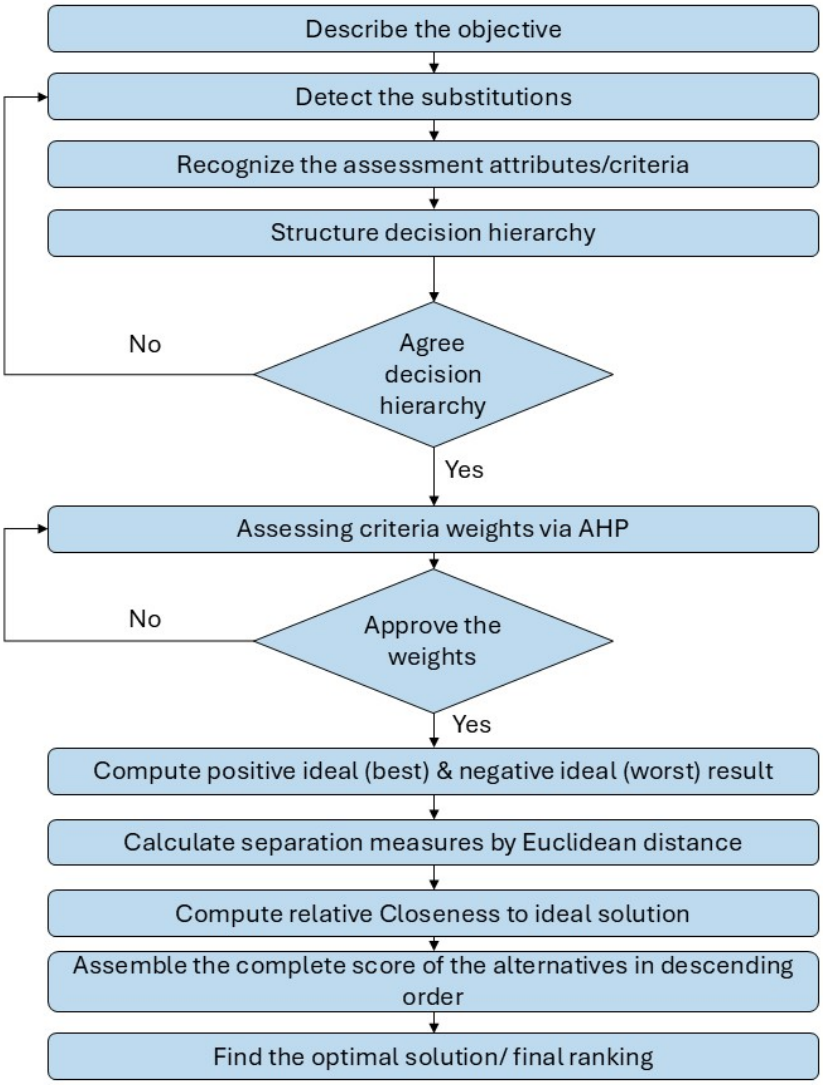

Figure II.31: Flow chart of TOPSIS method

II.6.5.5 Simple Additive Weighting (SAW)

Simple Additive Weighting (SAW) is a simple decision making method that converts the final pareto solution set into one objective value by summing normalized objective functions. The implementation of the SAW value is shown in eq. (II.80) [223]:

$$OF_{SAW}(\chi) = \sum_{i=1}^{3} \lambda_i \frac{OF_i(\chi) - OF_i^{min}(\chi)}{OF_i^{max}(\chi) - OF_i^{min}(\chi)} \tag{II.80}$$

$OF_i^{max}(\chi)$ and $OF_i^{min}(\chi)$ represent the maximum and the minimum values of the $i-th$ objective functions, respectively. λ_i is the weighting coefficients of the $i-th$ objective function

II.7 Conclusion

The detailed model for every component of the HRES was performed in chapter II, by setting a basis on how each element interacts within the whole system. Emphasis has been done on devising appropriate and realistic models that mimic energy sources such as photovoltaic panels and wind turbines, as well as energy storage solutions, such as Battery Energy Storage Systems and Hydrogen-based Energy Storage. It was here said that modeling the behavior of each component realistically for changes in environmental and operational variables is very important. Solar irradiance fluctuations and wind speed variations, for instance, were taken into consideration in modeling PV and wind turbines to account well for the variable nature of renewable sources. In the same manner, storage systems were modeled as dynamic systems representing charge/discharge cycles, efficiencies and depth-of-discharge limitations amongst others in the evaluation of long-term performances. The chapter also introduced the mathematical modeling of conventional backup sources, such as gas turbines, with a view to fuel consumption and resulting emissions. Such models are necessary in order to assess the environmental impact of the system and to find an optimum energy mix with a minimum greenhouse gas emission. In chapter II, the modeling of the HRES components was done in a very articulate and structured manner to ensure that every variable and constraint involved in the operation of such a system were put into consideration. This comprehensive modeling is very necessary for subsequent optimization processes where the models shall be used in finding the most efficient and sustainable configuration of the energy system. This chapter thus provides the knowledge based on which an initial process of refinement and testing can be started to integrate renewable energy sources into industrial applications, helping to achieve the overall objective of increasing energy efficiency and sustainability.

Chapter III

Simulation results, analysis and discussions

III.1 Introduction

In this section, the outcomes from the studied systems will be presented and thoroughly discussed. This section will provide a summary of key findings. The simulations for this study were conducted using MATLAB, with the coding. The simulations were performed on MATLAB 2024a, installed on a Windows 11 machine equipped with an Intel(R) Core (TM) i7-1065G7 CPU @ 1.30GHz, 1.50 GHz, and 16.0 GB of RAM. Certain simulation assumptions were made during the course of this study, and are also detailed as follows. the techno-econmic data inputs used for the simulation are presented in the the Appendix (Table A.1.

- The self-discharge of hydrogen in storage tanks is disregarded.
- Heat losses in the system components are not considered in the analysis.
- The price of fuel is assumed to remain constant throughout the study period, based on the Algerian market.
- The study does not account for potential failures of HRES components, nor does it consider transmission and distribution losses.
- The simulation starts at 00:00 on January 1st, which affects the results since solar energy is unavailable for approximately the first 7-8 hours.

- The analysis of load profiles and climatic data is conducted with an hourly time resolution, assuming that fluctuations within each hour are insignificant.

III.2 Reference system

The reference system in this study focuses on load electrification through a natural gas (NG) thermal power plant. The primary objective is to evaluate the techno-economic feasibility and environmental impact of integrating renewable energy sources (RES) with this conventional plant. The total annual load to be electrified is 83,470.035 MWh. From the simulation results, although the cost of energy production from the NG plant is relatively low, at around 0.7105 $kWh, the greenhouse gas (GHG) emissions from the plant are significant, posing a substantial threat to the environment. The total CO2-equivalent (CO2eq) emissions generated during the process of meeting full load amount to 49,009.47 kg, which corresponds to a carbon dioxide emission factor (CDE) of 0.5871 kg/MWh. This high emission rate not only raises environmental concerns but could also result in additional costs through carbon taxes or other regulatory penalties in the future. Another challenge associated with using an NG-based thermal plant is its relatively low efficiency. The simulation reveals that the average efficiency of converting natural gas into electricity is approximately 34%. Fig. III.1 illustrates the efficiency trend throughout the year, showing how efficiency varies over time, further emphasizing the limitations of the current system in terms of energy conversion. The overarching goal of this

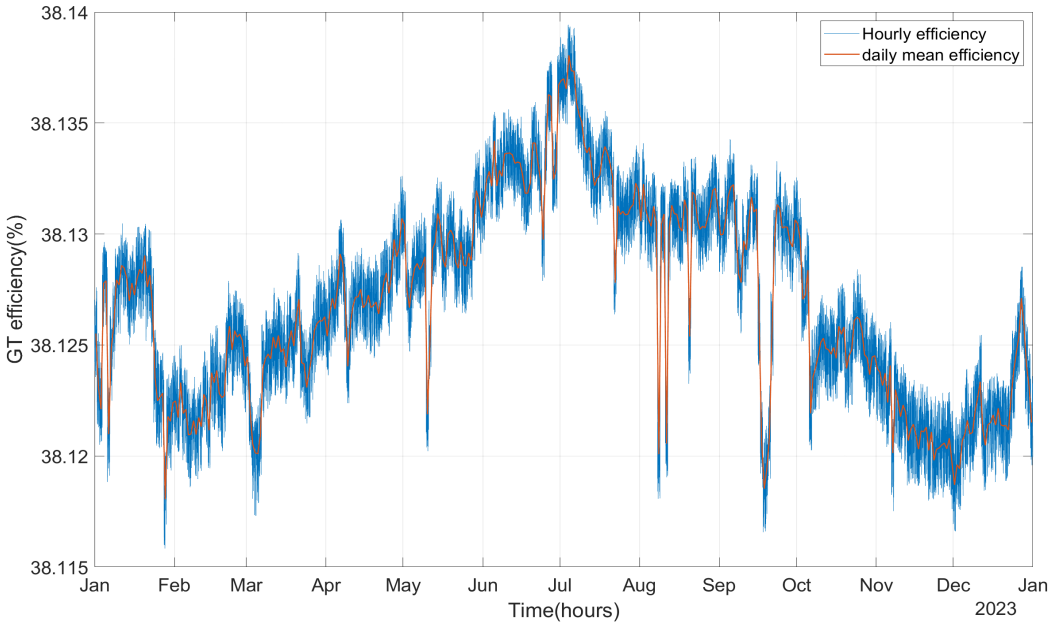

Figure III.1: GT conversion efficiency

study is to improve the technical, economic, and environmental performance of the oil and gas industry by integrating renewable energy sources along with energy storage systems. The aim is to ensure the full electrification of the load while minimizing the environmental footprint and improving the overall efficiency of the energy production system. The introduction of renewable energy sources and advanced storage solutions has the potential to significantly reduce GHG emissions, enhance system efficiency, and provide a more sustainable and cost-effective energy solution for the industry.

III.3 Integration of renewable energy

To address the technical and environmental challenges, the integration of renewable energy (RE) into the power plant is evaluated from technical, economic, and environmental perspectives.

III.3.1 Full renewable energy source integration

The first four case studies focus on a complete shift to renewable energy, meaning that the load is electrified solely from renewable sources. To mitigate the intermittency of renewable sources, HES and BES systems are considered. Additionally, the 100% shift to renewable energy is assessed with both single storage systems (BES or HES) and dual storage systems (BES and HES). In the dual storage scenario, each system is evaluated as either the primary or secondary storage means. Table III.1 summarizes these four case studies.

Table III.1: Full RE shift case studies description

Case Study	Source	Storage	Description
Case study 2	PV-WT	HES	100% shift with single HES system
Case study 3	PV-WT	BES	100% shift with single BES system
Case study 4	PV-WT	BES (1) - HES (2)	100% shift with dual storage (primary: BES, secondary: HES)
Case study 5	PV-WT	BES (2) - HES (1)	100% shift with dual storage (primary: HES, secondary: BES)

Comparing the four case studies reveals an increase in the COE compared to the reference system. However, this rise in COE is offset by the complete elimination of carbon dioxide emissions (CDE), as the full integration of renewable energy eliminates all emissions associated with the power plant. Systems utilizing a single storage option show that configurations relying solely on HES cannot achieve 0% LPSP. This limitation is largely due to the circularity constraints ((eqs. (II.64) and (II.65)): in section II.6.3) imposed on the system, requiring that the final hydrogen quantity in the tank must be

equal to or greater than the initial value to ensure hydrogen availability for future operational periods. These constraints restrict hydrogen consumption, thus reducing the amount of power that can be generated by Fuel Cells (FCs). Additionally, the upper limit of the hydrogen tank capacity, which is sized to hold a 24-hour full load, plays a critical role in the system's limitations.

In contrast, due to its superior charging and discharging efficiency, BES can achieve 0% LPSP. Even though BES and HES are subject to the same upper bound (sized to hold a 24-hour full load) and circularity constraints, BES performs better than HES in maintaining 0% case study 02 presents a COE of 0.1051$/kWh at a LPSP of 8.92% .

In the dual storage configurations, allocating short-term charging/discharging processes to BES proves to be more cost-effective. Case Study 4, where BES handles short-term storage, shows a COE of $0.1345/kWh compared to $0.2454/kWh in Case Study 5, where HES is used for short-term storage. This disparity arises because frequent charging and discharging cycles in HES system result in lower efficiencies; the theoretical charging/discharging efficiency of HES is around 40%, compared to 72% for BES. Therefore, it is more techno-economically feasible to assign short-term, hourly charging to BES while using HES for longer-term, daily charging/discharging cycles. In Case Study 4, HES helps to prevent overloading the BES, reducing the Depth of Discharge (DoD) to 73.53% compared to 79.46% in Case Study 3. This reduction in DoD extends the lifespan of the BES, with Case Study 4 offering a projected BES lifetime of 5.45 years compared to 5.10 years in Case Study 3.

Furthermore, alternative solutions from the Pareto-optimal curve may also be viable if the plant operator is willing to allow a small LPSP. Fig. III.2 presents the Pareto curve, offering a range of optimal solutions that can help the operator select a configuration that balances COE and LPSP according to their specific requirements and constraints. This approach enables operators to maintain a low COE while allowing an acceptable LPSP limit.

Figure III.3 shows the shares of different produced/consumed energy compared to the total load for each subsystem.

The cost breakdown analysis of the four "full renewable shift" case studies highlights the effectiveness of Case Study 4 (PV-WT-BES-HES). In this configuration, the incorporation of HES as a secondary, long-term daily storage backup demonstrates its superiority over other setups. This configuration not only achieves the lowest COE at 0% LPSP but also provides the most balanced distribution of costs, as shown in Fig. III.4.

In contrast, when BES is the sole storage system or when it serves as the primary long-term storage option, over 60% of the Total Annual Cost of System (TACS) is allocated to the BES

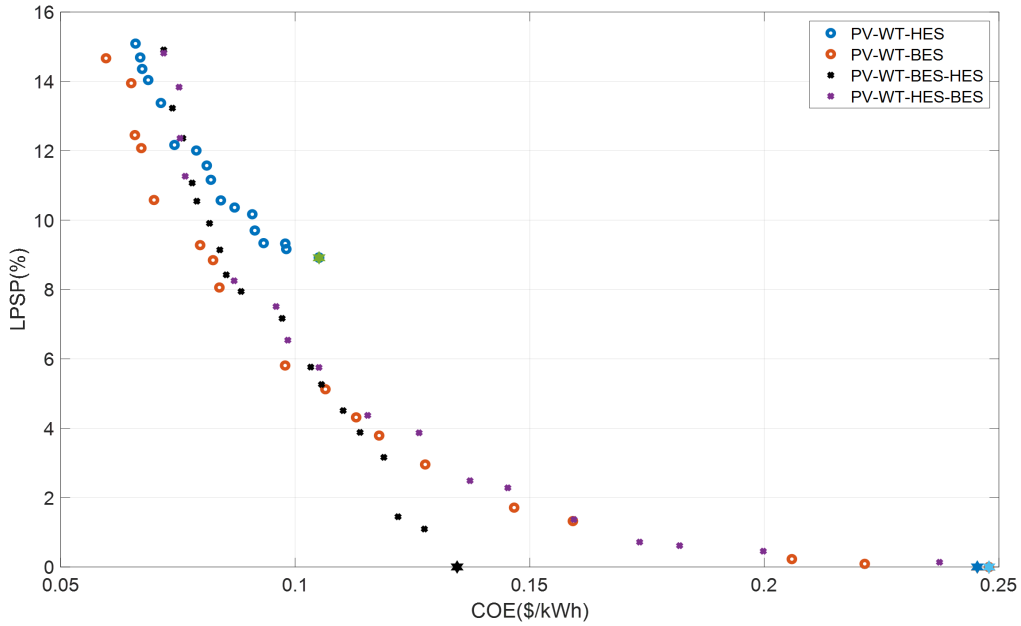

Figure III.2: Pareto optimal curves of complete RE shift

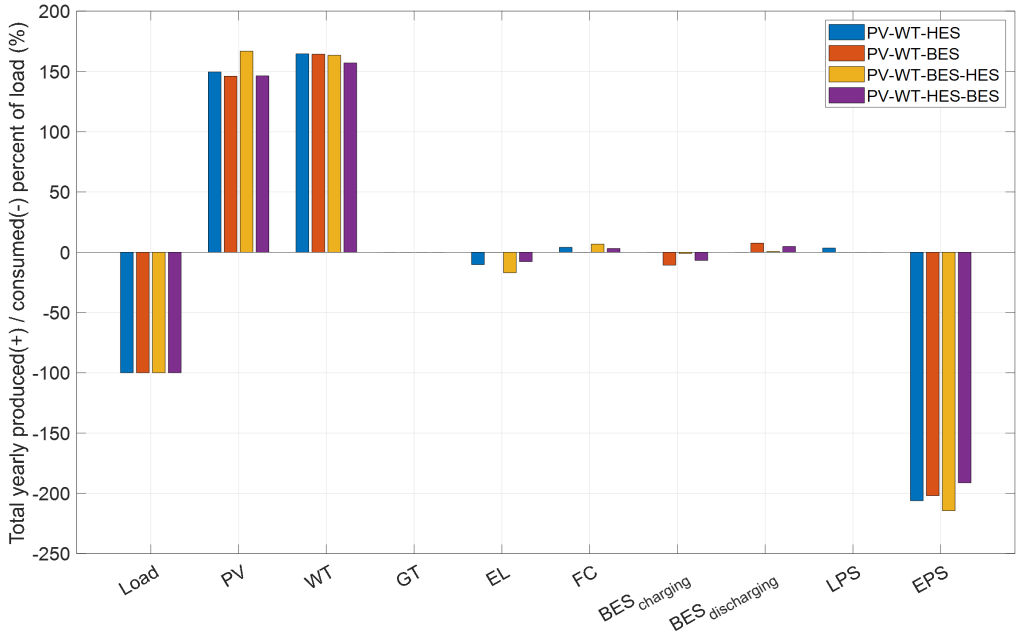

Figure III.3: Complete RE shift case studies Load sharing

component. These elevated costs are a result of ensuring circularity constraints, which require the final storage capacities to be equal to or greater than their initial values. This leads to higher expenses in maintaining the BES system over time. Given these factors, Case Study 4 (PV-WT-BES-HES) emerges as the optimal configuration for achieving a complete shift to renewable energy sources. It

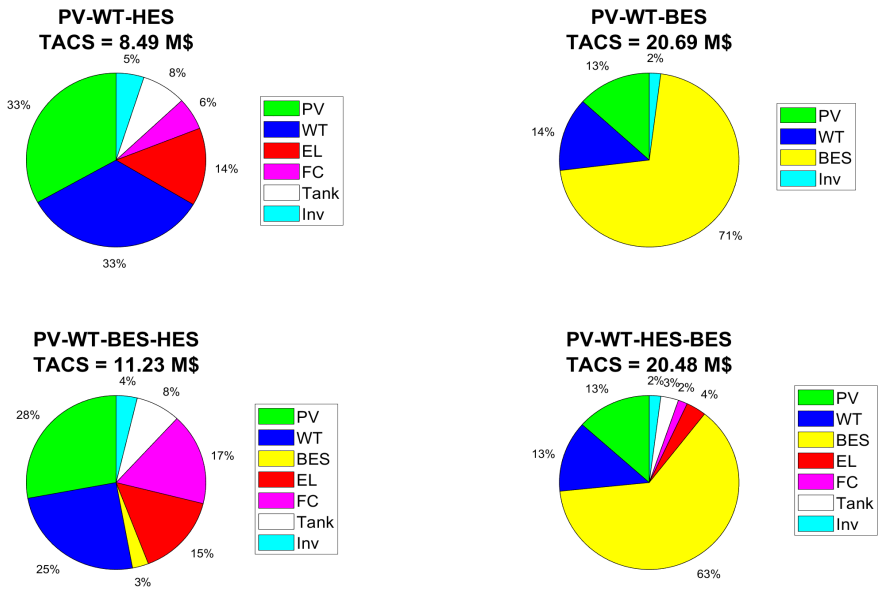

Figure III.4: complete RE shift case studies Cost sharing

balances cost efficiency and storage reliability, making it the most effective solution among the studied options.

III.3.2 Partial shift to renewable energy sources with single storage

A complete shift to renewable energy sources is sometimes infeasible due to techno-economic limitations, such as high initial investment and the challenge of maintaining a low LPSP given the intermittency of renewable sources. In such cases, a partial shift or integration of renewable energy with existing systems presents a more practical and promising solution [115]. To explore this, three case studies are considered (Table III.2), each representing a different level of renewable energy integration—20%, 50%, and 80%. These case studies are optimized based on set objectives and constraints, and they are evaluated in terms of their techno-economic and environmental performance. These case studies allow for a detailed examination of how different levels of renewable energy integration affect the overall performance of the system, with a focus on achieving a balance between technical feasibility, economic viability, and environmental sustainability.

Before proceeding with the techno-economic and environmental analysis of the three case studies, it is important to highlight that the simulation results for Case Study 8 reveal the infeasibility of achieving an 80% renewable energy integration with photovoltaic (PV) as the sole renewable energy source. In this case, it becomes necessary to incorporate an additional energy source capable of

Table III.2: Partial shift case study configurations (single storage)

Case Study	Sources	Storages	Description
Case study 6	PV (min 20%) - GT (max 80%)	HES	Minimum 20% integration of RE with HES system
Case study 7	PV (min 50%) - GT (max 50%)	HES	Minimum 50% integration of RE with HES system
Case study 8	PV-WT (min 80%) - GT (max 20%)	HES	Minimum 80% integration of RE with HES system

covering periods when PV energy is unavailable, such as during nighttime or low-irradiance conditions. Case Study 8, which comprises PV and wind turbines (WT) as energy sources, demonstrates that relying solely on PV is insufficient for maintaining the required load demand at such high levels of renewable integration. Therefore, in systems with higher renewable integration targets, a diversified energy portfolio, such as PV combined with WT or other renewable sources, is critical to ensure both reliability and sustainability.

The technical analysis of the effect of renewable integration rates on overall system performance is illustrated in Figs. III.5 and III.6 and table III.3. Based on Fig. III.5, for cases with zero LPSP, the COE is inversely correlated with the rate of renewable integration and carbon dioxide emissions (CDE). This trend arises because the initial investment cost for renewable energy systems is generally higher than for non-renewable systems, such as those based on gas turbines (GT). Additionally, integrating renewable energy into the system necessitates the incorporation of storage solutions, such as HES (comprising electrolyzers, fuel cells, and hydrogen tanks), which further increases the overall system cost.

On the other hand, partial renewable energy integration (at levels of 20%, 50% and 80%) increases the COE by approximately 42.94% and 59.50% respectively and a decrease by 1.66% for 80% level of renewable integration, while significantly reducing the CDE by 42.25, 53.86% and 80.77% for levels of RE integration of 20%, 50% and 80% respectively. This trade-off provides valuable insight for investors and plant operators, who can select the most suitable configuration that aligns with their technical, economic, and sustainability goals. Furthermore, plant developers can leverage this analysis to plan a gradual increase in renewable energy integration while understanding the impact on key performance indicators (KPIs) such as technical reliability, cost, and environmental impact.

Regarding the system constraints, even when the upper limits for renewable energy sources were set to 20%, 50% and 80% of the total load, the optimal results show a higher actual integration of 42.33, 53.86% and 80.92%, respectively. This outcome is due to the system's optimal decision variables that balance the objectives and constraints.

This finding underscores the need for further investigation into the optimal limit for renewable integration. In future studies, the renewable integration factor itself could be considered a decision variable to better explore its potential, although this approach is beyond the scope of the current study.

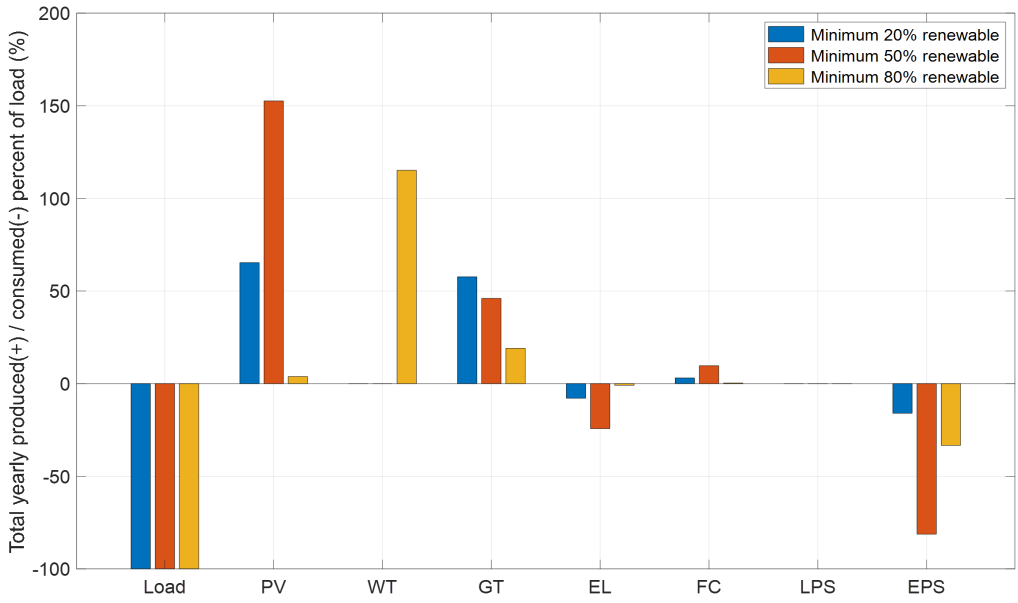

Figure III.5: partial integration of RE case studies Load sharing

Table III.3: Change in CDE and COE vs level of integration

RE limit	**0%**	**20%**	**50%**	**80%**
Change in CDE	0%	-42.25%	-53.86%	-80.77%
Change in cost	0%	42.94%	59.50%	-1.66%
EPS (% of load)	0%	15.98%	81.23%	33.33%

Due to the high marginal cost of the renewable sources compared to fossil fuel-based energy sources, the level of integration of RE highly affects the cost of each component. Additionally, from Table III.3, it is not only the level of renewable integration that affects the changes in COE and CDE, the excess of energy can also have an impact on the system performance. The best level of integration of renewable energy highly depends on limit of acceptable EPS and the way it may be used or handled. Nevertheless, it is vital to recognize that national energy policies may necessitate energy producers to uphold a minimum level of involvement in renewable energy and impose restrictions on greenhouse gas (GHG) emissions within their facilities.

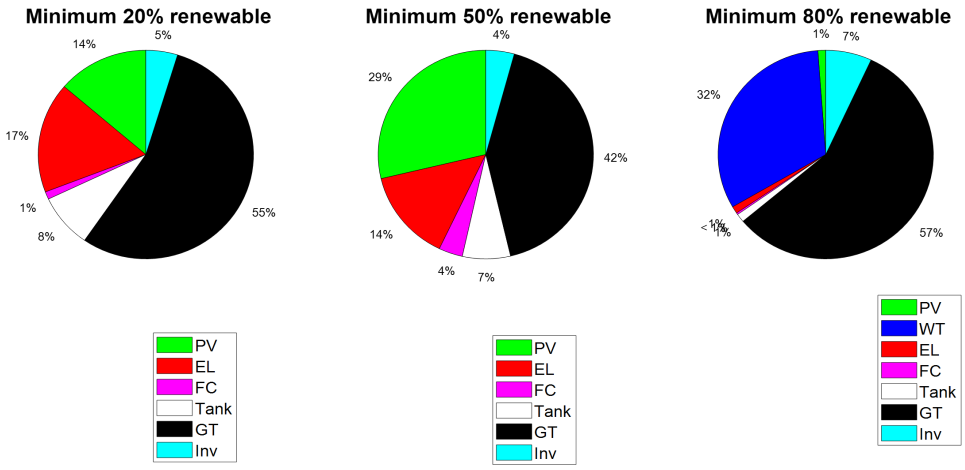

Figure III.6: Total Annual Cost of System (TACS) shares between different system components (partial integration)

The overall pareto curves of the three partial integration case studies are presented in Figs. III.7 and III.8. The techno-economic and environmental analysis of the pareto curves reveals that while Case Study 6 demonstrates a relatively low COE ranging from 0.0979 to 0.1320 $/kWh but higher (LPSP) of up to 15% and lower carbon dioxide emissions (CDE) of approximately between 0.2695 and 0.3391 kgCO2/kWh, Case Study 7 offers a more balanced approach with moderate increases in COE (0.1049-0.1329 $/kWh) and LPSP (0.0-15%), but a significant reduction in CDE (0.2551 -0.2947 kgCO2/kWh). Case Study 8, on the other hand, exhibits a COE (0.0563 -0.1129 $/kWh) and a lower CDE (0.0168 -0.1129 kgCO2/kWh). However, achieving such a high level of renewable energy integration solely with photovoltaic (PV) systems presents challenges, potentially requiring the addition of other renewable sources like wind turbines to maintain system feasibility.

III.3.3 Partial shift to renewable energy sources with dual storage

After assessing the behavior of the renewable integration on both level of integration (full shift and partial integration) , it is important to evaluate the techno-economic and environmental behavior of partial integration while considering dual storage system. As revealed in the section section III.3.1 above where case study 4 gives a promising performance toward achieving system objectives, additionally, taking into account the difficulty of full shift as stated in section III.3.2 above, a partial integration

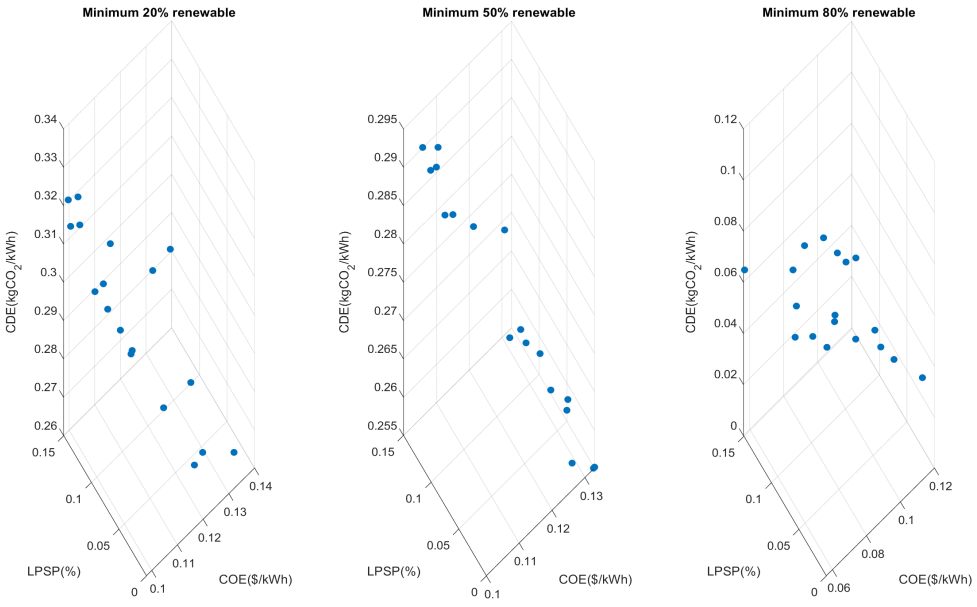

Figure III.7: Overall pareto curves (3D) of the three partial integration case studies

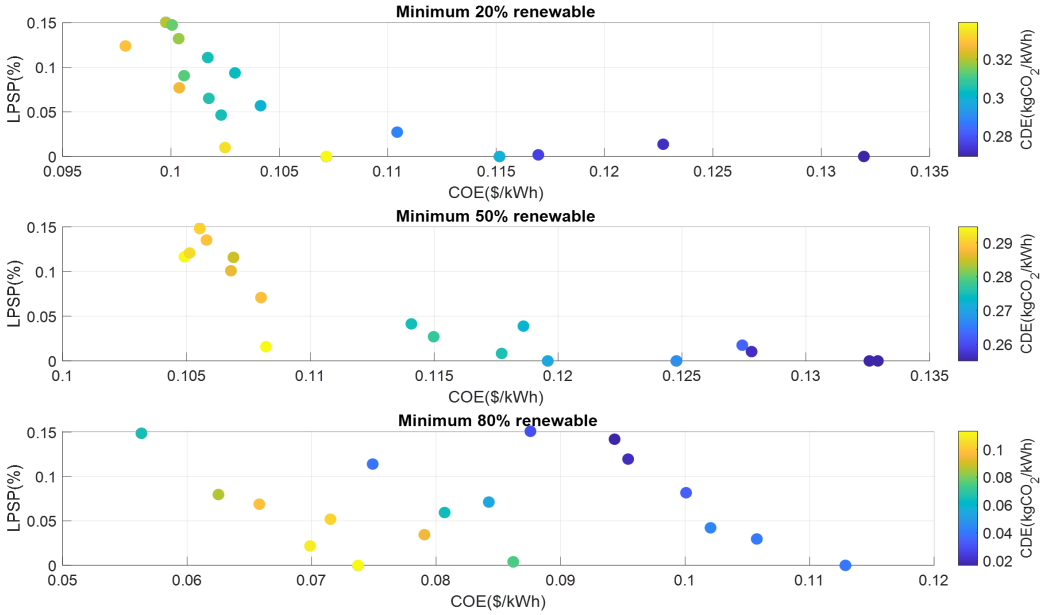

Figure III.8: Overall pareto curves (2D) of the three partial integration case studies

of 80% is considered. In this section 2 case studies are considered as presented in Table III.4. The first case study (Case study 9) considers the PV-WT as a renewable energy sources, BES-HES as a storage with priority to BES as a short run hourly charge/discharge priority and HES as a secondary long run daily charge/discharge mean. Additionally, GT is integrated into the system sources with a

limit of 20% of total load in order to limit the CDE. The second case study (Case study 10) to be evaluated in this section is same as case study 9 with storage charge/discharge priority is inversed making HES as the short run hourly priority whereas BES is considered as the long run daily storage mean.

Table III.4: Partial shift case study configurations (dual storage)

Case Study	Sources	Storages	Description
Case study 9	PV-WT (min 80%) - GT (max 20%)	BES-HES	Minimum 80% integration of RE with BES/HES storage system
Case study 10	PV-WT (min 80%) - GT (max 20%)	BES-HES	Minimum 80% integration of RE with HES/BES storage system

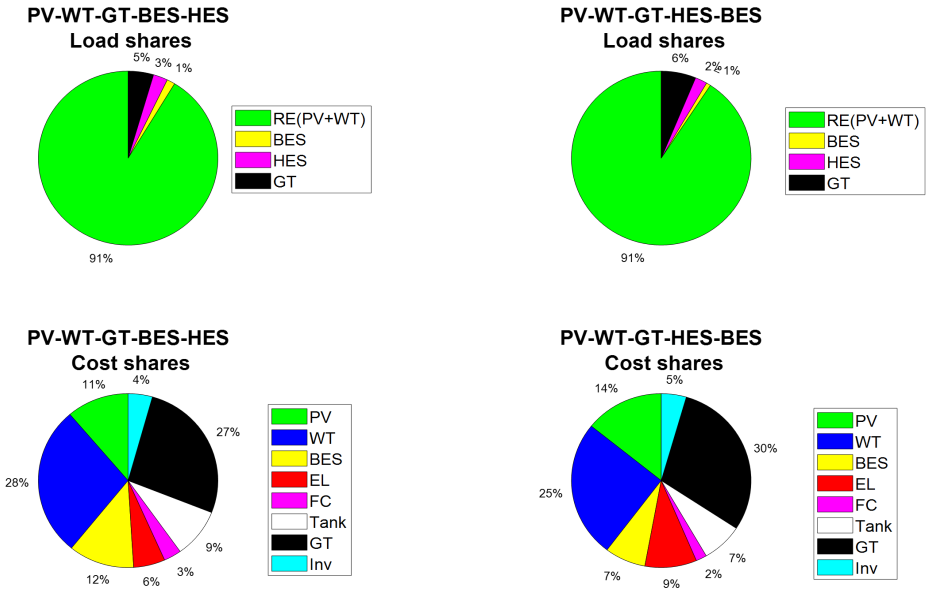

Figure III.9: Load and cost shares for partial integration with dual storage

With a null LPSP, case study 9 and 10 reach a low COE of 0.1169 $/kWh and 0.1134 $/kWh with a CDE of 0.0279 gCO2eq/kWh and 0.0377 gCO2eq/kWh respectively. This confirms effectiveness of reaching low COE and CDE when considering partial shift with dual storage, additionally, the conflicting between the COE and CDE is revealed, this behavior of conflicting can clearly show in Figs. III.10 and III.11 . Regarding the load sharing breakdown as shown in Fig. III.9 , for both storage priority strategy, the constraint of ensuring a level of 80% of renewable integration is ensured with only 4.57% and 6.26% of total annual load is ensured by GT for case study 9 and 10 respectively. The storage system participates to less than 3% for both HESS and BEES respectively. Talking about the cost sharing, and although the GT and storage systems participate to less that 10% of the total

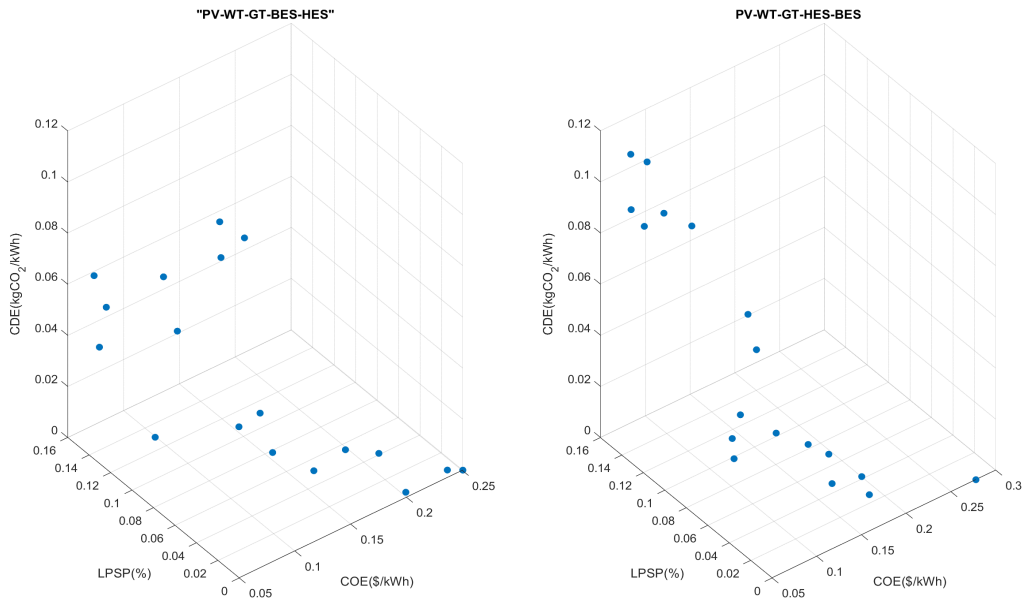

Figure III.10: 3D pareto curves of partial integration of RE (dual storage)

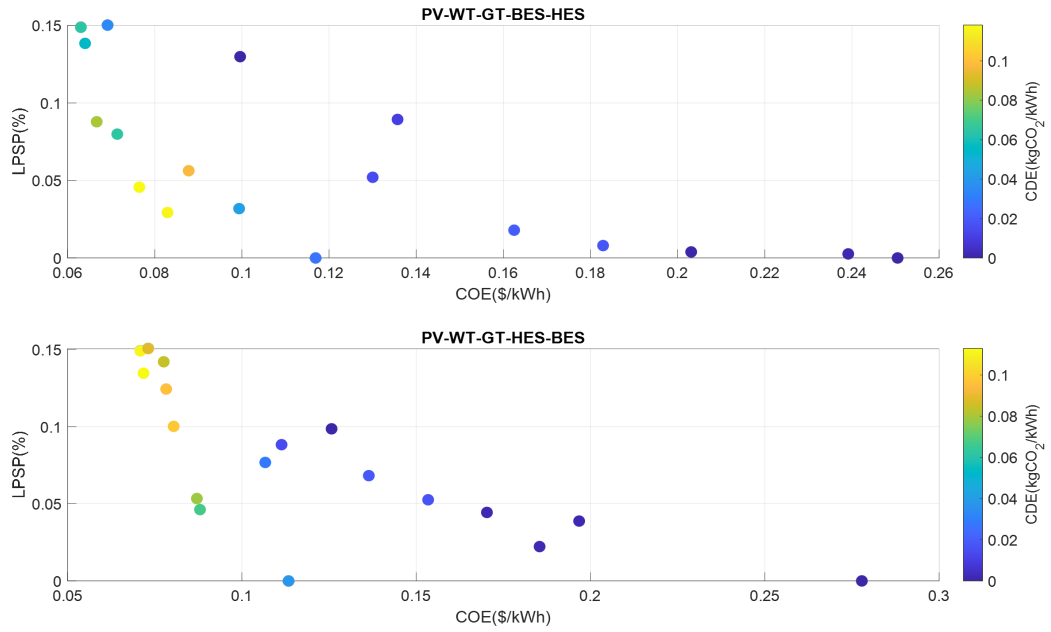

Figure III.11: Detailed pareto curves of partial integration of RE (dual storage)

load, their cost participation is relatively significant. For instance, and always taking the 0 of LPSP configuration, GT, BES system and HESS participate by (27%,12% and 18% respectively) for case study 9 and by (30%, 7% and 18% respectively) for case study 10. The other cost participation is shared between RE sources, usually the inverters participate of less than 5% for both case studies. For

further investigation, and if the operator may accept a certain level of non-null LPSP, the shares may differs and further techno-economic investigation is performed based on the chosen feasible solution from the pareto curve as shown in Figs. III.10 and III.11 . From this analysis, it is clear that even the backup system based on GT and storage system merely participate to the load shares, their presence is important to ensure the null LPSP. Additionally, their cost is significant due to initial, maintenance, operation and replacement expenditures.

III.3.4 Overall case studies optimal results comparison

After completing the overall optimization process, results of the output objective functions (COE, LPSP and CDE) are presented in Fig. III.12 , Tables III.5 and III.6. From these results, from the technical objective function, only case study 02 that cannot reach a null LPSP, the minimum reachable LPSP for this configuration accounts of 8.92%. alternatively, the economic and the environmental analysis of the obtained outputs at null LPSP reveals the confecting behavior between COE and CDE. For instance, case studies with full renewable shift (configurations 3,4,5) present a higher COE, this is due to the higher investment, replacement and OM for RE subsystems. In the other hand, when partial shift is considered, the systems present a reduction in COE compared to full shift system and a benefit in CDE reduction compared to reference system based on fossil fuel. In fact, case study 8 presents a COE similar to reference system with a huge amount of CDE reduction by -93.5733% to reach a CDE of 0.0377 (gCO2eq/kWh).

III.4 Trends of generated/consumed power

To provide a time-based analysis of the obtained results, since they presents the most complete systems and contain all the possible sources and storage strategies, case studies 9 and 10 are shown to present the trends of generated consumed power. In this section, the monthly trends of total load demand, energy produced, and energy consumed are presented, as shown in Fig. III.13 for Case Study 9. As previously noted in Fig. III.9, Fig. III.13 offers more detailed insights into the monthly distribution of produced and consumed power. The trends indicate that solar and wind energy reach their peak production levels during the summer months due to higher availability of renewable energy sources during this period. This reinforces the appropriateness of selecting solar and wind as the main renewable energy sources for this system configuration.

Since Case Study 9 sets a minimum renewable energy factor of 80%, the optimal solution results

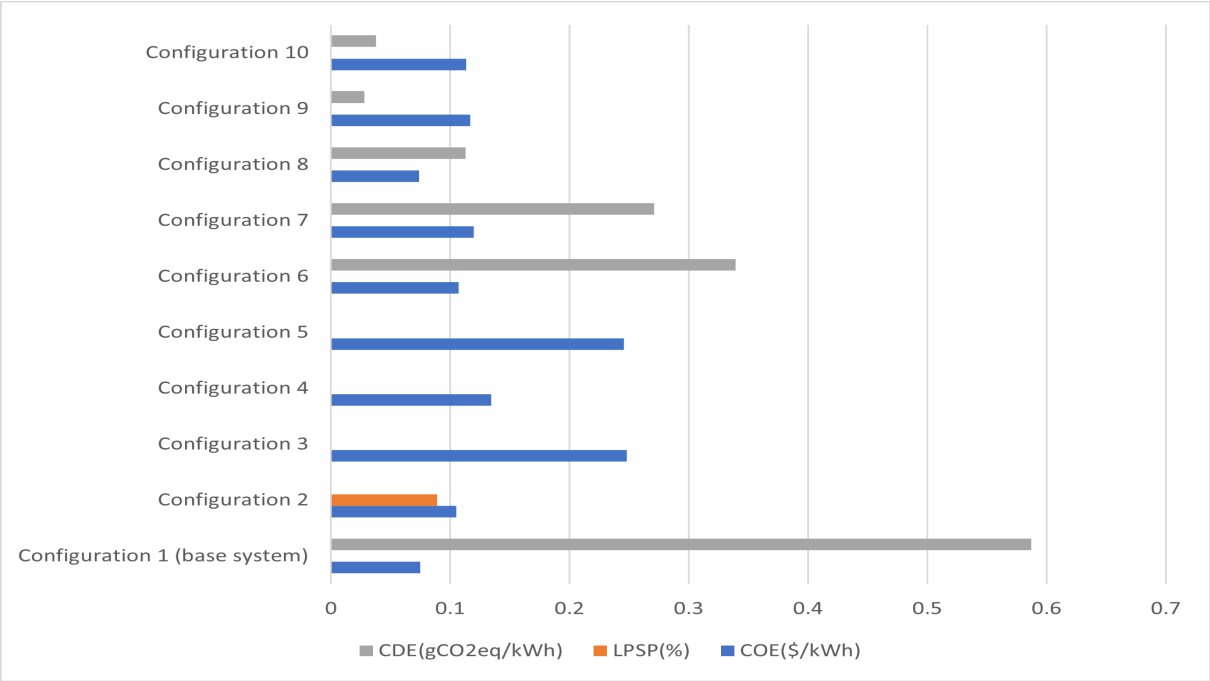

Figure III.12: Overall case studies optimal objective functions (COE, LPSP,CDE)

in a renewable energy factor exceeding 95%, mainly supplied by PV and WT. The remaining energy, which accounts for nearly half of the total produced renewable energy, is classified as Excess Power Supply (EPS). This significant level of excess energy is a result of the optimization process, which aims to ensure 0% LPSP. To achieve 0% LPSP, the system must fully supply the load during every hour of the year, necessitating higher-rated renewable energy systems. As a result, excess energy is generated during hours of high solar and wind availability.

Additionally, the Gas Turbine (GT) primarily operates during months with lower renewable energy production, such as January and November. During these months, GT contributes to approximately 10% of the total monthly load demand to compensate for the reduced availability of renewable sources. Ultimately, Fig. III.13 provides a clear depiction of the seasonal variations in energy production and consumption, illustrating the system's reliance on renewable sources during high-availability periods and the role of GT in ensuring reliability during low renewable production months.

Furthermore, storage system trends are examined based on Fig. III.14 graphics. For case study 9 the BES system varies in the range of 10.32 -16.87 MWh, with more charging discharging cycles during winter periods (periods with low RE energy sources availability), compared to case study 10, where the BES system become the secondary storage mean, the level of storage in most time stays between 06.42 and 10.2 MWh, with the same charging/discharging behavior as configuration 9. Talking about the HESS, for case study 9, the fluctuation in the HESS storage is limited to

Table III.5: Overall case studies optimal (Reference system + full shift to RE)

Configuration	**Configuration 1 (base system)**	**Configuration 2**	**Configuration 3**	**Configuration 4**	**Configuration 5**
	0% Renewable	**100% Renewable**	**100% Renewable**	**100% Renewable (dual storage)**	**100% Renewable (dual storage)**
PV		✓	✓	✓	✓
WT		✓	✓	✓	✓
GT	✓				
HESS		✓		✓	✓(p)
BES system			✓	✓(p)	✓
DoD			79.4618%	73.5300%	63.5400%
RE	0.0000%	100.0000%	100.0000%	100.0000%	100.0000%
COE ($/kWh)	0.0750	0.1051	0.2479	0.1345	0.2454
LPSP (%)	0.00%	8.92%	0.0000%	0.0000%	0.0000%
CDE (gCO2eq/kWh)	0.5872	0.0000	0.0000	0.0000	0.0000
Rated (MW) Load	11.5647	11.5647	11.5647	11.5647	11.5647
Rated (MW) PV	0.0000	57.4550	56.1274	64.0944	56.2038
Rated (MW) WT	0.0000	22.0400	22.0000	21.8800	21.0200
Rated (MW) GT	11.6000	0.0000	0.0000	0.0000	0.0000
Rated (MW) EL	0.0000	8.6940	0.0000	11.9532	5.1618
Rated (MW) FC	0.0000	3.3975	0.0000	13.0675	2.2675
Rated (kg) Tank	0.0000	11 137.0000	0.0000	14 815.0000	10 707.0000
Rated (MW) Bat charging	0.0000	0.0000	-58.7753	-4.1533	-52.6977
Rated (MW) Bat discharging	0.0000	0.0000	11.1164	2.9788	8.8489
Rated (MW) LPS	0.0000	7.7189	0.0000	0.0000	0.0000
Rated (MW) EPS	0.0000	72.5166	71.0657	79.4303	70.1680
Total yearly (MWh) Load	83 470.0353	83 470.0353	83 470.0353	83 470.0353	83 470.0353
Total yearly (MWh) PV	0.0000	124 825.3418	121 940.8584	139 249.8445	122 107.0169
Total yearly (MWh) WT	0.0000	137 392.9903	137 143.6382	136 395.5820	131 034.5125
Total yearly (MWh) GT	83 470.0353	0.0000	0.0000	0.0000	0.0000
Total yearly (MWh) EL	0.0000	8 557.5533	0.0000	14 224.5984	6 509.0089
Total yearly (MWh) FC	0.0000	3 414.8558	0.0000	5 637.3636	2 589.5693
Total yearly (MWh) Bat charging	0.0000	0.0000	-8 949.9278	-853.6951	-5 666.3307
Total yearly (MWh) Bat discharging	0.0000	0.0000	6 305.5510	615.1135	3 971.4151
Total yearly (MWh) LPS	0.0000	2 865.6544	0.0000	0.0000	0.0000
Total yearly (MWh) EPS	0.0000	172 078.0939	168 576.9247	178 956.4151	159 663.9791

daily charging/discharging cycle, and most of time the amount of stored hydrogen lays in the tanks maximum level of 14 672 kg, however , for case study 10, and since the primary storage mean is the HESS, the trends of the stored hydrogen in tank presents more hourly fluctuations with low level of

Table III.6: Overall case studies optimal (Partial shift to RE)

Configuration	**Configuration 6**	**Configuration 7**	**Configuration 8**	**Configuration 9**	**Configuration 10**
	HRES (RF≥20%)	**HRES (RF≥50%)**	**HRES (RF≥80%) - non feasible without WT**	**HRES (RF ≥80%)**	**HRES (RF ≥80%)**
PV	✓	✓	✓	✓	✓
WT			✓	✓	✓
GT	✓	✓	✓	✓	✓
HESS	✓	✓	✓	✓	✓(p)
BES system				✓(p)	✓
DoD				38.8058%	36.9700%
RE	42.33%	53.96%	80.92%	95.4261%	93.7400%
COE ($/kWh)	0.1072	0.1196	0.0737	0.1169	0.1134
LPSP (%)	0.00%	0.00%	0.00%	0.00%	0.00%
CDE (gCO2eq/kWh)	0.3391	0.2709	0.1129	0.0279	0.0377
Rated (MW) Load	11.5647	11.5647	11.5647	11.5647	11.5647
Rated (MW) PV	25.0941	58.6339	1.4768	22.4134	27.5325
Rated (MW) WT	0.0000	0.0000	15.4200	21.2000	18.7600
Rated (MW) GT	11.4000	10.1000	10.6000	8.9000	9.5000
Rated (MW) EL	10.8864	9.1098	0.4746	3.8556	6.3756
Rated (MW) FC	0.4250	1.5575	0.0900	2.0850	1.1725
Rated (kg) Tank	12 243.0000	11 804.0000	1 312.0000	14 672.0000	11 476.0000
Rated (MW) Bat charging	0.0000	0.0000	0.0000	-7.6986	-4.4389
Rated (MW) Bat discharging	0.0000	0.0000	0.0000	5.5626	3.2037
Rated (MW) LPS	0.0000	0.0000	0.0000	0.0000	0.0000
Rated (MW) EPS	16.4862	49.5590	7.8395	34.8225	37.7666
Total yearly (MWh) Load	83 470.0353	83 470.0353	83 470.0353	83 470.0353	83 470.0353
Total yearly (MWh) PV	54 518.7526	127 386.5462	3 208.4577	48 694.8631	59 816.3577
Total yearly (MWh) WT	0.0000	0.0000	96 125.2228	132 156.5968	116 946.1206
Total yearly (MWh) GT	48 136.0880	38 427.8826	15 929.5603	3 817.8380	5 223.0569
Total yearly (MWh) EL	6 553.1919	20 274.9296	698.4453	5 514.6911	4 621.6805
Total yearly (MWh) FC	2 570.2015	8 102.7920	277.7448	2 176.9121	1 807.9183
Total yearly (MWh) Bat charging	0.0000	0.0000	0.0000	-1 714.2716	-918.7573
Total yearly (MWh) Bat discharging	0.0000	0.0000	0.0000	1 230.3907	657.8663
Total yearly (MWh) LPS	0.0000	0.0000	0.0000	0.0000	0.0000
Total yearly (MWh) EPS	13 342.1336	67 801.6163	27 817.7430	93 185.3818	91 322.5847

variation in the total stored amounts in the tanks between 10000-11500 kg.

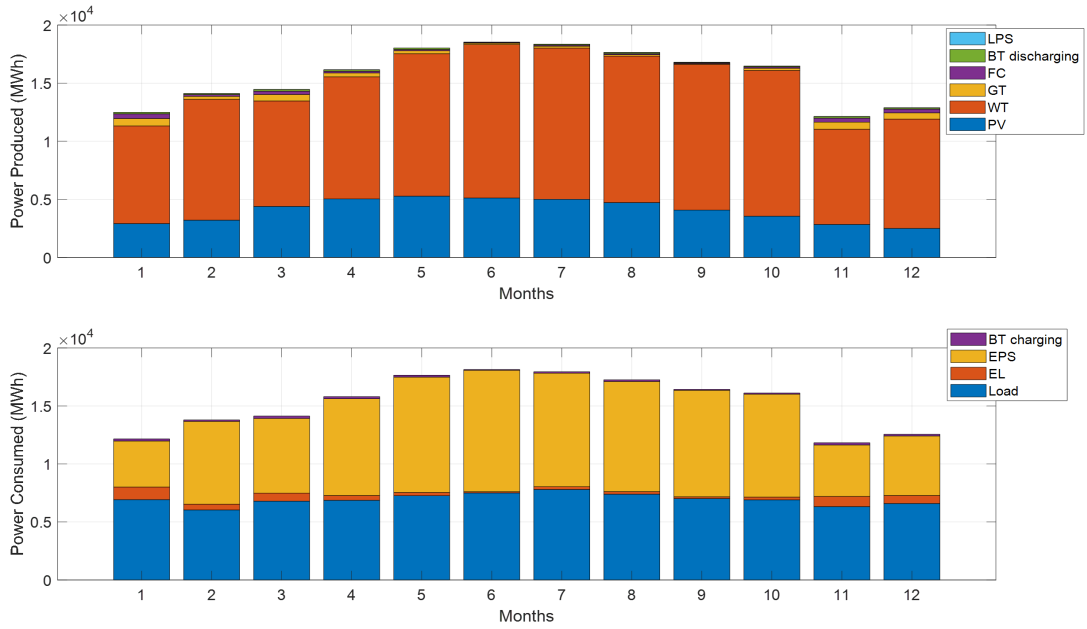

Figure III.13: Overall case studies optimal objective functions (COE, LPSP,CDE)

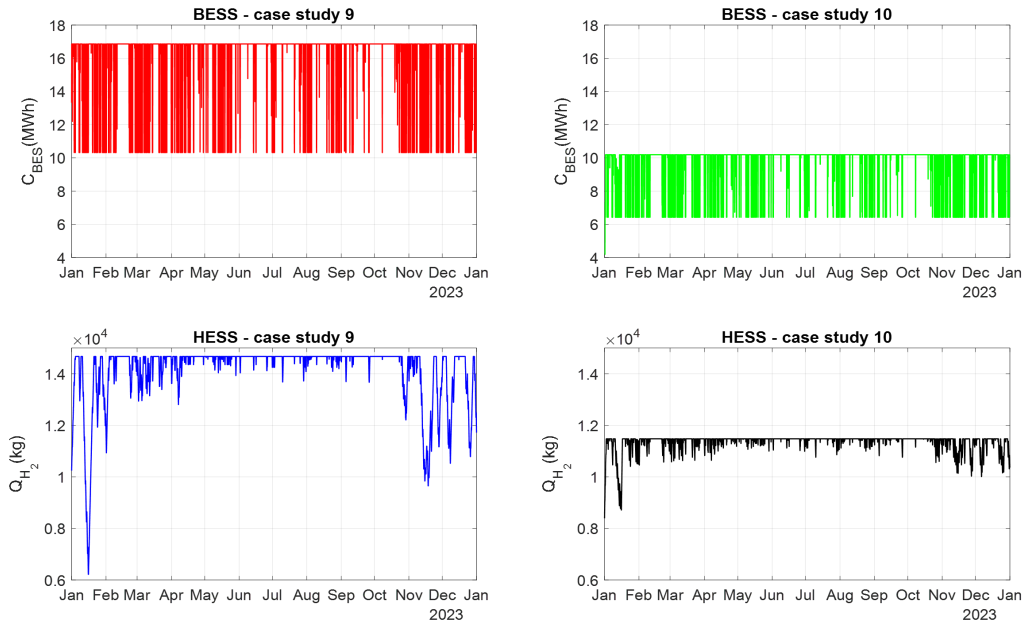

Figure III.14: Overall case studies optimal objective functions (COE, LPSP,CDE)

III.5 Comparison between optimization results with NSGA-II, MPSO and FLA

The optimization algorithm plays a crucial role in obtaining global optimal solution while keeping an eye on the performances and speed of reaching a global optimal solution. In this regard, a comparative study is conducted to evaluate the behavior of the 3 different chosen algorithms to solve the optimization problem. The case study 8 is chosen to be the base case study used to compare between algorithm performances. Firstly, NSGA-II and MOMSO result outcomes are compared based on the multi-objective outputs Table III.7, taking into account a null LPSP, the obtained COE is accounted for 0.07372687 and 0.113880991 for NSGA-II and MOMSO respectively. However, this difference is due to the level of renewable energy integration (RF). The RF for MOPSO 95.39% is much higher than that of NSGA-II (80.92%), this makes the COE for MOPSO results higher than that of NSGA-II, in contrast, the high level of RF leads to low CDE for MOPSO results 0.028097167 gCO2eq/kWh compared to a 0.112910888 gCO2eq/kWh for the NSGA-II, these differences confirms also the conflicting behavior of the objectives and confirms the necessity of applying a decision making process to help operators and investors choose the best configuration that aligns with their objectives, this decision making process is based on the pareto non dominant solution as presented in Fig. III.15. Additionally, from Table III.7, FLA can reach optimal results regarding ensuring a minimum non null LPSP, in this way the FLA algorithm reach a higher renewable energy integration more than 99% similar to a full shift system presented in configuration 2. Another important insight to take from these outcomes is about the difference between considering multi-objective optimization problem and converting a multi-objective problem into a single objective problem as done in the FLA case, in this case even the output optimal problem may be acceptable, although, it can hide another promising solution from pareto curve. This solution may have importance in the operators and investors point of view.

III.6 Decision making processes

In this section, and after obtaining a set of non-dominant optimal solutions using NSGA-II and MOPSO algorithms, it is crucial to use a well defined method to select the best tradeoff between objective functions in order to help operator and investor selecting the best configuration that leads to the satisfaction of their objectives. In this case the pareto curve obtained from NSGA-II of the

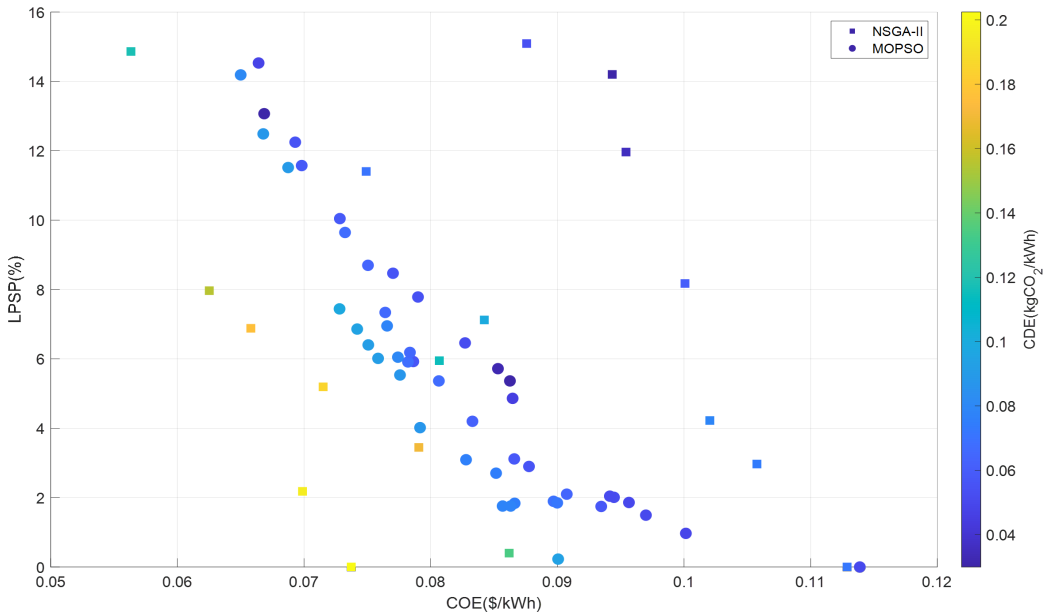

Figure III.15: Pareto non-dominant solution of NSGA-II vs MOPSO

case studies 9 and 10 are studied using both TOPSIS and SAW algorithms. Detailed obtained results are presented in Table III.8.

From Table III.8, overall TOPSIS and SAW decision making methods are presented and ranked based on their relative closeness as presented in previous chapter. From these outcomes, it is clear that strategy based on BES system as a primary storage system slightly surpass the strategy where HESS is considered as the primary storage mean, however, both strategies (9 and 10) can reach a null LPSP at a COE of 0.1169 $/kWhand 0.1134/kWh respectively, with a CDE of 0.0500 gCO2/kWh and 0.0676 gCO2/kWh. In another insight, if the system operators and investors would accept a lower value for LPSP in order to reduce the COE, another configuration from Table III.8 may be chosen. For instance, for case study 9 (configuration 29 in Table III.8) an acceptable LPSP of 4.5662% would reduce the COE by 34.60% to reach 0.0765 $/kWh, however this configuration presents an increase in CDE to 0.2117 gCO2/kWh but is still within the acceptable range of reducing 80% of CDE compared to reference system (Case study 1). Additionally, for case study 10 (configuration 20 in Table III.8), an acceptable LPSP of 4.6233% would reduce the COE by 22.41% to reach 0.0880 $/kWh, with also CDE withing 80% reduction limit. The analysis using the Decision-making methods shows the effectiveness of getting an overall vision and revealing the hidden configurations that help the operators, and the investors choose the optimal tradeoff that meet their objectives.

Furthermore, and in order to get deep into the trends of the obtained results, the yearly, monthly

Table III.7: Comparison between NSGA-II, MOPSO, and FLA optimal results

Parameter	**NSGA-II**	**MOPSO**	**FLA**
Configuration	Configuration 8	Configuration 8	Configuration 8
	HRES (RF ≥ 80%) - non feasible without WT	**HRES (RF ≥80%) - non feasible without WT**	**HRES (RF ≥80%) - non feasible without WT**
PV	✓	✓	✓
WT	✓	✓	✓
GT	✓	✓	✓
HESS	✓	✓	✓
BES system			
DoD			
RE	80.92%	95.39%	99.17%
COE ($/kWh)	0.0737	0.1139	0.0798
LPSP (%)	0.00%	0.00%	8.57%
CDE (gCO2eq/kWh)	0.1129	0.0281	0.0060
Load (MW)	11.5647	11.5647	11.5647
PV (MW)	1.4768	43.4278	20.4367
WT (MW)	15.42	14.0070	14.2620
GT (MW)	10.6000	10.2206	0.8322
EL (MW)	0.4746	3.2903	7.2190
FC (MW)	0.0900	6.0829	7.6877
Tank (kg)	1 312.0000	10 691.8486	8 232.4397
Bat charging (MW)	0	0	0
Bat discharging (MW)	0	0	0
LPS (MW)	0.0000	0.0000	9.6399
EPS (MW)	7.8395	49.2258	25.4598
Load (MWh)	83 470.0353	83 470.0353	83 470.0353
PV (MWh)	3 208.4577	94 350.0653	44 400.2824
WT (MWh)	96 125.2228	87 316.8729	88 906.5061
GT (MWh)	15 929.5603	3 850.5207	674.8232
EL (MWh)	698.4453	13 986.5642	17 843.4186
FC (MWh)	277.7448	5 747.0481	7 292.9611
Tank (kg)	0.0000	0.0000	0.0000
Bat charging (MWh)	0.0000	0.0000	0.0000
Bat discharging (MWh)	0.0000	0.0000	0.0000
LPS (MWh)	0.0000	0.0000	2 748.0785
EPS (MWh)	27 817.7430	89 617.4068	38 351.5547

and daily trends of the 04 previous cases are evaluated. This case are summarized and presented in Tables III.9 and III.10 and Figs. III.16 to III.24.

Table III.8: Overall Optimization Results for Case Studies 9 and 10

Config.	Case Study	COE ($/kWh)	LPSP (%)	CDE (gCO2 / kWh)	TOPSIS Relative Closeness	SAW Relative Closeness	TOPSIS Rank	SAW Rank
01	9	0.1169	0.0000	0.0500	81.0337	16.2253	1	1
02	10	0.1134	0.0000	0.0676	77.6749	18.4629	2	2
03	9	0.1625	1.7922	0.0365	74.1405	25.1376	3	6
04	9	0.1300	5.2055	0.0258	73.9826	25.9616	4	8
05	9	0.0994	3.1849	0.0774	72.9438	24.8648	5	5
06	10	0.1854	2.2260	0.0037	72.8087	24.5004	6	4
07	9	0.1829	0.7991	0.0324	72.2634	25.4608	7	7
08	9	0.2031	0.3881	0.0000	71.8873	22.5941	8	3
09	10	0.1703	4.4406	0.0025	71.8528	26.8529	9	9
10	10	0.1534	5.2626	0.0300	70.0690	30.3859	10	13
11	10	0.1967	3.8813	0.0028	68.7706	29.7774	11	12
12	10	0.1364	6.8265	0.0334	68.1412	31.7495	12	17
13	10	0.1067	7.6826	0.0500	66.8064	31.6378	13	16
14	10	0.1114	8.8356	0.0248	66.6395	30.9534	14	14
15	9	0.2391	0.2626	0.0027	66.6151	28.3396	15	10
16	9	0.2505	0.0000	0.0000	65.4945	29.0877	16	11
17	10	0.1257	9.8630	0.0000	65.1426	31.5455	17	15
18	9	0.1357	8.9384	0.0187	64.7180	33.9878	18	20
19	10	0.2778	0.0000	0.0000	62.2845	33.3333	19	19
20	10	0.0880	4.6233	0.1201	62.2008	33.0114	20	18
21	9	0.0996	12.9909	0.0000	60.4347	34.4090	21	21
22	9	0.0714	7.9909	0.1159	57.8773	37.2128	22	22
23	10	0.0871	5.3425	0.1408	57.1246	37.7154	23	23
24	9	0.0692	15.0228	0.0621	52.7522	43.9669	24	26
25	9	0.0667	8.7900	0.1508	51.2737	43.7506	25	25
26	9	0.0829	2.9338	0.2081	51.0053	42.3331	26	24
27	9	0.0878	5.6279	0.1758	50.9314	43.9733	27	27
28	9	0.0640	13.8470	0.0993	50.4457	46.4212	28	29
29	9	0.0765	4.5662	0.2117	48.9226	45.5159	29	28
30	9	0.0630	14.8858	0.1154	47.1279	51.1047	30	30
31	10	0.0804	10.0228	0.1760	44.5844	52.5758	31	31
32	10	0.0776	14.2123	0.1508	42.2737	57.4314	32	33
33	10	0.0783	12.4429	0.1707	42.0526	56.7599	33	32
34	10	0.0731	15.0685	0.1586	41.0143	59.8634	34	34
35	10	0.0718	13.4703	0.2023	38.7027	62.9998	35	35
36	10	0.0709	14.9201	0.1990	37.7950	65.5478	36	36

Table III.9: Rated power and working hours for each subsystem

Configuration	**Case study 09 – config. 01**	**Case study 10 – config. 02**	**Case study 09 – config. 29**	**Case study 10 – config. 20**
Storage priority	BES system	HESS	BES system	HESS
LPSP(%)	0%	0%	4.5662%	4.6233%
PV (MW)	22.4134	27.5325	18.8237	11.3616
WT (MW)	21.2000	18.7600	8.9400	15.0600
GT (MW)	8.9000	9.5000	8.1000	7.3000
BT charging rated (MW)	-7.6986	-4.4389	-1.1324	-2.4224
BT discharging rated (MW)	5.5626	3.2037	0.7459	1.7329
SOC_{init} (%)	42.8337	41.1505	37.2902	34.7712
SOC_{final} (%)	61.1942	63.0185	75.1010	72.7851
BT number of cycles (-)	284	185	404	237
BT working hours (charge/discharge)	7201 / 1559	7691 / 407	3424 / 5336	7736 / 409
FC (MW)	2.0850	1.1725	0.1575	0.4400
FC running hours (hours)	1165	1644	5177	2615
EL (MW)	3.8556	6.3756	1.2894	3.9690
EL running hours (hours)	1598	1135	1835	1163
Tanks (kg)	14 672	11 476	9 063	14 555
$H_{2\ init}$ (%)	69.8387	72.2398	80.4407	78.2856
$H_{2\ end}$ (%)	79.8596	90.2663	97.6545	92.1739

Table III.10: Optimal Rated Power for the Studied System (All Case Studies)

Configuration	**Case study 09 – config. 01**	**Case study 10 – config. 02**	**Case study 09 – config. 29**	**Case study 10 – config. 20**
Storage priority	BES system	HESS	BES system	HESS
LPSP (%)	0%	0%	4.57%	4.62%
PV (MWh)	48 694.8631	59 816.3577	40 895.8429	24 683.9199
WT (MWh)	132 156.5968	116 946.1206	55 730.1875	93 881.0541
GT (MWh)	3 817.8380	5 223.0569	16 606.8328	9 341.7457
BT charging (MWh)	-1 714.2716	-918.7573	-391.6644	-598.9061
BT discharging (MWh)	1 230.3907	657.8663	282.2462	427.3631
FC (MWh)	2 176.9121	1 807.9183	807.3876	1 124.0055
EL (MWh)	5 514.6911	4 621.6805	2 095.3033	2 909.5699
LPS (MWh)	0.0000	0.0000	324.7462	472.0883
EPS (MWh)	93 185.3818	91 322.5847	25 171.1244	39 050.1764

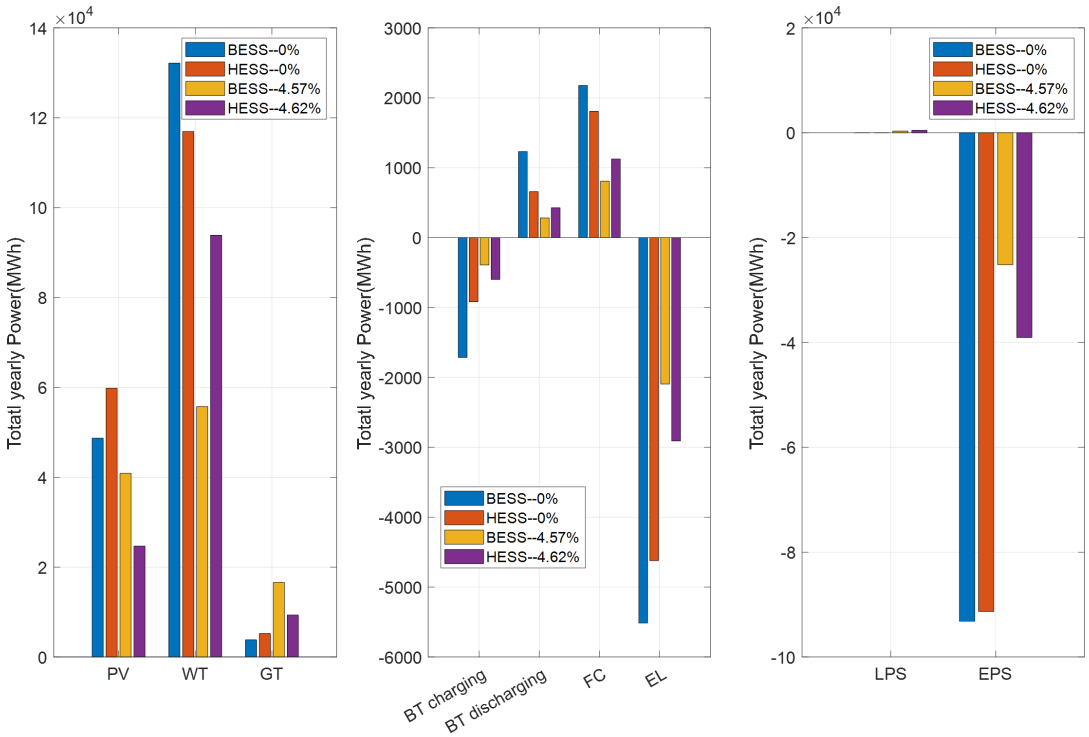

Figure III.16: Total yearly produced (+), consumed (-) power for each system component

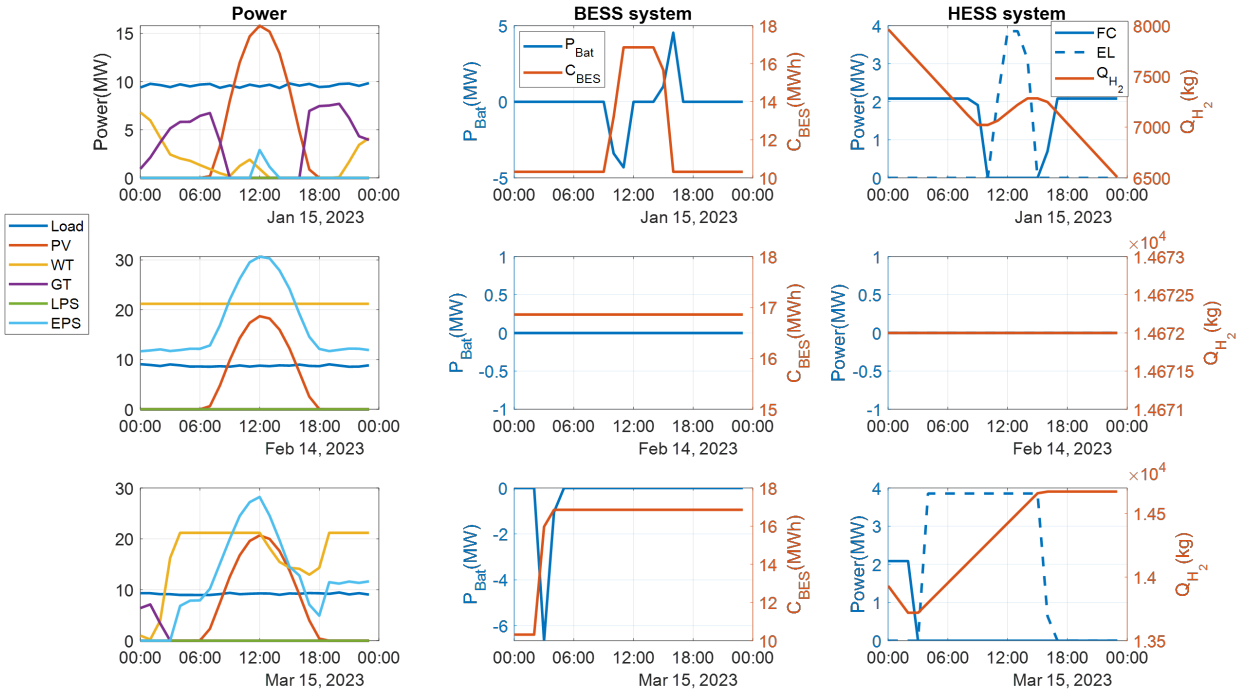

Figure III.17: case study 9 – configuration 01- (0% LPSP) - generated power (Jan, Feb, Mar)

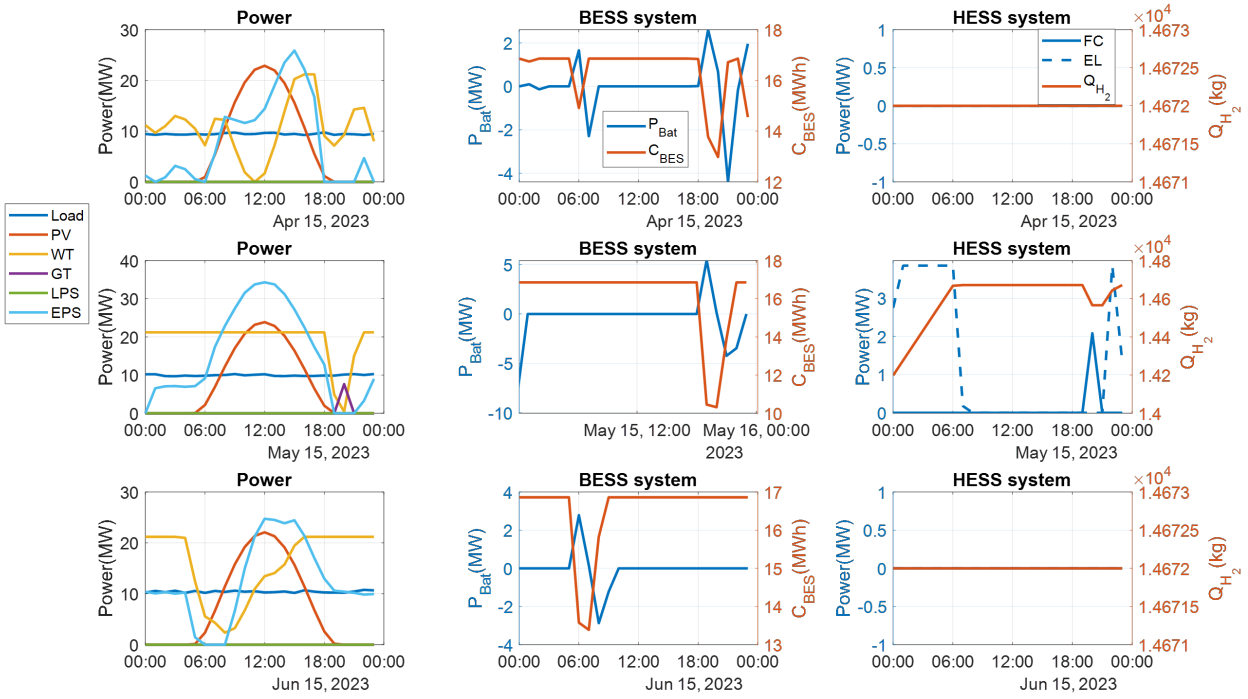

Figure III.18: case study 9 – configuration 01- (0% LPSP) - generated power (Apr, May, Jun)

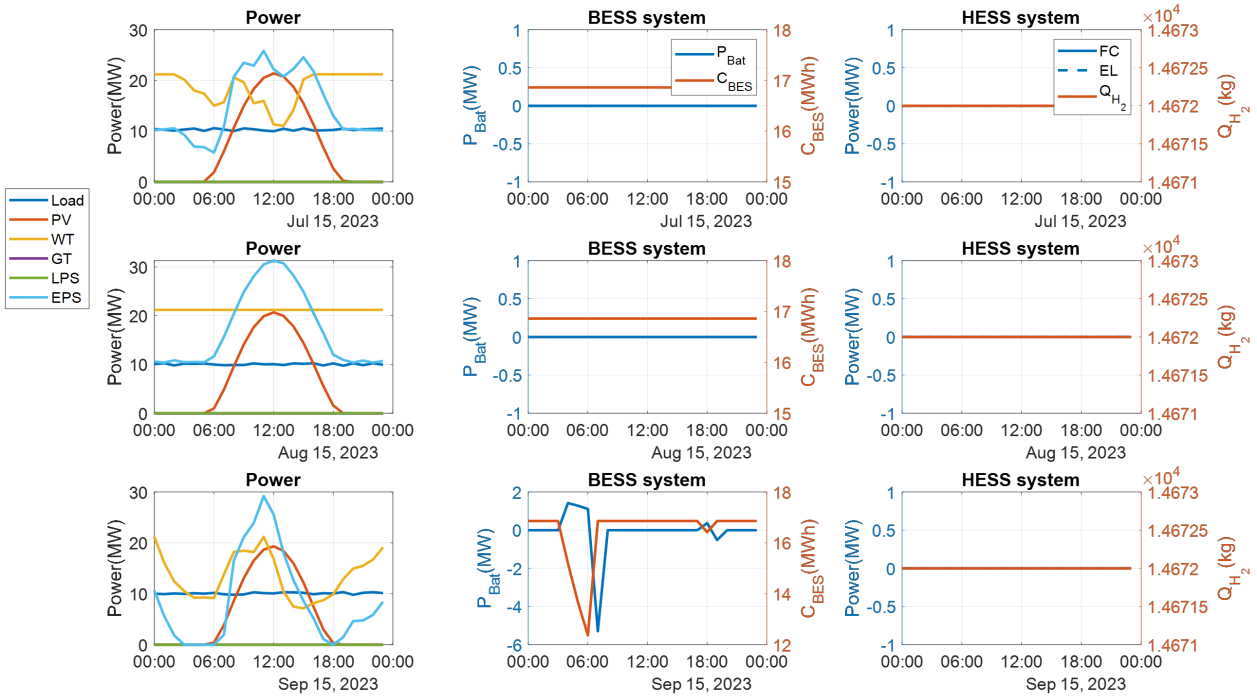

Figure III.19: case study 9 – configuration 01- (0% LPSP) - generated power (Jul, Aug, Sep)

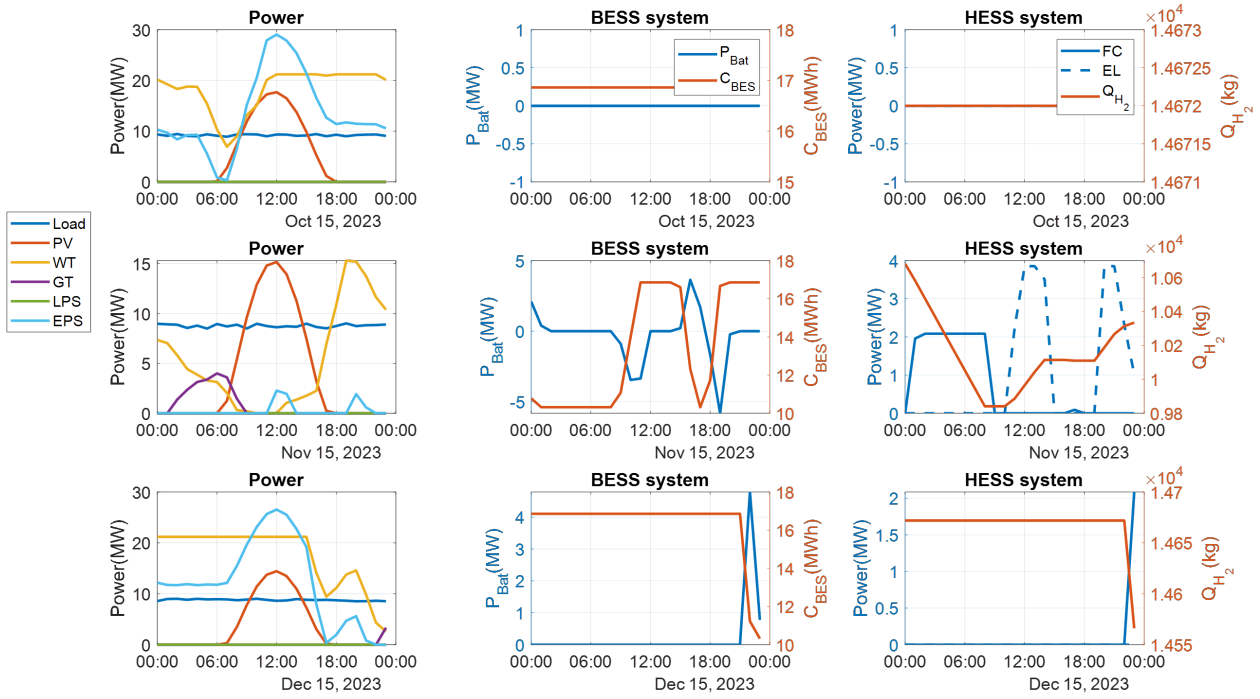

Figure III.20: case study 9 – configuration 01- (0% LPSP) - generated power (Oct., Nov., Dec.)

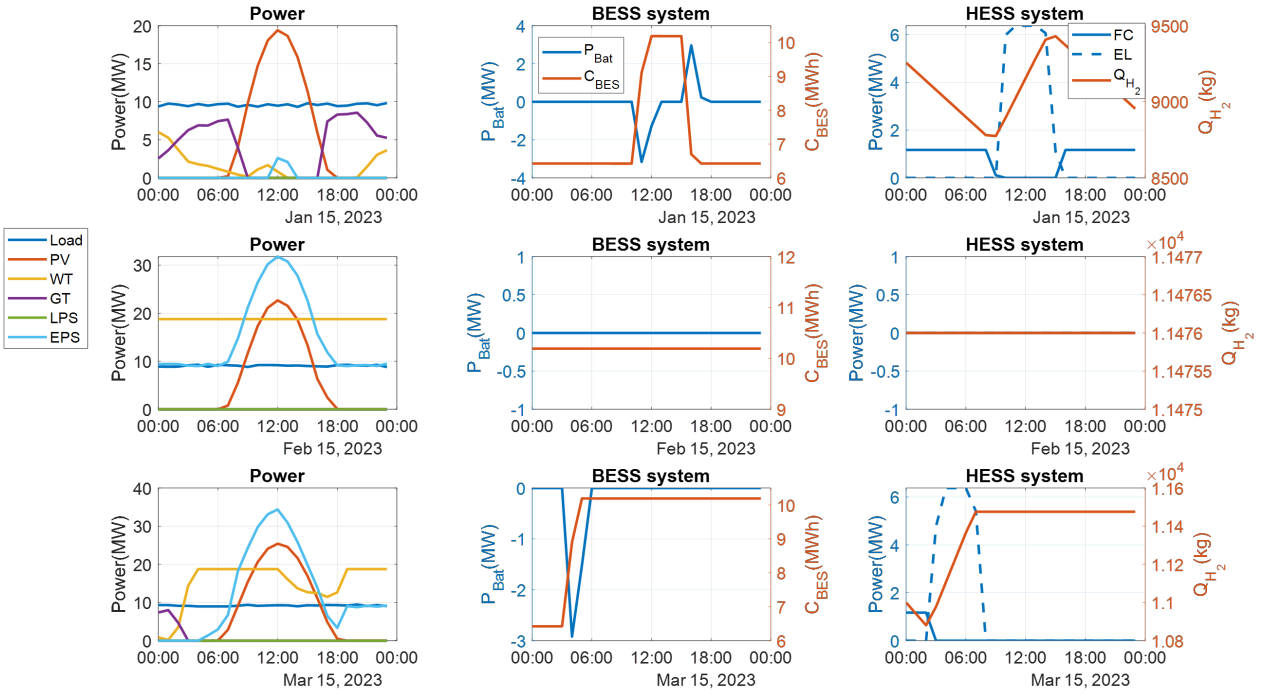

Figure III.21: case study 10 – configuration 02- (0% LPSP) - generated power (Jan, Feb, Mar)

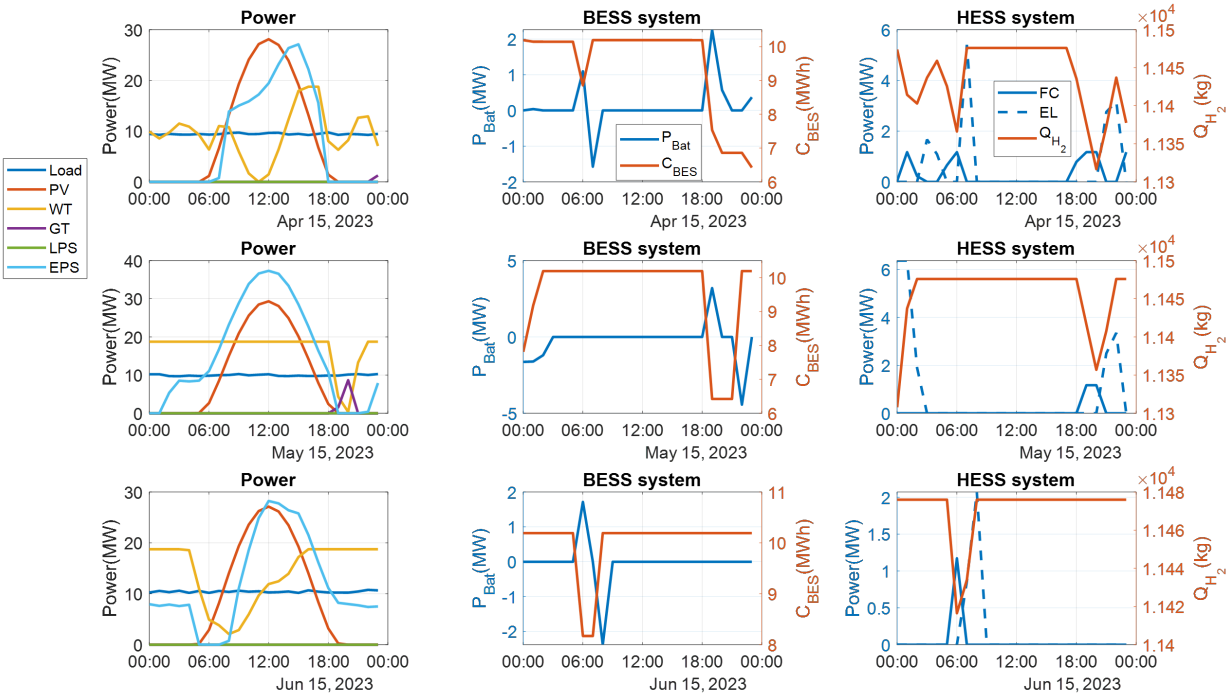

Figure III.22: case study 10 – configuration 02- (0% LPSP) - generated power (Apr, May, Jun)

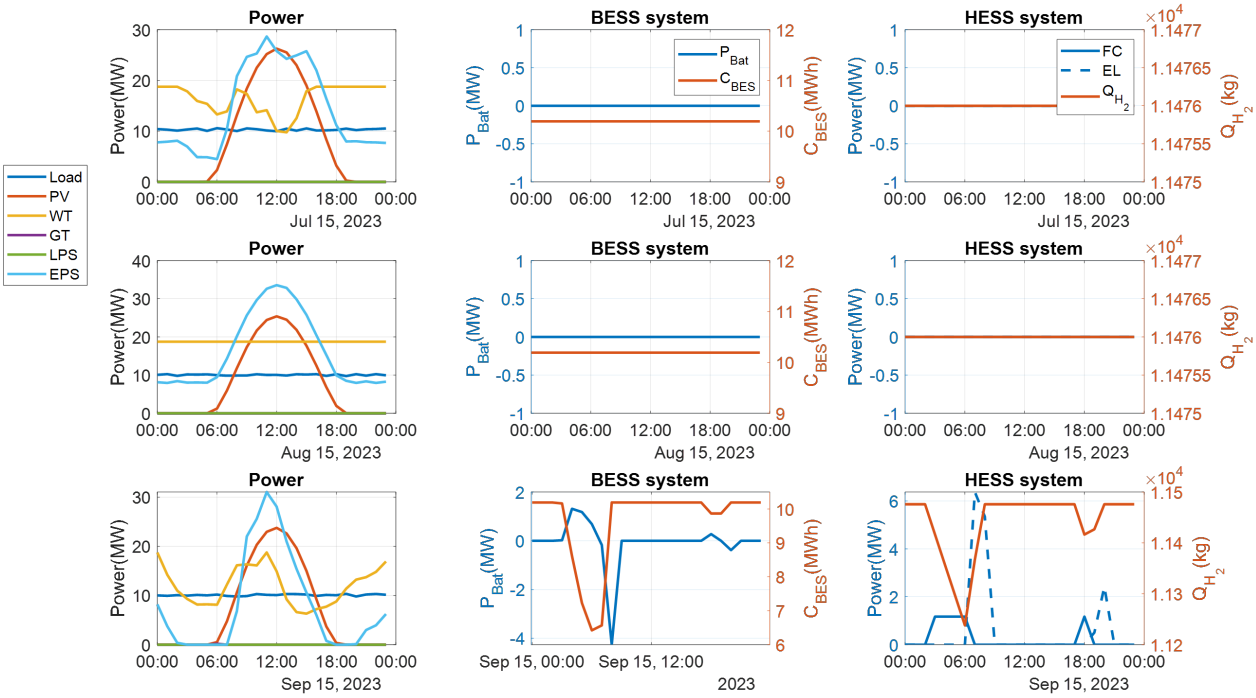

Figure III.23: case study 10 – configuration 02- (0% LPSP) - generated power (Jul, Aug, Sep)

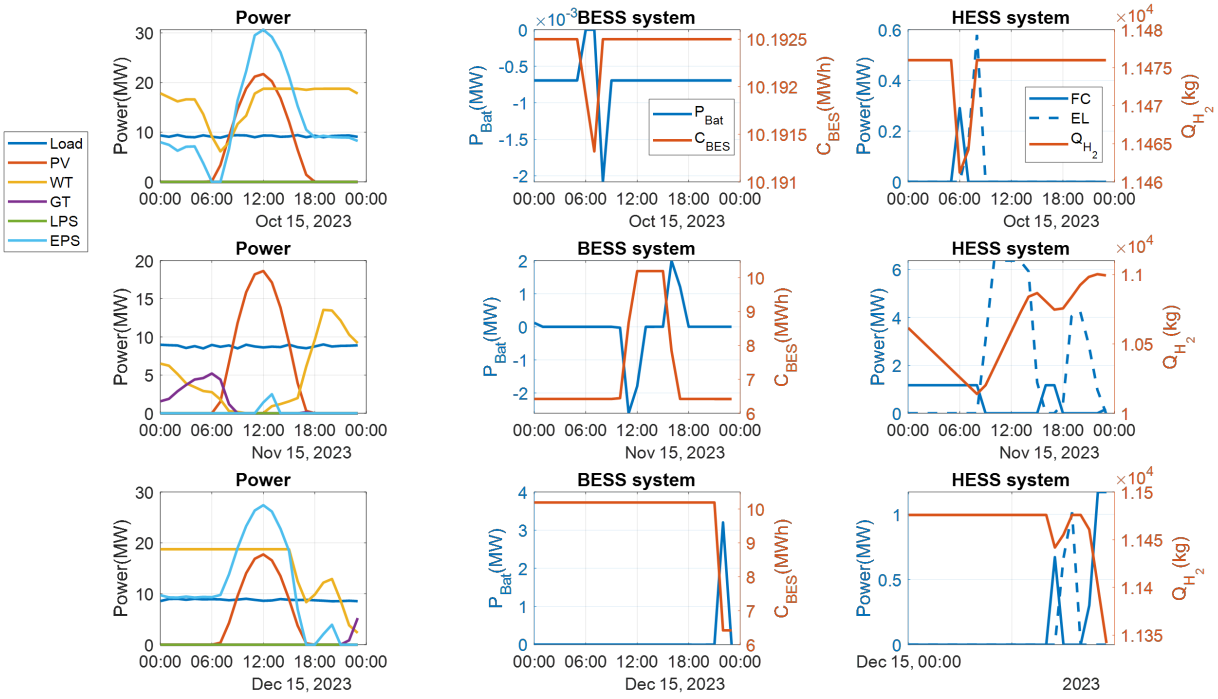

Figure III.24: case study 10 – configuration 02- (0% LPSP) - generated power (Oct., Nov., Dec.)

Based on tables III.9 and III.10 and Figs. III.17 to III.20, in order to achieve a null LPSP, the priority storage means presents the primary mean to address the intermittency of generated renewable power, for instance, in configuration 09, BESS has more number of cycles (284) and discharging periods (1559 hours) compared to the configuration 09 where HESS is the priority for the storage. In the case study 10, the BESS number of cycles is 185 and the discharging periods are only 407 hours reduced by 75%. In this case the reduced cycles and discharging periods may enhance the BESS and balance between BESS failure and HESS low roundtrip (charge /discharge) efficiency. On the other hand, the becomes the more important elements when HESS is the priority storage mean. For instance, the running hours for FC in the configuration 10 is more that 41% more compared to the running hours of FC in configuration 09, this confirms the system energy management strategy that assign short charging/discharging needs to the HESS system, the remaining needs for discharging to meet null LPSP is ensured firstly by BESS that using power from GT.

Furthermore, Figs. III.16 to III.24 gives an insightful graphic vision on the trends of generated power, load profile and storage systems on a seasonal basis for both case studies 09 and 09. A selected daily variation is presented for each month to visualize the trends of each energy quantity. The trends presented in these graphs confirms the effectiveness of the used modeling methods, of

the selected EMS and the adopted optimization algorithm

III.7 Conclusion

In this chapter, simulation results for a hybrid renewable energy system (HRES) for electrifying an oil and gas processing plant are conducted and presented. These results are obtained after a rigorous techno-economic and environmental multi-objective based optimal sizing of the study system. Different case study was considered including reference system with 100% fossil fuel-based system, full shift toward renewable energy systems and partial integration of renewable energy system considering single (HESS or BES system) and dual ((HESS and BES system) energy storage systems. the multi-objective optimization problem is solved using different type of optimization algorithms including (NSGA, MOPSO and FLA), the results obtained are assessed in all techno-economic and environmental performance indicators. Furthermore, the multi-objective optimization algorithm reveals different non-dominant solution configurations known as pareto curves, these results are evaluated using decision making methods including TOPSIS and SAW. The obtained results revel the effectiveness of considering a partial integration level of 80% of renewable energy, while considering a dual storage energy system based on BES system as the primary short run storage and HESS as the secondary long-run storage mean. In this situation, with the insurance of null Loss of Power Supply Probability (LPSP = 0%), the Cost of energy account 0.0737 $/kWh with a huge reduction in Carbon Dioxide Emission factor (CDE) by more than 80% compared to the reference system based on full fossil fuel power plant. All obtained outcomes shown the effectiveness of the adopted HRES, the modeling and optimization methods, and decision-making process.

General Conclusion

The main issue that oil and gas sector suffer from nowadays is its environmental burdens of these heavy energy industry. This issue is becoming a serious matter due to the increase demand of energy worldwide. In this regard, the objective of this work is to develop a techno-economically feasible solution to address this matter.

To do, several suggested systems are studied to meet the techno-economic and environmental feasibility of the energy system for the electrification of an oil and gas processing facility. The suggested system proposes different ways to address the problematic by considering systems based on renewable energy sources (RES).

The first part of this thesis is dedicated to the literature review of the study system. This review includes the previous works conducted in this field. The conducted review is defined into the sub-fields of optimal sizing of a Hybrid Renewable Energy System. The first field consists of the review the state of the art of Algerian energy sector which is mostly relies on oil and gas. Secondly, a review on HRES including the electrification of remote areas/load, the electrification using fossil fuel-based power plants and previous works on considering renewable energy sources to electrify remote loads. Another part of the literature review in this thesis consists of previous research works conducted in order to modeling and optimal sizing of HRES. The modeling part includes sources, storage and energy management methods used in HRES modeling. Additionally, different previous used methods in optimal sizing of a HRES are explored and presented including different methods of problem formulation and solution methods. Finally, the literature review is concluded by an exploration of remaining research gaps in this field, which must be addressed.

The second section of this works is devoted to the problem formulation, modeling and optimal sizing of hybrid renewable energy system for the electrification of an oil and gas processing facility located in the southeast region of Algeria. Firstly, the reference already existing power system is presented with a clear evaluation of its Cost of Energy and Carbon dioxide emission level. Afterward, and before conducting a detailed modeling of a HRES, Climate data and Load profile are acquired,

these data are crucial in conducting the modeling and the optimal sizing of HRES since they are considered as a required system inputs. Upon the acquisition of different system inputs, extensive models for different components of the HRES are developed including sources (PV module, Wind turbine, Gas Turbine, Fuel Cell, and Electrolyzer) as well as storage systems (Battery energy storage system and Hydrogen energy storage system). All these models are validated against experimental data before their use in the simulation process. In the same section, Energy management strategy (EMS) was developed, in our case, a rule-based EMS is considered in order to define the flow of power in each time step of the simulation period, additionally the EMS outputs the defined key performance indicators (KPIs) to be assessed at the end of the optimization process including technical, economic and environmental KPIs. The optimal sizing of the HRES is conducted using optimization algorithm is also conducted. Multi-objective optimization based on three solution algorithms including Non-Dominant Sorting Genetic Algorithm-II (NSGA-II), Multi-Objective Particle Swarm Optimization (MOPSO) algorithm and Fick's Law Algorithm (FLA). Finally, the pareto solution curves, after the multi-optimization process is finished, are analyzed using the decision-making (DM) methods. The Technique for Order Preference by Similarity to an Ideal Solution (TOPSIS) and Simple Additive Weighting (SAW) are the DM adopted in this study.

In the final stage of this thesis, simulation process of modeling and optimal sizing of a HRES are conducted under MATLAB. Additionally, the outcome of the simulation process are presented, analyzed and discussed based on different techno-economic and environmental aspects. Firstly, the reference system based on fossil fuel power plant is analyzed to reveal the actual COE and the environmental impact based on the Carbon Dioxide Emission (CDE) factor of the actual system. The simulation results for the reference reveal a COE of $71.05 per MWh and a CDE of 0.5871 kg/MWh of produced electricity, these values are used to compare and assess the effectiveness of the adopted HRES in both economic and environmental point of view. Additionally, other 09 HRES case studies are considered, these case studies are categorized into three categories (Full renewable energy source integration with single and dual storage means, Partial shift to renewable energy sources with single storage and Partial shift to renewable energy sources with dual storage), the case studies consider different levels of Renewable energy source integrations. The optimal sizing process of the adopted case studies outcome the effectiveness of case study with PV-WT-GT energy source and considering single or dual storage and a limit of minimum 80% of energy produced by renewable sources. The minimum COE account for 0.0737$/kWh is obtained from a PV-WT-GT system with HESS storage,

with a 80% of CDE is reduced to have a 0.0279 gCO2eq/kWh. Other system may also be feasible with a configuration based on PV-WT-GT system with dual storages may reach a 95% of renewable energy integration with relatively low COE of 0.1169$/kWh. The obtained outcomes also reveal the conflicting behavior between objectives and the decision-making methods become a necessity to help investors and operators of HRES in selecting the best tradeoff between different feasible solutions.

Finally, this work gives an insightful analysis of modeling, optimal sizing and energy management of a hybrid renewable energy systems for remote loads such as oil and gas sector in Algeria. In contrast, this work presents some other future perspectives including and not limited to:

- Considering a sensitivity analysis of load and renewable energy source variations. These inputs present an intermittent and stochastic behavior and may strongly affects the size and the performances of the studied system.

- In this study, a rule-based Energy management strategy is adopted, however, considering a machine learning based EMS may leads to better management to operations and the performance of the study systems especially in enhancing the performance of charging/discharging cycles of the storage systems.

- The storage systems chosen in this study are chemical (HESS) and electrochemical (BES system), however, assessing the effectiveness of other storage means such as thermal energy storage system may leads to better storage performances due to both high round-trip charging/discharging efficiency of thermal energy storage and the possibility of the needs in heat load demand for oil and gas facility.

References

[1] E. M. B. Messini, Y. Bourek, C. Ammari, A. Pesyridis, The integration of solar-hydrogen hybrid renewable energy systems in oil and gas industries for energy efficiency: Optimal sizing using fick's law optimisation algorithm, Energy Conversion and Management 308 (2024) 118372. doi:10.1016/j.enconman.2024.118372.

[2] Z. Abada, M. Bouharkat, Study of management strategy of energy resources in algeria, Energy Reports 4 (2018) 1–7. doi:10.1016/j.egyr.2017.09.004.

[3] K. Al-Khori, Y. Bicer, M. I. Aslam, M. Koç, Flare emission reduction utilizing solid oxide fuel cells at a natural gas processing plant, Energy Reports 7 (2021) 5627–5638. doi:10.1016/j.egyr.2021.08.164.

[4] A. ME, Algerian oil and gas map (2024).
URL https://www.energy.gov.dz/?rubrique=hydrocarbure

[5] O. B. Mya, Shale Gas in Algeria: The Future Environmental Disaster, 2022, pp. 565–570. doi:10.1007/978-3-030-76081-6_70.

[6] Y.-S. Park, S. Benayad, Hydrocarbons law and bidding opportunities in algeria, Journal of the Korean Society of Mineral and Energy Resources Engineers 50 (2013) 750–759. doi:10.32390/ksmer.2013.50.5.750.

[7] F. Sahnoune, K. Imessad, D. M. Bouakaz, Energy consumption renewable energy development and environmental impact in algeria - trend for 2030, 2017, p. 020072. doi:10.1063/1.4976291.

[8] A. B. Stambouli, Z. Khiat, S. Flazi, Y. Kitamura, A review on the renewable energy development in algeria: Current perspective, energy scenario and sustainability issues, Renewable and Sustainable Energy Reviews 16 (2012) 4445–4460. doi:10.1016/j.rser.2012.04.031.

[9] A. Kate, J. William, V. Valerie, Fossil fuel phase-out among options on cop28 table (2014).

[10] Y. Kebbati, L. Baghli, Design, modeling and control of a hybrid grid-connected photovoltaic-wind system for the region of adrar, algeria, International Journal of Environmental Science and Technology (8 2022). doi:10.1007/s13762-022-04426-y.

[11] V. K. Singh, S. Singal, Operation of hydro power plants-a review, Renewable and Sustainable Energy Reviews 69 (2017) 610–619. doi:10.1016/j.rser.2016.11.169.

[12] Y. W. Weldu, G. Assefa, Evaluating the environmental sustainability of biomass-based energy strategy: Using an impact matrix framework, Environmental Impact Assessment Review 60 (2016) 75–82. doi:10.1016/J.EIAR.2016.05.005.

[13] Y. W. Weldu, G. Assefa, The search for most cost-effective way of achieving environmental sustainability status in electricity generation: Environmental life cycle cost analysis of energy scenarios, Journal of Cleaner Production 142 (2017) 2296–2304. doi:10.1016/j.jclepro.2016.11.047.

[14] M. Bouznit, M. del P. Pablo-Romero, A. Sánchez-Braza, Measures to promote renewable energy for electricity generation in algeria, Sustainability 2020, Vol. 12, Page 1468 12 (2020) 1468. doi:10.3390/SU12041468.

[15] Y. Himri, S. Rehman, A. Mostafaeipour, S. Himri, A. Mellit, M. Merzouk, N. K. Merzouk, Overview of the role of energy resources in algeria's energy transition, Energies 15 (2022) 4731. doi:10.3390/en15134731.

[16] O. A. (2022), Renewables will be slow to take off in algeria, Emerald Expert Briefings oxan-db (2022). doi:10.1108/OXAN-DB266471.

[17] S. Sefiane, M. N. E. Hoda, H. Ahmed, Financial or socio-economic feasibility? potential assessment of renewable energy investment in algeria, Journal of Asian Energy Studies 6 (2022) 48–58. doi:10.24112/jaes.060004.

[18] Y. Zahraoui, M. R. B. Khan, I. AlHamrouni, S. Mekhilef, M. Ahmed, Current status, scenario, and prospective of renewable energy in algeria: A review, Energies 14 (2021) 2354. doi:10.3390/en14092354.

[19] M. de l'énergie, Energies nouvelles, renouvelables et maitrise de l'energie (2018).
URL https://tinyurl.com/algeriaRE

[20] A. M. A. Gama, F. Yettou, N. L. Panwar, Generation of solar irradiation maps for various applications under algerian clear-sky conditions, International Journal of Ambient Energy 39 (3) (2018) 243–256. arXiv:https://doi.org/10.1080/01430750.2017.1303630, doi:10.1080/01430750.2017.1303630.
URL https://doi.org/10.1080/01430750.2017.1303630

[21] H. Benamirouche, A. Megherbi, N. E. I. Djedaa, R. Bouferkas, Energy security index of algeria: an integrated approach, les cahiers du cread 38 (2022) 229–260. doi:10.4314/cread.v38i3.9.

[22] N. K. Merzouk, Wind energy potential of algeria, Renewable Energy 21 (2000) 553–562. doi:10.1016/S0960-1481(00)00090-2.

[23] R. Hammouche, Atlas vent de l'algerie, Office National de la Météorologie (1991).

[24] N. Sulmont, F. Meley, Les énergies renouvelables en algérie "chiffres clefs, service économique régional, Ambassade De France, Alger, Algérie (2013).

[25] IRENA, Renewable energy for remote communities: A guidebook for off-grid projects, International Renewable Energy Agency, 2023.
URL www.irena.org

[26] A. R. Barron, M. Domeshek, L. E. Metz, L. C. Draucker, A. L. Strong, Carbon neutrality should not be the end goal: Lessons for institutional climate action from u.s. higher education, One Earth 4 (2021) 1248–1258. doi:10.1016/j.oneear.2021.08.014.

[27] Y. Liu, S. Yu, Y. Zhu, D. Wang, J. Liu, Modeling, planning, application and management of energy systems for isolated areas: A review, Renewable and Sustainable Energy Reviews 82 (2018) 460–470. doi:10.1016/j.rser.2017.09.063.

[28] T. Luz, P. Moura, 100flexibility based on a multi-objective assessment, Applied Energy 255 (2019) 113819. doi:10.1016/j.apenergy.2019.113819.

[29] A. Roy, S. B. Kedare, S. Bandyopadhyay, Optimum sizing of wind-battery systems incorporating resource uncertainty, Applied Energy 87 (2010) 2712–2727. doi:10.1016/j.apenergy.2010.03.027.

[30] N. Singh, K. Patel, K. Patel, S. V. Pandey, P. Singh, A. K. Shukla, G. Dwivedi, Intermittency

Reduction Techniques in Hybrid Renewable Energy Systems: A Review, 2022, pp. 85–92. doi:10.1007/978-981-16-5371-1_9.

[31] C. Ammari, D. Belatrache, B. Touhami, S. Makhloufi, Sizing, optimization, control and energy management of hybrid renewable energy system—a review, Energy and Built Environment 3 (2022) 399–411. doi:10.1016/j.enbenv.2021.04.002.

[32] H. Girardet, M. Mendonça, A Renewable World: Energy, Ecology, Equality: A Report for the World Future Council, Green Books Totnes, 2009.

[33] Y. He, S. Guo, J. Zhou, G. Song, A. Kurban, H. Wang, The multi-stage framework for optimal sizing and operation of hybrid electrical-thermal energy storage system, Energy 245 (2022) 123248. doi:10.1016/j.energy.2022.123248.

[34] Y. He, S. Guo, J. Zhou, J. Ye, J. Huang, K. Zheng, X. Du, Multi-objective planning-operation co-optimization of renewable energy system with hybrid energy storages, Renewable Energy 184 (2022) 776–790. doi:10.1016/j.renene.2021.11.116.

[35] J. Lian, Y. Zhang, C. Ma, Y. Yang, E. Chaima, A review on recent sizing methodologies of hybrid renewable energy systems, Energy Conversion and Management 199 (2019) 112027. doi:10.1016/J.ENCONMAN.2019.112027.

[36] Y. He, S. Guo, P. Dong, Y. Zhang, J. Huang, J. Zhou, A state-of-the-art review and bibliometric analysis on the sizing optimization of off-grid hybrid renewable energy systems, Renewable and Sustainable Energy Reviews 183 (2023) 113476. doi:10.1016/j.rser.2023.113476.

[37] A. Kerboua, F. B. Hacene, M. F. Goosen, L. F. Ribeiro, Development of technical economic analysis for optimal sizing of a hybrid power system: A case study of an industrial site in tlemcen algeria, Results in Engineering 16 (2022) 100675. doi:10.1016/J.RINENG.2022.100675.

[38] A. Chebabhi, I. Tegani, A. D. Benhamadouche, O. Kraa, Optimal design and sizing of renewable energies in microgrids based on financial considerations a case study of biskra, algeria, Energy Conversion and Management 291 (2023) 117270. doi:10.1016/j.enconman.2023.117270.

[39] B. Bacha, H. Ghodbane, H. Dahmani, A. Betka, A. Toumi, A. Chouder, Optimal sizing of a hybrid microgrid system using solar, wind, diesel, and battery energy storage to alleviate energy poverty in a rural area of biskra, algeria, Journal of Energy Storage 84 (2024) 110651. doi:10.1016/j.est.2024.110651.

[40] A. Nekkache, B. Bouzidi, Y. Bakelli, A. Kaabeche, C. Larbes, Optimised sizing of a hybrid renewable water pumping system based on recent metaheuristic algorithms: a case study in algeria, International Journal of Ambient Energy 45 (12 2024). doi:10.1080/01430750.2023.2267569.

[41] S. T. Jan, A. Alanazi, M. Feroz, M. Alanazi, Techno-economic analysis of renewable energy sources' potential in the rural northern region of kalam in pakistan, Environment, Development and Sustainability (1 2024). doi:10.1007/s10668-023-04350-2.

[42] M. Kharrich, A. Selim, S. Kamel, J. Kim, An effective design of hybrid renewable energy system using an improved archimedes optimization algorithm: A case study of farafra, egypt, Energy Conversion and Management 283 (2023) 116907. doi:10.1016/j.enconman.2023.116907.

[43] S. Palanisamy, H. Lala, Optimal sizing of renewable energy powered hydrogen and electric vehicle charging station (hevcs), IEEE Access 12 (2024) 48239–48254. doi:10.1109/ACCESS.2024.3383960.

[44] M. Gökçek, N. Paltrinieri, Y. Liu, E. Badia, A. Şakir Dokuz, A. Erdoğmuş, B. B. Urhan, Özge Yoldaş, Optimum sizing of hybrid renewable power systems for on-site hydrogen refuelling stations: Case studies from türkiye and spain, International Journal of Hydrogen Energy 59 (2024) 715–729. doi:10.1016/j.ijhydene.2024.02.068.

[45] P. Kurukuri, M. R. Mohamed, P. H. Raavi, Y. Arya, Optimal planning and designing of microgrid systems with hybrid renewable energy technologies for sustainable environment in cities, Environmental Science and Pollution Research 31 (2024) 32264–32281. doi:10.1007/s11356-024-33254-5.

[46] T. Yuan, Y. Mu, T. Wang, Z. Liu, A. Pirouzi, Using firefly algorithm to optimally size a hybrid renewable energy system constrained by battery degradation and considering uncertainties of power sources and loads, Heliyon 10 (2024) e26961. doi:10.1016/j.heliyon.2024.e26961.

[47] A. M. García, J. Gallagher, J. A. R. Díaz, A. McNabola, An economic and environmental optimization model for sizing a hybrid renewable energy and battery storage system in off-grid farms, Renewable Energy 220 (2024) 119588. doi:10.1016/j.renene.2023.119588.

[48] S. M. S. Alavi, A. Maleki, A. Noroozian, A. Khaleghi, Simultaneous optimal site selection and sizing of a grid-independent hybrid wind/hydrogen system using a hybrid optimization method

based on electre: A case study in iran, International Journal of Hydrogen Energy 55 (2024) 970–983. doi:10.1016/j.ijhydene.2023.11.110.

[49] M. U. Manoo, F. Shaikh, L. Kumar, M. Arıcı, Comparative techno-economic analysis of various stand-alone and grid connected (solar/wind/fuel cell) renewable energy systems, International Journal of Hydrogen Energy 52 (2024) 397–414. doi:10.1016/j.ijhydene.2023.05.258.

[50] B. Yang, Y. Li, J. Huang, M. Li, R. Zheng, J. Duan, T. Fan, H. Zou, T. Liu, J. Wang, H. Shu, L. Jiang, Modular reconfiguration of hybrid pv-teg systems via artificial rabbit algorithm: Modelling, design and hil validation, Applied Energy 351 (2023) 121868. doi:10.1016/j.apenergy.2023.121868.

[51] G. Yang, H. Zhang, W. Wang, B. Liu, C. Lyu, D. Yang, Capacity optimization and economic analysis of pv–hydrogen hybrid systems with physical solar power curve modeling, Energy Conversion and Management 288 (2023) 117128. doi:10.1016/j.enconman.2023.117128.

[52] N. R. Deevela, B. Singh, T. C. Kandpal, Optimization and economic analysis of solar pv based hybrid system for powering base transceiver stations in india, Energy 283 (2023) 129160. doi:10.1016/j.energy.2023.129160.

[53] K. Zhu, H. Shi, S. Zheng, S. Michele, F. Cao, Hydrodynamic analysis of hybrid system with wind turbine and wave energy converter, Applied Energy 350 (2023) 121745. doi:10.1016/j.apenergy.2023.121745.

[54] Y. Wang, X. Wen, H. Su, J. Qin, L. Kong, Real-time dispatch of hydro-photovoltaic (pv) hybrid system based on dynamic load reserve capacity, Energy 285 (2023) 129420. doi:10.1016/j.energy.2023.129420.

[55] P. Jin, Z. Zheng, Z. Zhou, B. Zhou, L. Wang, Y. Yang, Y. Liu, Optimization and evaluation of a semi-submersible wind turbine and oscillating body wave energy converters hybrid system, Energy 282 (2023) 128889. doi:10.1016/j.energy.2023.128889.

[56] J. Zhang, Q. Sun, Z. Zheng, L. Huang, D. Chen, J. Yuan, Lightning surge analysis for hybrid wind turbine-photovoltaic-battery energy storage system, Electric Power Systems Research 225 (2023) 109803. doi:10.1016/j.epsr.2023.109803.

[57] B. Qiu, G. Li, X. Wei, M. Liu, J. Yan, System design and operation optimization on the hybrid system with nuclear power, concentrated solar, and thermal storage, Annals of Nuclear Energy 189 (2023) 109862. doi:10.1016/j.anucene.2023.109862.

[58] A. S. Irshad, W. K. Samadi, A. M. Fazli, A. G. Noori, A. S. Amin, M. N. Zakir, I. A. Bakhtyal, B. A. Karimi, G. A. Ludin, T. Senjyu, Resilience and reliable integration of pv-wind and hydropower based 100system without any energy storage system for inaccessible area electrification, Energy 282 (2023) 128823. doi:10.1016/j.energy.2023.128823.

[59] I. V, S. V, L. R, Resources, configurations, and soft computing techniques for power management and control of pv/wind hybrid system, Renewable and Sustainable Energy Reviews 69 (2017) 129–143. doi:10.1016/j.rser.2016.11.209.

[60] D. H. Muhsen, T. Khatib, H. T. Haider, A feasibility and load sensitivity analysis of photovoltaic water pumping system with battery and diesel generator, Energy Conversion and Management 148 (2017) 287–304. doi:10.1016/j.enconman.2017.06.007.

[61] Y. He, S. Guo, J. Zhou, J. Wang, W. Ji, T. Song, Province-level techno-economic feasibility analysis of baseload supply from hybrid renewable energy systems in china, Energy Conversion and Management 268 (2022) 116037. doi:10.1016/j.enconman.2022.116037.

[62] D. T. Hermann, N. Donatien, T. K. F. Armel, T. René, Techno-economic and environmental feasibility study with demand-side management of photovoltaic/wind/hydroelectricity/battery/diesel: A case study in sub-saharan africa, Energy Conversion and Management 258 (2022) 115494. doi:10.1016/j.enconman.2022.115494.

[63] O. D. T. Odou, R. Bhandari, R. Adamou, Hybrid off-grid renewable power system for sustainable rural electrification in benin, Renewable Energy 145 (2020) 1266–1279. doi:10.1016/j.renene.2019.06.032.

[64] Y. Yang, S. Guo, D. Liu, R. Li, Y. Chu, Operation optimization strategy for wind-concentrated solar power hybrid power generation system, Energy Conversion and Management 160 (2018) 243–250. doi:10.1016/j.enconman.2018.01.040.

[65] A. R. Starke, J. M. Cardemil, R. Escobar, S. Colle, Multi-objective optimization of hybrid csp+pv system using genetic algorithm, Energy 147 (2018) 490–503. doi:10.1016/j.energy.2017.12.116.

[66] R. Li, S. Guo, Y. Yang, D. Liu, Optimal sizing of wind/ concentrated solar plant/ electric heater hybrid renewable energy system based on two-stage stochastic programming, Energy 209 (2020) 118472. doi:10.1016/j.energy.2020.118472.

[67] J. Lata-García, F. Jurado, L. M. Fernández-Ramírez, H. Sánchez-Sainz, Optimal hydrokinetic turbine location and techno-economic analysis of a hybrid system based on photovoltaic/hydrokinetic/hydrogen/battery, Energy 159 (2018) 611–620. doi:10.1016/j.energy.2018.06.183.

[68] M. M. Ibrahim, N. H. Mostafa, A. H. Osman, A. Hesham, Performance analysis of a standalone hybrid energy system for desalination unit in egypt, Energy Conversion and Management 215 (2020) 112941. doi:10.1016/j.enconman.2020.112941.

[69] B. K. Das, R. Hassan, M. S. H. Tushar, F. Zaman, M. Hasan, P. Das, Techno-economic and environmental assessment of a hybrid renewable energy system using multi-objective genetic algorithm: A case study for remote island in bangladesh, Energy Conversion and Management 230 (2021) 113823. doi:10.1016/j.enconman.2020.113823.

[70] J. Rugolo, M. J. Aziz, Electricity storage for intermittent renewable sources, Energy Environmental Science 5 (2012) 7151. doi:10.1039/c2ee02542f.

[71] F. Nadeem, S. M. S. Hussain, P. K. Tiwari, A. K. Goswami, T. S. Ustun, Comparative review of energy storage systems, their roles, and impacts on future power systems, IEEE Access 7 (2019) 4555–4585. doi:10.1109/ACCESS.2018.2888497.

[72] A. Emrani, A. Berrada, A comprehensive review on techno-economic assessment of hybrid energy storage systems integrated with renewable energy, Journal of Energy Storage 84 (2024) 111010. doi:10.1016/j.est.2024.111010.

[73] O. Schmidt, S. Melchior, A. Hawkes, I. Staffell, Projecting the future levelized cost of electricity storage technologies, Joule 3 (2019) 81–100. doi:10.1016/j.joule.2018.12.008.

[74] T. B. Nkwanyana, M. W. Siti, Z. Wang, I. Toudjeu, N. T. Mbungu, W. Mulumba, An assessment of hybrid-energy storage systems in the renewable environments, Journal of Energy Storage 72 (2023) 108307. doi:10.1016/j.est.2023.108307.

[75] A. Kaabeche, Y. Bakelli, Renewable hybrid system size optimization considering various electrochemical energy storage technologies, Energy Conversion and Management 193 (2019) 162–175. doi:10.1016/j.enconman.2019.04.064.

[76] B. K. Das, F. Zaman, Performance analysis of a pv/diesel hybrid system for a remote area in bangladesh: Effects of dispatch strategies, batteries, and generator selection, Energy 169 (2019) 263–276. doi:10.1016/j.energy.2018.12.014.

[77] Y. Jiang, L. Kang, Y. Liu, A unified model to optimize configuration of battery energy storage systems with multiple types of batteries, Energy 176 (2019) 552–560. doi:10.1016/j.energy.2019.04.018.

[78] H. M. Ridha, C. Gomes, H. Hazim, M. Ahmadipour, Sizing and implementing off-grid standalone photovoltaic/battery systems based on multi-objective optimization and techno-economic (made) analysis, Energy 207 (2020) 118163. doi:10.1016/j.energy.2020.118163.

[79] C. Li, D. Zhou, H. Wang, H. Cheng, D. Li, Feasibility assessment of a hybrid pv/diesel/battery power system for a housing estate in the severe cold zone—a case study of harbin, china, Energy 185 (2019) 671–681. doi:10.1016/j.energy.2019.07.079.

[80] P. Arévalo, D. Benavides, J. Lata-García, F. Jurado, Energy control and size optimization of a hybrid system (photovoltaic-hidrokinetic) using various storage technologies, Sustainable Cities and Society 52 (2020) 101773. doi:10.1016/J.SCS.2019.101773.

[81] P. Kumar, N. Pal, H. Sharma, Techno-economic analysis of solar photo-voltaic/diesel generator hybrid system using different energy storage technologies for isolated islands of india, Journal of Energy Storage 41 (2021) 102965. doi:10.1016/j.est.2021.102965.

[82] S. Bandyopadhyay, G. R. C. Mouli, Z. Qin, L. R. Elizondo, P. Bauer, Techno-economical model based optimal sizing of pv-battery systems for microgrids, IEEE Transactions on Sustainable Energy 11 (2020) 1657–1668. doi:10.1109/TSTE.2019.2936129.

[83] M. A. Miller, J. Petrasch, K. Randhir, N. Rahmatian, J. Klausner, Chemical energy storage, Elsevier, 2021, pp. 249–292. doi:10.1016/B978-0-12-819892-6.00005-8.

[84] B. Modu, M. P. Abdullah, A. L. Bukar, M. F. Hamza, A systematic review of hybrid renewable energy systems with hydrogen storage: Sizing, optimization, and energy management strategy, International Journal of Hydrogen Energy 48 (2023) 38354–38373. doi:10.1016/j.ijhydene.2023.06.126.

[85] I. Dincer, H. Ishaq, Solar Energy-Based Hydrogen Production, Elsevier, 2022, pp. 91–122. doi:10.1016/B978-0-323-85176-3.00009-3.

[86] J. Wang, K. Xue, Y. Guo, J. Ma, X. Zhou, M. Liu, J. Yan, Multi-objective capacity programming and operation optimization of an integrated energy system considering hydrogen energy storage for collective energy communities, Energy Conversion and Management 268 (2022) 116057. doi:10.1016/j.enconman.2022.116057.

[87] A. Izadi, M. Shahafve, P. Ahmadi, Neural network genetic algorithm optimization of a transient hybrid renewable energy system with solar/wind and hydrogen storage system for zero energy buildings at various climate conditions, Energy Conversion and Management 260 (2022) 115593. doi:10.1016/j.enconman.2022.115593.

[88] H. Sun, A. G. Ebadi, M. Toughani, S. A. Nowdeh, A. Naderipour, A. Abdullah, Designing framework of hybrid photovoltaic-biowaste energy system with hydrogen storage considering economic and technical indices using whale optimization algorithm, Energy 238 (2022) 121555. doi:10.1016/j.energy.2021.121555.

[89] C. Ammari, D. Belatrache, S. Makhloufi, N. Saifi, Techno-economic analysis of a stand-alone photovoltaic system with three different storage systems for feeding isolated houses in south algeria, Energy Storage 3 (2 2021). doi:10.1002/est2.211.

[90] J. Mitali, S. Dhinakaran, A. Mohamad, Energy storage systems: a review, Energy Storage and Saving 1 (2022) 166–216. doi:10.1016/j.enss.2022.07.002.

[91] E. K. Gøtske, G. B. Andresen, M. Victoria, Cost and efficiency requirements for successful electricity storage in a highly renewable european energy system, PRX Energy 2 (2023) 023006. doi:10.1103/PRXEnergy.2.023006.

[92] K. R. Gautam, G. B. Andresen, M. Victoria, Review and techno-economic analysis of emerging thermo-mechanical energy storage technologies, Energies 15 (2022) 6328. doi:10.3390/en15176328.

[93] A. Lyden, C. Brown, I. Kolo, G. Falcone, D. Friedrich, Seasonal thermal energy storage in smart energy systems: District-level applications and modelling approaches, Renewable and Sustainable Energy Reviews 167 (2022) 112760. doi:10.1016/j.rser.2022.112760.

[94] T. Liu, J. Yang, Z. Yang, Y. Duan, Techno-economic feasibility of solar power plants considering pv/csp with electrical/thermal energy storage system, Energy Conversion and Management 255 (2022) 115308. doi:10.1016/j.enconman.2022.115308.

[95] S. Guo, Y. He, H. Pei, S. Wu, The multi-objective capacity optimization of wind-photovoltaic-thermal energy storage hybrid power system with electric heater, Solar Energy 195 (2020) 138–149. doi:10.1016/j.solener.2019.11.063.

[96] H. Liu, R. Zhai, K. Patchigolla, P. Turner, X. Yu, P. Wang, Multi-objective optimisation of a thermal-storage pv-csp-wind hybrid power system in three operation modes, Energy 284 (2023) 129255. doi:10.1016/j.energy.2023.129255.

[97] Y. Xi, Z. Zhang, J. Zhang, Multi-objective optimization strategy for regional multi-energy systems integrated with medium-high temperature solar thermal technology, Energy 300 (2024) 131545. doi:10.1016/j.energy.2024.131545.

[98] Y. Xiao, C. Zou, M. Dong, H. Chi, Y. Yan, S. Jiang, Feasibility study: Economic and technical analysis of optimal configuration and operation of a hybrid csp/pv/wind power cogeneration system with energy storage, Renewable Energy 225 (2024) 120273. doi:10.1016/j.renene.2024.120273.

[99] T. Ma, H. Yang, L. Lu, Development of hybrid battery–supercapacitor energy storage for remote area renewable energy systems, Applied Energy 153 (2015) 56–62. doi:10.1016/j.apenergy.2014.12.008.

[100] H. I. Alhammad, K. A. Khan, O. F. Konash, M. Khalid, Deployment of battery energy storage system in a renewable integrated distribution network based on long-term load expansion, Proceedings of 2021 31st Australasian Universities Power Engineering Conference, AUPEC 2021 (2021). doi:10.1109/AUPEC52110.2021.9597750.

[101] S. Sinha, S. S. Chandel, Review of recent trends in optimization techniques for solar photovoltaic–wind based hybrid energy systems, Renewable and Sustainable Energy Reviews 50 (2015) 755–769. doi:10.1016/J.RSER.2015.05.040.

[102] B. Bendjedia, F. Bouchafaa, N. Rizoug, M. Boukhnifer, Comparative study between battery and supercapacitor hybridization with fuel cells for automotive applications, in: 2017 4th International Conference on Control, Decision and Information Technologies (CoDIT), IEEE, 2017, pp. 0833–0838. doi:10.1109/CoDIT.2017.8102698.

[103] R. Mishra, R. Saxena, Comprehensive review of control schemes for battery and super-capacitor energy storage system, in: 2017 7th International Conference on Power Systems (ICPS), IEEE, 2017, pp. 702–707. doi:10.1109/ICPES.2017.8387381.

[104] C. Zhu, R. Lu, L. Tian, Q. Wang, The development of an electric bus with super-capacitors as unique energy storage, in: 2006 IEEE Vehicle Power and Propulsion Conference, IEEE, 2006, pp. 1–5. doi:10.1109/VPPC.2006.364372.

[105] J. Schindall, The charge of the ultracapacitors, IEEE Spectrum 44 (2007) 42–46. doi:10.1109/MSPEC.2007.4378458.

[106] V. Ganesh, S. Pitchumani, V. Lakshminarayanan, New symmetric and asymmetric supercapacitors based on high surface area porous nickel and activated carbon, Journal of Power Sources 158 (2006) 1523–1532. doi:10.1016/j.jpowsour.2005.10.090.

[107] C.-W. Liew, S. Ramesh, A. Arof, Enhanced capacitance of edlcs (electrical double layer capacitors) based on ionic liquid-added polymer electrolytes, Energy 109 (2016) 546–556. doi:10.1016/j.energy.2016.05.019.

[108] J. M. Crider, S. D. Sudhoff, Reducing impact of pulsed power loads on microgrid power systems, IEEE Transactions on Smart Grid 1 (2010) 270–277. doi:10.1109/TSG.2010.2080329.

[109] M. F. Elmorshedy, M. Elkadeem, K. M. Kotb, I. B. Taha, D. Mazzeo, Optimal design and energy management of an isolated fully renewable energy system integrating batteries and supercapacitors, Energy Conversion and Management 245 (2021) 114584. doi:10.1016/j.enconman.2021.114584.

[110] A. L. Bukar, C. W. Tan, A review on stand-alone photovoltaic-wind energy system with fuel cell: System optimization and energy management strategy, Journal of Cleaner Production 221 (2019) 73–88. doi:10.1016/j.jclepro.2019.02.228.

[111] F. Vivas, A. D. las Heras, F. Segura, J. Andújar, A review of energy management strategies for renewable hybrid energy systems with hydrogen backup, Renewable and Sustainable Energy Reviews 82 (2018) 126–155. doi:10.1016/j.rser.2017.09.014.

[112] P. Palensky, D. Dietrich, Demand side management: Demand response, intelligent energy systems, and smart loads, IEEE Transactions on Industrial Informatics 7 (2011) 381–388. doi:10.1109/TII.2011.2158841.

[113] M. Guezgouz, J. Jurasz, B. Bekkouche, T. Ma, M. S. Javed, A. Kies, Optimal hybrid pumped hydro-battery storage scheme for off-grid renewable energy systems, Energy Conversion and Management 199 (2019) 112046. doi:10.1016/j.enconman.2019.112046.

[114] J. Yang, Z. Yang, Y. Duan, Optimal capacity and operation strategy of a solar-wind hybrid renewable energy system, Energy Conversion and Management 244 (2021) 114519. doi:10.1016/j.enconman.2021.114519.

[115] E. M. B. Messini, Y. Bourek, C. Ammari, A. Zouaghi, L. Pace, Optimization and decision-making approach for energy storage strategies in a natural gas processing facility with photovoltaic renewable energy supply, Journal of Energy Storage (2025). doi:10.1016/j.est.2025.115431.

[116] A. M. Abdelshafy, J. Jurasz, H. Hassan, A. M. Mohamed, Optimized energy management strategy for grid connected double storage (pumped storage-battery) system powered by renewable energy resources, Energy 192 (2020) 116615. doi:10.1016/j.energy.2019.116615.

[117] M. R. Quitoras, P. E. Campana, P. Rowley, C. Crawford, Remote community integrated energy system optimization including building enclosure improvements and quantitative energy trilemma metrics, Applied Energy 267 (2020) 115017. doi:10.1016/j.apenergy.2020.115017.

[118] J. J. D. Nesamalar, S. Suruthi, S. C. Raja, K. Tamilarasu, Techno-economic analysis of both on-grid and off-grid hybrid energy system with sensitivity analysis for an educational institution, Energy Conversion and Management 239 (2021) 114188. doi:10.1016/j.enconman.2021.114188.

[119] G. T. Udeh, S. Michailos, D. Ingham, K. J. Hughes, L. Ma, M. Pourkashanian, Optimal sizing of a hybrid pv-wt-battery storage system: Effects of split-st and combined st + orc back-ups in circuit charging and load following, Energy Conversion and Management 256 (2022) 115370. doi:10.1016/j.enconman.2022.115370.

[120] Y. Khawaja, A. Allahham, D. Giaouris, C. Patsios, S. Walker, I. Qiqieh, An integrated framework for sizing and energy management of hybrid energy systems using finite automata, Applied Energy 250 (2019) 257–272. doi:10.1016/j.apenergy.2019.04.185.

[121] K. Lee, D. Kum, Complete design space exploration of isolated hybrid renewable energy system via dynamic programming, Energy Conversion and Management 196 (2019) 920–934. doi:10.1016/j.enconman.2019.05.078.

[122] R. Chedid, A. Sawwas, D. Fares, Optimal design of a university campus micro-grid operating under unreliable grid considering pv and battery storage, Energy 200 (2020) 117510. doi:10.1016/J.ENERGY.2020.117510.

[123] X. Xu, W. Hu, D. Cao, Q. Huang, W. Liu, Z. Liu, Z. Chen, H. Lund, Designing a standalone wind-diesel-caes hybrid energy system by using a scenario-based bi-level programming method,

Energy Conversion and Management 211 (2020) 112759. doi:10.1016/j.enconman.2020.112759.

[124] A. B. Forough, R. Roshandel, Lifetime optimization framework for a hybrid renewable energy system based on receding horizon optimization, Energy 150 (2018) 617–630. doi:10.1016/j.energy.2018.02.158.

[125] D. Fioriti, S. Pintus, G. Lutzemberger, D. Poli, Economic multi-objective approach to design off-grid microgrids: A support for business decision making, Renewable Energy 159 (2020) 693–704. doi:10.1016/j.renene.2020.05.154.

[126] S. Swaminathan, G. S. Pavlak, J. Freihaut, Sizing and dispatch of an islanded microgrid with energy flexible buildings, Applied Energy 276 (2020) 115355. doi:10.1016/j.apenergy.2020.115355.

[127] P. Rullo, L. Braccia, P. Luppi, D. Zumoffen, D. Feroldi, Integration of sizing and energy management based on economic predictive control for standalone hybrid renewable energy systems, Renewable Energy 140 (2019) 436–451. doi:10.1016/j.renene.2019.03.074.

[128] Z. Roumila, D. Rekioua, T. Rekioua, Energy management based fuzzy logic controller of hybrid system wind/photovoltaic/diesel with storage battery, International Journal of Hydrogen Energy 42 (2017) 19525–19535. doi:10.1016/j.ijhydene.2017.06.006.

[129] M. Thirunavukkarasu, Y. Sawle, H. Lala, A comprehensive review on optimization of hybrid renewable energy systems using various optimization techniques, Renewable and Sustainable Energy Reviews 176 (2023) 113192. doi:10.1016/j.rser.2023.113192.

[130] M. Atef, T. Khatib, M. F. Abdullah, M. F. Romlie, Optimization of a hybrid solar pv and gas turbine generator system using the loss of load probability index, Clean Technologies 2 (2020) 240–251. doi:10.3390/cleantechnol2030016.

[131] S. Sanajaoba, E. Fernandez, Maiden application of cuckoo search algorithm for optimal sizing of a remote hybrid renewable energy system, Renewable Energy 96 (2016) 1–10. doi:10.1016/j.renene.2016.04.069.

[132] A. Kaabeche, M. Belhamel, R. Ibtiouen, Sizing optimization of grid-independent hybrid photovoltaic/wind power generation system, Energy 36 (2011) 1214–1222. doi:10.1016/j.energy.2010.11.024.

[133] M. J. H. Moghaddam, A. Kalam, S. A. Nowdeh, A. Ahmadi, M. Babanezhad, S. Saha, Optimal sizing and energy management of stand-alone hybrid photovoltaic/wind system based on hydrogen storage considering loee and lole reliability indices using flower pollination algorithm, Renewable Energy 135 (2019) 1412–1434. doi:10.1016/j.renene.2018.09.078.

[134] R. Kaur, V. Krishnasamy, N. K. Kandasamy, S. Kumar, Discrete multiobjective grey wolf algorithm based optimal sizing and sensitivity analysis of pv-wind-battery system for rural telecom towers, IEEE Systems Journal 14 (2020) 729–737. doi:10.1109/JSYST.2019.2912899.

[135] M. Jamshidi, A. Askarzadeh, Techno-economic analysis and size optimization of an off-grid hybrid photovoltaic, fuel cell and diesel generator system, Sustainable Cities and Society 44 (2019) 310–320. doi:10.1016/j.scs.2018.10.021.

[136] H. A. El-Sattar, H. M. Sultan, S. Kamel, A. S. Menesy, C. Rahmann, Optimal design of hybrid stand-alone microgrids using tunicate swarm algorithm, in: 2021 IEEE International Conference on Automation/XXIV Congress of the Chilean Association of Automatic Control (ICA-ACCA), IEEE, 2021, pp. 1–6. doi:10.1109/ICAACCA51523.2021.9465283.

[137] A. Tabak, E. Kayabasi, M. T. Guneser, M. Ozkaymak, Grey wolf optimization for optimum sizing and controlling of a pv/wt/bm hybrid energy system considering tnpc, lpsp, and lcoe concepts, Energy Sources, Part A: Recovery, Utilization and Environmental Effects 44 (2022) 1508–1528. doi:10.1080/15567036.2019.1668880.

[138] H. T. Nguyen, U. Safder, X. N. Nguyen, C. Yoo, Multi-objective decision-making and optimal sizing of a hybrid renewable energy system to meet the dynamic energy demands of a wastewater treatment plant, Energy 191 (2020) 116570. doi:10.1016/j.energy.2019.116570.

[139] D. Xu, T. Acker, X. Zhang, Size optimization of a hybrid pv/wind/diesel/battery power system for reverse osmosis desalination, Journal of Water Reuse and Desalination 9 (2019) 405–422. doi:10.2166/wrd.2019.019.

[140] B. O. Bilal, D. Nourou, V. Sambou, A. P. Ndiaye, M. Ndongo, Multi-objective optimization of hybrid pv/wind/diesel/battery systems for decentralized application by minimizing the levelized cost of energy and the co2 emissions, International Journal of Physical Sciences 10 (2015) 192–203. doi:10.5897/IJPS2014.4251.

[141] M. Kharrich, O. Mohammed, M. Akherraz, Design of hybrid microgrid pv/wind/diesel/battery

system: Case study for rabat and baghdad, EAI Endorsed Transactions on Energy Web 0 (2018) 162692. doi:10.4108/eai.13-7-2018.162692.

[142] J. Zhang, S. Liang, X. Feng, A novel multi-effect methanol distillation process, Chemical Engineering and Processing: Process Intensification 49 (2010) 1031–1037. doi:10.1016/j.cep.2010.07.003.

[143] A. Ogunjuyigbe, T. Ayodele, O. Akinola, Optimal allocation and sizing of pv/wind/split-diesel/battery hybrid energy system for minimizing life cycle cost, carbon emission and dump energy of remote residential building, Applied Energy 171 (2016) 153–171. doi:10.1016/j.apenergy.2016.03.051.

[144] B. Shi, W. Wu, L. Yan, Size optimization of stand-alone pv/wind/diesel hybrid power generation systems, Journal of the Taiwan Institute of Chemical Engineers 73 (2017) 93–101. doi:10.1016/j.jtice.2016.07.047.

[145] P. Suhane, S. Rangnekar, A. Mittal, A. Khare, Sizing and performance analysis of standalone wind-photovoltaic based hybrid energy system using ant colony optimisation, IET Renewable Power Generation 10 (2016) 964–972. doi:10.1049/iet-rpg.2015.0394.

[146] A. Khan, N. Javaid, S. Javaid, Optimum unit sizing of stand-alone pv-wt-battery hybrid system components using jaya, in: 2018 IEEE 21st International Multi-Topic Conference (INMIC), IEEE, 2018, pp. 1–8. doi:10.1109/INMIC.2018.8595678.

[147] A. Maleki, M. G. Khajeh, M. Ameri, Optimal sizing of a grid independent hybrid renewable energy system incorporating resource uncertainty, and load uncertainty, International Journal of Electrical Power Energy Systems 83 (2016) 514–524. doi:10.1016/j.ijepes.2016.04.008.

[148] B. O. Bilal, V. Sambou, P. Ndiaye, C. Kébé, M. Ndongo, Optimal design of a hybrid solar–wind-battery system using the minimization of the annualized cost system and the minimization of the loss of power supply probability (lpsp), Renewable Energy 35 (2010) 2388–2390. doi:10.1016/j.renene.2010.03.004.

[149] Z. Shi, R. Wang, T. Zhang, Multi-objective optimal design of hybrid renewable energy systems using preference-inspired coevolutionary approach, Solar Energy 118 (2015) 96–106. doi:10.1016/j.solener.2015.03.052.

[150] H. Lan, S. Wen, Y.-Y. Hong, D. C. Yu, L. Zhang, Optimal sizing of hybrid pv/diesel/battery in ship power system, Applied Energy 158 (2015) 26–34. doi:10.1016/j.apenergy.2015.08.031.

[151] J. Schmidt, R. Cancella, A. O. Pereira, An optimal mix of solar pv, wind and hydro power for a low-carbon electricity supply in brazil, Renewable Energy 85 (2016) 137–147. doi:10.1016/j.renene.2015.06.010.

[152] D. Abbes, A. Martinez, G. Champenois, Life cycle cost, embodied energy and loss of power supply probability for the optimal design of hybrid power systems, Mathematics and Computers in Simulation 98 (2014) 46–62. doi:10.1016/j.matcom.2013.05.004.

[153] A. Gonzalez, J.-R. Riba, B. Esteban, A. Rius, Environmental and cost optimal design of a biomass–wind–pv electricity generation system, Renewable Energy 126 (2018) 420–430. doi:10.1016/j.renene.2018.03.062.

[154] M. Bortolini, M. Gamberi, A. Graziani, F. Pilati, Economic and environmental bi-objective design of an off-grid photovoltaic–battery–diesel generator hybrid energy system, Energy Conversion and Management 106 (2015) 1024–1038. doi:10.1016/j.enconman.2015.10.051. URL https://linkinghub.elsevier.com/retrieve/pii/S0196890415009735

[155] J. M. Aberilla, A. Gallego-Schmid, L. Stamford, A. Azapagic, Design and environmental sustainability assessment of small-scale off-grid energy systems for remote rural communities, Applied Energy 258 (2020) 114004. doi:10.1016/j.apenergy.2019.114004.

[156] B. Fleck, M. Huot, Comparative life-cycle assessment of a small wind turbine for residential off-grid use, Renewable Energy 34 (2009) 2688–2696. doi:10.1016/j.renene.2009.06.016.

[157] Y. Lechón, C. de la Rúa, R. Sáez, Life cycle environmental impacts of electricity production by solarthermal power plants in spain, Journal of Solar Energy Engineering 130 (5 2008). doi:10.1115/1.2888754.

[158] Y. Bicer, I. Dincer, Life cycle environmental impact assessments and comparisons of alternative fuels for clean vehicles, Resources, Conservation and Recycling 132 (2018) 141–157. doi:10.1016/j.resconrec.2018.01.036.

[159] S. Sadeghi, S. Ghandehariun, M. A. Rosen, Comparative economic and life cycle assessment of solar-based hydrogen production for oil and gas industries, Energy 208 (2020) 118347. doi:10.1016/j.energy.2020.118347.

[160] Y. Sawle, S. C. Gupta, A. K. Bohre, Socio-techno-economic design of hybrid renewable energy system using optimization techniques, Renewable Energy 119 (2018) 459–472. doi:10.1016/j.renene.2017.11.058.

[161] H. Yang, Z. Wei, L. Chengzhi, Optimal design and techno-economic analysis of a hybrid solar-wind power generation system, Applied Energy 86 (2009) 163–169. doi:10.1016/j.apenergy.2008.03.008.

[162] F. A. Khan, N. Pal, S. H. Saeed, Optimization and sizing of spv/wind hybrid renewable energy system: A techno-economic and social perspective, Energy 233 (2021) 121114. doi:10.1016/j.energy.2021.121114.

[163] M. Petrelli, D. Fioriti, A. Berizzi, C. Bovo, D. Poli, A novel multi-objective method with online pareto pruning for multi-year optimization of rural microgrids, Applied Energy 299 (2021) 117283. doi:10.1016/j.apenergy.2021.117283.

[164] J. L. C. Meza, M. B. Yildirim, A. S. M. Masud, A model for the multiperiod multiobjective power generation expansion problem, IEEE Transactions on Power Systems 22 (2007) 871–878. doi:10.1109/TPWRS.2007.895178.

[165] S. Awerbuch, Portfolio-based electricity generation planning: Policy implications for renewables and energy security, Mitigation and Adaptation Strategies for Global Change 11 (2006) 693–710. doi:10.1007/s11027-006-4754-4.

[166] S. Upadhyay, M. Sharma, A review on configurations, control and sizing methodologies of hybrid energy systems, Renewable and Sustainable Energy Reviews 38 (2014) 47–63. doi:10.1016/j.rser.2014.05.057.

[167] D. P. Neto, E. G. Domingues, A. P. Coimbra, A. T. de Almeida, A. J. Alves, W. P. Calixto, Portfolio optimization of renewable energy assets: Hydro, wind, and photovoltaic energy in the regulated market in brazil, Energy Economics 64 (2017) 238–250. doi:10.1016/j.eneco.2017.03.020.

[168] T. Khatib, I. A. Ibrahim, A. Mohamed, A review on sizing methodologies of photovoltaic array and storage battery in a standalone photovoltaic system, Energy Conversion and Management 120 (2016) 430–448. doi:10.1016/j.enconman.2016.05.011.

[169] P. Paliwal, N. Patidar, R. Nema, Determination of reliability constrained optimal resource mix for an autonomous hybrid power system using particle swarm optimization, Renewable Energy 63 (2014) 194–204. doi:10.1016/j.renene.2013.09.003.

[170] J. Jurasz, B. Ciapała, Integrating photovoltaics into energy systems by using a run-off-river power plant with pondage to smooth energy exchange with the power gird, Applied Energy 198 (2017) 21–35. doi:10.1016/j.apenergy.2017.04.042.

[171] A. Q. Jakhrani, A.-K. Othman, A. R. H. Rigit, S. R. Samo, S. A. Kamboh, A novel analytical model for optimal sizing of standalone photovoltaic systems, Energy 46 (2012) 675–682. doi:10.1016/j.energy.2012.05.020.

[172] T. Markvart, Sizing of hybrid photovoltaic-wind energy systems, Solar Energy 57 (1996) 277–281. doi:10.1016/S0038-092X(96)00106-5.

[173] J. G. G. Clúa, R. J. Mantz, H. D. Battista, Optimal sizing of a grid-assisted wind-hydrogen system, Energy Conversion and Management 166 (2018) 402–408. doi:10.1016/j.enconman.2018.04.047.

[174] A. Giallanza, M. Porretto, G. L. Puma, G. Marannano, A sizing approach for stand-alone hybrid photovoltaic-wind-battery systems: A sicilian case study, Journal of Cleaner Production 199 (2018) 817–830. doi:10.1016/j.jclepro.2018.07.223.

[175] H. A. Kazem, T. Khatib, K. Sopian, Sizing of a standalone photovoltaic/battery system at minimum cost for remote housing electrification in sohar, oman, Energy and Buildings 61 (2013) 108–115. doi:10.1016/j.enbuild.2013.02.011.

[176] W. Ma, X. Xue, G. Liu, Techno-economic evaluation for hybrid renewable energy system: Application and merits, Energy 159 (2018) 385–409. doi:10.1016/j.energy.2018.06.101.

[177] M. Elkadeem, A. Younes, S. W. Sharshir, P. E. Campana, S. Wang, Sustainable siting and design optimization of hybrid renewable energy system: A geospatial multi-criteria analysis, Applied Energy 295 (2021) 117071. doi:10.1016/j.apenergy.2021.117071.

[178] T. Tawfik, M. Badr, E. El-Kady, O. Abdellatif, Optimization and energy management of hybrid standalone energy system: a case study, Renewable Energy Focus 25 (2018) 48–56. doi:10.1016/j.ref.2018.03.004.

[179] R. Figaj, M. Żołądek, W. Goryl, Dynamic simulation and energy economic analysis of a household hybrid ground-solar-wind system using trnsys software, Energies 13 (2020) 3523. doi:10.3390/en13143523.

[180] K.-H. Lee, D.-W. Lee, N.-C. Baek, H.-M. Kwon, C.-J. Lee, Preliminary determination of optimal size for renewable energy resources in buildings using retscreen, Energy 47 (2012) 83–96. doi:10.1016/j.energy.2012.08.040.

[181] F. A. Hashim, R. R. Mostafa, A. G. Hussien, S. Mirjalili, K. M. Sallam, Fick's law algorithm: A physical law-based algorithm for numerical optimization, Knowledge-Based Systems 260 (2023) 110146. doi:10.1016/j.knosys.2022.110146.

[182] A. Mahesh, K. S. Sandhu, A genetic algorithm based improved optimal sizing strategy for solar-wind-battery hybrid system using energy filter algorithm, Frontiers in Energy 14 (2020) 139–151. doi:10.1007/s11708-017-0484-4.

[183] A. Abdelkader, A. Rabeh, D. M. Ali, J. Mohamed, Multi-objective genetic algorithm based sizing optimization of a stand-alone wind/pv power supply system with enhanced battery/supercapacitor hybrid energy storage, Energy 163 (2018) 351–363. doi:10.1016/j.energy.2018.08.135.

[184] J. H. Holland, Genetic algorithms, Scientific American 267 (1992) 66–72. doi:10.1038/scientificamerican0792-66.

[185] S. Kirkpatrick, C. D. Gelatt, M. P. Vecchi, Optimization by simulated annealing, Science 220 (1983) 671–680. doi:10.1126/science.220.4598.671.

[186] W. Zhang, A. Maleki, M. A. Rosen, J. Liu, Optimization with a simulated annealing algorithm of a hybrid system for renewable energy including battery and hydrogen storage, Energy 163 (2018) 191–207. doi:10.1016/j.energy.2018.08.112.

[187] S. Hakimi, S. Moghaddas-Tafreshi, Optimal sizing of a stand-alone hybrid power system via particle swarm optimization for kahnouj area in south-east of iran, Renewable Energy 34 (2009) 1855–1862. doi:10.1016/j.renene.2008.11.022.

[188] A. K. Pandey, S. Kirmani, Optimal location and sizing of hybrid system by analytical crow search optimization algorithm, International Transactions on Electrical Energy Systems 30 (5 2020). doi:10.1002/2050-7038.12327.

[189] O. Llerena-Pizarro, N. Proenza-Perez, C. E. Tuna, J. L. Silveira, A pso-bpso technique for hybrid power generation system sizing, IEEE Latin America Transactions 18 (2020) 1362–1370. doi:10.1109/TLA.2020.9111671.

[190] J. Kennedy, R. Eberhart, Particle swarm optimization, in: Proceedings of ICNN'95 - International Conference on Neural Networks, IEEE, 1995, pp. 1942–1948. doi:10.1109/ICNN.1995.488968.

[191] S. Mirjalili, S. M. Mirjalili, A. Lewis, Grey wolf optimizer, Advances in Engineering Software 69 (2014) 46–61. doi:10.1016/j.advengsoft.2013.12.007.

[192] Z. W. Geem, J. H. Kim, G. Loganathan, A new heuristic optimization algorithm: Harmony search, SIMULATION 76 (2001) 60–68. doi:10.1177/003754970107600201.

[193] D. Fares, M. Fathi, S. Mekhilef, Performance evaluation of metaheuristic techniques for optimal sizing of a stand-alone hybrid pv/wind/battery system, Applied Energy 305 (2022) 117823. doi:10.1016/j.apenergy.2021.117823.

[194] S. Mohseni, A. C. Brent, D. Burmester, A comparison of metaheuristics for the optimal capacity planning of an isolated, battery-less, hydrogen-based micro-grid, Applied Energy 259 (2020) 114224. doi:10.1016/j.apenergy.2019.114224.

[195] E. Koepf, I. Alxneit, C. Wieckert, A. Meier, A review of high temperature solar driven reactor technology: 25years of experience in research and development at the paul scherrer institute, Applied Energy 188 (2017) 620–651. doi:10.1016/j.apenergy.2016.11.088.

[196] D. Gu, N. Shao, Y. Zhu, H. Wu, B. Wang, Solar-driven thermo- and electrochemical degradation of nitrobenzene in wastewater: Adaptation and adoption of solar step concept, Journal of Hazardous Materials 321 (2017) 703–710. doi:10.1016/j.jhazmat.2016.09.069.

[197] C. Likkasit, A. Maroufmashat, A. Elkamel, H. ming Ku, M. Fowler, Solar-aided hydrogen production methods for the integration of renewable energies into oil amp; gas industries, Energy Conversion and Management 168 (2018) 395–406. doi:10.1016/j.enconman.2018.04.057.

[198] F. Sayedin, A. Maroufmashat, R. Roshandel, S. S. Khavas, Optimal design and operation of a photovoltaic–electrolyser system using particle swarm optimisation, International Journal of Sustainable Energy 35 (2016) 566–582. doi:10.1080/14786451.2014.922974.

[199] D. TROMMER, F. NOEMBRINI, M. FASCIANA, D. RODRIGUEZ, A. MORALES, M. ROMERO, A. STEINFELD, Hydrogen production by steam-gasification of petroleum coke using concentrated solar power?i. thermodynamic and kinetic analyses, International Journal of Hydrogen Energy 30 (2005) 605–618. doi:10.1016/j.ijhydene.2004.06.002.

[200] C. Li, M. Wang, N. Li, D. Gu, C. Yan, D. Yuan, H. Jiang, B. Wang, X. Wang, Solar oil refinery: Solar-driven hybrid chemical cracking of residual oil towards efficiently upgrading fuel and abundantly generating hydrogen, Energy Conversion and Management 300 (2024) 117900. doi:10.1016/j.enconman.2023.117900.

[201] A. S. Nafey, M. Mohamad, S. El-Helaby, M. Sharaf, Theoretical and experimental study of a small unit for solar desalination using flashing process, Energy Conversion and Management 48 (2007) 528–538. doi:10.1016/j.enconman.2006.06.010.

[202] M. N. Mistry, et al., Comparison of weather station and climate reanalysis data for modelling temperature-related mortality, Scientific Reports 12 (2022) 5178. doi:10.1038/s41598-022-09049-4.

[203] J. M. Sabater, et al., Era5-land hourly data from 1981 to present, Copernicus Climate Change Service (C3S) Climate Data Store (CDS) 10 (2019).

[204] A. Berchiche, M. Guenoune, S. Belaadi, G. Léonard, Optimal energy integration and off-design analysis of an amine-based natural gas sweetening unit, Applied Sciences 13 (2023) 6559. doi:10.3390/app13116559.

[205] Z. Gu, G. Xiong, X. Fu, Parameter extraction of solar photovoltaic cell and module models with metaheuristic algorithms: A review, Sustainability 15 (2023) 3312. doi:10.3390/su15043312.

[206] V. Kachitvichyanukul, Comparison of three evolutionary algorithms: Ga, pso, and de, Industrial Engineering and Management Systems 11 (2012) 215–223. doi:10.7232/iems.2012.11.3.215.

[207] Y. He, S. Guo, J. Zhou, F. Wu, J. Huang, H. Pei, The quantitative techno-economic comparisons and multi-objective capacity optimization of wind-photovoltaic hybrid power system considering different energy storage technologies, Energy Conversion and Management 229 (2021) 113779. doi:10.1016/j.enconman.2020.113779.

[208] L. Olatomiwa, S. Mekhilef, A. S. N. Huda, K. Sanusi, Techno-economic analysis of hybrid ¡scp¿pv¡/scp¿ –diesel–battery and ¡scp¿pv¡/scp¿ –wind–diesel–battery power systems for mobile ¡scp¿bts¡/scp¿ : the way forward for rural development, Energy Science Engineering 3 (2015) 271–285. doi:10.1002/ese3.71.

[209] A. Fathy, A reliable methodology based on mine blast optimization algorithm for optimal sizing of hybrid pv-wind-fc system for remote area in egypt, Renewable Energy 95 (2016) 367–380. doi:10.1016/j.renene.2016.04.030.

[210] M. H. Amrollahi, S. M. T. Bathaee, Techno-economic optimization of hybrid photovoltaic/wind generation together with energy storage system in a stand-alone micro-grid subjected to demand response, Applied Energy 202 (2017) 66–77. doi:10.1016/j.apenergy.2017.05.116.

[211] F. Bauelos-Ruedas, C. Angeles-Camacho, Sebastin, Methodologies Used in the Extrapolation of Wind Speed Data at Different Heights and Its Impact in the Wind Energy Resource Assessment in a Region, InTech, 2011. doi:10.5772/20669.

[212] E. M. B. Messini, Y. Bourek, C. Ammari, Comparative analysis of pv module models using ai-based metaheuristic optimization techniques, in: M. Hatti (Ed.), Smart Computing and Control Renewable Energy Systems, Springer Nature Switzerland, Cham, 2025, pp. 207–216. doi:10.1007/978-3-031-80301-7_23.

[213] M. El-Shafie, Hydrogen production by water electrolysis technologies: A review, Results in Engineering 20 (2023) 101426. doi:10.1016/j.rineng.2023.101426.

[214] Y. Bourek, E. M. B. Messini, C. Ammari, M. Guenoune, B. Chabira, B. K. Saha, A hybrid renewable energy system for hassi messaoud region of algeria: Modeling and optimal sizing, Energy Storage and Saving 4 (1) (2025) 56–69. doi:https://doi.org/10.1016/j.enss.2024.10.002.

[215] D. Ghribi, A. Khelifa, S. Diaf, M. Belhamel, Study of hydrogen production system by using pv solar energy and pem electrolyser in algeria, International Journal of Hydrogen Energy 38 (2013) 8480–8490. doi:10.1016/j.ijhydene.2012.09.175.

[216] D. Ipsakis, S. Voutetakis, P. Seferlis, F. Stergiopoulos, C. Elmasides, Power management strategies for a stand-alone power system using renewable energy sources and hydrogen storage, International Journal of Hydrogen Energy 34 (2009) 7081–7095. doi:10.1016/j.ijhydene.2008.06.051.

[217] Øystein Ulleberg, Stand-alone power systems for the future: optimal design, operation and control of solar-hydrogen energy systems, Ph.D. thesis, Norwegian University of Science and Technology Trondheim, Trondheim, Norway, phD Thesis (1998).

[218] A. A. El-Fergany, Extracting optimal parameters of pem fuel cells using salp swarm optimizer, Renewable Energy 119 (2018) 641–648. doi:10.1016/j.renene.2017.12.051.

[219] R. Dufo-López, J. L. Bernal-Agustín, J. Contreras, Optimization of control strategies for stand-alone renewable energy systems with hydrogen storage, Renewable Energy 32 (2007) 1102–1126. doi:10.1016/j.renene.2006.04.013.

[220] K. Deb, A. Pratap, S. Agarwal, T. Meyarivan, A fast and elitist multiobjective genetic algorithm: Nsga-ii, IEEE Transactions on Evolutionary Computation 6 (2002) 182–197. doi:10.1109/4235.996017.

[221] F. Ren, J. Wang, S. Zhu, Y. Chen, Multi-objective optimization of combined cooling, heating and power system integrated with solar and geothermal energies, Energy Conversion and Management 197 (2019) 111866. doi:10.1016/j.enconman.2019.111866.

[222] M. Reyes-Sierra, C. A. C. Coello, et al., Multi-objective particle swarm optimizers: A survey of the state-of-the-art, International journal of computational intelligence research 2 (2006) 287–308.

[223] N. Delgarm, B. Sajadi, F. Kowsary, S. Delgarm, Multi-objective optimization of the building energy performance: A simulation-based approach by means of particle swarm optimization (pso), Applied Energy 170 (2016) 293–303. doi:10.1016/j.apenergy.2016.02.141.

[224] F. Ciardiello, A. Genovese, A comparison between topsis and saw methods, Annals of Operations Research 325 (2023) 967–994. doi:10.1007/s10479-023-05339-w.

[225] T. Niknam, M. Bornapour, A. Gheisari, Combined heat, power and hydrogen production optimal planning of fuel cell power plants in distribution networks, Energy Conversion and Management 66 (2013) 11–25. doi:10.1016/j.enconman.2012.08.016.

[226] Z. Yue, A method for group decision-making based on determining weights of decision makers using topsis, Applied Mathematical Modelling 35 (2011) 1926–1936. doi:10.1016/j.apm.2010.11.001.

[227] R. Kumar, S. Singal, Penstock material selection in small hydropower plants using madm methods, Renewable and Sustainable Energy Reviews 52 (2015) 240–255. doi:10.1016/j.rser.2015.07.018.

[228] M. Madanchian, H. Taherdoost, A comprehensive guide to the topsis method for multi-criteria decision making, Sustainable Social Development 1 (8 2023). doi:10.54517/ssd.v1i1.2220.

Appendix A

Techo-economic data

Table A.1: Economic Parameters of System Components

Component	**Lifetime (years)**	**Capital Cost**	**O&M Cost Yearly**	**Replacement Cost (% of Capital Cost)**
PV	25	350 $/kW	3% of yearly capital	100%
WT	20	2500 $/kW	50 $/year	70%
GT	10	1840 $/kW	0.02 $/year + fuel price	100%
EL	10	1000 $/kW	0.05 $/per working hour	7%
FC	10	1000 $/kW	0.05 $/per working hour	7%
H_2 ST	25	100 $/$m^3$	50% of yearly capital	100%
BT	5 @ 80% DoD	481.5 $/kWh	0.5% of yearly capital	100%
Inverter	15	300 $/kW	0	100%

Appendix B

Data for Electrolyzer modelling

Table B.1: Parameter values for the model

Parameter	Value
r_1	7.331×10^{-5}
r_2	-1.107×10^{-7}
r_3	0
s_1	1.586×10^{-1}
s_2	1.378×10^{-3}
s_3	-1.606×10^{-5}
t_1	1.599×10^{-2}
t_2	-1.302
t_3	4.213×10^{2}

Appendix C

Data for BES modelling

Table C.1: Battery Energy Storage (BES) System Parameters

Parameter	**Description**	**Value**
η_{BES}^{char}	Charging efficiency of the BES system	85%
$\eta_{BES}^{dischar}$	Discharging efficiency of the BES system	85%
$C_{\text{Bat-nom}}$	Nominal capacity of a single battery accumulator	13.5 kWh
SoC_{max}	Maximum allowable state of charge	100%
SoC_{min}	Minimum allowable state of charge	20%
$I_{BES-max}$	Maximum allowable current	1800 A
$V_{BES-nom}$	Nominal battery voltage	12 V
σ_{BES}	Self-discharge of BES during time	5.7870×10^{-5} per hour. (eq. 50% self-discharge each year)